The University of Nottingham

Hybrid quadrupole linear ion trap mass spectrometry: application to metabolites

Peter Christensen BSc.

Thesis submitted to the University of Nottingham for the Degree of Doctor of Philosophy

July 2009

Abstract

The capability of the QqQLit hybrid triple quadrupole linear ion trap mass spectrometer to profile endogenous metabolites has been assessed by the analysis of three different families of metabolites; nucleotides from bacteria and N-acyl ethanolamines and N-acyl glycerols from rat tissues.

Mass spectrometry methods were developed based on employing a survey scan, either precursor ion or neutral loss, coupled with full product ion spectra. This approach identified families of metabolites with a common structural core and provided the structural information for the reliable identification of known and unknown metabolites. By targeting structural similarities, this approach has opened the window of metabolites that can be profiled beyond the constraints of available references standards.

A method to profile phosphate containing endogenous metabolites, particularly nucleotide metabolites, was based on the identification of the phosphate moiety following collision induced dissociation. Employing a precursor ion scan, this approach was successfully applied to the analysis of nucleotides in bacterial samples *Escherichia coli* MG1655 and *Pseudomonas aeruginosa.* A more comprehensive profile of nucleotides was observed compared to targeted approaches. Furthermore, a considerable number of additional analytes were identified which were unlikely to be nucleotides and probably result from other endogenous phosphate containing metabolites, demonstrating the scope of the approach outside nucleotides alone.

The use of this methodology was also successful in the profiling of N-acyl ethanolamines and N-acyl glycerols. Targeting core structures common to each family of metabolite, the ethanolmine and glycerol moiety, precursor ion and neutral loss survey scans were successfully employed in identifying a wider number of these metabolites in various rat tissues than previously reported. The profile of rat testi was notably different from other

tissues investigated due to the presence of MAG and NAE C22:5; analytes not detected in other tissues by this method. Furthermore, as far as it can be ascertained, MAG C22:5 has not been previously reported in rat tissues.

A quantitative method based on precursor ion - product ion transitions was developed based on the NAEs and MAGs identified by the survey scans. By employing this method to analyze various rat tissues harvested immediately after death and five hours post mortem, quantitative data was obtained not only for a broad range of NAEs and MAGs at basal levels but also an insight into postmortem changes of these analytes.

Acknowledgements

Firstly I would like to thank my supervisors Dave Barrett and Cath Ortori for their advice and support throughout this work. Many thanks also to Dave Kendall, Vicky Chapman, Stephen Alexander, and Nigel Halliday for supplying samples and for their advice.

A very big thank you to Anahi who gave me constant love, support and encouragement throughout the rigors of the PhD and was there to pick me when the going got tough.

Many thanks to everyone in the lab and house mates who made the days fly by and made life easier when the instrumentation was misbehaving.

Thanks also to my parents and my sister who supported me through the PhD and especially the writing up.

Finally I'd like to thank the BBSRC for their funding which made this project possible.

Table of contents

List of abbreviations

2-AG, C20:4	2-arachidonylglycerol
2-LG, C18:2	2-linoleoyl glycerol
ADP	Adenine 5' - diphosphate
AMP	Adenine 5' - monophosphate
Anandamide, AEA C20:4	N-arachidonylethanolamine
ATP	Adenine 5' - triphosphate
cAMP	Cyclic adenine 2', 3' - monophosphate
CB_1 / CB_2	cannabinoid receptors 1 and 2
CDP	Cytidine 5' diphosphate
CE	Collision energy
cGMP	Cyclic guanosin 2', 3' - monophosphate
CID	Collision induced dissociation
CMP	Cytidine 5' monophosphate
CNS	Central nervous system
COX-2	Cyclooxygenase
CP450	Cytochrome P450
CTP	Cytidine 5' - triphosphate
dADP	Deoxyadenosine 5' - diphosphate
DAG	Diacylglycerol
dATP	Deoxyadenosine 5' - triphosphate
dCDP	Deoxycytidine 5' - diphosphate
DEA, C22:4	Docosatetraenoyl ethanolamide
DMHA	N,N-dimethylhexylamine
DNA	Deoxyribonucleic acid
DP	Declustering potential
dTMP	Deoxythymidine 5' - monophosphate
dTTP	Deoxythymidine 5'- triphosphate
EC	Endocannabinoid
EMC	Enhanced multiple charged
EMS	Enhanced single MS
EPI	Enhanced product ion
ER	Enhanced resolution

ESI	Electrospray ionisation
ETE-EA	Epoxyeicosatrienoic acid ethanolamine
FAAH	Fatty acid amide hydrolase
FAD	Flavin adenine dinucleotide
FT-ICR	Fourier-transform ion cyclotron resonance mass spectrometry
FWHM	Full width at half maximum
GC-MS	Gas chromatography mass spectometry
GC-TOF	Gas chromatography time of flight mass spectometry
GDP	Guanosin 5' - diphosphate
GMP	Guanosin 5' - monophosphate
GP-NArE	Glycerophopspho-N-arachidonoylethanolamine
GTP	Guanosin 5'- triphosphate
HETE-EA	Hydroxyeicosatetraenoic acid ethanolamine
HPLC	High performance liquid chromatography
LC-MS	Liquid chromatography mass spectometry
LIT	Linear ion trap
LLOD	Lower limit of detection
LLOQ	Lower limit of quantification
LOX	Lipoxygenases
MAG	Mono-acylglycerol
MGL	Monoacylglycerol lipase
mRNA	messenger ribonucleic acid
NAAA	*N* – acylethanolamine-hydrolyzing acid amidase
NAD^+ / NADH	Nicotinamide adenine dinucleotide / reduced form
$NADP^+$ / NADPH	Nicotinamide adenine dinucleotide phosphate / reduced form
NAE	*N*-acylethanolamine
NAPE	*N*-acyl phosphatidylethanolamine
NAT	*N*-acyltransferase
NE	Noladin Ether
NL	Neutral loss
OEA, C18:1	*N*-oleoylethanolamine
PC	Precursor ion
PEA, C16:0	*N*-pamitoylethanolmine
PhosC	Phosphatidylcholine
PhosEA	Phosphatidylethanolamine
ppm	Parts per million
QqQLIT	Hybrid quadrupole linear ion trap mass spectrometer

Q-TOF	Quadrupole time of flight mass spectrometer
RNA	Ribonucleic acid
RSD	Relative standard deviation
S/N	Signal to noise ratio
SRM	Selected reaction monitoring
TDF	Time delay fragmentation
TOF	Quadrupole time of flight mass spectrometer
UDP	Uridine diphosphate
UDP(G)	Uridine diphosphate glucose/galactose
UMP	Uridine monophosphate
UTP	Uridine triphosphate
UV/VIS	Ultraviolet / visible light

List of figures

List of tables

CHAPTER 1

1 Introduction

1.1 Metabolite Profiling

Primary and secondary metabolites are relatively small molecules (<1500 Daltons) present in biological systems. Primary metabolites are found in all prokaryotic and eukaryotic cells and are involved in growth, development, and reproduction where secondary metabolites, commonly found in plants, are involved in traits such as crop resistance, taste, colour, and aroma (Laurentin *et al.*, 2008). The presence and relative levels of these compounds are the result of gene expression and environmental factors (Ceglarek *et al.*, 2009b). As such metabolite profiling methods have become one of the tools employed in the understanding of gene function, drug metabolism, disease and diet (Ceglarek *et al.*, 2009b; Cunnick *et al.*, 1972; Raamsdonk *et al.*, 2001). Essentially, metabolite profiling or metabolomics is the study of metabolites, involving identifying and/or measuring levels of these analytes in biological materials. The terms metabolomics, metabonomics and metabolite profiling have essentially become interchangeable, although there have been calls for the phrase metabolomics to be used only where the analysis of metabolites is in reference to the genome (Villas-Boas *et al.*, 2005).

Metabolomics complement other 'omics' such as transcriptomics and proteomics to provide a greater understanding of a given biological system (Witkamp, 2005). The study of transcriptomics measures the levels of messenger ribonucleic acid (mRNA) resulting from the transcription of a gene (Feng *et al.*, 2008). This however does not necessarily accurately describe the amount of active protein synthesized at the ribosomes because of mRNA splicing and post-translational modification such as phosphorylation and glycosylation, mechanisms employed to control protein activity (Cho, 2007). Complementary to this approach is proteomics, described as the analysis of the all proteins expressed by a genome or cell or tissue type, including post translational modifications (Dierick *et al.*, 2002). Metabolomics is the analyses of small molecules

which can be synthesised / catabolised by active proteins and as such complements the other two areas of analysis, providing an insight into the workings of a biological system.

The study of metabolomics has found application in understanding silent gene function. By the disruption or mutation of a gene of interest, a possible function can be identified by measuring the metabolite phenotype resulting from the genetic change (Fiehn, 2001). Such an approach is advantageous when assigning function to silent genes which, when deleted, can appear to have no obvious measurable influence on an organism's phenotype, such as cell growth. The lack of phenotypical change can be due to compensation at the metabolite level, which however can be measured, and the role of the silent gene may be characterized (Raamsdonk *et al.*, 2001).

Measuring changes and relative levels of metabolites has been successfully employed in the identification of disease states that are due to inherited genetic disorders, pathogens or other health issues such as diabetes. Inherited genetic disorders are commonly screened in new born babies (Horning and Horning, 1971; Jones and Bennett, 2002) using a targeted approach to measure metabolites which are biomarkers for a given illness. Disease states caused by pathogens, such as urinary tract infection, can affect metabolite levels, and it has been demonstrated that a select number of amino acids and related compounds can be used as biomarkers for the presence of one of the causes of this infection (Ramautar *et al.*, 2008). Diseases such as diabetes, gout and alcoholic liver disease have also been identified by the measurement of specific metabolites (Cunnick *et al.*, 1972).

The analysis of metabolites, particularly the monitoring of multiple metabolites, is not a simple task because of the nature of their chemistry and wide-ranging dynamic levels (Stitt and Fernie, 2003). There are a large number of metabolites, although numbers vary considerably depending on the biological source. Within the plant kingdom there are an

estimated 200,000 metabolites, combining both primary and secondary metabolites (Fiehn, 2001), where species of yeast and bacteria have been reported to have approximately 600 and 1692 metabolites respectively (Luo *et al.*, 2007). Metabolite vary greatly in structures, although fractions of these metabolites (e.g. lipids) do possess a common structural backbone (Schwab, 2003). Furthermore, metabolite – enzyme reactions can be very quick, from time scales of half an hour to fractions of a second (Stitt and Fernie, 2003). This requires stringent sample extraction and preparation, ensuring all biological processes are stopped at the time of sample collection, leading to accurate metabolite profiles comparable between experiments.

1.1.1 Approaches to metabolite profiling

Metabolite profiling can be undertaken by two main analytical approaches, a targeted methodology or global methodology (Ceglarek *et al.*, 2009b). A targeted approach is commonly adopted where the metabolites of interest are known prior to analysis and hence only a predetermined list of analytes is measured. If performed using mass spectrometry, this methodology is typically very specific and sensitive. An example of this targeted approach was the successful profile of twenty nucleotides and structural analogous from stimulated and unstimulated Chinese hamster ovary cells (Cordell *et al.*, 2008). Both the extraction and analysis were biased towards predetermined analytes. This approach is the more widely used of the two methods and, in some respects, the simpler, although the principle has drawbacks. The obvious issue is that metabolites of interest must be known prior to analysis, so the approach is not suitable for an unknown metabolic pathway. Furthermore, reference standards are commonly employed to optimize instrumental conditions. For the investigation of a gene for which the biological role is unknown, this approach is not appropriate as it would be difficult to predict which analytes to measure. Furthermore, the effects of disease or drugs can also cause a new, untargeted metabolite to be produced, which could be of biological significance but, as it is unknown, will not be observed or measured (Fiehn, 2001; Raamsdonk *et al.*, 2001; Stitt and Fernie, 2003).

The alternative methodology is a global approach, where the approach is not biased towards a specific group of analytes and the aim is to detect all the metabolites within a biological sample. Such an approach is more appropriate where it is not clear from the outset exactly which metabolites are of interest, and in this case it is common to compare a control group against an 'altered' group (Ceglarek *et al.*, 2009b). Although this approach will provide a wide picture of the metabolites present, it has the potential of missing low-level analytes due to the non-biased approach. Furthermore, this methodology has difficulties due to the potentially huge number of detected analytes and the requirements of identifying unknown compounds. To help with this issue, this approach is commonly supplemented by multivariate analysis methods, such as principle components analysis. By reducing the volume of data obtained, analytes which vary between a control and an affected can be more easily observed (Fiehn, 2001). This approach has been successfully employed in identifying metabolite variation in wild type and gene knockout plants. Using a global approach, employing gas chromatography time of flight mass spectometer (GC-TOF), $\approx$ 1000 peaks were detected from leaf extracts and $\approx$ 500 from the plants tubers, enabling comparison of metabolite levels to be undertaken by multivariate approaches (Weckwerth *et al.*, 2004). This publication highlights another limitation to this approach, namely the difficulty in identifying the considerable number of analytes detected. While spectral libraries help, and are more prominent for gas chromatography mass spectometry (GC-MS), a number of analytes could not be identified at the time consequently making links to known biological networks difficult. The use of accurate mass instrumentation for such profiling can provide information, such as an analytes empirical formula, aiding the identification of unknowns

1.2 Instrumentation for metabolite profiling

The study of endogenous metabolites can be challenging due to the diversity and sometimes the low levels of analytes of interest. A number of analytical approaches have been employed to tackle this task, commonly being highly specific or sensitive, or both. Nuclear magnetic resonance is a technique that has been employed extensively in the field of metabolomics and metabolite profiling, commonly in a global approach. Coupled

with multivariate data processing techniques, this analytical tool has been applied to the analysis of genetically modified mice modelling neurological disorders found in children (Pears *et al.*, 2005), the identification of individuals with and without coronary heart disease (Brindle *et al.*, 2002), and the source of various ginseng samples by profiling of metabolites (Kang *et al.*, 2008). Structural elucidation, as with certain types of mass spectrometry techniques, can be undertaken by nuclear magnetic resonance, enabling the approach to be a useful tool for unknowns (Skoog D *et al.*, 1998).

Various chromatography methods have also been employed extensively in the analysis of endogenous metabolites, commonly coupled to detectors such as Ultraviolet / visible light (UV/VIS) but more recently, to mass spectrometry. Capillary electrophoresis has found successful application in the analysis of nucleotides (Grob *et al.*, 2003; Lin *et al.*, 1997; Nguyen *et al.*, 1990; Oneill *et al.*, 1994). Gas chromatography (GC) and high performance liquid chromatography (HPLC) have also been used in the field of endogenous metabolites (Jhaveri *et al.*, 2006; Kondo *et al.*, 1998a; Maccarrone *et al.*, 2001; Richardson *et al.*, 2007). Mass spectrometry has also been employed extensively in this scientific field and is discussed in more detail in the following sections.

1.2.1 Mass Spectrometry

Alongside nuclear magnetic resonance, mass spectrometry has been one of the major analytical tools in the field of metabolomics, due to high specificity and sensitivity. The principles by which mass spectrometers work vary; however, the premise that all mass spectrometers adhere to is the measurement of an ion's mass to charge ratio (*m/z*) (Hoffmann, 1996). The internal workings of all mass spectrometer instruments can be can be divided into three discreet roles: the ionization of molecules of interest, the mass analyzer (an area of the instrument where analytes are discriminated by their mass to charge ratio) and the detector, which detects and reports a signal from any ions emerging from the mass analyzer. The first two will be considered in greater detail in the following sections

1.2.1.1 Ion sources

A number of ionization mechanisms have been employed in the introduction of analytes into a mass spectrometer, however, chromatography is commonly employed in conjunction with mass spectrometry in the field of metabolite profiling and hence the ion sources which bridge the gap between these two techniques are described.

Electron ionization

Electron ionization is a technique based on the bombardment of electrons onto an analyte in gaseous form, producing radical cations or anions under a vacuum. As such, this method is used extensively as an interface between gas chromatography and the mass spectrometer, commonly a single quadrupole (although GCTOF and GC-MS/MS are commercial available at this time). This ionization method is suitable for relatively small, thermally stable molecules. The use of this approach has been successfully applied to the unbiased analysis and comparison of wild type versus genetically modified *Arabidopsis* plants (Fiehn *et al.*, 2000). 326 analytes were quantified, although only half were identified using reference standards and MS libraries. A drawback to this approach is that additional derivatization steps are sometimes required to improve chromatography or analyte volatility, and this ionization technique is not suitable for large biological molecules, which can undergo complete fragmentation, resulting in few structurally significant ions. Furthermore, it is not uncommon for the molecular ion to be either fully fragmented or to be only present at very low intensities (Hoffman and Stroobant, 2005).

Atmospheric pressure ionization

The development of atmospheric pressure ionization made a huge impact in the analysis of large, thermally labile biological molecules, such as proteins as well as non-volatile small molecules from solution. Furthermore, the approach enabled the coupling of liquid chromatography with mass spectrometry, combining the advantages of both techniques (Hoffman and Stroobant, 2005). The development was so important to the field of bioanalysis that the Nobel prize was awarded to John B. Fenn for his roles in its

conception[1]. Electrospray ionization, commonly referred to as ESI, was the first of the atmospheric pressure ionization techniques to be developed. Ions are formed by elution of solvent and analytes through a capillary with a high potential voltage. Highly charged small droplets are formed and travel down a pressure and potential gradient towards the inlet of the MS (Yamashita and Fenn, 1984), see **Error! Reference source not found.**. There are two theories as to analyte ion formation. The first is that with the additional presence of an inert gas (commonly nitrogen) and temperatures between ~25 and 300 °C, droplets desolvate and subsequently reduce in size to a point where coulombic forces on the surface overcome surface tensions and the droplets breakup into smaller droplets. This mechanism continues until the solvent has completely desolvated, leaving a single ion. An alternative mechanism suggests that charged ions are repelled from the surface of the droplet by the charges on the solvent (Gaskell, 1997; Griffiths *et al.*, 2001). Ions formed are subsequently pulled into the MS by a potential gradient. The ions formed are typically the result of the addition or loss of a proton, depending on the functional groups on the molecule. Furthermore, molecules with multiple sites of protonation / deprotonation can form multiple charges; this is especially true of large biomolecules such as proteins and peptides (Hoffman and Stroobant, 2005). Therefore, the *m/z* of a protonated ion can be described as:-

$$m/z = [M + nH] / nH$$

Where *m/z* - mass to charge ration
M - mass of a molecule (amu)
nH - number of protons

However, other adducts can also form an ion with an analyte, such as sodium or NH_4^+.

Since the invention of ESI, alternative atmospheric ionization techniques have been explored that rely on some of the principles of ESI, atmospheric pressure chemical

[1] http://nobelprize.org/nobel_prizes/chemistry/laureates/2002/public.html - accessed on 15th June 2009

ionization in particular. These methods share similarities with ESI. Atmospheric pressure chemical ionization is a technique that is more typically applied to more polar compounds. As with ESI, analytes in solution elute out of a capillary under a stream of warm nitrogen to facilitate desolvation. A corona needle is present within the source at a high electrical potential. Mobile phase molecules, which are gaseous as this stage, become protonated (or otherwise charged by an adduct) due to the corona needle and subsequently pass the charge onto the gaseous analyte present (Hoffman and Stroobant, 2005).

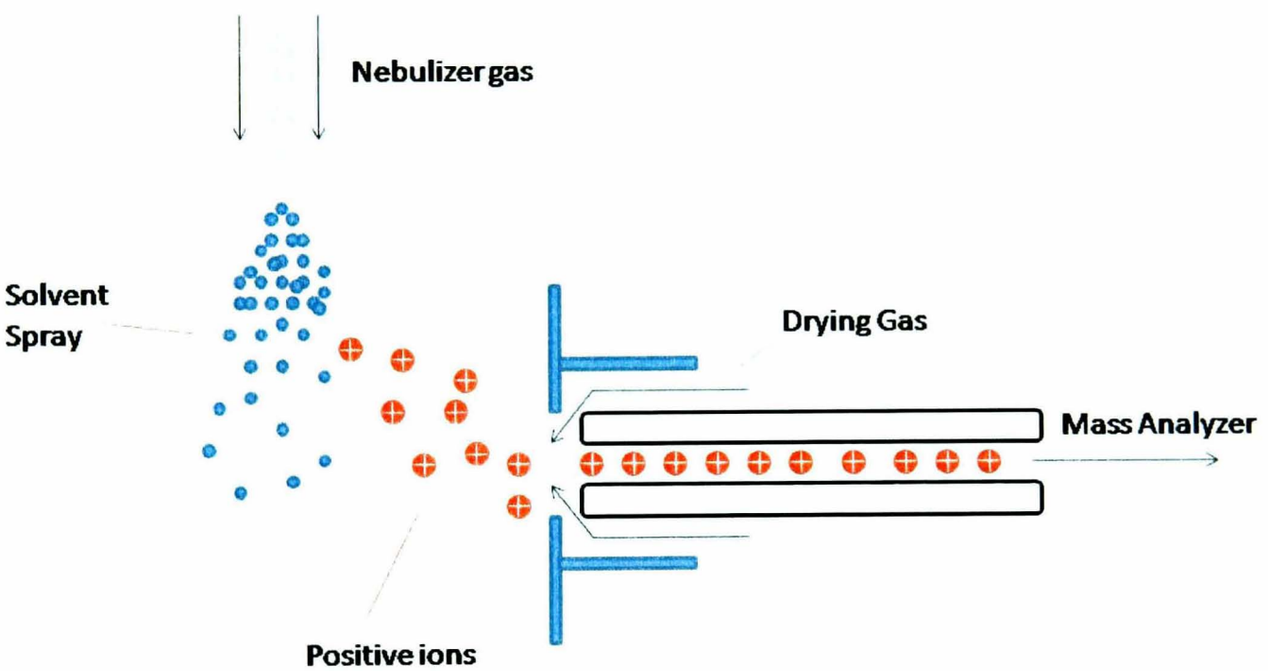

Figure 1.1. Pictorial representation of atmospheric pressure ionization forming positive ions. Reproduced from Basics of LC-MS Primer – Agilent technologies

1.2.1.2 Quadrupoles

Quadrupole mass analyzers are comprised of four parallel rods, which are either circular or hyperbolic in cross section. Each opposing rod has a RF/DC voltage applied that alternates, causing attraction and repulsion for a given charge and thereby causing it to oscillate between the rods. The voltage and frequency applied is specific for the stable flight for a given *m/z*. Ions with an alternative *m/z* have an unstable flight, causing the ion to be lost via contact with the rods. The quadrupole essentially works as a mass filter, varying the voltage and frequency of the rods so that only one *m/z* can pass through the quadrupole at a time. Unlike other mass analyzers, such as time of flight, this form of mass filter has nominal mass resolution of approximately 1 amu (Hoffman and Stroobant, 2005; Hoffmann, 1996).

A further development of this technique is the addition of a collision cell which enables the formation of product ions through collision induced dissociation (CID). This section of the instrument is typically of a quadrupole or hexapole arrangement, but only with an RF voltage applied, pulling and focusing the ions through the cell. The cell is filled with an inert gas, typically either helium or nitrogen, and ions are accelerated into the inert molecules, converting their kinetic energy into internal energy. With sufficient internal energy, bonds are broken and/or rearranged and product ions are formed. The conversion of kinetic energy into internal energy is dependent on the mass of the neutral molecule, molecular weight of the analyte, kinetic energy applied and the charge on the ion (Wells and McLuckey, 2005). The conversion of kinetic energy into internal energy for a singularly charged ion can be described as follows:-

$$E_{com} = \left(\frac{N}{m_p + N}\right) E_{Lab}$$

Where

E_{com}	=	Total available energy translated from kinetic to internal
N	=	mass of the neutral molecule
m_p	=	molecular weight of the analyte
E_{lab}	=	kinetic energy

The collision energies involved in CID within tandem quadrupoles or ion traps are commonly within 1 – 150 V. Fragmentation by this route favors an even electron ion and formation coupled with a neutral species, as described below (for a protonated species):-

$$[M + H]^+ \rightarrow A^+ + B$$

Where

$[M+H]^+$	=	protonated precursor ion
A^+	=	product ion
B	=	Neutral fragment

Ions are formed predominately by either a simple bond cleavage or a rearrangement (Sleno and Volmer, 2004) although charge remote fragmentation, where the charge on the ion is not directly responsible for the fragmentation can occur; this can be common in alkyl chains (Thomas *et al.*, 2009).

The collision cell sits between the first mass filter and a second mass filter so that pseudomolecular ions are initially selected, fragmented, and the resulting product ions identified by the second mass filter. Such an arrangement is commonly called a triple quadrupole mass spectrometer, although technically the collision cell is not always of a quadrupole design, and hence the phrase tandem quadrupole mass spectrometer has also been used to describe this MS/MS arrangement (Hoffmann, 1996).

Tandem quadrupole mass spectrometer instruments are very sensitive, selective instruments, especially when operated in multiple reaction monitoring (SRM) mode, and are commonly used in quantitative analysis. In such a mode the instrument's quadrupoles are set to allow only a specific pseudomolecular ion and the resulting product ion through

the instrument to the detector. If more than one analyte is to be monitored, the instrument skips from one mass transition to the next, rather than scan through all possible masses. Because of the selectivity and sensitivity of such an instrument run in a multiple reaction monitoring (SRM) mode, this technique has been employed extensively in the targeted analysis of metabolites (Kingsley and Marnett, 2007; Magnes C *et al.*, 2005; Richardson *et al.*, 2007; Williams *et al.*, 2007). Tandem quadrupole mass spectrometer instruments can be run in full scan mode, recording full product ion spectra; however, this is not a common approach, especially when combined with liquid chromatography, due to the constraint of comparatively slow scan speeds and the reduced sensitivity (Hoffman and Stroobant, 2005; Li A *et al.*, 2005).

Due to the nature of the tandem quadrupole mass spectrometer alignment, alternative scanning methodologies can be applied that have found a place in the analysis of drug metabolites as well as endogenous metabolites; namely, precursor ion or neutral loss scans. In either case, the quadrupoles scan through a preselected mass range and identify either a product ion or a neutral loss, which represents a core structure common to a group or family of analytes. The precursor ion scan employs the first quadrupole to scan through the mass range, the pseudomolecular ions are fragmented in the collision cell and the third quadrupole is fixed, only allowing product ions of a preselected *m/z* to pass onto the detector. The neutral loss scan is performed in a similar manner although the third quadrupole scans through the mass range but offset by a mass equivalent to the mass of the neutral sought (Hoffmann, 1996). The subsequent total ion chromatogram produced demonstrates the intensity and the pseudomolecular ion of compounds identified by this approach. However, full product ion spectra of the analyte of interest are not identified by this approach (Hoffman and Stroobant, 2005). Further confirmation of knowns or identification of unknowns would require other instrumentation to full product ion spectra or accurate mass measurements of the pseudomolecular ion.

1.2.1.3 Ion trap

Ion trap mass spectrometers can be sub-divided into 3D ion traps and 2D linear ion traps; however, they both perform a similar function when measuring analytes. Unlike a triple quadrupole instrument, where ions are filtered by their respective *m/z* as they pass through a quadrupole, ion traps store all the ions present in a region of space and subsequently expel them to measure the relative intensities of the ions present. By the nature of their operation, full product ion spectra are produced. This makes these instruments ideal for the analysis of compounds where strong confirmation of a known analyte is required or where structural elucidation is needed. Furthermore, full product ion spectra can help in the identification of unknowns (Ortori *et al.*, 2007). These instruments have been successfully employed in quantification, although 3D traps are relatively smaller than linear ion traps and can suffer from space charging effects to a greater degree (Mueller C A *et al.*, 2005). This is a phenomenon where too many ions in the trap cause a shielding effect, reducing the effect of the voltages applied to the ions in the trap (Hoffmann, 1996). Some instruments, however, have addition scan steps to limit the effects of this problem.

Ion traps have been applied to the analysis of endogenous and drug metabolites, predominantly in a targeted role (Fu *et al.*, 2007; Hansen *et al.*, 2001; Liu *et al.*, 2005; Zhang *et al.*, 2009b). Although it is stated that ion traps cannot perform precursor ion or neutral loss survey scans (Hoffman and Stroobant, 2005), it could be argued that this is not strictly true, although it is fair to say that the precursor ion or neutral loss survey scans performed only consider a relatively small number of the most intense pseudomolecular ion in any given scan. As such, the precursor ion or neutral loss capabilities of an ion trap are not as complete as a tandem quadrupole instrument Nevertheless, ions traps have been employed in the determination of endogenous and drug metabolites using precursor ion and neutral loss scans from *in vivo* samples (Rochfort *et al.*, 2008; Triolo *et al.*, 2005).

The full product ion spectra obtained from an ion trap instrument can provide greater confidence in the identification of analytes as compared to single SRM transitions

commonly used by tandem quadrupole instruments (Thomas *et al.*, 2009). As with quadrupole instruments, the mass accuracy of ion traps is classed as nominal.

1.2.1.4 Time of flight and quadrupole time of flight mass spectrometers

Time of flight instruments work on a different principle than quadrupole and ion traps and consequently offer advantages and disadvantages compared to the other techniques. Where quadrupole and ion traps instruments rely on an ion's stability within a RF/DC field to identify the *m/z*, TOF calculates an ion's *m/z* by the time it takes to travel a predetermined distance. More recent TOF instruments employ a number of features to improve mass accuracy and resolution, such as reflectors and ion pushers, but the discussion of such techniques falls outside the scope of this thesis (Hoffman and Stroobant, 2005).

An advantage of TOF instruments over quadrupole or ions traps is the increased mass accuracy and resolution, with modern instruments measuring accurately down to 5 parts per million (ppm) or better and a resolution of around 20000 full width at half maximum (FWHM)[2]. As such, known analytes can be identified with confidence and unknowns can be theorized because of the empirical formula calculated from the ions recorded *m/z*. However, it should be borne in mind that, as the mass of an analyte increases, so does the number of possible empirical formulas that match the measured *m/z*.

TOF instruments do not technically 'scan' through the *m/z* of ions, but rather collect all the ions present in a pulse, a feature which makes TOF instruments suitable for the global metabolite profiling methodology (Chan and Cai, 2008; Plumb *et al.*, 2006; Ramautar *et al.*, 2008). Because of the mode of operation, a large mass range is measured without the subsequent loss of scan speed or resolution. Furthermore, TOF instruments can be combined with a quadrupole and a collision cell, enabling not only accurate mass measurements of pseudomolecular ions but also allowing them to obtain accurate mass of

[2] Agilent 6200 TOF - http://www.chem.agilent.com/en-us/products/instruments/ms/6220accurate-masstoflcms/pages/default.aspx - accessed 16th June 2009

the resulting product ions. Such an orientation is a useful tool in the analysis of unknowns that may arise in a global metabolite profile. Using a QTOF, novel brain lipid N-acyl Taurines were identified by comparison of reference standards with those obtained from biological material (Saghatelian and Cravatt, 2005).

1.2.1.5 Orbitrap

The Orbitrap is a relatively new mass analyzer manufactured by Thermo Scientific. Ions are trapped and constrained around a central electrode and two outer electrodes. Electrostatic and centrifugal forces cause the ions to oscillate in both radial and axial directions and it is the detection of the axial oscillation frequency which enables a give ions *m/z* to be calculated. The Orbitrap has similar or slightly better mass accuracy and resolution when compared to time of flight instruments, with accuracy of < 2 parts per million (ppm) and mass resolution of up to 60000 (FWHM) (Dunn *et al.*, 2008). There is however a tradeoff between mass resolution and scan speed (Lim *et al.*, 2007). The Orbitrap has been successfully employed in quantification and compares well against a tandem quadrupole instrument, when run in relatively low resolution mode of 15000 FWHM (Zhang *et al.*, 2009a). Due to the instrument's accuracy and resolution, coupled in some cases with a linear trap, it has potential for the analysis of drug or endogenous metabolites. Consequently, the instrument has been successfully employed in the analysis of drug interactions with human liver microsomes, identifying up to 58 drug metabolites (Lim *et al.*, 2007)

1.2.2 Hybrid quadrupole linear ion trap

The hybrid quadrupole linear ion trap mass spectrometer (QqQLit) is a relatively new mass spectrometer manufactured by Applied Biosystems and sold under the commercial name of QTrap®. The configuration of the instrument is that of a tandem quadrupole mass spectrometer, but with the unique feature of converting the last quadrupole into an ion trap on demand. Scan functions common to both tandem quadrupole and ion trap instruments are possible using this instrument; however, the capability to perform

multiple scan functions one after the other has great potential for the analysis of endogenous metabolite and is not possible using a tandem quadrupole or an ion trap alone. A schematic diagram of the instrument can be found in Figure 1.2.

1.2.2.1 Scan Functions of the QqQLit

A list of the various scan functions of the QqQLit can be found in Table 1.1. A number of these functions have direct relevance to the analysis of endogenous analytes and are described in more detail.

Enhanced product ion scan

Enhanced product ion (EPI) scan is a specific term adopted by Applied Biosystems to describe a scan function which produces a full product ion spectrum from a selected pseudomolecular ion. This scan is performed by the selection of pseudomolecular ions by the first quadrupole, the fragmentation in the collision cell and the accumulation and subsequent expulsion of product ions in the third quadrupole while acting as an ion trap. Where the instrument can perform such a task while running Q3 as a standard quadrupole mass filter, scan speeds are slower (Hopfgartner *et al.*, 2004).

It should be noted that a feature of the EPI spectra scan function has an advantage over MS/MS spectra obtained in 3D or 2D linear ion traps. Product ion formation within ion traps is typically formed by the isolation of a pseudomolecular ion, followed by fragmentation and the subsequent ejection of the resulting product ions (Douglas D *et al.*, 2005). In this instance, there is a low mass cut-off in which ions less than approximately one-third of the *m/z* of the pseudomolecular ion are unstable and are lost from the trap (Hopfgartner *et al.*, 2004). This low cut-off does not apply to the QqQLit, as product ions from the pseudomolecular ion are not formed in the third quadrupole acting as an ion trap but rather in the collision cell, and the subsequent issue with stability of low mass ions below one-third of the *m/z* of the pseudomolecular ion is negated. The observation

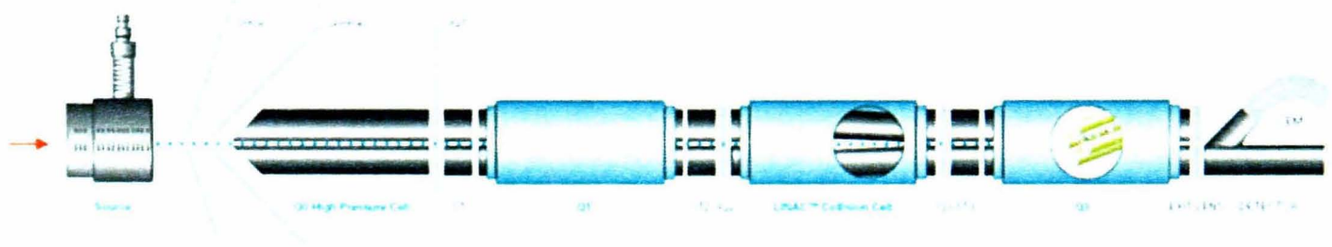

Figure 1.2. A schematic diagram of the QqQLit tandem quadrupole linear ion trap. Q1 acts as mass filters, where the collision cells either act as an ion guide, allowing the flow of pseudomolecular ions through, or cause the fragmentation of ions by the application of collision energy. Q3 can either act as a mass filter or, unique to this instrument, act as a linear ion trap, where either pseudomolecular ions or product ions can be stored and subsequently ejected. Q0 can be used as an ion store when scan functions, such as enhanced production spectra, are performed. Image obtained from QqQLit brochure[3]

[3] http://www3.appliedbiosystems.com/cms/groups/psm_marketing/documents/generaldocuments/cms_040200.pdf - accessed on 15th June 2009

Table 1.1. A list of possible scan functions of the QqQLit and the modes in which each section of the instrument is run. The capability to perform such scans, and perhaps more importantly the ability to perform a number of scans in succession makes this MS instrument a potentially useful tool in the analysis of endogenous metabolites. Scan functions were obtained from literature reference (Hopfgartner *et al.*, 2003).

Scan mode	Q1	Collision cell	Q3
Q1	Scanning	Ion guide	Ion guide
Q3	Ion guide	Ion guide	Scanning
Product ion scan	Fixed	Fragment	Scanning
Precursor ion scan	Scanning	Fragment	Fixed
Neutral loss scan	Scanning	Fragment	Scanning (with offset)
SRM	Fixed	Fragment	Fixed
Enhanced single MS (EMS)	Ion guide	Ion guide	Trap / scan
Enhanced product ion (EPI)	Fixed	Fragment	Trap / scan
MS^3	Fixed	Fragment	Isolate / fragment trap / scan
Time delayed fragmentation (TDF)	Fixed	Trap / no fragmentation	Fragment / trap / scan
Enhanced resolution (ER)	Ion guide	Ion guide	Trap / scan
Enhanced multiple charged (EMC)	Ion guide	Ion guide	Trap / scan

of low mass ions can be advantageous as they may provide structural information for the elucidation of unknowns but also as they could play a pivotal role in precursor ion scans.

Enhanced resolution scan

Enhanced resolution on the QqQLit is a useful scan function that is more applicable to the analysis of peptides than smaller molecules; nevertheless, the information provided can be of use in the analysis of small endogenous metabolites. The enhanced resolution scan collects ions within a 30 amu of the pseudomolecular ion of interest in Q3, following which a slow scan at 250 amu / sec is performed. The resolution of the scan is considerably better than that demonstrated for EPI spectra (6000 compared to 0.3 – 0.5 FWHM at 1000 amu / sec). Consequently, this slow scan enables the isotopic distribution of the pseudomolecular ions to be calculated and hence the charge state (Hopfgartner *et al.*, 2004).

The novel scan methodologies of this instrument have started to find analytical applications, although it would be fair to say the instrument has also been employed as a standard tandem quadrupole instrument in the analysis of drugs, drug metabolites and sterols (Bueno *et al.*, 2007; Coles and Kharasch, 2007; Li A *et al.*, 2005; McDonald *et al.*, 2007).

1.2.2.2 Scan combinations using information dependent acquisition

The feature of the QqQLit which sets it apart from QQQ and ion trap instruments is the capability to link a number of the scan functions in detailed Table 1.1 together on the fly. In such an orientation, the first scan is commonly in the form of survey scan, following which, if the detected analyte signal meets certain criteria (such as intensity), further scans will be initiated to provide a more targeted analysis of the analyte of interest. Four combined scan functions that have application in the analysis of endogenous and drug metabolites are set out in Table 1.2.

EMS – EPI(*n*) – MS^3

This compilation of scan methods, as described in Table 1.2, is an approach that could be employed in the analysis of endogenous analytes. The instrument is set to scan for the most intense pseudomolecular ions and an EPI spectrum is performed for each ion detected in each survey scan. MS^3 can also be performed if further elucidation of the spectra is required. This approach is limited in respect to analyte intensity. Unless the analytes of interest are the most intense in a given scan, they are not selected for EPI spectra and hence overlooked. Proficient sample clean up is therefore required to remove interfering analytes, which would otherwise cause difficulties. Alternatively, inclusion or exclusion lists can be applied, but this requires knowledge of expected analytes or interfering compounds.

Phospholipids have been investigated *in vitro* in cell cultures using the EMS – EPI(*n*) scan function. Extracted samples were analyzed by an enhanced MS scan, identifying the most prominent pseudomolecular ion and subsequently recording an EPI spectrum to add confidence in the identification (Zhao *et al.*, 2008).

SRM – EPI(*n*)

This method is a more selective approach than EMS – EPI(*n*) – MS^3. Predetermined lists of analytes are identified by both their pseudomolecular and product ion transition and an EPI spectrum is obtained for detected analytes present at levels above a specified threshold. This is a specific method producing results similar to a targeted method, using either 3D or 2D linear ion traps (Fu *et al.*, 2007; Hansen *et al.*, 2001). Drug and potential phase I and phase II drug metabolite toxicology screening methods have employed the SRM – EPI(n) method to identify known analytes of interest and to obtain greater confidence in identification than possible with SRM transitions alone (Herrin *et al.*, 2005; Li A *et al.*, 2005; Mueller C A *et al.*, 2005). This approach has also been successfully applied in the analysis of endogenous metabolites. The investigation of endocannabinoids in human plasma has been successfully undertaken by this approach, with the EPI spectra providing greater confidence in the identification of an analyte than if an SRM approach alone had been used (Thomas *et al.*, 2009).

Table 1.2. A list of scan combinations possible with the QqQLit mass spectrometer. Information obtained from recent publication of the QqQLit (Hopfgartner *et al.*, 2004).

Combination	Description	Comments
EMS – EPI(*n*) – MS^3	Screening method coupled with EPI spectra	Scans for the most intense pseudomolecular ions and produces a full product ion spectra
SRM – EPI(*n*)	Targeted SRM method coupled with EPI spectra	Identifies predetermined analytes following which full product ion spectra is obtained for confirmation
PC – ER – EPI(*n*)	Precursor ion screening method coupled with EPI spectra	Identifies analytes with a common moiety and obtains full product ion spectra for confirmation
NL – ER – EPI(*n*)	Neutral loss screening method coupled with EPI spectra	Identifies analytes with a common moiety and obtains full product ion spectra for confirmation

This approach has also been applied to the profiling of endogenous steroids in human serum for the identification of endocrine diseases by identifying imbalances of known steroids levels (Ceglarek *et al.*, 2009a).

The approach described is dependent on understanding in advance the analytes of interest and reference standards are often required for SRM transition optimization. This approach does not take into account analytes that may be present, and of biological relevance, but are not preselected for analysis, either because of a lack of reference standards or because they are unknown.

PC – ER – EPI(n) / NL – ER – EPI(n)

The coupling of precursor ion or neutral loss survey scans with an enhanced resolution scan, followed by an EPI scan, is an alternative approach to either the global or targeted metabolite profiling approaches. Rather than a targeted methodology, this approach identifies analogous analytes that have a similar structural moiety that form either an ion or a neutral under collision-induced dissociation. As such, a full quota of reference standards is not required, although an understanding of the fragmentation is necessary (Hopfgartner *et al.*, 2004). The use of precursor ion or neutral loss scans for the identification of analytes is a common approach for tandem quadrupole instruments (Hoffman and Stroobant, 2005; Hoffmann, 1996). The drawback to performing precursor ion or neutral loss survey scans on traditional tandem quadrupole instruments is the lack of information gleaned regarding the analytes of interest, specifically product ions. The QqQLit, however, enables a combined scan of both precursor ion / neutral loss survey scans and EPI spectra, providing greater confidence in analyte identification and also helping identify unknowns.

The methodology of precursor ion scans coupled with EPI spectra has found successful application in the analysis of endogenous metabolites. Endogenous long chain fatty Acyl-CoAs have been studied by the neutral loss scanning of 507 daltons, targeting the adenine diphosphate moiety. Subsequent identification was obtained from the EPI spectrum (Magnes C *et al.*, 2005). N-acylhomoserine lactones, quorum sensing

molecules employed by bacteria Yersinia pseudotuberculosis to determine population density, have been investigated by this approach (Ortori *et al.*, 2007). Furthermore, this approach has been employed to identify sphingolipids in cell cultures. By the use of three precursor ion scans, sphingolipids and sphingolipids subspecies were identified and an SRM method was developed to quantify the analytes detected (Shaner *et al.*, 2008).

1.2.3 Application of QqQLIT technology to metabolite profiling

The PC – ER – EPI(n) / NL – ER – EPI(n) methods sits in-between the two common approaches for metabolite profiling. Consequently, it is not as stringent as the targeted methodology, which only identifies preselected analytes and, conversely, it is not as broad as the global methodology, targeting families of metabolites rather than all detectable analytes. Targeted approaches, commonly employing SRM scans, often require a full range of references standards for each analyte to be analyzed. Where commercially available or in house synthesis is possible, such methods can be developed. However, if such reference standards are not easily available it can limit the scope of analysis, usually to the analytes where such standards are commercially available and ignoring potentially biologically relevant metabolites (Fiehn, 2008). Furthermore, targeted approaches can make the assumption that all the relevant metabolites of a given biological process are known. This may not be the case and potentially important metabolites could be overlooked. Conversely, global approaches do not generally make an assumption of the analytes present in the matrix; hence there is not a bias towards any particular analytes. However, in cases where a broad class of compounds are of interests such as lipids, there may be some bias towards this group as a whole. Nevertheless, when attempting to identify as many analytes as possible, low level analytes could be missed, especially where instrumental settings are not specifically optimized. Furthermore, global approaches collate a considerable volume of data which often requires complicated analysis, typically with multivariate approaches (Fiehn, 2001).

By targeting a core structural similarity of endogenous metabolites, this approach has the potential to identify families of metabolites, both known and unknown analogues.

Although reference standards are required for initial instrumental optimization and to gleam an understanding of the fragmentation patterns of a given class of analytes, a full complement of standards are not required unlike the targeted approach. Additionally, it is not assumed that all the analytes are known prior to analysis, with the possibility of identifying previously unknown analytes or for compounds where reference standards are not readily available.

There is an inherent bias in this approach, both for instrumental setting but also chromatography (if performed). This is potentially advantageous for those analytes which are present at low levels and require such steps for successful analysis. Where it has been previously been noted that global methodologies using GC-MS observe a large number of analytes of which only a subsection are identified (Fiehn, 2008; Weckwerth *et al.*, 2004). The more focused approach of identifying families of metabolites may allow the job of identifying unknowns easier. Furthermore, the volume of data obtain by this approach will not be as great as global methodologies and would not require complicated data processing, although this could be applied if required. Hence, there is potential to apply the novel scanning modes available in a QqQLIT mass spectrometer to provide an alternative approach to metabolite profiling.

1.2.4 Aims of the thesis

- To evaluate and optimise QqQLIT mass spectrometry for profiling of endogenous metabolites that consist of structural analogues or have a core structural moiety
- To develop a method for the analysis of phosphate-containing metabolite families focused on a precursor ion or neutral loss survey scan coupled with EPI spectra and application of the method to mammalian and bacterial samples.
- To develop and apply the QqQLIT profiling approach to two families of bioactive lipid molecules (N-acylethanolamines and mono-acylgycerols) and to assess the methods capabilities for endogenous metabolite profiling in rat tissues.

CHAPTER 2

2 Use of Hybrid Quadrupole Linear Ion Trap Mass Spectrometry for Profiling of Phosphate Containing Metabolites

2.1 Introduction

Phosphate containing metabolites, including the nucleotide family and related biological compounds, were initially selected to assess the capabilities of the hybrid quadrupole-linear ion trap (QqQLit) in detecting and profiling endogenous metabolites. Nucleotides are relatively small molecules with a molecular weight of less than 600 Da. The structure of this family can be broken down into three constituent groups: a base, the most common being adenine, cytidine, guanine, uracil, and thymine). Bases are attached to a five carbon sugar, either ribose or 2'- deoxyribose (deoxyribose lack an OH groups from the 2' - carbon), forming a nucleoside (thymine is commonly attached to a deoxyribose). The addition of one to three phosphate groups to the ribose sugar via an ester linkage, commonly at the 5 position (although linkages at 2 and 3 are also known), forms a nucleotide (Mathews *et al.*, 1998; Stryer, 1999). Typical structures can be found in Figure 2.1

Within biological systems, the role of nucleotides is varied. Monophosphate nucleotide polymers form the base of deoxyribonucleic acid (DNA) and ribonucleic acid (RNA). Adenosine triphosphate (ATP) is commonly used in the cell as a source of energy, although guanine triphosphate (GTP) can also play this role (Stryer, 1999). Cyclic adenosine monphosphate (cAMP) has a role as secondary messenger, affecting metabolism within a cell and is found in both pro- and eukaryotic cells (Antoni, 2000). Uracil diphosphate (UDP) has the role of carrying glucose, forming UDP glucose, an intermediate in the production of the glucose polymer glycogen, an important store of chemical energy (Mathews *et al.*, 1998).

Other endogenous molecules synthesized from adenine nucleotides such as nicotinamide adenine dinucleotide (NAD^+), nicotinamide adenine dinucleotide phosphate ($NADP^+$) and flavin adenine dinucleotide (FAD) are structurally similar to nucleotides (Stryer, 1999). These molecules contain a base and a ribose sugar in addition to two phosphate groups and act as co-enzymes, predominantly in oxidation reactions (in the case of NAD^+ and FAD) or reduction (in the case of $NADP^+$) (Mathews *et al.*, 1998). Acetyl CoA, an important precursor in the production of fatty acids palmitate, has ADP as a core part of the structure (Mathews *et al.*, 1998).

2.1.1 Nucleotide extraction methods

A number of sample preparation methods have been successfully applied to the extraction of nucleotides from both prokaryotic and eucaryotic cells. Acidic extractions have been demonstrated to be successful as a method for the removal of proteins from a sample matrix (Polson *et al.*, 2003) by precipitation. Acetic acid followed by filtering of debris was applied in the extraction of triphosphates from *Escherichia coli MG1655* cells (Nazar *et al.*, 1970). It is worth noting that extraction was approximately five times more efficient with the additional freeze thaw stage prior to acid extraction, aiding in cell lysis. Trichloroacetic acid followed by neutralization using sodium hydroxide was applied to the extraction of nucleotide from fish tissue. In this instance, a phosphate buffer was also used to control pH; however, this buffer is not compatible with electrospray ionisation (ESI), as it can cause ion suppression (Nguyen *et al.*, 1990). Trichloroacetic acid has also been applied in the extraction of nucleotide in human plasma (Lin *et al.*, 1997). However trifloroacetic acid has been compared against trichloroacetic acid and formic acid for nucleotide recoveries from *Escherichia coli MG1655* cells and was found to perform slightly better. Again, a neutralization step was required (Dutta and O'Donovan, 1987). Alternatively, perchloric acid has been successfully used in the extraction from cell cultures (Oneill *et al.*, 1994), however it has been reported to leave a precipitate once neutralized and dried down, which is incompatible with LC-MS (Cordell *et al.*, 2008). Nevertheless, the

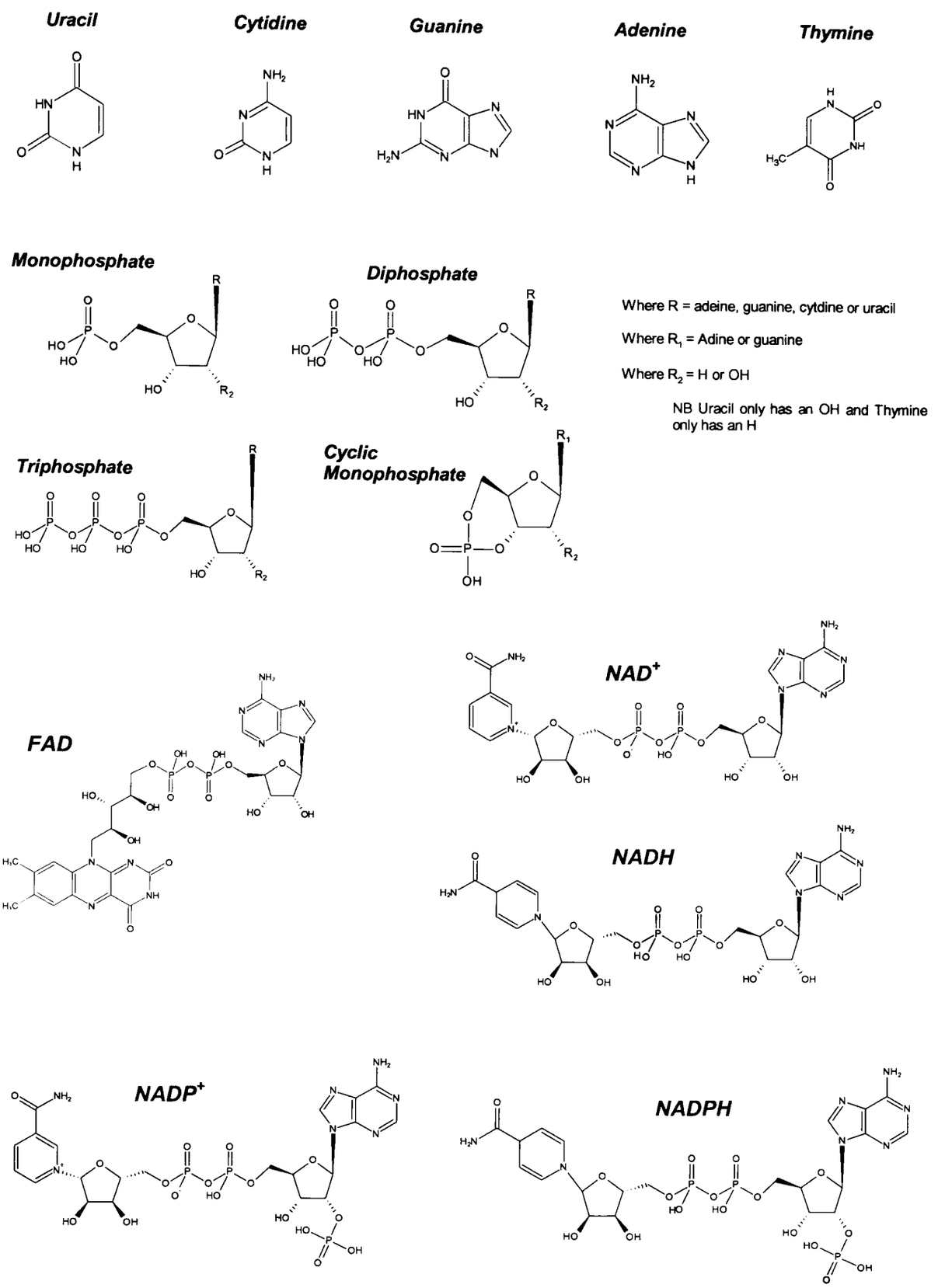

Figure 2.1. Structure of nucleotides and other phosphate – based containing compounds.

analysis of nucleotides by LC-MS has been successfully accomplished with use of perchloric acid as an extractant from plant and mammalian cells (Cai *et al.*, 2002; Richards *et al.*, 2002). The disadvantage of the use of acid extraction is the requirement for a further neutralization step and the potential degradation due to the low pH.

Organic solvents have also been used in the extraction of nucleotides and, where they have been demonstrated to precipitate proteins, they do not need the additional step of neutralization. A comparative study of organic and acid extraction methods was assessed on African green monkey kidney cells. Using trichloroacetic acid (5 and 10%), perchloric acid and methanol, it was reported that methanol gave the highest recoveries - approximately 2-4 times greater than perchloric acid (which gave better results than either trichloroacetic acid extractions), although the authors admit the increase in recoveries could be due to the speed at which the organic extraction took place compared to the acid extractions (Loregian et al., 1994). Acetonitrile and ethanol have also been demonstrated to work as extract solvents for nucleotides (Grob *et al.*, 2003) and the use of hexane following a methanol extraction has been shown to improve peak shapes by the subsequent removal of the endogenous phospholipids (Cordell *et al.*, 2008).

2.1.2 Methods of nucleotide analysis

The analysis of nucleotides has been undertaken by a variety of approaches, although the majority have been focused on separation by chromatography techniques, typically high performance liquid chromatography using anion exchange, reversed phase or ion pair modes (Werner, 1993). The chromatographic techniques have been coupled predominantly with UV as a tool for identification, although more recently mass spectrometry has also been employed due to greater specificity and sensitivity (Cordell et al., 2008).

2.1.2.1 Nucleotide analysis by capillary electrophoresis

Capillary electrophoresis is an established separation technique and is advantageous compared to HPLC due to the small sample volumes required (Ng et al., 1992). This

approach has been employed in a number of nucleotide assays. The analysis of adenine, guanine, uracil and cytidine mono-, di- and triphosphates in mouse lymphona cells using capillary electrophoresis coupled with a UV detector has been reported (Grob et al., 2003). Nucleotides AMP and GMP along with their respective nucleosides, have been successfully analyzed in human plasma using capillary electrophoresis coupled with an amperometric detector (Lin et al., 1997). Mono-, di- and triphosphates have also been identified in hybridoma cells using capillary electrophoresis (Oneill et al., 1994) and capillary electrophoresis was employed in comparing nucleotide extraction methods from mouse lymphoma cells (Grob et al., 2003). A drawback to capillary electrophoresis can be limited sensitivity compared to HPLC (Grob et al., 2003) and its difficulty with connecting to MS.

2.1.2.2 High performance liquid chromatography

The use of HPLC has been extensive in the analysis of nucleotides. Early methods used ion exchange chromatography as a tool in the separation of these endogenous analytes. Mouse fibroblast cells and rat liver were successfully investigated for the presence of ribose and deoxyriboes nucleotides by the use of an anion exchange column for the fractionation of nucleotides, followed by reversed phase chromatography (Maybaum et al., 1980). Triphosphate nucleotides have been investigated in bacterial samples of *Escherichia coli Luria strain B* and *Pseudomonas aeruginosa* using an anion exchange column coupled with UV detection (Dutta and O'Donovan, 1987). Anion exchange chromatography was again employed in the analysis of triphosphate nucleotides, but in eucaryotic monkey kidney cells (Loregian et al., 1994). A slightly wider group of nucleotides were analyzed using anion exchange coupled with reverse phase chromatography in fibroblast cells. Uracil, cytidine and thymine deoxyribose and ribose mono-, di- and triphosphates were successfully detected by this method, although the use of two separation techniques is time consuming (Maybaum et al., 1980).

A feature of ion exchange chromatography is elution of salts, which are required to displace analytes retained in the stationary phase. Such salts are less than ideal if MS is

to replace less specific techniques, such as UV (Tuytten et al., 2002). An alternative to ion exchange chromatography is the use of ion pairing agents, which, when added to the mobile phase, aid in the separation of polar analytes by helping with retention in the hydrophobic stationary phase without the elution of strong concentrations of salts (Snyder et al., 1997). The use of ion pair reversed phase chromatography has become the preferred method of nucleotide separation (Werner, 1993) and has been successfully used in the analysis of adenine monophosphate (AMP), adenine diphosphate (ADP) and ATP from myocard tissue (Ingebretsen et al., 1982) and in the analysis of adenine and guaranine mono-, di- and triphosphates, as well as of inosine monophosphate from small intestine mucosa (Tikhonov Yu et al., 1990). In both those instances, UV was used as the detector. However, not all ion pairing agents are compatible with mass spectrometry, particularly those based on a quaternary ammonium structure such as tetrabutylammonium phosphate and tetraethylbutylammonium phosphate as they are non volatile (Cai *et al.*, 2002; Luo *et al.*, 2007). Nevertheless, volatile ion pairing agents such as N,N-dimethylhexylamine (DMHA) are available have been successfully employed in the separation and analysis of nucleotides by reversed phase HPLC and mass spectrometry (Cai *et al.*, 2002; Cordell *et al.*, 2008; Tuytten *et al.*, 2002).

2.1.2.3 LC-MS

The coupling of MS to HPLC has a number of advantages over the use of UV detection that can aid in the analysis of these compounds. The number of possible nucleotides, the range of endogenous concentrations (mM to below nM) and the endogenous background matrix have all made the analysis of a large number of nucleotides by UV detection challenging (Maybaum et al., 1980). MS, however, with increased selectivity and sensitivity is better suited to the analysis of these analytes.

HPLC with the addition of an ion paring agent has been coupled with quadrupole time of flight (QTOF) in the analysis of ATP and GTP (both reoxyribose and ribose sugars) from glioma cells (Cai et al., 2002). LC-MS/MS have also been employed in the selective analysis of AMP, GMP, cyclic adenine monophosphate (cAMP) and cyclic guanosin

monophosphate (cGMP), (Witters et al., 1996) in addition to the identification of deoxyribose triphosphates from blood (Hennere et al., 2003). Ion traps have been used in conjunction with HPLC in the targeted analysis of NAD^+ in eukaryotic cells (Evans et al., 2002), and in the analysis of cyclic monophosphates in tobacco plant cells (Richards et al., 2002)

Despite the advantages of LC-MS few methods have widened the range of possible nucleotide analytes. A method for the simultaneous analysis of mono-, di- and triphosphates of the bases adenine, gurnine, cyticine and uracil was developed (Tuytten et al., 2002). This assay targeted a greater number of nucleotides than most other methods published previously, but did not include deoxyribose nucleotides or cyclic nucleotides such as cAMP and cGMP. Another methodologies have increased the number of nucleotides identified even further to include the cyclic nucleotides and co-factors such as NAD^+, $NADP^+$, FMN and FAD, but again the deoxyribose nucleotides were not included in the targeted analysis (Cordell et al., 2008).

2.1.2.4 An alternative approach to MS nucleotide analysis

An issue with the targeted LC-MS approaches is that although highly selective and specific, there is an inherent reliance on reference standards for the optimum tuning of the instrument and selective reaction monitoring (SRM) transition selection. Consequently, only analytes preselected are identified. The possibility of employing the QqQLit to undertake survey scans, such as precursor ion or neutral loss, to target a core structural similarity present in families of endogenous metabolites leads to an approach less reliant on reference standards and enables, in theory, the identification of all analytes with the selected core structure. This includes unknowns which would be overlooked by a targeted method but could be biologically relevant. With full product ion spectra for each analyte confident identification of known analytes and identification of unknowns is possible.

In the case of phosphate containing endogenous metabolites, in particularly nucleotides, a precursor ion scan can be employed to target the resulting phosphate ion $[PO_3]^-$ formed the under collision induced dissociation (CID). With the addition of an enhanced resolution scan to more accurately identify the pseudomolecular ion and its charge state, coupled with an EPI scan to obtained full product ion spectra, the method will be able to identify nucleotides by the pseudomolecular ion and product ion spectra. Furthermore, analytes for which reference standards are not immediately available may be tentatively identified by an understanding of the product ion spectrum. This approach, although it requires reference standards to initially understand nucleotide CID fragmentation patterns and optimize MS parameters such as collision energies and declustering potentials, is not as targeted as a SRM methods. The approach has the potential to identify any analyte which forms a $[PO_3]^-$ under CID conditions. This not only includes nucleotides and structural analogous but endogenous metabolites such as phosphorlated carbohydrates, sugar nucleotides, and glycerophospholipids.

2.1.3 Aims

The aims of this chapter are as follows:

- To develop a method for the analysis of nucleotides based around the identification of a core structure present in all nucleotides.
- To assess the methodology for the analysis of nucleotides in biological materials.

2.2 Methods

2.2.1 Chemicals

All nucleotide standards AMP, ADP, ATP, cAMP, GMP, GDP, GTP, cGMP, UMP, UDP, UTP, CMP, CDP, CTP, NAD^+, NADH, $NADP^+$, NADPH, FAD (see Figure 2.1) and 8-bromoadenosine 3′,5′- cyclic monophosphate (employed as an internal standard) were purchased from Sigma Aldrich (Poole, UK). N,N-dimethylhexylamine (DMHA) and acetic acid were purchased from Acros Organics (Geel, Belgium). Methanol (HPLC grade) was purchased from Fisher (Loughborough, UK). Water was filtered through a Milli-Q system (18.2 mΩ) and all mobile phases were filtered through a 0.47 μm nylon filter (Watman, Maidstone, UK) before use.

2.2.2 Liquid chromatography equipment and conditions

Chromatography was carried out on a Shimadzu series 10AD μVP liquid chromatography system equipped with binary pumps, a vacuum degasser and a SILHTc autosampler and column oven (Shimadzu, Columbia, MD, USA).

The liquid chromatography method was based on work carried out by Dr. Rebecca Cordell (Cordell et al., 2008), a former PhD in the School of Pharmacy, Nottingham University, but subsequently adjusted by Monika Huszar, a PhD student visiting the laboratory on an Erasmus scheme. All separations were conducted on a Waters Symmetry (C18 150 x 2.1 mm; 3.5 μm particle size) column with a flow rate of 0.2 mL/min gradient elution mobile phase consisting of A (95% water, 5% methanol and 5 mM DHMA, adjusted to pH7 with acetic acid) and B (20% water, 80% methanol and 5 mM DHMA). The gradient started at 0% B, increasing to 53% B after 15 min; this was maintained for 7 min following which %B was reduced to 0 after 3 min and the column re-equilibrated at 0% B for 5 min. Column temperature was maintained at 40°C and sample temperature was maintained at 4°C in the autosampler during analysis. Injection

volume was 10 µL. DHMA was employed as an ion pairing agent to improve retention of polar nucleotides on a reverse phase column

2.2.3 Mass spectrometry equipment and development

All MS experiments were conducted on a 4000 QTrap® hybrid triple-quadruple–linear ion trap mass spectrometer (Applied Biosystem, Foster City, CA, USA) equipped with a TurboIon source used in ESI⁻. A Windows XP (Microsoft, Redmond, WA, USA) workstation running Analyst (version 1.4.1) was used for data acquisition and processing.

2.2.3.1 Initial instrumental tuning for nucleotide analysis

Tuning of the instrument was conducted by direct infusion of nucleotide standards at a concentration of 10 µM in ESI-. The optimum source temperature was set at 300 oC, N2 gas flow at 20 mL/min, N2 curtain gas at 25 mL/min and the ion spray voltage at -4200 V.

2.2.3.2 Development of a precursor ion survey scan coupled with enhanced resolution and enhanced product ion spectra

The MS method developed for the detection of nucleotides comprised a number of scans that ran sequentially. Initial identification of nucleotides was performed by a precursor ion scan, following by an enhanced resolution scan which performed a more accurate scan of the target pseudomolecular ion. Information-dependant acquisition selected (or deselected) the target ion according to a set criteria, following which an EPI scan was performed to obtain the full product ion spectra of the target ion. A flow diagram depicting the various scan functions and conditions optimized for the precursor ion scan used to investigate nucleotides can be found in Figure 2.2.

Precursor ion scan

The precursor ion survey scan method was initially developed by direct infusion of reference standards and obtaining full product ion spectra under CID in ESI⁻. Following the identification of a product ion common to all nucleotides, a phosphate

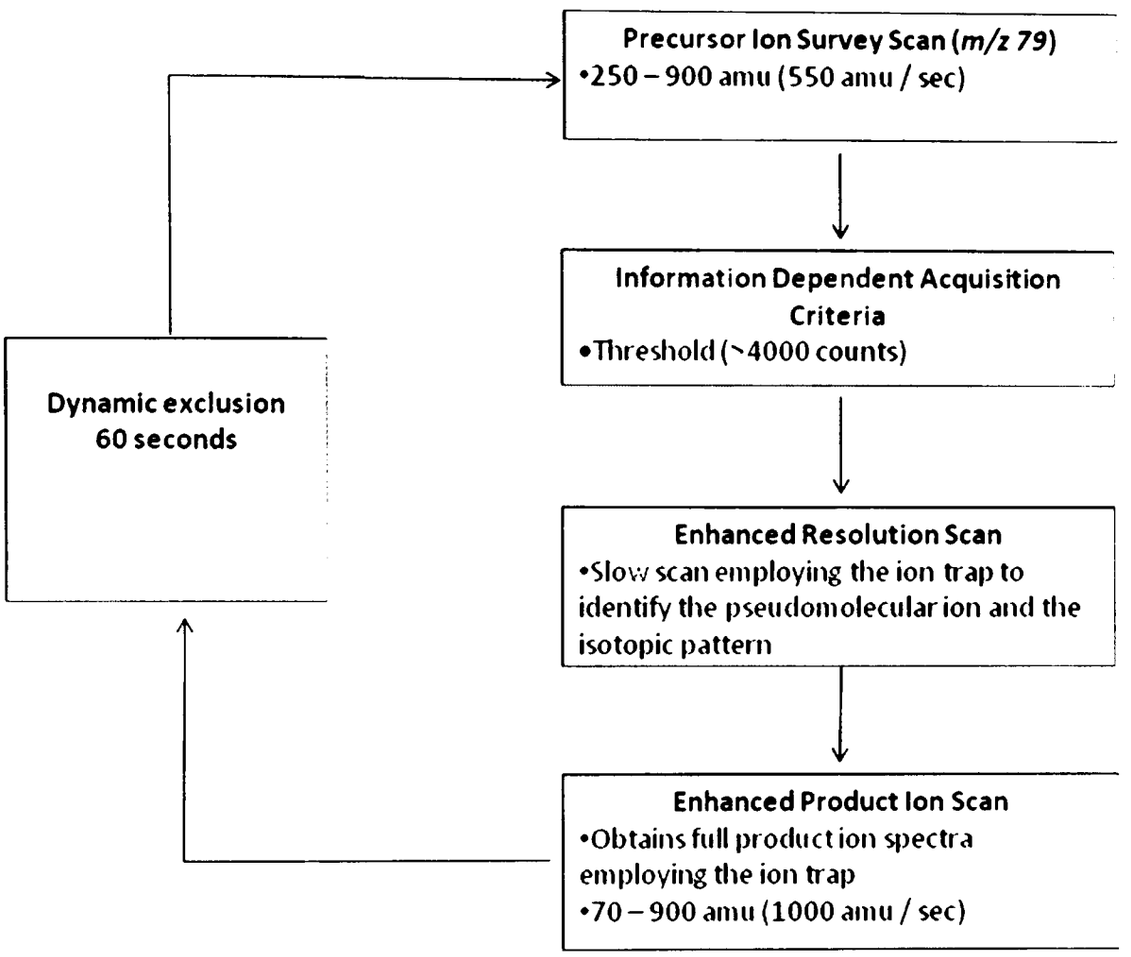

Figure 2.2. A flow diagram demonstrating the various scan functions involved in precursor ion survey scan used for the analysis of nucleotides.

moiety *m/z* 79, an optimum collision energy and declustering potential of -80 and -80 V, suitable for all analytes, was selected.

The mass accuracy of the precursor ion survey scan was assessed to evaluate whether an enhanced resolution scan was necessary. Precursor ion scan speeds of 275, 550 and 1100 amu / sec were employed to measure the mass of the nucleotide reference standards (10 μM, n=6). Furthermore, the precision of the precursor scans, run at increasing scan speeds, was assessed on reference standards (10μM, n=6). Two methods comprised of precursor ion scans of 500 and 1000 amu /sec coupled with an EPI scan at 1000 amu / sec, resulting in total cycle times of 2.4 and 2.04 sec respectively. The third method had a precursor ion scan of 1000 amu /sec but an EPI scan speed of 4000 amu / sec, resulting in a total cycle time of 1.4 sec. The extracted ion chromatograms from each reference standard were plotted and the peak areas calculated. The scan speed of 500 amu/sec was subsequently chosen for all analysis on the basis of mass accuracy, see Table 2.1.

Information independent acquisition

Inclusion and exclusion lists were not employed and the cut off, by which ions exceeding a specific number of counts caused the instrument to perform an EPI spectra, was set at 4000 counts. Former target ions were excluded for 60 sec.

Enhanced resolution

The enhanced resolution scan parameters were not adjusted from those preselected and optimised by the software. The scan rate was 250 amu / sec with a linear ion trap fill time of 20 msec. At this scan speed the resolution will be in the order of 6000 FWHM and capable of accurately identifying the pseudomolecular ion and charge state.

Enhanced product ion scan

Following the precursor ion scan and enhanced resolution scan, an EPI scan was attached to the method to obtain full product ion spectra from analytes identified by the precursor ion scan to containing a phosphate moiety (denoted by a product ion of *m/z* 79). EPI scan is a specific term adopted by Applied Biosystems to describe a scan function which

produces a full product ion spectrum by the selection of pseudomolecular ions by the first quadrupole, the fragmentation in the collision cell and the accumulation and subsequent ejection of product ions out of the third quadrupole while acting as an ion trap (Hopfgartner et al., 2004).

A collision energy for the EPI scan was required that would produce structurally significant product ions for a range of analytes. Unlike an SRM experiment, one collision energy is allowed for the EPI scan and must be acceptable, as far as that is possible, for all analytes expected. However, a spread of that collision energy is possible to increase range of product ions formed. To this end reference standards (10 μM) were infused directly into the ESI source, the collision energy ramped and the full product ion spectra collected. Taking all reference standards into account, a compromise of -30 ± 20 V was selected which, for the most part, demonstrated the structurally significant product ions for each analyte. The EPI scan mass range was from 70 to 900 amu and scanned at a speed of 1000 amu / sec and a fixed ion trap fill time of 100 ms was selected.

2.2.3.3 Development of an SRM method

To evaluate the extraction methods (see 2.2.5), a sensitive and specific assay was developed using a specific targeted SRM scan. Reference standards (see Table 2.3) were infused at a concentration of 10 μM and ions formed in ESI^-. The automated SRM development software was used to optimize declustering potential, collision energy and optimum product ion fragment for each analyte. The most intense parent ion for each analyte, the deprotonated pseudomolecular ion $[M-H]^-$, was selected as the precursor for each analyte and the most abundant product ion was chosen as the transition ion. A dwell time of 15 msec was chosen for each SRM transition. 8-bromoadenosine 3′,5′-cyclic monophosphate was used as an internal standard, as successfully applied previously (Cordell et al., 2008).

2.2.4 Application on biological samples

To evaluate the capabilities of the QqQLit for the analysis of nucleotides, bacteria were selected as the biological source because of the ease in production. *Pseudomonas aeruginosa* PA01 and *Escherichia coli* MG1655 were available and kindly supplied by Nigel Halliday, Institute of Infection, Immunity and Inflammation, Medical School, University of Nottingham. Sample preparation was as follows:

Escherichia coli MG1655 was grown on agar medium and stored at -80°C until ready to be used. A colony was removed and placed in LB growth medium overnight, following which three 1:1000 dilutions were made of the overnight culture in LB growth medium. These cultures were grown for a further five hours, the optical densities measured (650 nm) as a gauge of cell growth and resulting broths pooled. 5.0 ml of bacterial culture were rapidly drawn up into a 20 ml syringe containing 15 ml of precooled (-20°C) quenching fluid (70 mM HEPES solution in 60% (v/v) methanol, pH adjusted to 7 with aqueous sodium hydroxide) and mixed. The suspension was centrifuged for 10 min, 10,000 g at -20°C and the supernatant discarded. PBS (5ml) was added and then vortexed. The suspension was then spun down for 10 min at 10,000 g at -20°C, the supernatant discarded and the cell pellet stored at -80°C until extracted.

Pseudomonas aeruginosa PA01 was grown as a batch culture in Nutrient Yeast Broth. (Nutrient broth No.2 25.0 g/l, yeast extract 5.0 g/l), at 37 °C on an orbital shaker at 200 r.p.m. Cell density (OD_{600nm}) was determined using a Thermo Scientific Biomate 3 spectrophotometer measuring at a wavelength of 600 nm.

At a cell density of $OD_{600nm} \approx 2.0$, samples were harvested by rapid addition and mixing of 5 ml of the bacterial culture into 15 ml of ice cold 0.9% (w/v) sodium chloride. A volume of the quenched culture, equivalent to 2.5 ml of a culture with $OD_{600}=1.0$, was pelleted by centrifugation (5 min, 5 000 r.c.f., at -5 °C), to produce a standard size cell pellet. Once the supernatant was discarded, cell pellets were washed by resuspending in a 10 ml aliquot of the ice cold saline solution, and pelleted again by centrifugation (5 min,

5 000 r.c.f., at -5 °C). After discarding the supernatant the cell pellets were stored at -80 °C until metabolite extraction was carried out.

2.2.5 Extraction method selection

A number of approaches have been used in recent years for the extraction of nucleotides. Acid extractions have been employed numerous times, including perchloric acid, trifluoroacetic acid, tricloroacetic acid and acetic acid however degradation of nucleotides has been noted (Grob *et al.*, 2003; Nazar *et al.*, 1970). Solvent extractions, which do not require a neutralization step, have also been demonstrated to work (Loregian et al., 1994). Hence, the optimum extraction method was investigated a little further. Three methods, based on those previously described in the literature (Cordell *et al.*, 2008; Dutta and O'Donovan, 1987; Grob *et al.*, 2003; Nazar *et al.*, 1970; Ng *et al.*, 1992), were assessed on the basis of precision and recovery of nucleotide reference standard peak areas (10μM, n=6) using an SRM method developed. The methods were based on an acid extraction, acid extraction followed by neutralization and an organic extraction using methanol and hexane. The acidic extraction employed acetic acid rather than other acids, such as perchloric, which has been noted to leave insoluble precipitate post-neutralization which can causes losses due to adsorption (Cordell *et al.*, 2008; Perrett *et al.*, 1989) and can give poorer yields (Nazar et al., 1970). The most successful of the three methods was then assessed for reproducibility of endogenous nucleotides determined in *Pseudomonas aeruginosa* bacterial extracts. Extraction methods were as follows:

Acetic acid extraction method

500 μL of aqueous acetic acid (1 M) stored at -20°C was added to the cell pellet along with 8 – Bromoadenosine 3', 5' – cyclic monophosphate (acting as an internal standard). (100 μl of 10 μM solution). Samples were homogenized, following which two freeze thaw cycles were performed using liquid nitrogen twice (mixed between each stage). The resulting solution was spun down (-5°C) and the supernatant removed to a clean tube.

Samples were evaporated to dryness using a rotory evaporation and stored at -80°C until ready for analysis. Extracts were reconstituted in 50 µl mobile phase A prior to analysis.

Acetic acid & sodium hydroxide method

The same procedure as for the acetic acid extraction was followed, except for the addition of 500 µl of 1M sodium hydroxide to the recovered supernatant to provide an expected pH 7 (ratio of acid to base was measure using a pH meter on acetic acid and sodium hydroxide alone).

Organic solvent extraction method

500 µL methanol:H_2O (1:1) stored at -20°C was added to the cell pellet along with 8 – Bromoadenosine 3', 5' – cyclic monophosphate (acting as an internal standard) (100 µl of 10 µM solution). Samples were homogenized, following which two freeze thaw cycles were performed using liquid nitrogen. The resulting solution was spun down (-5°C) supernatant removed. Ice-cold hexane (1 mL) was added to the supernatant and the solution mixed and again spun down for 5 min (-5°C). The methanol / aqueous layer was removed and stored at -80°C until ready for analysis. Extracts were reconstituted in 50 µl mobile phase A prior to analysis.

All standards and biological samples/extracts were kept in ice when not being physically handled.

The evaluation of the extraction methods was conducted in collaboration with Monika Huszar, a PhD student visiting the laboratory on an Erasmus scheme from Hungary.

2.3 Results and discussion

2.3.1 Survey scan ion selection

Nucleotide reference standards were infused in ESI^- ion and product ion spectra examined for common structural fragments with the potential of being a marker for nucleotides or structural analogues. The instrument was run in ESI^- rather than ESI^+ because of the better overall signal. Nucleotides in ESI^+ have been observed to form $[M+Na]^+$ and $[M + N,N\text{-}DMHA + H]^+$ (when employing DHMA as an ion pairing agent) adducts (Cai *et al.*, 2002; Witters *et al.*, 1996), which essentially dilute the signal strength of the analyte of interest, whereas in ESI^-mode only the $[M-H]^-$ pseudomolecular ion has been reported to be formed (Tuytten et al., 2002).

It was observed that all reference standards fragmented under CID generate a *m/z* 79 $[PO_3]^-$ and a *m/z* 97 $[PO_4H_2]^-$ product ion; see Figure 2.3. Such fragments have been previously reported in monophosphates, diphosphates and cyclic cytidine monophosphate (cCMP), cyclic guanosine monophosphate (cGMP), and cyclic adenosine monophosphate (cAMP) and used as transitions for SRM experiments (Cordell *et al.*, 2008; Tuytten *et al.*, 2002; Witters *et al.*, 1996). In an effort to select the more appropriate of these two ions for a precursor ion scan, the profile of intensity against collision energy was plotted (see Figure 2.4; in this instance only the triphosphates have been plotted for the sake of clarity). It was observed that of the two product ions, *m/z* 79 generated a more intense signal for all mono, di and triphosphates reference standards. As this would result in greater sensitivity, *m/z* 79 was chosen as the signature product ion for the precursor ion scan.

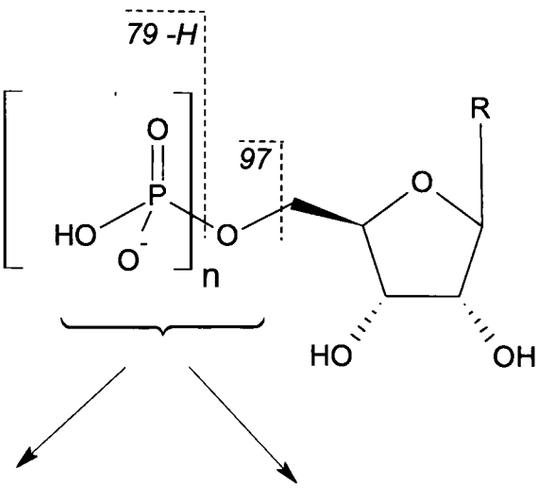

Molecular Formula	= O_3P	Molecular Formula	= H_2O_4P
Monoisotopic Mass	= 79 Da	Monoisotopic Mass	= 97 Da

Where R = Nucleotide base

n = Number of phosphate groups, 1 to 3

Figure 2.3 Common product ions observed under CID for all nucleotide (and structural analog) reference standards. The ion of *m/z* 79 has previously been assigned in mono and di phosphates as well as cAMP, cCMP, cGMP (Cordell *et al.*, 2008; Tuytten *et al.*, 2002; Witters *et al.*, 1996)

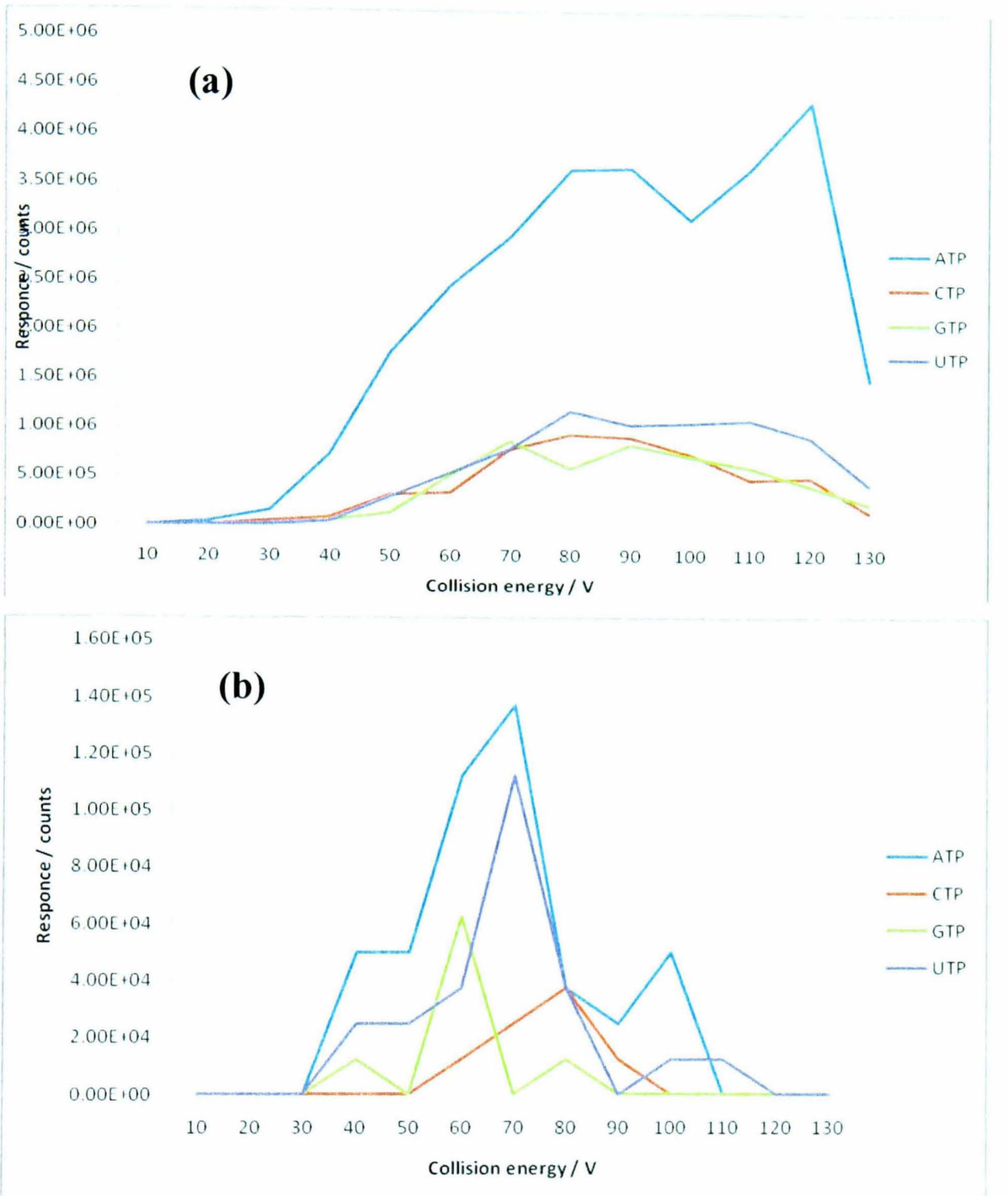

Figure 2.4. Plots demonstrate the collision energy differences between generating a *m/z* 79 and 97 for the triphosphates. The (a) *m/z* 79 ion generates a more intense signal compared to (b) *m/z* 97, making it more suitable as marker for the precursor ion scans.

2.3.2 Mass accuracy of the precursor ion scan and use of the enhanced resolution scan

2.3.2.1 Precursor ion scan speed

The survey scan mode in the QqQLit is used to identify possible analytes of interest which, if preceded by an enhanced production scan, will be used to assign the *m/z* of the compound designated to undergo EPI spectra (Hopfgartner et al., 2004). If the survey scan is a precursor ion scan (or neutral loss), as is the instance in this case, then it is recommended that an enhanced resolution scan is used to more accurately depict the *m/z* of the pseudomolecular ion of interest rather than relying on the mass accuracy of the precursor ion (or neutral loss) scan alone. In an attempt to identify the mass accuracy of the precursor ion scan and potentially reduce the complexity and time of the overall scan by removing the enhanced resolution scan, the influence of precursor ion scan speed on mass accuracy was investigated.

Mass Accuracy of the precursor ion scan

Using the same mass range, three scan speeds were selected: 275, 550 and 1100 amu / sec, and the *m/z* of the pseudomolecular ion of nucleotide reference standards was measured. The mass accuracy of the precursor ion scan was found to be dependent on the scan speed, with a slow precursor ion scan of 275 amu / sec demonstrating a mean accuracy of -0.2, the scan of 550 amu / sec gave a mean accuracy of 0.2 greater than expected and the faster scan of 1100 amu / sec is, on average, +0.4 amu greater than expected. Following consultation with an instrumental specialist at Applied Biosystems it became apparent that the QqQLit does not compensate for mass accuracy shifts caused by a change in the speed of the survey scan. Therefore, for the identification of pseudomolecular ions of interest, the enhanced resolution scan is more accurate than the precursor ion scan alone, even if a reasonable scan speed of 550 amu / sec is employed.

An additional reason for the use of the enhanced resolution scan is the increased resolution it has compared to the precursor ion scan; see Figure 2.5. This is of importance when measuring the isotopic cluster of the pseudomolecular ion, its charge

state and consequently the mass of the molecule. The *m/z* of pseudomolecular ion (deprotonated in ESI$^-$) is calculated by:

$$m/z = [M - nH] / nH$$

Where *m/z* - mass to charge ration
M - mass of a molecule (amu)
nH - number of protons

The compounds of interest in this work will have a pseudomolecular carbon isotope cluster of M and M+1 corresponding to C^{12} and C^{13}, the latter being present at 1.1%. O^{17} is also present but only at 0.04% (McLafferty and Turecek, 1993). If the pseudomolecular is singularly deprotonated then the two isotopes of the pseudomolecular ion will be one amu apart. However, if the pseudomolecular ion is doubly charged (the result of a loss of two protons in ESI$^-$) then subsequently the mass difference between the isotope cluster will be half an amu apart (Hoffman and Stroobant, 2005). As such the charge state and mass of an analyte can be calculated. The enhanced resolution scan option enables the identification of the charge state of the pseudomolecular ion where the precursor ion does not have the necessary resolution (see Figure 2.5); hence this scan function was employed in all precursor ion scans.

Precursor ion precision

The peak area precision of extracted ion chromatograms from a precursor ion scan was assessed at different precursor ion scan speeds on nucleotide reference standards. Three methods were evaluated, two composed of precursor ion scans of 500 and 1000 amu /sec coupled with an EPI scan at 1000 amu / sec, resulting in total cycle times of 2.4 and 2.04 sec respectively. The third method had a precursor ion scan of 1000 amu /sec, but an EPI scan speed of 4000 amu / sec, resulting in a total cycle time of 1.4 sec. Reference standards were separated by the chromatography described in section 2.2.2 and peak areas were measured from the extracted ion

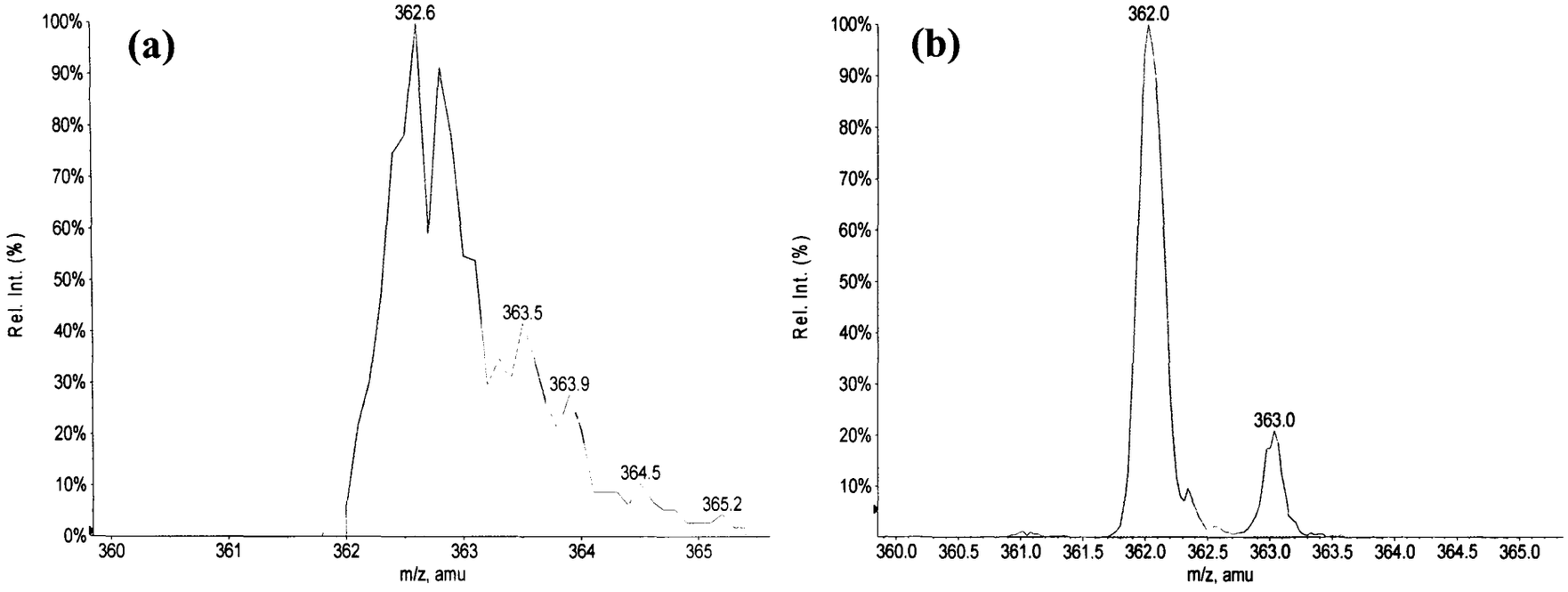

Figure 2.5. A comparison of the (a) precursor ion scan and the (b) enhanced resolution scan of the $[M-H]^-$ ion of GMP observed after a precursor ion scan (coupled with EPI) at 550 amu / sec. The resolution of the enhanced resolution is greater than the precursor ion scan and allows for the identification of the isotopic pattern, confirming the charge state of the ion and subsequent identification of the molecular mass.

chromatograms of nucleotide reference standards. The measured precision for each reference standard can be found in Table 2.1. The reproducibility of all the methods appear poor in Table 2.1 and outside the accepted limits for bioanalytical methods (US Department of Health and Human Services, 2001). This is to be expected as the number of data points across the chromatography peak is on average six and hence does not accurately describe the peak shape, although the precision and number of data points improved with the fastest scan. It has been previously demonstrated that a precursor ion scan on a QqQLit has successfully been used as a quantitative method in the analysis of N-acylhomoserine lactones (Ortori et al., 2007). If such an approach was required for the investigation of nucleotides, a faster precursor ion scan could be employed, reducing the overall cycle time and increasing the number of data points across the peak. As such, quantification of nucleotides by the survey scan was not investigated further.

2.3.3 Nucleotide fragmentation patterns

The precursor ion survey scan coupled with the full product ion spectra has the potential to identify the nucleotide reference standards described in Figure 2.1, as well as structural analogues that have a phosphate moiety. To this end an understanding of the product ion spectra of nucleotide reference standards was required, not only to confirm the identity of known analytes but to aid in identifying analytes which were structurally similar. Furthermore, the phosphate moiety is not specific to nucleotides but is found in other endogenous biological compounds such as phospholipids. An understanding of nucleotide fragmentation under CID should aid in the identification of analytes that belong to the nucleotide family. The EPI spectra of reference standards were examined for product ions relating to common structural similarities. The fragmentation patterns of the reference standards can be found in Figure 2.6, Figure 2.7, Figure 2.8, Figure 2.9 and Figure 2.10.

All nucleotide reference standards demonstrated a *m/z* 79 ion under EPI conditions, be it at a relatively low ion intensity, but the larger molecules such as FAD, NAD^+, $NADP^+$ did

Table 2.1 Precision of precursor ion survey scan method on nucleotide standards (10pM, n=6). The effect of [illegible] one different EPI scan speed was assessed on peak area precision. PI – precursor ion scan, EPI – enhanced product ion scan

Scan speed of survey scan constituents (amu / sec)	Total cycle Time (sec)	Precision of extracted ion chromatogram %RSD (n=6)													
		AMP	GMP	CMP	UMP	ADP	GDP	CDP	UDP	ATP	GTP	CTP	UTP	cAMP	cGMP
PI - 500 EPI - 1000	2.4 sec	62.1	56.5	82.3	64.6	75.0	64.8	53.7	46.9	68.4	64.3	70.9	108.0	125.1	54.3
PI - 1100 EPI - 1000	2.0 sec	64.4	48.4	34.9	79.0	40.2	84.7	50.2	41.3-	63.4	83.4	68.0	60.5	41.1	92.2
PI – 1100 EPI - 4000	1.4	56.8	44.7	27.6	45.7	33.6	30.5	44.6	32.2	49.6	76.4	63.0	49.4	50.4	69.9

not. The optimum collision energy required to generate a *m/z* 79 ion (-80 V) is relatively high for other structurally significant ions, causing such ions to further fragment. Therefore, where a spread of collision energies were applied for the EPI scan, they are relatively low and result in low intensity or unobservable *m/z* 79 product ions. The lack of this ion is not critical as the triggering of the EPI scan by the PI scan demonstrates the presence of the *m/z* 79 ion for a given analyte.

All nucleotides tested appear to fragment forming an ion of the respective base. Adenine nucleotides form an *m/z* 134 ion $[C_5H_4N_5]^-$ under CID, uracil nucleotides form an *m/z* 111 ion $[C_4H_3N_2O_2]^-$, guanine nucleotides form an *m/z* 150 ion $[C_5H_4N_5O]^-$ and cytidine nucleotides form a *m/z* 110 ion $[C_4H_3N_3O]^-$. Base ions have been previously observed for the cyclic nucleotides, cAMP and cGMP (Witters et al., 1997). Furthermore, adenine and guanine nucleosides have been observed to cleave between the sugar and the base forming a base ion, however this was under ESI^+ conditions (Zhu et al., 2001) Such fragments are diagnostic in the identification of unknowns as it demonstrates the presence of a base, strongly suggesting a nucleotide or structurally similar compound.

Diphosphate reference standards fragmented to form a product ions at *m/z* 159. This ion is likely to be $[HP_2O_6]^-$ by the loss of two phosphates. The *m/z* 273 ion observed in diphosphate fragmentation is likely to be the ribose sugar and two phosphates but with the loss of water $[C_5H_7O_9P_2]^-$. It is not clear at this time where the loss of H_2O occurs, be it from the ribose sugar or from one of the phosphate moieties. There appears to be little information in the literature regarding this fragment and it would mostly likely be the product of a number of fragmentation steps.

Triphosphate reference standards also form *m/z* 159 product ions (as observed with diphosphates) and has been previously reported to be the loss of two phosphates as $[HP_2O_6]^-$ (Tuytten et al., 2002). Furthermore deoxyribose triphosphates have also been observed to form this ion under CID conditions (Hennere et al., 2003). Triphosphates also appear to lose $[H_3PO_4]$ as a neutral, forming product ions of *m/z* 480, 384, 385 and 424 for ATP, CTP, UTP and GTP respectively (Buckstein *et al.*, 2008; Chen *et al.*, 2009).

As observed with diphosphates, triphosphates also form a *m/z* 273 ion. Again this ion is likely to be $[C_5H_7O_9P_2]^-$ and as with diphosphates, the mechanisms involved in its formation is likely to be by a number of fragmentations steps. The presence of these two ions, *m/z* 159 and *m/z* 273, indicates the presence of two or more phosphates and can be used as a diagnostic tool.

Cyclic AMP and cyclic GMP reference standards fragment to generate a product ion spectra similar to AMP and GMP. Both cyclic nucleotides demonstrate a loss of the *m/z* 79 $[PO_3]^-$ ion, along with their respective bases of *m/z* 134 ion $[C_5H_4N_5]^-$ and *m/z* 150 ion $[C_5H_4N_5O]^-$, and are comparable with previously reported spectra (Buchholz *et al.*, 2001; Witters *et al.*, 1996; Witters *et al.*, 1997).

NAD^+, $NADP^+$, NADH and NADPH have strong structural similarities and demonstrate similar product ion spectra to adenine nucleotides. The base ion at *m/z* 134 ion was formed under CID, as were the ions indicative of two or more phosphates moieties, *m/z* 159 and *m/z* 273. Both NAD^+ and $NADP^+$ form ions at *m/z* 540 and 640 respectively with the loss of nicotinic acid as a natural (Buchholz et al., 2001) and FAD fragments to form AMP as an ion at *m/z* 437 as previously observed (Buchholz et al., 2001)

The EPI spectra of the nucleotide reference standards investigated show structurally significant ions that not only provide strong evidence in the identification of knowns but will also aid in the identification of unknowns. The optimization of the collision energy is not ideal for all reference standards investigated and a number of structurally important ions have relatively low intensities. However, for the most part, identification of an ion indicative of a nucleotide base and the presence of one or more than one phosphate group was achieved. A list of prominent production ions for each reference standard can be found in Table 2.2

Table 2.2. The pseudomolecular ion and prominent product ions of nucleotides and structurally related analytes. Reference standards were infused into the QqQLit (10μM) in ESI$^-$ and fragmented under CID with a collision energy of -35 ± 20V.

Analyte	$[M-H]^-$ (*m/z*)	Prominent product ions (*m/z*)
AMP	346	211, 134, 79
UMP	322.97	211, 97, 79
CMP	322.1	211, 110, 97, 79
GMP	362	211, 150, 79
ADP	425.93	328, 273, 159, 134, 79
UDP	402.95	273, 159, 111, 79
CDP	401.99	304, 273, 175, 159, 79
GDP	441.92	344, 159, 150, 79
ATP	505.99	408, 273, 159, 79
UTP	483	385, 273, 159, 111, 79
CTP	482	358, 273, 159, 79
GTP	522.02	273, 159,150, 79
NAD^+	662.1	540, 273, 328, 79
$NADP^+$	742.1	79, 620, 408, 274, 159, 79
FAD	784.18	437, 346, 241, 79
NADH	663	541, 426,329, 273, 159, 134
NADPH	744	684, 622, 561, 408, 273, 159, 134
cAMP	328	134, 79
cGMP	344	150, 79

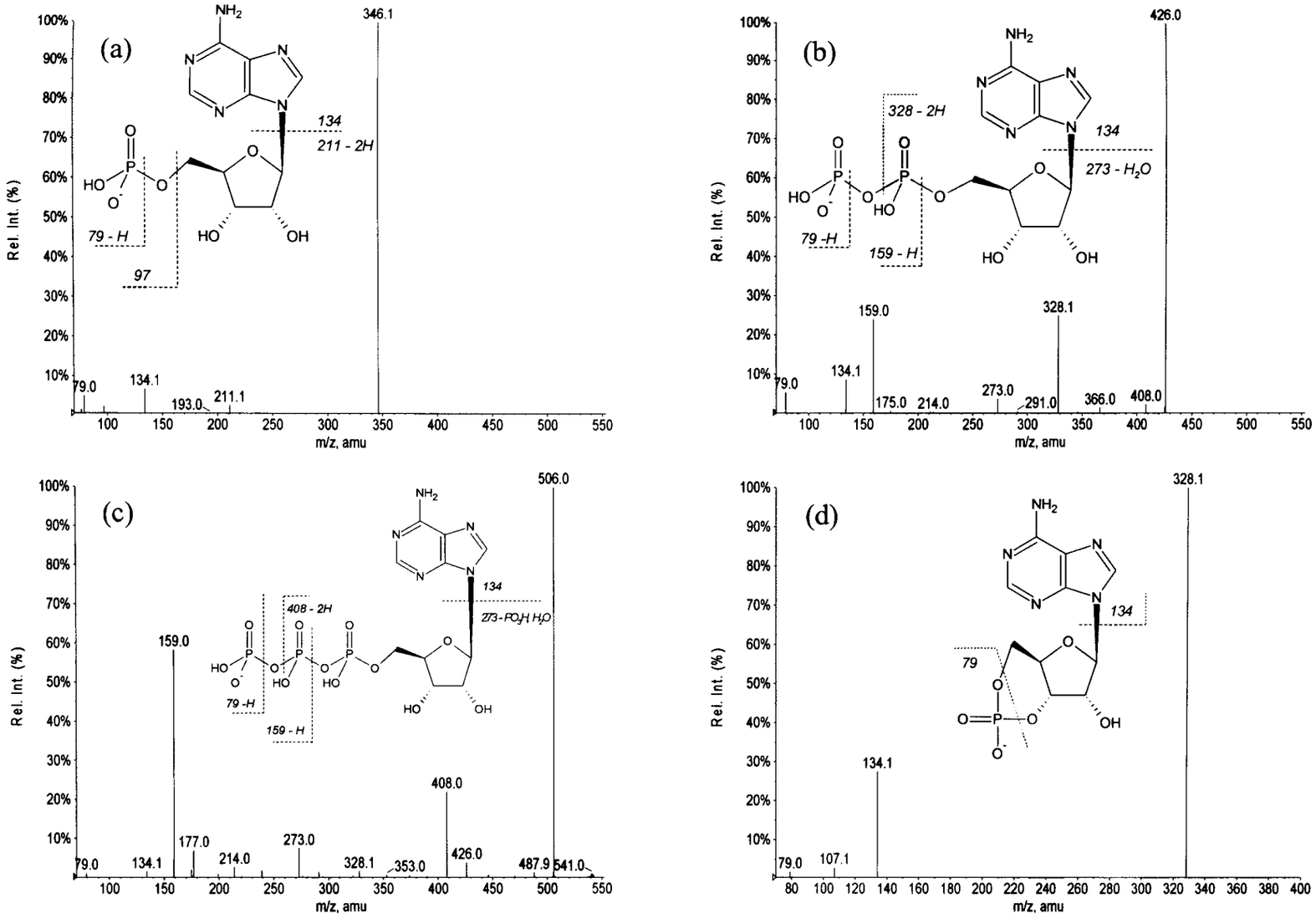

Figure 2.6. EPI spectra of (a) AMP, (b) ADP, (c) ATP and (d) cAMP reference standards and proposed fragmentation under CID with a collision energy of 30 ± 20 V. Ions were formed under ESI⁻ conditions by direct infusion of reference standards.

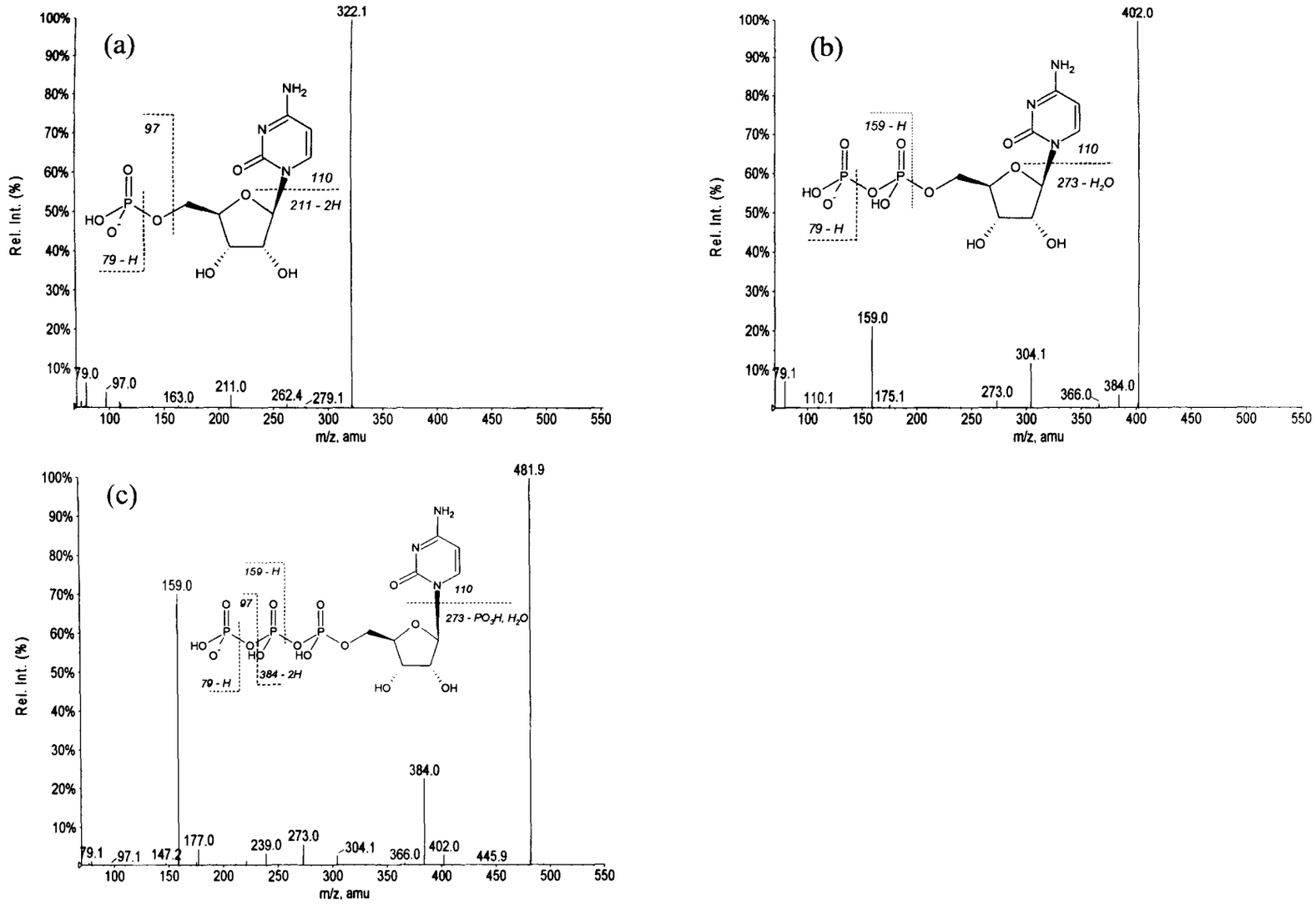

Figure 2.7. EPI spectra of a) CMP, (b) CDP and (c) CTP reference standards and proposed fragmentation under CID with a collision energy of 30 ± 20 V. Ions were formed under ESI$^-$ conditions by direct infused of reference standards.

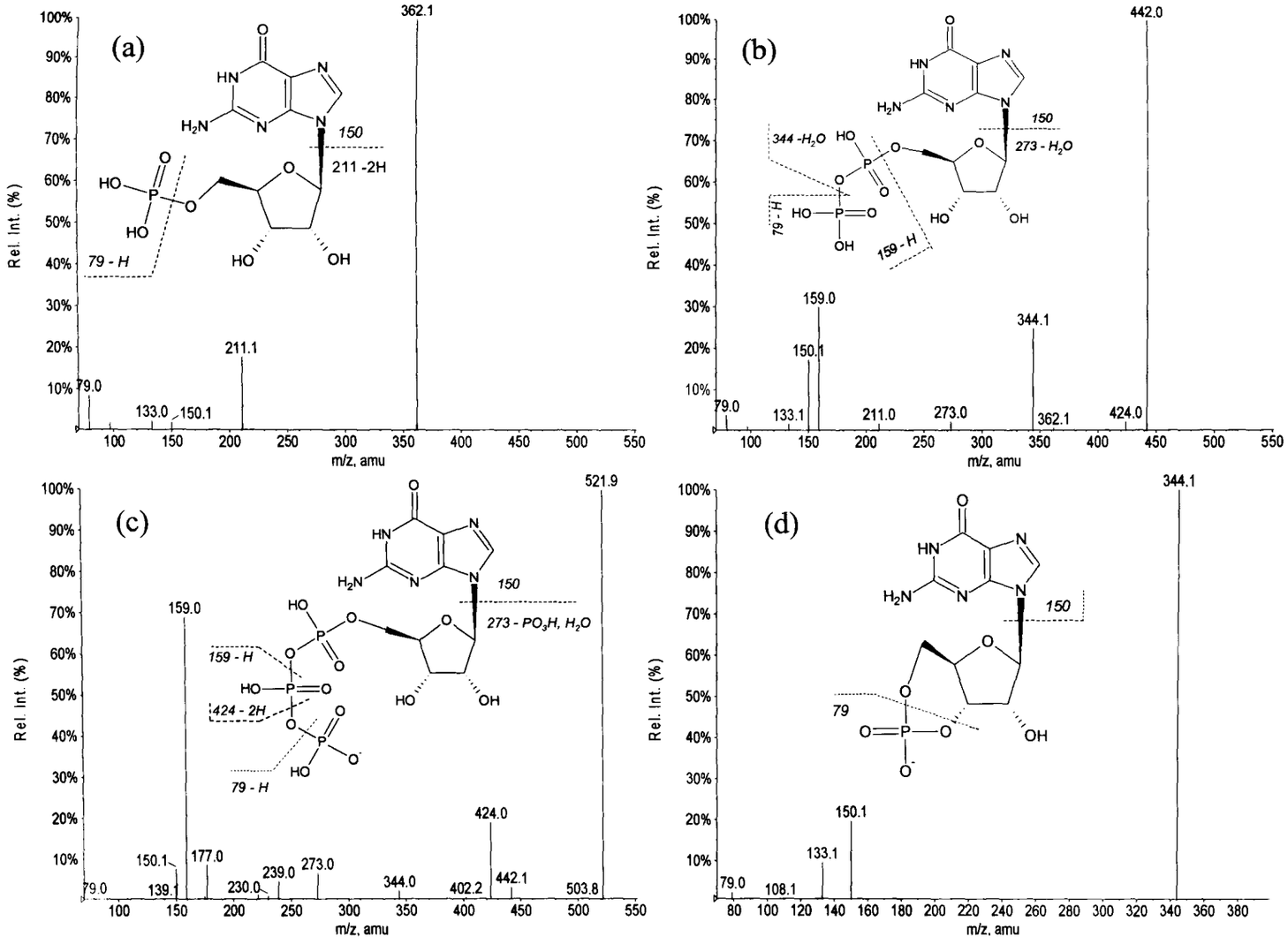

Figure 2.8. EPI spectra of (a) GMP, (b) GDP, (c) GTP, (d) cGMP and proposed fragmentation under CID with a collision energy of 30 ± 20 V. Ions were formed under ESI⁻ conditions by direct infused of reference standards.

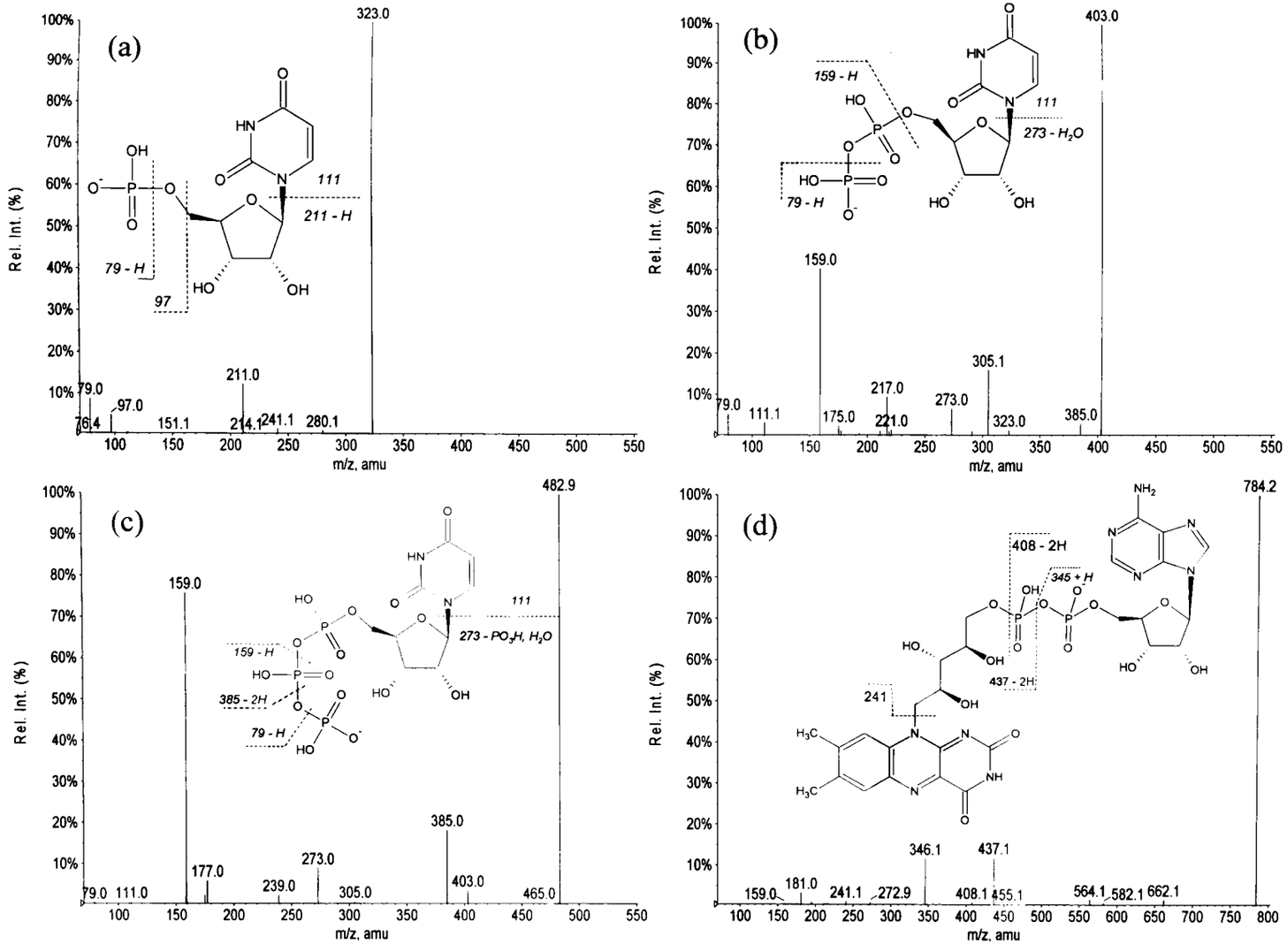

Figure 2.9. EPI spectra of (a) UMP, (b) UDP, (c) UTP and (d) FAD and proposed fragmentation under CID with a collision energy of 30 ± 20 V. Ions were formed under ESI⁻ conditions by direct infused of reference standards.

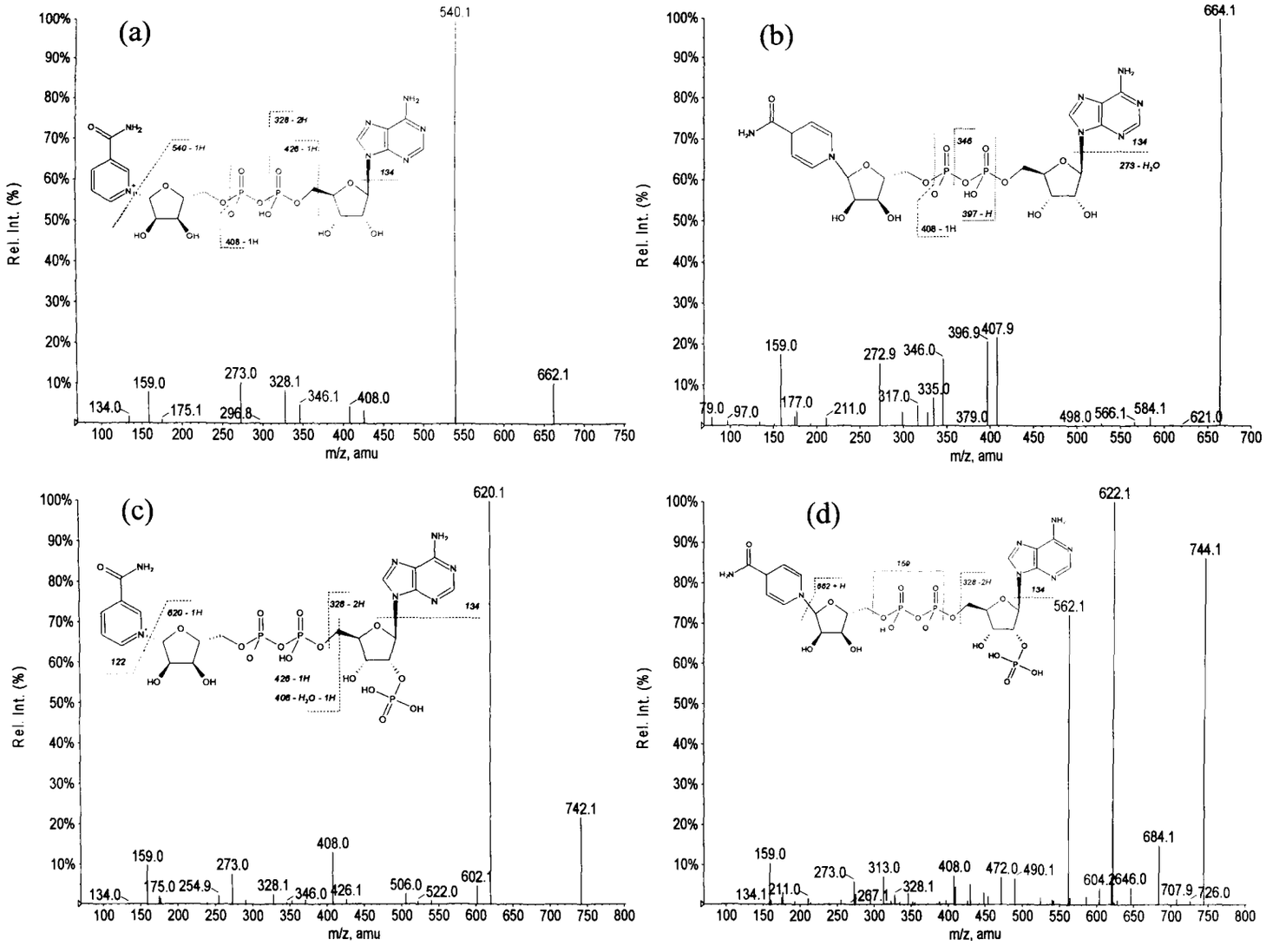

Figure 2.10. EPI spectra of (a) NAD^+, (b) NADH, (c) $NADP^+$ and (d) NADPH and proposed fragmentation under CID with a collision energy of 30 ± 20 V. Ions were formed under ESI^- conditions by direct infused of reference standards.

2.3.4 Assessment of the precursor ion scan coupled with EPI to identify nucleotide reference standards in a chromatographic run

The ability of the precursor ion scan to correctly identify reference standards (10 μM) was subsequently assessed along with the expected EPI spectra. Successful identification of all nucleotide reference standards (mono-, di- and triphosphates, as well as cAMP, cGMP, FAD, NAD^+, NADH, $NADP^+$ and NADPH) and EPI spectra was obtained for all standards; a total ion current can be found in Figure 2.11

2.3.5 SRM method for nucleotide measurements

To establish the most appropriate extraction method, a multiple reaction monitoring method was developed to assess the most appropriate extraction method on recovery and precision. Triple quadrupole instruments are typically run in SRM mode when quantification is required due to the sensitivity and selectivity the approach affords (Hoffman and Stroobant, 2005).

Nucleotide precursor ions were selected on intensity; in the case of all standards measured this was a de-protonated pseudomolecular ion $[M-H]^-$. Product ions were again selected on intensity, and one SRM transition per analyte was selected on this basis. Each SRM transition, optimum declustering potential and collision energy can be found in Table 2.3. The transitions selected are in accordance with previously published methods where mono and diphosphates generate an intense *m/z* 79 ion $[PO_3]^-$ and where triphosphates generate a more abundant *m/z* 159 $[HP_2O_6]^-$ (Hennere *et al.*, 2003; Tuytten *et al.*, 2002). Another published method reports using a different set of product ions with the aim of increasing the selectivity of analytes one amu apart (Cordell et al., 2008), however the SRM transitions selected here demonstrated the required specificity.

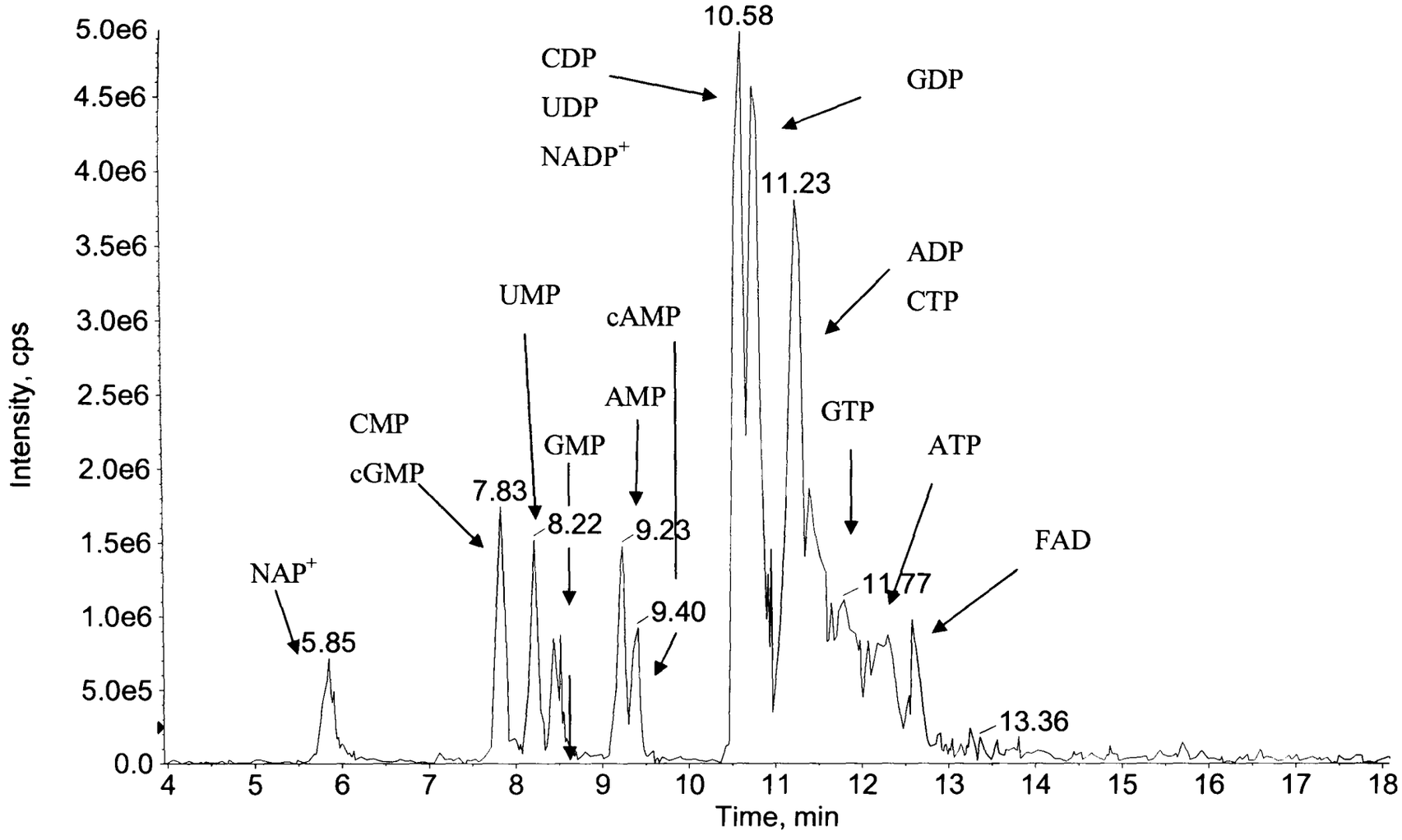

Figure 2.11. Total ion current of nucleotide reference standards (10μM) successfully identified by the use of the precursor ion scan identifying analytes with a product ion of *m/z* 79. Each analyte triggered a comparable enhanced spectra with those obtained from direct infusion experiments. .

2.3.6 Nucleotide extraction from biological matrix

2.3.6.1 Optimum extraction method

The three extraction methods were initially evaluated on mono-, di- and triphosphate reference standards. An acidic extraction, acidic extraction followed by sodium hydroxide and an organic extraction method. The recoveries and precision can be seen in Table 2.4. The acetic acidic extraction demonstrates a few erroneous results. ADP, CDP, GDP, cAMP and cGMP all exhibit reproducibility worse than expected, and ATP recoveries at 125.6% demonstrate that the extraction method is possibly enhancing the signal artificially. The cause of this is unknown at this time. The acetic acid / sodium hydroxide method again demonstrated variability greater than expected, especially for UMP, CMP, GMP and cGMP. Both methods centered on the acid extraction demonstrated poor chromatography compared to the organic extract and this is likely to be reason for the poor reproducibility of some of the analytes. The cause of this may be due to phospholipids which were predominantly removed in the organic extraction by the use of hexane. It is fair to say that the extraction recoveries are quite varied between analytes for each extraction method, an explanation for this is not currently forthcoming although it might be due to the poor stability of these compounds at room temperature although care was taken to keep all sample extracts on ice where ever possible. The organic extraction demonstrated better precision than either of the other two extraction methods and the recoveries are also acceptable, being comparable with those previously reported (Cordell et al., 2008). Furthermore, the organic extraction method has an additional hexane step that should have the advantage of removing some of the hydrophobic lipids present, which could be a source of ion suppression. For these reasons, the organic extraction was deemed the most suitable method to proceed with. To demonstrate that the method was capable of extraction from biological samples and to evaluate reproducibility, the methodology was further tested on *Pseudomonas aeruginosa* samples (n=6); see Table 2.5.

The reproducibility is reasonable and within expected tolerances (US Department of Health and Human Services, 2001). Although reproducibility should be within 15% or 20% if at the LLOQ, the LLOQ has not been established, so a value of 20% was allowed.

An organic extraction was also assessed without the use of hexane on *Pseudomonas aeruginosa* bacterial samples, but very poor peak shape was observed, probably due to co-eluting phospholipids compounds, leading to difficulties in peak assignment and very poor reproducibility. Similar results have been reported when extracting nucleotides from Chinese hamster ovary cells (Cordell et al., 2008).

2.3.7 Nucleotides detected in Pseudomonas aeruginosa and Escherichia coli MG1655 bacteria using the precursor ion survey scan

Following the optimum extraction method selection an analysis of *Pseudomonas aeruginosa* and *Escherichia coli MG1655* samples was carried out using the precursor ion survey scan previously described to evaluate the approach for the profiling of nucleotide in biological samples. An organic extraction, as described in section 2.2.5, was used on both bacterial strains (n=6).

Pseudomonas aeruginosa

Nucleotides detected in *Pseudomonas aeruginosa* can be found in Table 2.6. All but CMP, CTP, cAMP, NADH and NADPH were identified. Those observed were identified on the basis of retention time and enhanced production ion spectra compared to reference standards, see Figure 2.12, Figure 2.13, and Figure 2.14. Whereas the identification of most nucleotides detected can be confirmed by reference spectra, a number of analytes were tentatively identified as nucleotides when reference standards were not available at the time for confirmation. Identification was based upon the pseudomolecular ion and the resulting EPI spectra and discussed in section 2.3.7.1.

Table 2.3. Optimum SRM transition, declustering potential and collision energies for nucleotide and base – phosphate related reference standards. Reference standards were infused under ESI⁻ conditions, source temperature was set at 300 °C, N_2 gas flow set at 20 mL/min, N_2 curtain gas of 25 mL/min and an ion spay voltage of -4200 V.

Reference standard	Retention time / min	Precursor ion (*m/z*)	Product ion (*m/z*)	DP (V)	CE (V)
AMP	8.5	346.0	78.9	-90	-66
UMP	7.2	322.9	79.0	-70	-58
CMP	6.6	322.0	79.0	-75	-76
GMP	6.5	362.0	79.1	-95	-72
ADP	11.7	425.9	79.1	-100	-86
UDP	11.0	402.9	78.9	-100	-88
CDP	12.7	401.9	78.8	-100	-74
GDP	10.8	441.9	78.9	-105	-88
ATP	13.6	505.9	158.8	-90	-46
UTP	13.2	483.0	158.8	-100	-46
CTP	13.1	481.9	158.8	-105	-38
GTP	13.2	522.0	158.9	-110	-46
NAD^+	6.3	662.1	540.2	-80	-18
$NADP^+$	11.2	742.1	620	-85	-22
FAD	14.6	784.2	97.1	-140	-84
NADH	8.5	663.2	541	-80	-18
NADPH	13.2	744.1	622.1	-95	-20
cAMP	10.4	327.9	134	-95	-34
cGAMP	8.56	343.9	150.1	-95	-34
cAMP-BR	12.2	406.0	212.0	-120	-40

Table 2.4. Precision and recovery of various extraction methods on nucleotide reference standards (10μM), analyzed by an SRM method

Nucleotide	Acetic acidic		Acetic acidic/sodium hydroxide		Methanol / hexane	
	Precision (%RSD)	Recovery (%)	Precision (%RSD)	Recovery (%)	Precision (%RSD)	Recovery (%)
AMP	8.1	71.3	14.5	55.7	12.9	51.0
UMP	7.3	104.9	35.3	71.6	11.8	70.8
CMP	7.5	63.4	33.7	39.0	15.3	46.2
GMP	10.0	80.8	23.9	80.5	14.3	79.7
ADP	47.0	63.4	11.3	69.2	13.4	68.6
UDP	16.0	73.7	14.1	65.5	11.1	60.6
CDP	46.9	67.0	23.7	64.4	13.0	65.9
GDP	52.3	76.9	6.8	85.9	8.8	87.8
ATP	7.3	125.6	18.2	93.3	10.7	91.8
UTP	7.3	56.9	14.8	51.6	9.4	53.7
CTP	12.2	80.5	19.9	53.1	19.9	62.6
GTP	20.9	50.0	16.1	56.1	11.6	37.7
cAMP	50.4	63.5	12.7	55.7	9.3	52.3
cGMP	50.2	49.6	22.9	47.1	16.1	51.3

Table 2.5 Precision of a methanol / hexane extraction method on nucleotides from *Pseudomonas aeruginosa* bacteria, analyzed by an SRM method.

Statistic	Nucleotide													
	AMP	UMP	CMP	GMP	ADP	UDP	CDP	GDP	ATP	UTP	CTP	GTP	cAMP	cGMP
%RSD	21.2	11.5	14	20.2	16.7	20.5	8.5	15.4	20.8	10.6	3.3	17.1	-	-

Table 2.6. Nucleotides and structurally similar compounds detected in *Pseudomonas aeruginosa* bacteria using a precursor ion survey scan coupled with an EPI spectra. The retention times, pseudomolecular ion and prominent product ions are listed. Analytes in grey are tentative identifications of other nucleotides or structural analogues highlighted and identified by the precursor ion survey scan (*m/z* 79) and the EPI spectra.

Analyte	Retention time (min)	$[M-H]^-$ (*m/z*)	Prominent product ions
AMP	7.9	346.0	211, 134, 79
UMP	7.1	322.9	211, 111, 97, 79
GMP	6.7	362.0	211, 150, 79
ADP	11.5	425.9	328, 273, 159, 134, 79
UDP	10.4	402.9	273, 159, 111, 79
CDP	11.5	401.9	304, 273, 159, 79
GDP	10.8	441.9	344, 273, 159, 150, 79
ATP	12.5	505.9	408, 273, 159, 79
UTP	13.4	483.0	385, 273, 159, 111
GTP	13.3	522.0	273, 159,150, 79
NAD^+	5.9	662.1	540, 426, 408, 328, 273, 159, 134
$NADP^+$	11.3	742.1	620, 540, 408, 273, 159
FAD	14.6	784.2	437, 346, 241, 97
dAMP	9.8	330.1	195, 134, 97, 79
dCDP	9.5	386.0	159, 79
dTDP	11.4	401.0	275, 159, 97, 79
UDP(G)	7.7	565.1	403, 385, 323, 273, 159, 111, 97, 79,
Acetyl Co A	16.5	808.1	728.3, 461, 408, 273, 159, 134, 79

Table 2.7. Nucleotide and structurally similar phosphate containing endogenous analytes detected in Escherichia coli MG1655. Analytes were identified using a precursor ion survey scan (*m/z* 79) and confirmed by comparison of EPI spectra with reference standard spectra. Analytes in grey are tentative identifications of other nucleotides or structural analogues highlighted and identified by the precursor ion survey scan (*m/z* 79) and the EPI spectra.

Analyte	Retention time (min)	$[M-H]^-$ (*m/z*)	Prominent product ions
AMP	7.7	346.0	211, 134, 79
UMP	6.7	322.9	211, 111, 97, 79
GMP	7.0	362.0	211, 150, 79
ADP	9.8	425.9	328, 273, 159, 134, 79
UDP	9.5	402.9	273, 159, 79
CDP	8.9	401.9	304, 273, 159, 79
GDP	9.3	441.9	344, 159, 150, 79
ATP	10.4	505.9	408, 273, 159, 79
UTP	10.3	483.0	385, 273, 159, 79
CTP	9.7	481.9	385, 273, 159, 79
GTP	11.5	522.0	425, 159, 79
NAD^+	4.5	662.1	540, 426, 408, 328, 273, 159, 134
FAD	11.76	784.1	437, 346, 79
dADP	14.6	410.0	134, 159, 79
dATP	15.9	490.0	159, 257, 392, 410, 79
dCDP	12.62	386.0	159, 257, 79
dTMP	9.5	321.0	195, 79
dTTP	14.3	481.0	159, 257, 401, 79
UDP(G)	6.6	565.1	403, 385, 323, 273, 159, 111, 97, 79,
Acetyl CoA	16.5	808.1	728.3, 461, 408, 273, 159, 134, 79

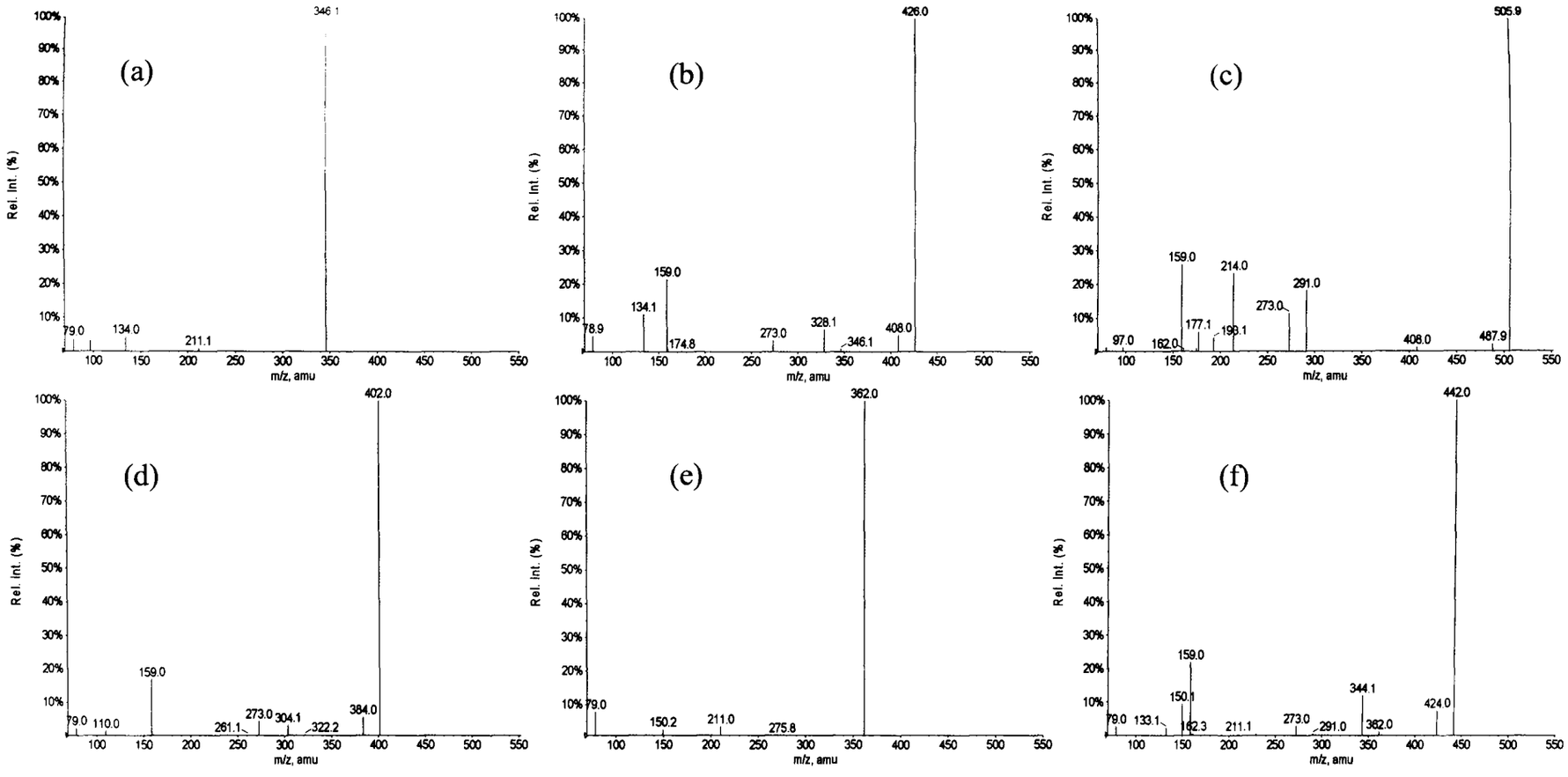

Figure 2.12 EPI spectra of nucleotides (a) AMP, (b) ADP, (c) ATP, (d) CDP, (e) GMP and (f) GDP detected in *Pseudomonas aeruginosa* bacteria using a precursor ion survey scan and confirmed by comparison of EPI spectra with reference standard spectra.

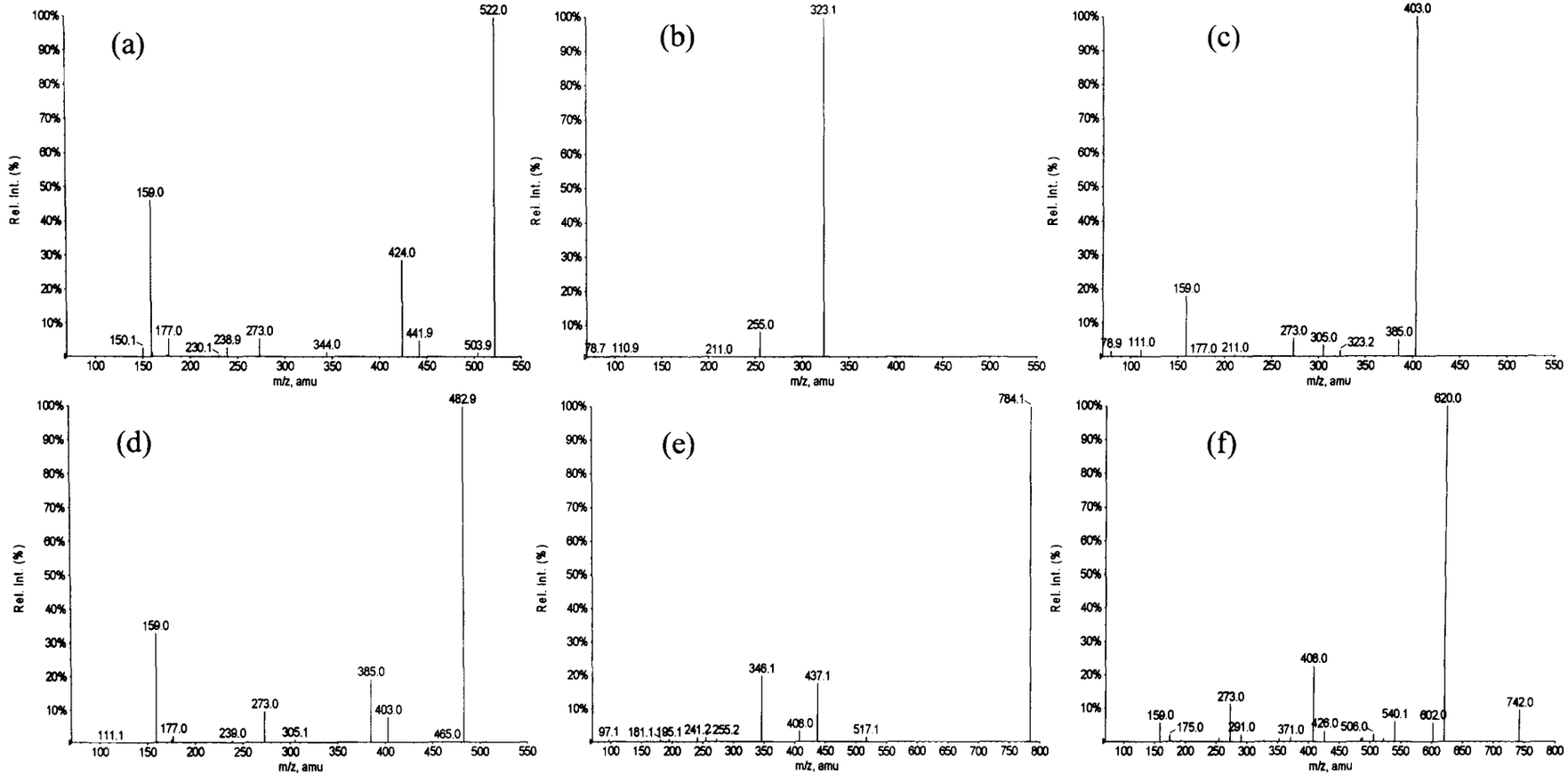

Figure 2.13 EPI spectra of nucleotides (a) GTP (b) UMP, (c) UDP, (d)UTP, (e) FAD, and (f) $NADP^+$ detected in *Pseudomonas aeruginosa* bacteria using a precursor ion survey scan and confirmed by comparison of EPI spectra with reference standard spectra.

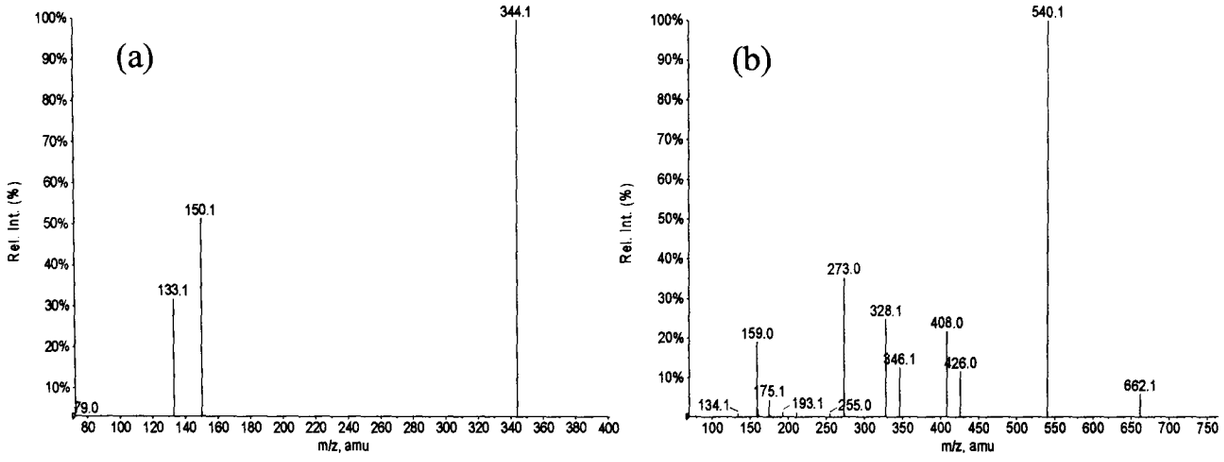

Figure 2.14. EPI spectra of nucleotides (a) cGMP and (b) NAD^+ detected in *Pseudomonas aeruginosa* bacteria using a precursor ion survey scan and confirmed by comparison of EPI spectra with reference standard spectra

Escherichia coli MG1655

The majority of nucleotides for which reference standards were readily available were identified in Escherichia coli MG1655 and can be found in Table 2.8, excluding CMP, $NADP^+$, NADH, NADPH, cAMP and cGMP. Furthermore a number of analytes were tentatively identified as nucleotides but reference standards were not immediately available to confirm identification. Identification was based upon the pseudomolecular ion and similar product ions observed in the EPI spectra of nucleotide reference standards and discussed in section 2.3.7.1.

Ten additional nucleotides or structurally similar compounds were flagged by the precursor ion scan and tentatively identified. Deoxyribose adenine monophosphate (dAMP), deoxyribose cytidine diphosphate (dCDP), deoxyribose thymine diphosphate (dTDP), uridine diphosphate glucose/galactose (UDP(G) and *Acetyl CoA* were tentatively identified in *Pseudomonas aeruginosa* and deoxyribose adenine diphosphate (dADP), deoxyribose adenine triphosphate (dATP), deoxyribose cytidine diphosphate (dCDP), deoxyribose thymine monophosphate (dTMP), deoxyribose thymine triphosphate (dTTP), uridine diphosphate glucose/galactose (UDP(G) and *Acetyl CoA* were tentatively identified in *Escherichia coli* MG1655 . Identification was undertaken by examining the EPI spectrum for ions observed in previously in the literature or in structurally similar reference standards, ie AMP and dAMP. See section 2.3.7.1

There appear to be few analytical approaches that have performed a wide profile of nucleotides in biological materials, so it is difficult to make an absolute comparison between intracellular analytes detected here and those previously reported. Furthermore, it has been reported that comparisons between nucleotides from bacterial samples that have been extracted by different protocols can produce different results (Buckstein et al., 2008). Nevertheless, one published technique has demonstrated a method to quantify a relatively large profile of intracellular nucleotides from *Escherichia coli* MG1655 (Buckstein et al., 2008), for which comparisons can be made. The overlap of nucleotides identified compares well with those observed by the precursor ion method, identifying ADP, UDP, ATP, UTP, CTP, GTP, FAD, dATP, dTTP, UDP(G) and acetyl CoA.

However, CDP, GDP, cCDP and dTMP identified in this chapter were not identified in the previously reported *Escherichia coli MG1655* extract, nor were any monophospates as reference standards were not used. The triphosphates have also been identified previously in *Escherichia coli* using HPLC and UV (Dutta and O'Donovan, 1987).

CMP, NADP, NADH, NADPH, cAMP and cGMP were not detected by the precursor ion methodology, suggesting that if they are present in the *Escherichia coli* extracts, they are below the limit of quantification. Both dTMP and dCDP, tentatively identified by this method, have been previously observed in *Escherichia coli* MG1655 (Sandlie and Kleppe, 1982; Weiss, 2007). The triphosphates observed in the *Pseudomonas aeruginosa* extracts here have been observed previously (Dutta and O'Donovan, 1987). Furthermore, AMP, ADP and ATP have all been previously identified in *Pseudomonas aeruginosa* as part of an effort to optimize extraction (Lundin and Thore, 1975). Overall, the method based on the precursor ion scan of the phosphate group (coupled with EPI spectra) profiled a greater number of nucleotides than previously observed by targeted methods.

2.3.7.1 Arguments for the tentative nucleotide identification of certain nucleotide in bacterial samples

The nucleotide dAMP was tentatively identified in *Pseudomonas aeruginosa* by the EPI spectra Figure 2.15. The pseudomolecular ion at *m/z* 330.1 is as expected for the $[M-H]^-$ ion. A low intensity ion at *m/z* 195 could be a cleavage between the base and the ribose sugar resulting in an ionised deoxyribose group with one phosphate. The product ion *m/z* 134 ion is indicative of adenine and has been previously observed for structurally similar analyte AMP and cAMP (Cordell *et al.*, 2008; Witters *et al.*, 1996). The ions *m/z* 79 and 97 are present, indicative of a phosphate moiety, and have previously been reported for structurally similar nucleotide AMP (Cordell *et al.*, 2008; Tuytten *et al.*, 2002).

Tentative identification of dCDP was made in both *Escherichia coli* MG1655 and *Pseudomonas aeruginosa* by the EPI spectra, see Figure 2.15 (only spectrum of dCDP from *Escherichia coli* MG1655 shown for sake of repetition). The pseudomolecular ion

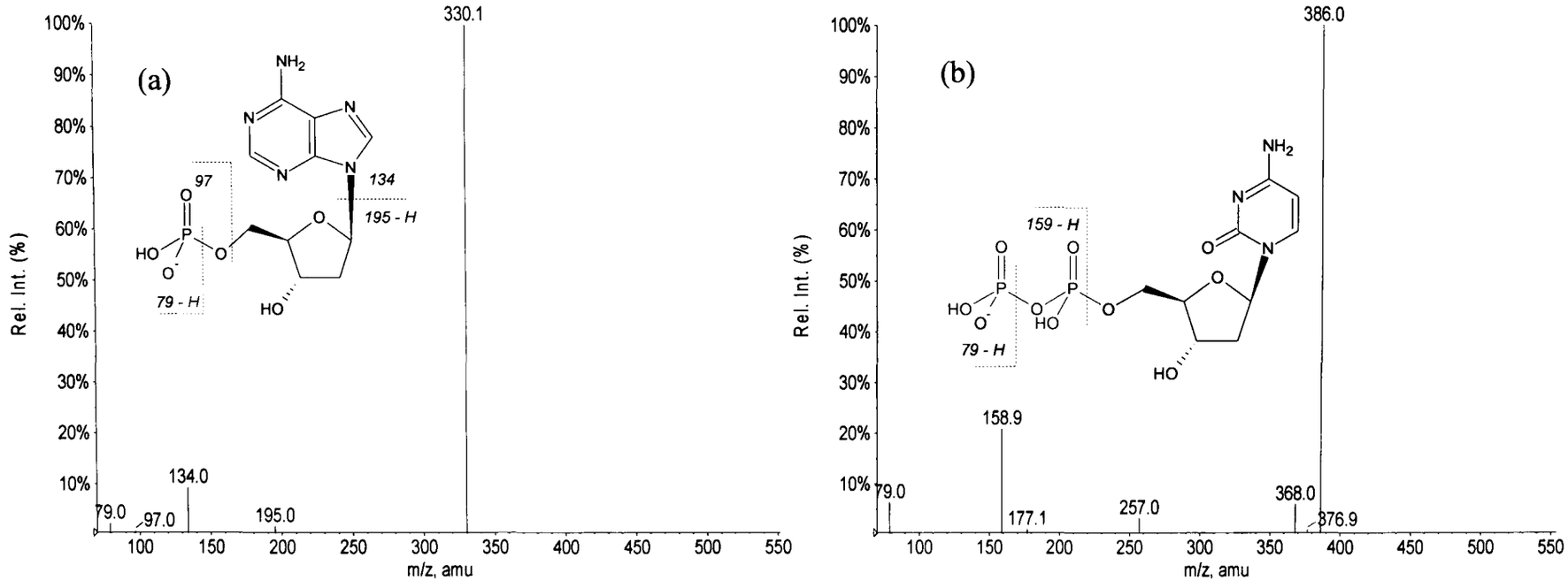

Figure 2.15 EPI spectra of tentatively identified (a) dAMP in *Pseudomonas aeruginosa* and (b) dCDP in *Pseudomonas aeruginosa and Escherichia coli MG1655*. Tentative identification was obtained using the precursor ion survey scan (*m/z* 79) and EPI spectra.

$[M-H]^-$ at *m/z* 386 is as expected. An *m/z* 79 is observed along with an *m/z* 159 ion, indicating the presence of at least two phosphate groups. Both ions have been previously identified as phosphate product ions of CDP, the ribose form of this nucleotide (Cordell *et al.*, 2008; Tuytten *et al.*, 2002). There lack of both a base ion and the ion comprised of two phosphates and a ribose sugar ($-H_2O$) observed in CDP could make this identification a little weak.

dTDP was tentatively identified in *Pseudomonas aeruginosa* by the resulting product ion spectra Figure 2.16. The pseudomolecular ion matches the expected $[M-H]^-$. An ion at *m/z* 275 is detected and is consistent with a deoxyribose and two phosphates. There is no observable ion indicative of the thymine base; however it is seen as a neutral loss with the cleavage of the *m/z* 275 from the pseudomolecular ion. A *m/z* 79 is observed along with an *m/z* 159 ion, indicating the presence of at least two phosphate groups. A *m/z* 79 has previously been shown previously to result from the loss of $[PO_3]^-$ from nucleotide (Cordell et al., 2008) where *m/z* 159 has been identified to be resulting from dTTP (Hennere et al., 2003)

UDP(G) was tentatively identified in both *Escherichia coli* MG1655 and *Pseudomonas aeruginosa* by the resulting EPI spectra (see Figure 2.16. Only the spectrum from *Escherichia coli* MG1655 is shown for sake of repetition). The identification of the terminal sugar, whether it was glucose or galactose, could not be established. The difference between the two sugars is the orientation of the hydroxyl groups and, as such, identification by the methodology described in this chapter was not possible. The pseudomolecular ion matches the expected $[M-H]^-$ and has been previously reported (Coulier et al., 2006). The EPI spectra of tentatively identified UDP(G) and UDP reference standard (see Figure 2.9) have strong similarities. Both fragment to form *m/z* 79 and m/z 159 ion, indicating the presence of phosphate moieties (Cordell *et al.*, 2008; Tuytten *et al.*, 2002). A *m/z* 273 ion is also observed, as with all di and tri phosphate nucleotides observed in this chapter, indicating the presence of two or more phosphate moieties plus a ribose sugar. The base ion is also observed at *m/z* 111. An ion at *m/z* 403 is probably the result of a cleavage between the terminal phosphate and the glucose,

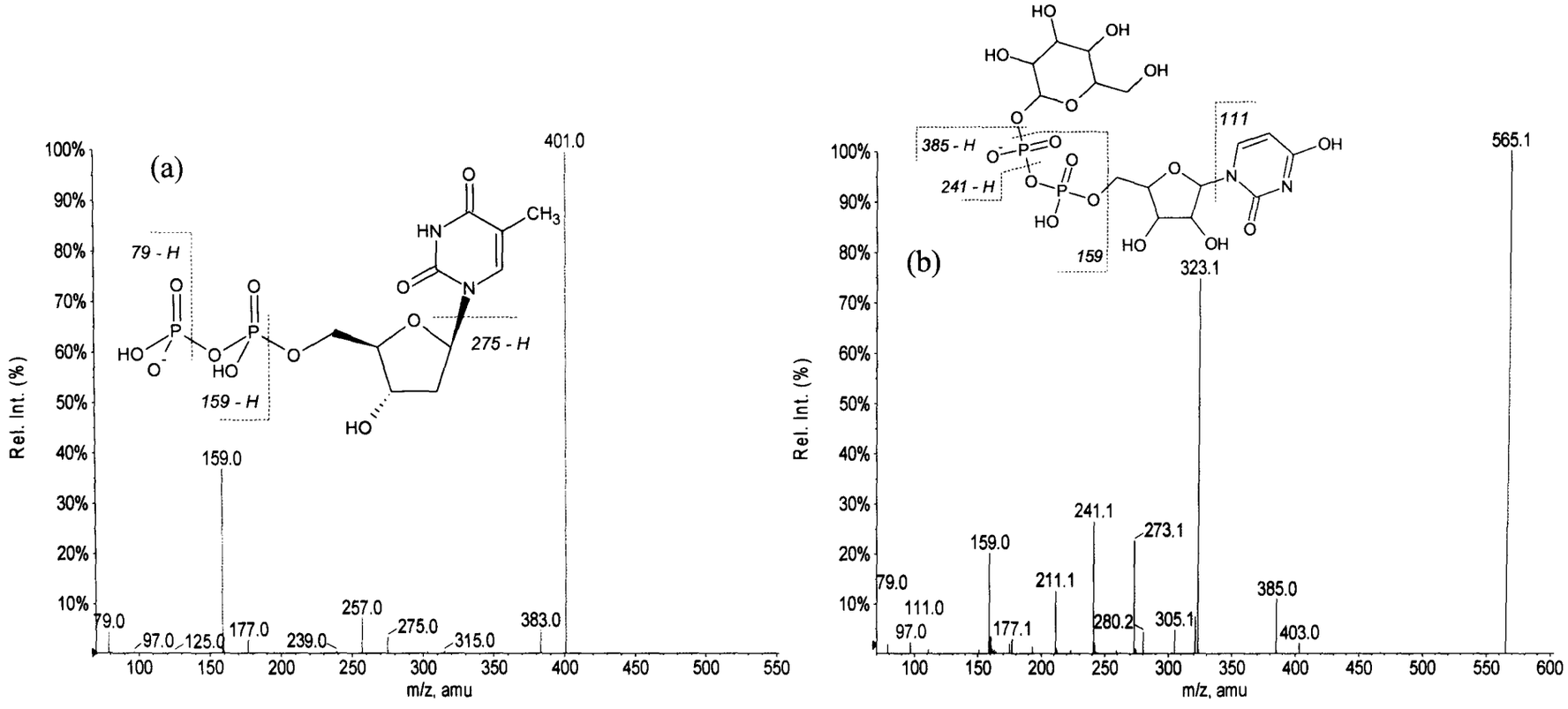

Figure 2.16. EPI spectra of tentatively identified dTDP from (a) *Pseudomonas aeruginosa* and (b) UDP(G) from *Pseudomonas aeruginosa and Escherichia coli* MG1655 . Tentative identification was obtained using the precursor ion survey scan (*m/z* 79) and EPI spectra.

forming UDP as an ion.

Acetyl CoA was tentatively identified again in both *Escherichia coli* MG1655 and *Pseudomonas aeruginosa* extract; EPI spectrum can be found in Figure 2.17. The EPI spectra appears to have a number of ions in common with ADP and has aided in the identification. Where Acetyl CoA has been studied in the past by MS, it has predominantly but not exclusively been under ESI^+ conditions (Burns *et al.*, 2005; Gao *et al.*, 2007; Kaushik *et al.*, 2009). The pseudomolecular ion matches the expected $[M-H]^-$ of 808.1 and has been previously reported (Coulier et al., 2006). The ion at *m/z* 728 would fit the ion with the loss of $[PO_3H_2]$ from position 2 of the ribose sugar. The ion at *m/z* 408, previously observed as a product ion of acetyl Co A (Hennere et al., 2003) could be the formation of ADP after the loss of $[PO_4H_2]$ from position 2 of the ribose sugar. An ion at *m/z* 159 is observed indicating the presence of two or more phosphate moieties. Furthermore, an ion at *m/z* 273 is present, indicating two or more phosphate moieties plus a ribose sugar. The adenine base is observed, although relatively small, at *m/z* 134.

Tentative identification of dADP was made in *Escherichia coli* MG1655 extract by the resulting EPI spectra, see Figure 2.18. and shares similar product ions with the EPI spectra of ADP; see Figure 2.18. The pseudomolecular ion at *m/z* 410.0 was as expected for the $[M-H]^-$ ion. A low intensity ion at *m/z* 275 was indicative of the deoxyribose joined to two phosphate groups, where the m/z 134 ion was indicative of adenine. An *m/z* 79 $[PO_3^-]$ was present indicating one phosphate group as observed with ADP (Cordell et al., 2008) as was m/z 159, previously observed in triphosphate and thought to be $[HP_2O_6]^-$, indicative of two phosphate groups (Tuytten et al., 2002).

Tentatively identified dATP also demonstrates structurally informative EPI spectra; see Figure 2.18, a demonstrates similarities to ATP. The pseudomolecular ion at *m/z* 490.0 was as expected for the $[M-H]^-$ ion (Chen et al., 2009). A m/z 79 ion is present, albeit at a low intensity, along with *m/z* 159, indicating two or more phosphate moieties and was previously observed (Hennere et al., 2003). An ion at *m/z* 329 was observed and has been previously reported as the result of the terminal phosphate $[PO_4H_3]$ lost as neutral

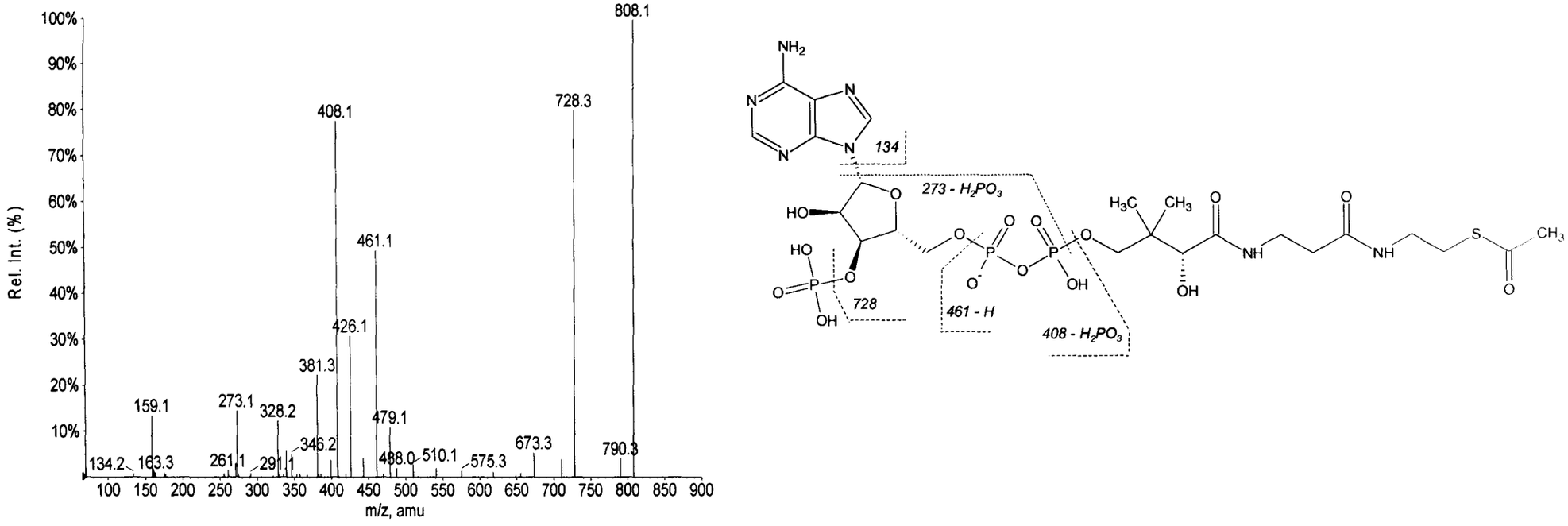

Figure 2.17. EPI spectra of tentatively identified *Acetyl CoA* in *Pseudomonas aeruginosa and Escherichia coli* MG1655. Tentative identification was obtained using the precursor ion survey scan (*m/z* 79) and EPI spectra. Location of the charge is a best estimate.

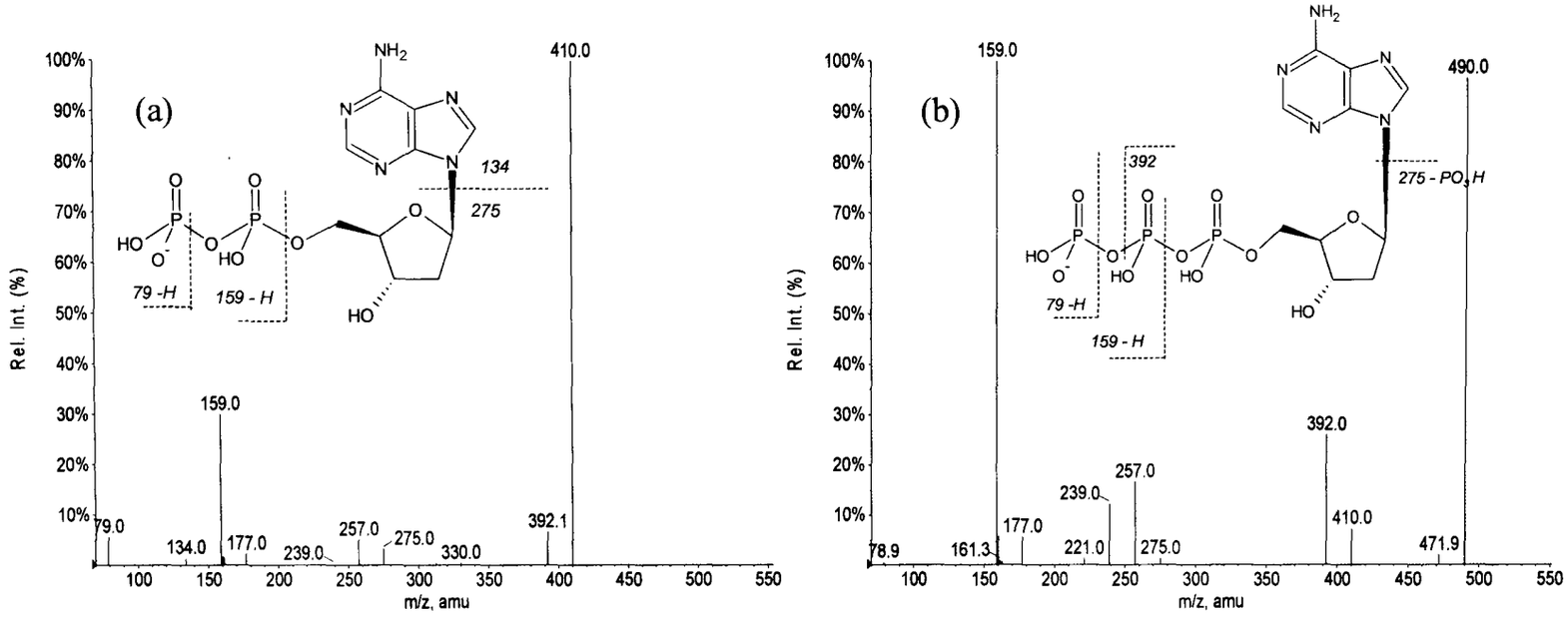

Figure 2.18. EPI spectra of tentatively identified of (a) dADP and (b) dATP in *Escherichia coli* MG1655. Tentative identification was obtained using the precursor ion survey scan (*m/z* 79) and *EPI* spectra.

(Chen et al., 2009) Additionally *m/z* 275 is detected, indicative of the deoxyribose joined to two phosphate groups. dTMP has a relatively simple EPI spectra, as do the other monophosphates observed in this chapter; see Figure 2.19. The pseudomolecular ion at *m/z* 321.1 was as expected for the $[M-H]^-$ ion. The cleavage yielding a *m/z* 79.0 ion indicates a phosphate moiety where the ion at *m/z* 195.1 is most likely the cleavage of the base as a neutral, leaving the deoxyribose adjoined to a phosphate as an ion. A small base ion is observed at *m/z* 125.1, but it is likely most of the base is lost as a neutral through the generation of *m/z* 195 ion.

The EPI spectra of dTTP is more informative than dTMP; see Figure 2.19. The pseudomolecular ion at *m/z* 481.0 was as expected for the $[M-H]^-$ ion (Chen et al., 2009). A small *m/z* 79 $[PO_3^-]$ phosphate ion is observed. The ion *m/z* 159 $[HP_2O_6]^-$is observed and indicative of two phosphates and has been previously observed in the CID product ion spectrum of dTTP (Hennere et al., 2003). An ion indicative of the loss of the terminal phosphate group as a neutral $[PO_4H_3]$ is observed at *m/z* 383 and has been previously assigned (Chen et al., 2009). Intestinally no thymine base ion is observed, nor is a neutral loss seen. However, it could be speculated that the ion associated with the neutral loss of the thymine base underwent further fragmentation, losing a phosphate moiety and forming the ion at *m/z* 275.

It is worth noting that AMP, ADP and ATP have the same molecular formula as dGMP, dGDP and dGTP respectively and therefore would be isobaric and could not be discriminated by their respective pseudomolecular ions. Deoxyribose guanine standards were not available at the time of this work and so identification by retention times could not be ascertained although it is unlikely that AxP and dGxP would coelute because of structural differences. Furthermore, it would be expected that dGMP, dGDP and dGTP would fragment under CID to form a base ion at *m/z* 150 as observed for GMP, GDP and GTP reference standards and cGMP (Witters et al., 1996). As this ion was not observed in any EPI spectra or AMP, ADP, and ATP spectra, it is assumed that if present, these three deoxyribose guanine nucleotides were below the limit of detection.

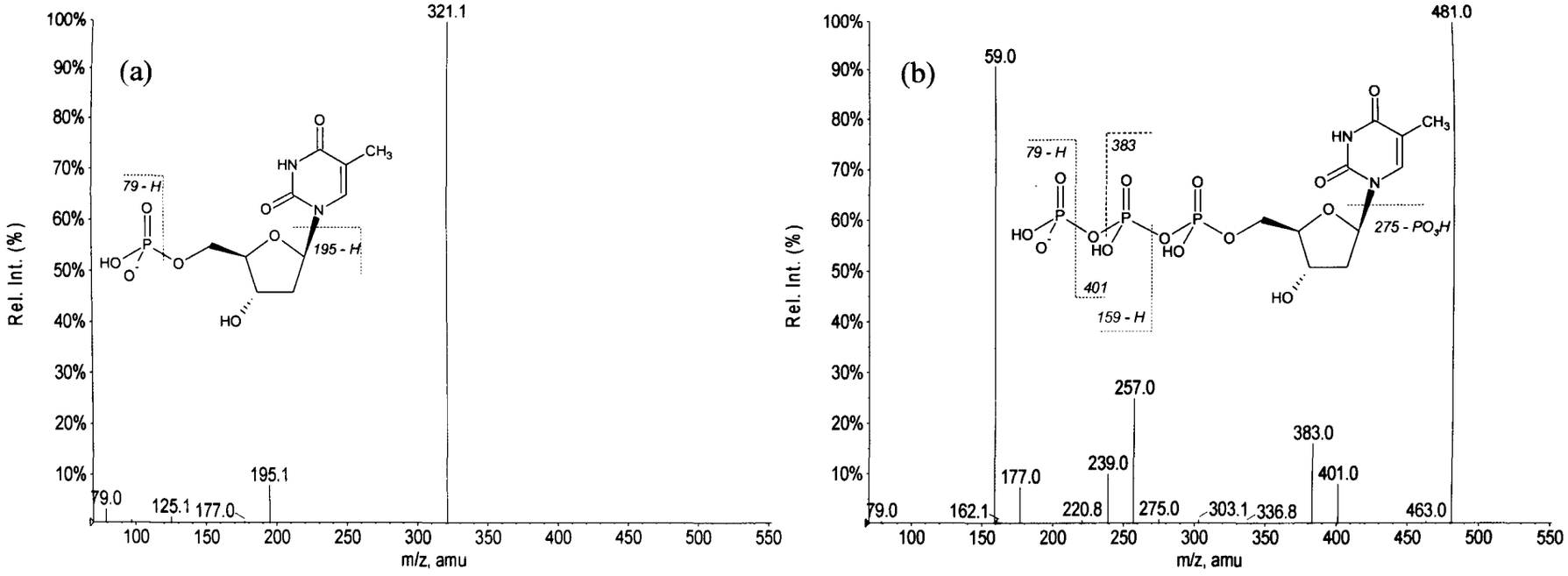

Figure 2.19. EPI spectra of tentatively identified of (a) dTMP and (b) dTTP in *Escherichia coli* MG1655. Tentative identification was obtained using the precursor ion survey scan (*m/z* 79) and confirmation based on the EPI spectra.

2.3.8 Additional analytes containing a phosphate group

Where a number of nucleotides and tentatively identified nucleotides have been successfully profiled in the two bacterial samples, a wide number of other analytes have also triggered the enhanced production ion scan. In both *Pseudomonas aeruginosa* and *Escherichia coli* MG1655 samples, conservatively 70 other compounds triggered an enhanced production ion scan due to the presence of a phosphate group, see Table 2.9 and Table 2.10. These spectra have a number of product ions coupled with a extracted ion chromatographic peak of an S:N of at least 3:1. It was not possible to identify these analytes as nucleotides and hence, the majority of phosphate containing metabolites remain unidentified.

There are a number of possible classes of compounds the unidentified analytes could belong to. Glycerophospholipids, for example, are prevalent in the cell walls of gram negative bacteria (Nikaido and Vaara, 1985; Stryer, 1999) and it has been demonstrated that at least one subclass of glycerophospholipids (See Figure 2.20) can undergo CID to generate an *m/z* 79 with the appropriate collision energy[4].

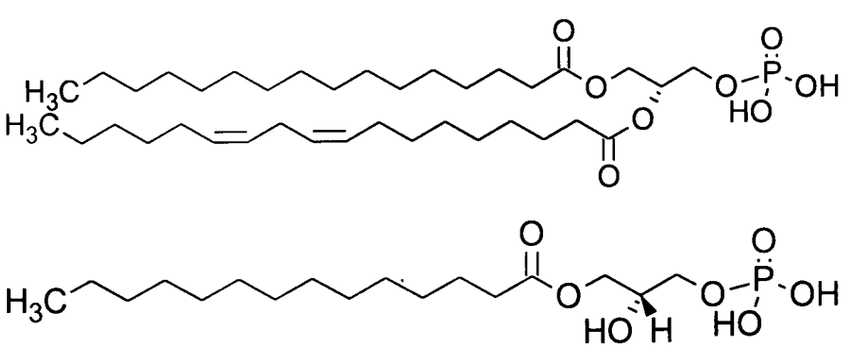

Figure 2.20. Diacylglycerophosphate and monoacylglycerophosphate have been demonstrated to fragment yielding a *m/z* 79 product ion under CID.

[4] http://www.lipidmaps.org/ - accessed on 20th May 2009

Table 2.9. Unidentified analytes containing a phosphate, detected in *Pseudomonas aeruginosa* using the precursor ion survey scan coupled with EPI spectra. Analytes in italics are possibly the same compound, differing by $[M-H]^-$ and $[M+Na-2H]^-$ adducts. Such adducts have been previously reported in ESI^- (Keller *et al.*, 2008; Tong *et al.*, 1999)

Unknowns detected in *Pseudomonas aeruginosa* extract					
Analyte (*m/z*)	Retention time (min)	Charge state	Analtye (*m/z*)	Retention time (min)	Charge state
296.8	1.3	1	606	9.2	1
245.2	2.5	1	618	9.5	1
293	3.3	1	547.1	9.7	1
412.8	3.8	1	442	10.8	1
292.9	***4.2***	***1***	448	11.6	1
314.9	***4.3***	***1***	661.1	12.4	1
412.8	4.64	1	678.1	12.7	1
292.8	4.8	1	595.7	13.9	2
390.8	4.8	1	399.1	14.0	1
456.9	5.2	1	549.3	15.2	1
562.1	6.1	1	535.1	15.3	2
531.1	6.8	1	432.5	17.0	2
565.1	7.0	1	660.8	18.8	2
466	8.8	1	483.6	22.2	2

Table 2.10. Unidentified analytes containing a phosphate, detected in *Escherichia coli* MG1655 using the precursor ion survey scan coupled with EPI spectra. Analytes in italics are possibly the same compound, differing by $[M-H]^-$ and $[M+Na-2H]^-$ adducts. Such adducts have been previously reported in ESI^- (Keller *et al.*, 2008; Tong *et al.*, 1999)

Unknowns detected in *Escherichia coli MG1655* extract					
Analyte (*m/z*)	Retention time (min)	Charge state	Analyte (*m/z*)	Retention time (min)	Charge state
562.6	4.4	1	329.9	12.5	1
289	5.7	1	363	12.6	1
259.9	5.8	1	423.9	12.7	1
261	6.4	1	***678.1***	***13.3***	***1***
259	6.6	1	***700***	***13.4***	***1***
288.9	6.8	1	463.9	13.5	1
587	7.3	1	424	13.8	1
241	7.3	1	595.7	15.2	2
606.1	7.6	1	339	15.4	1
625.3	7.9	1	495.1	15.8	2
563.1	8.3	1	490	16.0	1
565	8.9	1	417	16.7	2
394.8	9.0	1	535.1	17.9	2
618.2	***9.5***	***1***	382.5	18.4	2
640.2	***9.5***	***1***	403.8	18.9	2
618.2	9.5	1	725.1	20.0	2
547.1	9.7	1	560.1	20.2	2
569.1	9.9	1	731.3	20.3	1
302	10	1	660.7	20.9	2
321.1	10.1	1	775.4	21.4	1
547.1	10.3	1	509.7	21.56	3
512.8	11.7	1	765.1	21.6	2
207.5	12.1	1			

There are a number of other glycerophospholipids subclasses present in a biological system that could also, in theory, trigger an EPI scan due to the presence of a phosphate moiety. The use of the hexane in the extraction process is likely to have removed a number of lipids from the extract (Cordell et al., 2008) and precludes them from being the additional source of endogenous phosphate moieties, however, they demonstrate that other phosphate containing compounds can breakdown under CID to generate a *m/z* 79 product ion. Another class of endogenous metabolites to contain phosphate metabolites are the phosphorylated carbohydrates involved in glycolysis, the conversion of glucose into pyruvate. Glucose-6-phosphate, fructose 1,6-bisphosphate and 6-phosphogluconate are representative of the small molecules involved in this wide spread metabolomic pathway (Stryer, 1999). These molecules contain one or more phosphates and have been demonstrated to fragment under CID to form *m/z* 79 $[PO_3]^-$ and / or *m/z* 97 $[H_2PO_3]^-$ and have been found in *Escherichia Coli K12* (Buchholz et al., 2001).

It is worth noting that some co-eluting analytes in Table 2.9 and Table 2.10 (highlighted in bold) are probably different adducts of the same compound. Each pair is 22 amu apart and might be the result of a deprotonated molecule $[M-H]^-$ and a doubly deprotonated molecule with the addition of a sodium adduct $[M+Na-2H]^-$. Although the latter adduct has been previously reported (Keller *et al.*, 2008; Tong *et al.*, 1999), it might be rather unusual.

It could be said that the prevalence of the phosphate group in biological systems demonstrates a limitation of the methodology when applied solely to the analysis of nucleotides. Where the approach taken in this chapter has successfully identified a number of nucleotides in bacterial samples and tentatively identified others, the method is not selective for the detection of nucleotides alone because of the prevalence of the phosphate group in many endogenous compounds. Where such analytes can, on the most part, be distinguished from nucleotides, their presence causes the data analysis task to be considerably more complex and time consuming.

2.4 Conclusion

The analytical approach taken in this chapter has been to use the QqQLit mass spectrometer for the analysis of phosphate containing endogenous analytes, although the analysis has been predominantly focused towards nucleotides and structural analogs. By the use of a precursor ion scan, coupled with full product ion spectra, known analytes and analytes for which reference standards were not immediately available were identified.

By monitoring a common structural moiety, the methodology is not as targeted as SRM approaches commonly taken, consequently, the scope of analytes identified is not limited by the availability of reference standards. In comparison to a previous, relatively broad targeted method (Buckstein et al., 2008), analyzing nucleotide in *Escherichia coli* MG1655, the method described in this chapter compared well. All analytes identified in that previous work were identified by the method described in this chapter; furthermore, a number of deoxy nucleotides were also identified. As such this method is advantageous over other methods currently purposed for nucleotide analysis. Where previous methods have led a targeted approach, in most instances the scope of analytes has been relatively limited, this approach is not so reliant on reference standards and as such a greater number of nucleotides and structurally related analytes have been identified in one method than previously reported.

If this method was to be applied to answer biological questions, the identification of those analytes tentative ascertained would be required. This could be achieved by the purchasing of standards and comparing product ions spectra or, if difficult to obtain, by obtaining the accurate mass of those endogenous compounds by TOF or FTICR to obtain a likely empirical formula.

The precursor ion survey scan speed was assessed on the basis of mass accuracy with the aim of removing the enhanced resolution scan if redundant. It was found that the mass accuracy of the precursor ion scan was dependant on scan speed, and the speed recommended by the software gave the best accuracy of +0.2amu. Faster precursor ion

scan could be used, although the resulting mass shift should be remembered when interpreting the results. Furthermore, the enhanced resolution step provides greater resolution of the pseudomolecular ions of interest, allowing the charge state to be identified. The precision of extracted ion peak areas obtained from a precursor ion scan was also assessed. Although the speeds assessed were too slow for reproducible measurements to be made, by increasing the scan speed an improvement in precision was observed. Quantification of nucleotides by a precursor ion scan could in theory be achievable by increasing the scan speeds further if such an approach was required, although knowledge of the resulting mass shift would be needed.

Where nucleotides have been the focus of the work in this chapter, the phosphate moiety has been the target for this method and it is clear that a wider range of phosphate containing analytes have been identified other than nucleotides alone. Although commonly found in glycerolphosolipids, these lipids had to be removed during extraction due to the overwhelming signal produced and detrimental effect on chromatography. However, other endogenous phosphate containing compounds are likely to be present and contribute to the wide number of unknowns detected. Phosphorylated carbohydrates and nucleotide sugar have all been previously demonstrated to fragment under the correct CID conditions to yield a *m/z* 79 ion. Where the tentative identification of nucleotides, for which reference standards were not immediately available, was achieved by an understanding of the CID product ion spectra, this was difficult for other classes of analytes without a knowledge of prominent product ions. Hence, if this approach were to be more focused on other such analytes, the use of reference standards would be required to understand the resulting fragmentation patters. A full range of reference standards is not required but rather enough to understand likely product ions.

The scope of the methodology outlined in this chapter falls wider than profiling of just endogenous metabolites. The use of the precursor ion scanning method has found application in the field of proteomics, specifically in the analysis of phosphorlayted proteins. Where a number of MS approaches have been applied to the analysis of these proteins and peptide digests, a *m/z* 79 product ions have been observed for

phosphorlayted amino acids serine, threonine and, tyrosine (Annan *et al.*, 2001; Edelson-Averbukh *et al.*, 2006). Furthermore a similar approach outlined in this chapter, employing the QqQLit to monitor *m/z* 79 product ions, has been applied to the analysis of phosphorlayted peptides (Williamson et al., 2006).

It has been demonstrated here that the approach of targeting a common structural moiety can be a successful method for the profiling of endogenous metabolites. Where this method has been used to profile nucleotides, there are other endogenous families of metabolites for which this method could equally be applied, and its application to two related families of bioactive lipids is considered in the next chapters of this thesis.

CHAPTER 3

3 Investigation of endocannabinoids and structural analogs using the QqQLIT

3.1 Introduction

N-acylethanolamines (NAEs) and mono-acylglycerols (MAGs) are lipid classes of which some specific compounds are known to act as signaling molecules in the nervous system (on CB1 and CB2 receptors) and other tissues/organs (Devane et al., 1992). The most widely known of these endocannabinoids are N-arachidonylethanolamine (anandamide, AEA C20:4 ethanolamine) and 2-arachidonylglycerol (2-AG, C20:4 glycerol). Structurally similar compounds N-palmitoylethanolmine (PEA, C16:0 ethanolamine), N-oleoylethanolamine (OEA, C18:1 ethanolamine) and 2-linoleoyl glycerol (2-LG, C18:2 glycerol) can modulate the effect of AEA C20:4 and 2-AG C20:4 via competition for catabolic pathways but are not agonists for CB1 and CB2 receptors and have been called entourage compounds (Ben-Shabat *et al.*, 1998; Di Marzo, 1998; Hanus *et al.*, 2001; Porter *et al.*, 2002; Sugiura *et al.*, 1995); see Figure 3.1. These classes of compounds are comprised of an acyl chain of varying length and degree of saturation coupled to an ethanolamine or glycerol moiety. Previous studies have identified a range of NAEs and MAGs in mammalian tissue (Fu *et al.*, 2007; Kondo *et al.*, 1998a; Mechoulam *et al.*, 1995), but relatively few of these have been investigated for pharmacological and physiological relevance. The presence of a wide range of N-acylethanolamines (NAE) and mono-acylglycerols (MAG) with acyl chains of differing length and degrees of saturation suggest that mammalian tissues can synthesize these compounds from a range of precursor lipids. Despite the discovery of several bioactive NAEs and MAGs, there have been few detailed studies of the NAE and MAG profiles of tissues/organs in mammalian species (Huang *et al.*, 2001; Saghatelian *et al.*, 2004). The reason for this absence of information is mainly due to the lack of suitable analytical methods to provide comprehensive profiling of the individual members of the of NAE and MAG lipid groups.

3.1.1 Nomenclature

Endocannabinoids have been referred to in the literature by a number of nomenclatures. Full systematic names and shorthand names and nomenclatures are all commonly used when describing lipids, detailing the number of carbons, double bonds and positioning of double bonds. For this work the latter approach will be taken, following the method set out for naming fatty acids (IUPAC-IUBMB, 1992), and which has also been previously used to describe endocannabinoids (Leung *et al.*, 2006; Saghatelian and Cravatt, 2005). For example, N-acylethanolamine C20:4 n-6 describes a compound with 20 carbons counting from the carbonyl group. The 4 depicts 4 double bonds and n-6 describes the position of the first double bond, counting from terminal carbon. Further double bonds have a saturated carbon in between. As NAEs and MAG have similar structures apart from the end moiety, NAE or MAG will be placed before the name. Additionally, short hand names for some of the more commonly studied analytes will be used.

3.1.2 Endocannabinoids and their biological action

Interest in these endogenous lipid classes has arisen due to their affinity for and ability to modulate the cannabinoid receptors 1 and 2 (CB_1 and CB_2) and G-protein-coupled receptors found in mammalian tissue (Mathews et al., 1998). CB_1 receptors are predominantly found in the central nervous system (CNS) in the end terminus of nerve cells. These receptors are also detected in the pituitary gland, immune cells and reproductive tissues. CB_2 occurs predominately in immune cells but not exclusively, having also been identified in the CNS (Howlett, 2002; Pertwee, 2006).

The role of the CB1 receptor and its associated agonists on the CNS has been of interest due to its effect on pain relief (Jhaveri *et al.*, 2006; Walker and Huang, 2002; Walker *et al.*, 2002). Activation of the CB1 receptors limits neurotransmitters crossing the presynaptic cleft by modulating function of Ca^{2+} and Na^{+} channels. See Figure 3.2 for a diagrammatical description (Rea *et al.*, 2007).

Arachidonoylethanolamide (20:4)

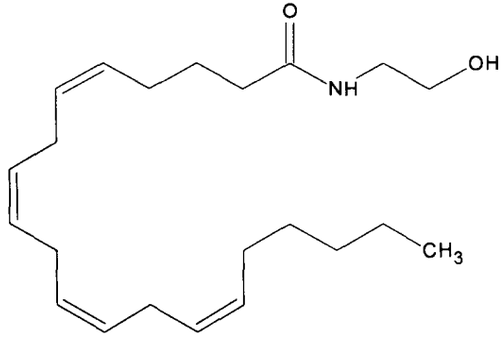

Molecular Formula = $C_{22}H_{37}NO_2$
Monoisotopic Mass = 347.2824 Da

N-Palmitoylethanolamide (16:0)

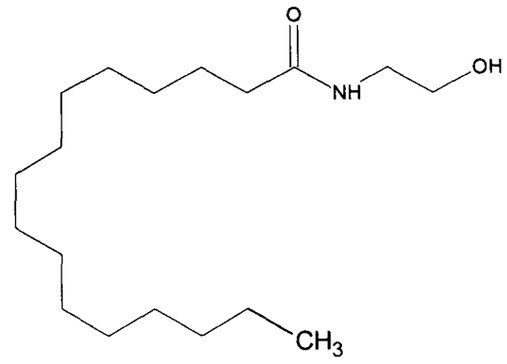

Molecular Formula = $C_{18}H_{37}NO_2$
Monoisotopic Mass = 299.2824 Da

Oleoylethanolamide (18:1)

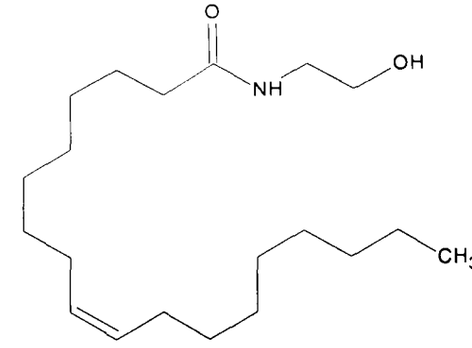

Molecular Formula = $C_{20}H_{39}NO_2$
Monoisotopic Mass = 325.2981 Da

2-Arachidonoyl-glycerol (20:4)

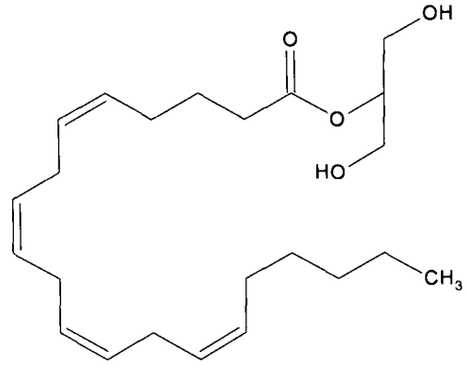

Molecular Formula = $C_{23}H_{38}O_4$
Monoisotopic Mass = 378.2770 Da

2-Linoleoyl Glycerol (18:2)

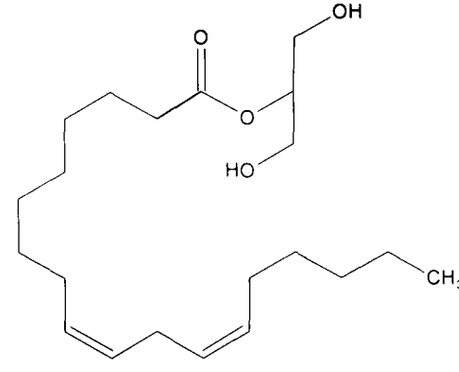

Molecular Formula = $C_{21}H_{38}O_4$
Monoisotopic Mass = 354.2770 Da

Noladin Ether (20:4)

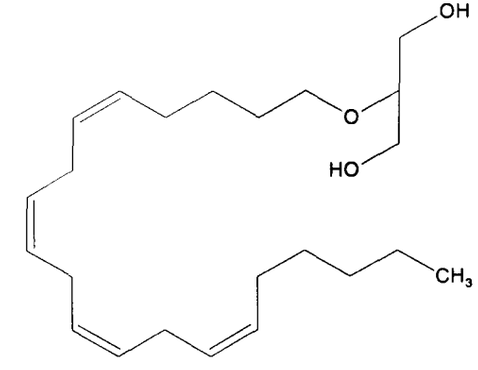

Molecular Formula = $C_{23}H_{40}O_3$
Monoisotopic Mass = 364.2978 Da

Figure 3.1. Known endocannabinoids and entourage compounds.

Endocannabinoids have been identified to have roles outside pain. Embroyonic development may also appear be affected by this class of compounds. Work reported in the literature (Maccarrone et al., 2000) demonstrated a link between decreased expression and inactivity of fatty acid amide hydrolase (a major metabolic route for AEA) in peripheral lymphocytes and an increased risk of miscarriage. It has been demonstrated that boar spermatozoa contain AEA, CB1 receptors and also N-acylphosphatidylethanolamine-selective phospholipase D (NAPE) and fatty acid amide hydrolase (FAAH), enzymes involved in the synthesis and metabolism of AEA (Maccarrone et al., 2005). Endocannabinoids have also been demonstrated to affect appetite (Mechoulam et al., 2006) and have been linked to obesity (Sharkey, 2006).

The biosynthetic pathway for NAEs and MAGs are only partially understood (Ahn *et al.*, 2008; Simon and Cravatt, 2008) at this time. Known routes for synthesis and degradation are described in Figure 3.3. These include metabolic pathways demonstrated *in vitro* but not been observed *in vivo*. Metabolic pathways are similar to arachidonic acid, which is a precursor of many biologically active compounds. The involvement of endocannabinoid signaling in a variety of different pathways has triggered a need to measure changes in endocannabinoid levels in tissues.

3.1.3 Measurement of Endocannabinoids

The analysis of endocannabinoids in biological tissues provides information as to the basal levels of compounds of interest and to changes that may occur following interventions. For such analysis, methodologies must be sensitive, selective and robust. Sensitivity is particularly important in the analysis of endocannabinoids, as some analytes are detected in the low pmol/g concentration range (Richardson *et al.*, 2007; Williams *et al.*, 2007). The most prevalent tool for the analysis of endocannabinoids to date has been chromatography coupled with mass spectrometry.

The methodologies employed in the analysis of endocannabinoids in biological tissues to date fall under three broad categories:

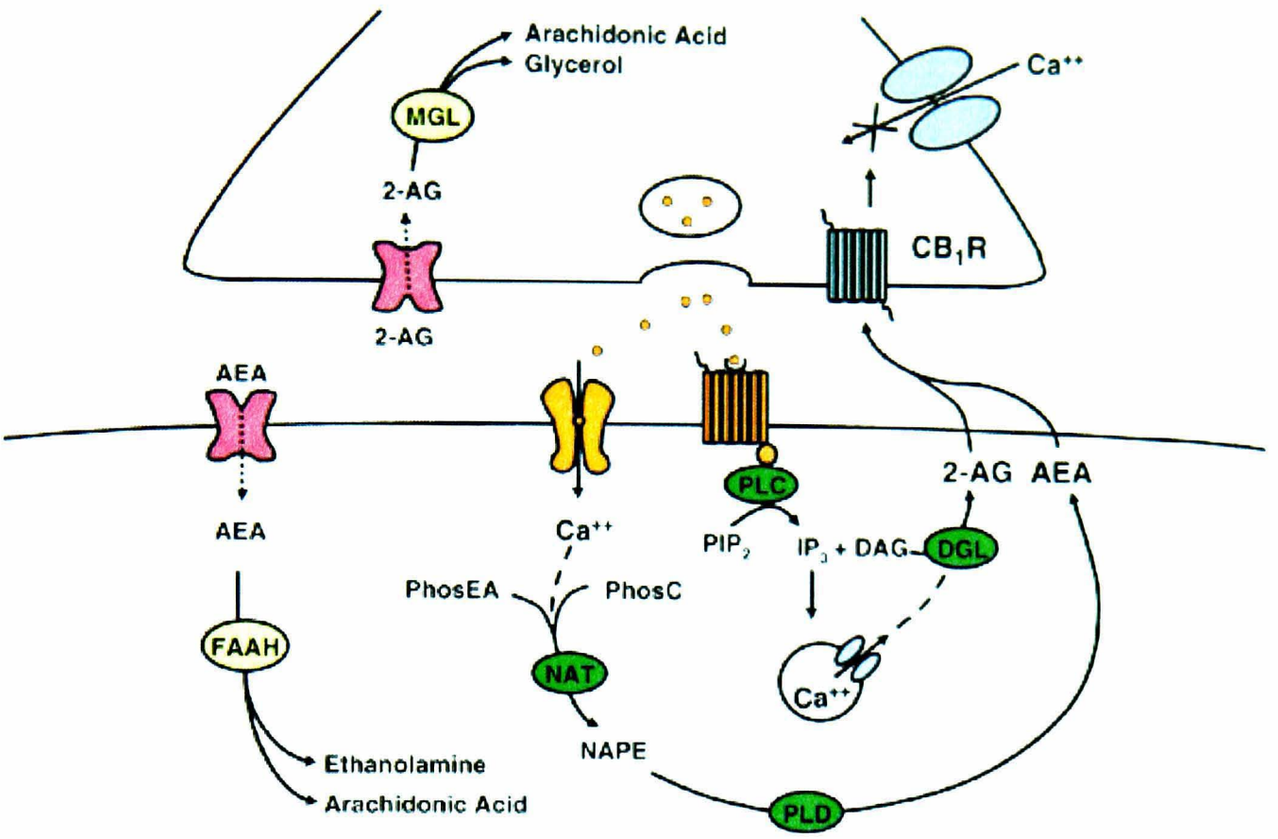

Figure 3.2 - A diagram describing the role of endocannabinoids and CB1 receptors on the mediation of neurotransmitters. Anandamide (AEA C20:4) and 2-arachidonylglycerol (2-AG C20:4) are synthesized on demand following an increase of Ca^{++} from activation of a postsynaptic ion channel. Ca^{++} levels cause the formation of *N*-acyl phosphatidylethanolamine (NAPE) from phosphatidylethanolamine (PhosEA) and phosphatidylcholine (PhosC) via the *N*-acyltransferase (NAT). 2-AG is synthesized from diacylglycerol (DAG) to 2-AG by diacylglycerol lipase (DGL). Both AEA and 2-AG travel to the presynaptic neuron where CB receptors are activated, which in turn inhibit Ca^{++} channels and reduce neural activity. 2-AG is metabolized by monoacylglycerol lipase (MGL) to arachidonyl acid and glycerol where AEA is metabolized by fatty acid amide hydrolase (FAAH) to arachidonic acid and ethanolamine. The diagram was obtained from the literature (Rea et al., 2007) and reproduced with the kind permission of Dr David Finn.

- Targeted, which relies upon the use of standards to optimize the instrument for source/ion optic voltages as well collision energies. Additionally, the fragmentation pattern of each compound is required before selecting the transition ions for multiple reaction monitoring (SRM). Not all standards are commercially available or easily synthesized.
- Global. Reliant on either a knowledge of compounds of interest or studying two or more different biological samples and identifying differences. Access to a comprehensive list of standards is not a pre-requisite for such an approach
- Hypothesizing possible compounds and confirming those by the use of accurate mass and the fragmentation patterns compared to standards.

The coupling of chromatography and mass spectrometry can take a number of forms, but the two that have been most widely used in the analysis of endocannabinoids are GC-MS and LC-MS or LC-MS/MS. Several groups have successfully employed GC-MS in the analysis of endocannabinoids from biological tissues (Bisogno *et al.*, 1997; Fontana *et al.*, 1995; Kondo *et al.*, 1998a; Maccarrone *et al.*, 2001; Obata *et al.*, 2003). While this technique has been successfully used, prior to analysis a lengthy derivatization step is required as well as extraction and purification, making this a complex and difficult procedure. LC-MS alternatively does not require a derivatization step and is therefore advantageous in comparison to GC-MS. Furthermore, the use of LC-MS/MS adds a further mass filter that GC-MS does not process, improving sensitivity and selectivity.

Early methods of endocannabinoid analysis used single quadrupole instruments (Carrier *et al.*, 2004; de Lago *et al.*, 2005; Huang *et al.*, 1999; Wagner *et al.*, 2001). Identification was based on the parent ion mass to charge (*m/z*) ration and retention time compared to standards. Such methodologies required a targeted approach with an understanding of the analytes of interest prior to analysis. With the use of triple quadrupoles, greater selectivity and sensitivity have been achieved and a number of targeted, quantitative methods have been reported in recent years

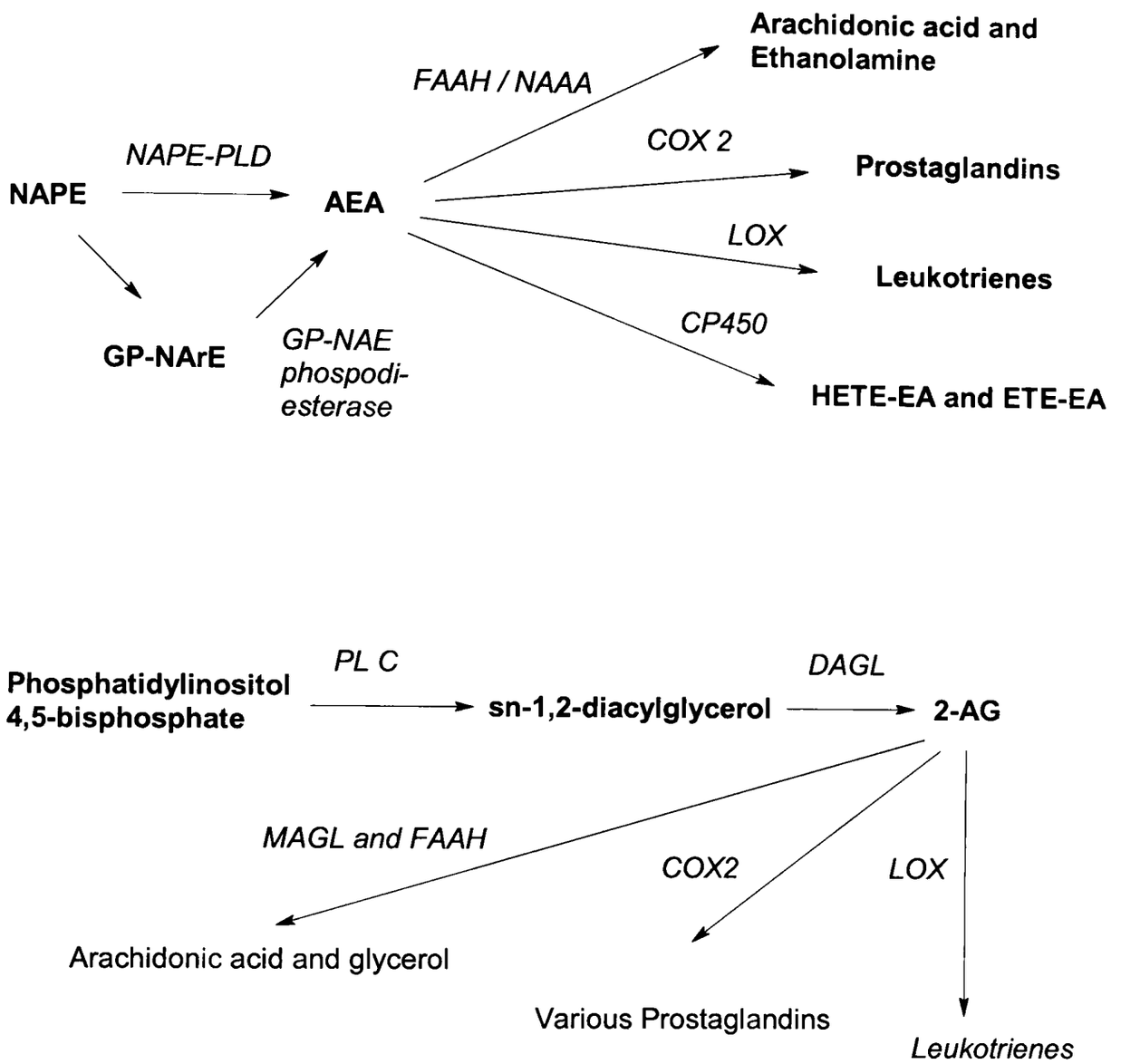

Figure 3.3. Biosynthetic and metabolomic pathways of AEA and 2-AG from *in vitro* and *in vivo* studies. Metabolomic pathways are similar to arachidonic acid, which metabolizes to form biologically active compounds. Abbreviations are *N*-acyl-phosphatidylethanolamines (NAPE), glycerophopspho-N-arachidonoylethanolamine (GP-NArE), fatty acid amide hydrolase (FAAH), *N* – acylethanolamine-hydrolyzing acid amidase (NAAA), cyclooxygenase (COX), lipoxygenases (LOX), cytochrome P450 (CP450), hydroxyeicosatetraenoic acid ethanolamine (HETE-EA), epoxyeicosatrienoic acid ethanolamine (ETE-EA), monoacylglycerol lipase (MAGL) and diacylglycerol lipase (DAGL). Based on information in publications (Ahn *et al.*, 2008; Moody *et al.*, 2001; Simon and Cravatt, 2008; Snider *et al.*, 2007; Tsuboi *et al.*, 2007; Yu *et al.*, 1997)

(Felder *et al.*, 1996; Kingsley and Marnett, 2007; Movahed *et al.*, 2005; Richardson *et al.*, 2007; Vogeser *et al.*, 2006; Vogeser and Schelling, 2007; Williams *et al.*, 2007). Ion traps have also been employed in this field, providing targeted analysis with the additional benefit of full product ion spectra for greater selectivity (Fu *et al.*, 2007; Hansen *et al.*, 2001). A global approach, identifying known and novel endocannabinoids, was demonstrated using a mass spectrometer to scan through potential analytes rather than specifying those of interest beforehand (Saghatelian and Cravatt, 2005; Saghatelian *et al.*, 2004). By the comparison of tissues from wild type and FAAH (an enzyme known to catabolise AEA C20:4 among other NAEs) defective mice, the pseudomolecular ions of NAEs and MAGs varying in concentrations were identified and quantified. Additionally, a novel class of compounds was detected, containing compounds that were also substrates of FAAH; the *N*-acyl taurines, C22:0, C23:0, C24:0 and C24:1. Further work was required to identify the novel class and Fourier-transform ion cyclotron resonance mass spectrometry (FT-ICR) was employed to obtain an accurate mass measurement and consequently an empirical formula. Standards were subsequently synthesized and the MS/MS spectra compared against those observed in biological tissues.

Further work again employed an untargeted global approach to investigate tissues from wild type and fatty acid amide hydrolase defective mice (Mulder and Cravatt, 2006). This work led to the identification of *O*-phoshorylcholine-AEA and a proposed alternative route for NAE catabolism.

A different methodology to identify novel endocannabinoids has been used with some success (Huang et al., 2001). Using LC coupled with an ion trap and a Q-TOF, hypothetical endocannabinoid structures were studied and subsequently targeted in extracted bovine brain. This approach heralded the discovery of *N*-arachidonyl γ-aminobutyric acid and *N*-arachidonylalanine. The use of accurate mass and product ion spectra from both an ion trap and Q-TOF enhanced identification. Such an approach has the obvious limitation that it is reliant on correctly hypothesizing unknown structures.

3.1.3.1 Scope of Quantitative Analysis

Since the identification of AEA C20:4 (Devane et al., 1992) and 2-AG C20:4 (Mechoulam et al., 1995), a number of targeted LC-MS/MS methods have been developed to qualify and quantify these compounds in biological tissues. While AEA C20:4 was identified as a CB1 agonist, docosatetraenylethanolamide (DEA, C22:4) and homo-γ-linolenylethanolamide (20:3) have also been observed to mediate the CB1 receptor (Hanus et al., 1993). However, there are few reported methods which actively look for these two CB1 agonists alongside AEA and 2-AG C20:4. In fact, a search on AEA in Pub Med gives 1947 hits, whereas a search on docosatetraenylethanolamide gives 6. Entourage compounds (PEA C16:0, OEA C18:1, 2-LG C18:1), although not active at cannabinoid receptors, can modulate endocannabinoid actions by influencing their metabolism (Mechoulam et al., 1998). Again, such compounds are only quantified in a relatively small number of targeted approaches (Nomura *et al.*, 2008; Richardson *et al.*, 2007; Williams *et al.*, 2007) or identified by global methodologies where metabolism was interrupted (Nomura et al., 2008).

Table 3.1 and Table 3.2 demonstrate the range of N-acylethanolamines and mono-acylglycerols that have either being identified in biological tissue or have been synthesized and tested for CB1 and CB2 activity. The list is pooled from a number of publications; as of yet, no one methodology has been demonstrated to identify all of these classes of compounds.

The ability of the QqQLIT instrument to survey for structurally similar compounds, coupled with EPI spectra to aid in the identification, could potentially be used in the identification of NAEs, MAGs and other structurally similar metabolites. As demonstrated with nucleotides, compounds with a common structural moiety can be identified using the approaches of precursor ion scanning coupled with full product ion spectra. NAEs such as anandamide NAE C20:4, OEA NAE C18:1 and PEA NAE C16:0 all contain an ethanolamine moiety that could be used in identification. MAGs 2-AG C20:4 and 2-LG C18:1 contain a glycerol moiety that again could be used in

identification. Other NAEs or MAGs consisting of such moieties should also be detectable by such an approach.

The targeted approaches to date are limited by the need for standards for instrumental setup and optimization. The lack of standards covering the range of known NAEs and MAGs has limited the scope of these methods. The purpose of this chapter is to access the survey scan – product ion scan methodology employed in identifying nucleotides to identify NAEs and MAGs. The method, identifying NAEs and MAGs by structural similarities that each class contains, has the potential to identify a far greater range of analytes without the need for standards for each compound. Additionally, it has the potential to identify structural analogs which have not been previously identified.

The role and function of NAEs and MAGs in various tissues has yet to be fully understood and the ability to provide a fuller picture of the analytes present in a given tissue will aid in understanding the role of these compounds.

3.1.4 Aims

The aims of this chapter were:

- To establish an analytical method to identify NAEs and MAGs using survey scans coupled with full product ion spectra.
- Apply the methodology to identify known and novel NAEs or MAGs in rat brain.

Table 3.1. A list of known NAEs taken from the following publications: (Fontana *et al.*, 1995; Hanus *et al.*, 1993; Kondo *et al.*, 1998a; Nomura *et al.*, 2008; Sheskin *et al.*, 1997; Sugiura *et al.*, 1999; Sugiura *et al.*, 2000; Williams *et al.*, 2007).

Acyl Chain	Routinely Studied	Identified but not routinely studied	Synthesized and assessed for CB1 / CB2 activity
C24:1	-	✓	-
C22:6	-	✓	✓
C22:5	-	✓	✓
C22:4	-	✓	✓
C22:1	-	-	-
C22:0	-	✓	-
AEA C20:4	✓	✓	✓
C20:3	-	✓	✓
C20:2	-		✓
C20:1	-	✓	✓
C20:0	-	✓	
C18:2	-	✓	✓
OEA C18:1	✓	✓	✓
C18:0	-	✓	✓
PEA C16:0	✓	✓	✓

Table 3.2. A list of known MAGs taken from the following publications: (Hanus *et al.*, 1993; Kondo *et al.*, 1998a; Nomura *et al.*, 2008; Sheskin *et al.*, 1997; Sugiura *et al.*, 1999; Sugiura *et al.*, 2000; Williams *et al.*, 2007)

Acyl Chain	Routinely Studied	Identified but not routinely studied	Synthesized and assessed for CB1 / CB2 activity
C22:6	-	-	-
C22:5	-	-	-
C22:4	-	-	✓
C22:1	-	-	-
C22:0	-	-	-
C20:5	-	✓	-
2-AG C20:4	✓	✓	-
C20:3	-	-	✓
C20:2	-	-	-
C20:1	-	✓	-
C20:0	-	-	-
C18:3	-	-	✓
2-LG C18:2	-	✓	✓
C18:1	-	✓	✓
C18:0	-	✓	-
C16:0	-	✓	✓

3.2 Methods

3.2.1 Chemicals

Acetonitrile, anhydrous chloroform, ethanol, toluene, ethyl acetate, hexane, ammonium acetate and formic acid were obtained from Fisher Scientific (Loughborough, UK). Anandamide, 2-AG, virodhamine, 2-LG, OEA, PEA, prostaglandin E2 glycerol ester, prostaglandin D2 glycerol ester, prostaglandin $F2_{\alpha}$ glycerol ester, deuterated anandamide (AEA-d8) and deuterated 2-AG (2-AG-d8) were obtained from Cayman Chemicals/ Alexis (Nottingham, UK). Noladin ether was obtained from Tocris Cookson (Bristol, UK). HPLC grade water, purified using an Elga system to 18Ω (Elga, High Wycombe, UK), was used for all experiments. All glassware used in the endocannabinoid extraction method was silanized using trichlorotrimethyl silane, obtained from Sigma–Aldrich (Steinheim, Germany), followed by wash stages with toluene and then methanol prior to use. All solvents and chemicals were of HPLC grade or higher.

Mobile phases were filtered using 0.47 μm nylon filters (Whatman, Maidstone, UK) before use.

3.2.2 Tissue collection

Whole brains were collected from Sprague-Dawley rats (Charles River, UK, fed on 2018 teklad global 18% protein rodent diet). The animals were stunned by a blow to the head followed rapidly by decapitation, typically within 3–4 seconds. Brain tissues were immediately collected and frozen on dry ice. All samples were stored at -80°C until required. Tissue collection was carried out by Professor David Kendall and Dr. Victoria Chapman, School of Biomedical Sciences, University of Nottingham

3.2.3 Tissue extraction

Tissues were extracted by a previously published method (Richardson et al., 2007). The left hemisphere of each brain was homogenized by hand in a silanized glass homogenizer in 8 ml of ethyl acetate / hexane (9:1 v/v). Water (10% of extracted volume) was added and the content transferred to a centrifuge tube. Centrifugation was performed at 7000 x g for 15 min and the temperature maintained at 4°C, resulting in two layers. The supernatant was removed and the process repeated a further two times to optimize recovery. Supernatants were then subsequently pooled and the solvent removed by centrifugal evaporation, set at room temperature, for approximately 40 min.

3.2.4 Preparation of standards

AEA, AEA-d8, OEA and PEA 1mM stock solutions were prepared in ethanol. 2-AG, AG-d8 and 2-LG were prepared in acetonitrile. All stock solutions were stored at -80°C and diluted as appropriate in ethanol, acetonitrile or mobile phase immediately before sample preparation and analysis.

3.2.5 LC-MS/MS instrumentation and conditions

All survey and MS/MS experiments were conducted on a 4000 QTRAP® (QqQLit) (Applied Biosystem, Foster City, CA, USA) equipped with a TurboIon source used in positive ion electrospray mode. A Windows XP (Microsoft, Redmond, WA, USA) workstation running Analyst (version 1.4.1) was used for data acquisition and processing.

Accurate mass measurements were conducted on a Waters Q-TOF (Waters, UK) and controlled by a Windows XP workstation running MassLynx (version 1.4). Initial instrument setup was performed by direct infusions of standards AEA and 2-AG (25μM). Masses between *m/z* 60 and 1000 were collected using a ramped cone voltage of 18 and 25 V. The instrument was run in single stage MS mode with the reflector set to V formation. Monoisotopic masses of potential NAEs and MAGs were obtained and

compared against theoretical values. The difference was reported in parts per million (ppm) (Huang et al., 2001) and calculated as follows :

$$ppm = (measured\ mass - theoretical\ mass / theoretical\ mass) * 10^6$$

3.2.5.1 MS parameters

Initial instrumental settings were obtained using direct infusion of AEA, OEA, PEA and 2-AG in 1:1 (v/v) mobile phase A and B. All compounds form strong $[M+H]^+$ pseudo molecular ions.

3.2.5.2 Declustering potential

Declustering potential (DP) is a manufacture-specific name for the voltage applied to draw ions into the mass spectrometer from the ionsource (referred to as cone voltage by other instrument manufacturers). The DP can have a profound effect on the sensitivity of a method: too low a value and too few ions are drawn in, too high and the ions can fragment prior to reaching the first quadrupole and are not detected. The DP applied for the survey scan methodology was required to cover the range of known and potentially unknowns analytes found in biological tissues. Using NAE standards, the optimum DP was assessed.

The optimum DP for each of the standards was obtained by direct infusion of standards in 50:50 (v/v) mobile phase A:B and fitted with an ESI source in positive mode while systematically increasing the declustering potential from 0 to 400 V. The DP for ethanolamine survey scans was set at 60 V and at 90 V for the glycerol survey scan.

3.2.5.3 Survey scan collision energy

PI or NL survey scans are designed to identify a specific *m/z* product ion or neutral loss resulting from CID fragmentation of the pseudomolecular ion. One parameter crucial for the formation of these ions is the collision energy (CE), not to be confused with the CE

associated with the EPI scan following a PI or NL scan, which is separate. As with the DP, to establish the optimum CE for NAEs and MAGs, reference standards were employed.

AEA C20:4, OEA C18:1, PEA C16:0 and 2-AG C20:4 were infused, the collision energy increased between 5 and 130 volts and the intensity of the product ion *m/z* 62 (ethanolamine moiety) for NAEs and *m/z* 287 for MAGs was plotted. A CE of 35V was selected for NAEs and 20 V for MAGs.

3.2.5.4 Precursor ion and neutral loss scan parameters

The *m/z* 62 precursor ion scan ranged from 200 to 800 amu in 2 seconds and the *m/z* 92 neutral loss scan ranged from 200 to 800 amu in 2.2 seconds. In both methods the quadrupoles were set to unit resolution. The mass range chosen was thought to cover the range of analytes expected. The scan speed was chosen by the software but was subsequently tested and used on the basis of mass accuracy, with such a speed providing measurements no greater than +0.3 amu in error. Such errors are inherent in these scans on this instrument, and are corrected for by the enhanced resolution scan that follows each survey scan.

3.2.5.5 EPI optimization

The EPI scan function utilizes the linear ion trap to store, concentrate and scan product ion spectra. A critical factor for the production of product ion spectra is the collision energy applied to the molecular ion. In this instance, where a variety of structures and masses are analyzed, a spread of collision energies was applied. AEA C20:4, OEA C18:1, PEA C16:0 and 2-AG C20:4 were infused and the collision energy and collision energy spread increased. Where the optimum CE for survey scans should yield the most intense signal, this is not necessarily the case for the EPI scan. In this instance the desired result is a spread of structurally significant product ions. Achieving this can be a fine balancing act due to the limited number of reference standards available and the

prospect of unknowns with a variety of masses and structures. Consequently, Collision energies of 35 ± 20 V for NAEs and 30 ± 10 V for MAGs were chosen.

3.2.5.6 Limit of detection

To compare the sensitivity of the survey scans with other analytical methods, the lower limit of detection (LLOD) was determined. The LLOD is often defined in terms of signal to noise ratio (*S/N*) - the lowest concentration that demonstrates an analyte signal three time that of the background noise (Kharbouche *et al.*, 2009; Martens-Lobenhoffer *et al.*, 2009).

The LLOD for PI 62 and NL 92 survey scans (coupled with EPI scanning) was calculated on standards AEA, OEA, PEA and 2-AG using the LC-MS/MS method. Three injections were carried out per concentration. Due to the slow duty cycle of these scans, and to the consequently reduced number of data points across a peak, it was not always possible to achieve an *S/N* value of 3:1; therefore the lowest detectable peak and the resulting *S/N* was recorded.

3.2.5.7 Chromatography

Chromatography was performed as described in a published method (Richardson et al., 2007) and carried out on a Shimadzu series 10AD VP liquid chromatography system equipped with binary pumps, a vacuum degasser, a SILHTc autosampler and column oven (Shimadzu, Columbia, MD, USA). The LC column was a Thermo Hypersil–Keystone HyPurity Advance column (100 x 2.1mm i.d., 3 µm particle size) with a mobile phase flow rate of 0.3ml/min. Gradient elution mobile phases consisted of A (water, 1 g/L ammonium acetate and 0.1% formic acid) and B (acetonitrile, 1 g/L ammonium acetate and 0.1% formic acid). The gradient started at 45% B, increasing to 55% after 2 min and then increasing again to 65% at 6.5 min; this was maintained until 9 min, with subsequent re-equilibration at 45% B for a 6 min period. Column temperature

was maintained at 40°C and sample temperature was maintained at 4°C in the auto sampler during analysis.

3.2.6 Compound identification and wider searching

Identification of unknowns was based upon the *m/z* of the pseudomolecular ion and the resulting product ions, comparing common fragment patterns with structurally similar reference standards. To further identify compounds, and to identify them within the literature, two approaches were taken. One was to search for chemical names in literature search engines. This approach had mixed results, as not all publications describe analytes by their full systematic name. The other was by structural / empirical searches on web-based databases that link to the literature. No one approach was sufficient, and instead a mixed approach, using both methods, was required to uncover the appropriate information. The databases used are listed below:-

- National Institute of Health's molecular libraries initiative (http://pubchem.ncbi.nlm.nih.gov/)
- Lipid Maps (http://www.lipidmaps.org/)
- Lipid Library (http://www.lipidlibrary.co.uk/)
- SciFinder (http://www.cas.org/products/scifindr/sfweb/)

3.3 Results and discussion

3.3.1 Optimization of MS parameters

3.3.1.1 Declustering potential

The optimum declustering potential (DP) for each of the standards was obtained by direct infusion while systematically increasing the declustering potential from 0 to 400V. Optimum values of 51, 70, 50 and 60 V respectively were obtained; see Figure 3.4. Over the range of saturation (4 double bonds to an unsaturated acyl chain) and acyl chain length (C20 down to C16) of the standards infused, there is significant overlap in the optimum declustering potentials for the NAEs. For MS experiments where only one DP is employed, this fortuitous overlap enables one value to be applicable to reference standards and also to be the best estimate of an optimum value for untested NAEs that might be encountered in biological tissues.

For MAGs, only MAG 2-AG C20:4 was available at the time of this work and the declustering potential for all MAGs is consequently taken from MAG 2-AG C20:4.

3.3.1.2 Survey scan collision energy

AEA C20:4, OEA C18:1, PEA C16:0 and 2-AG C20:4 were infused and the collision energy increased between 5 and 130 volts and the intensity of the product ion *m/z* 62 (ethanolamine moiety) for NAEs and *m/z* 287 for MAGs was plotted; see Figure 3.5. Optimum values of 41, 35 and 35 were obtained for NAEs. With a wide optimum value and overlap of the NAEs, a CE of 35V was selected. Only 2-AG was available for MAGs and consequently the optimum CE (20V) for MAGs was taken from this standard.

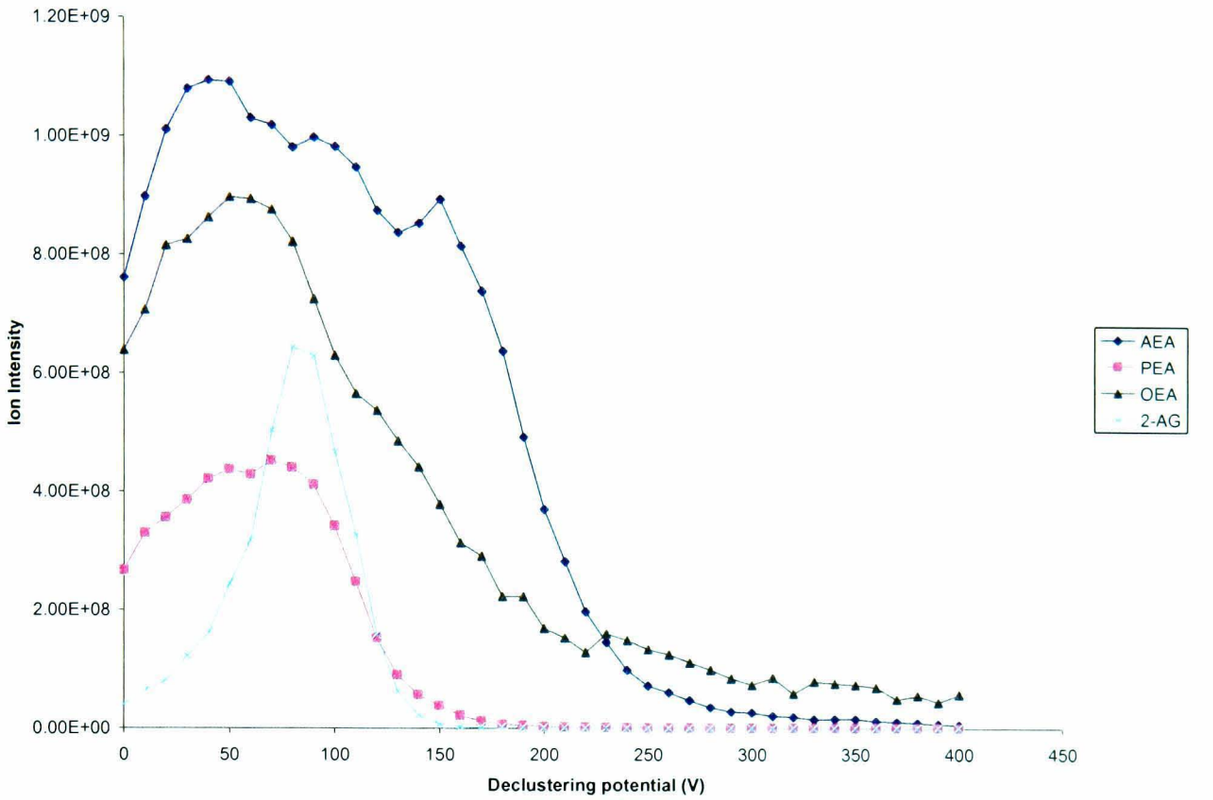

Figure 3.4. Optimum declustering potential for the pseudomolecular ions of AEA, OEA, PEA and 2-AG. The NAEs demonstrate significant overlap, enabling a general value of 60V to be chosen which will be applicable not only to the standards infused but more likely than not also to other, unobtainable NAEs. For MAGs, only 2-AG was available at the time of this work; hence the declustering potential for all MAGs is taken from 2-AG.

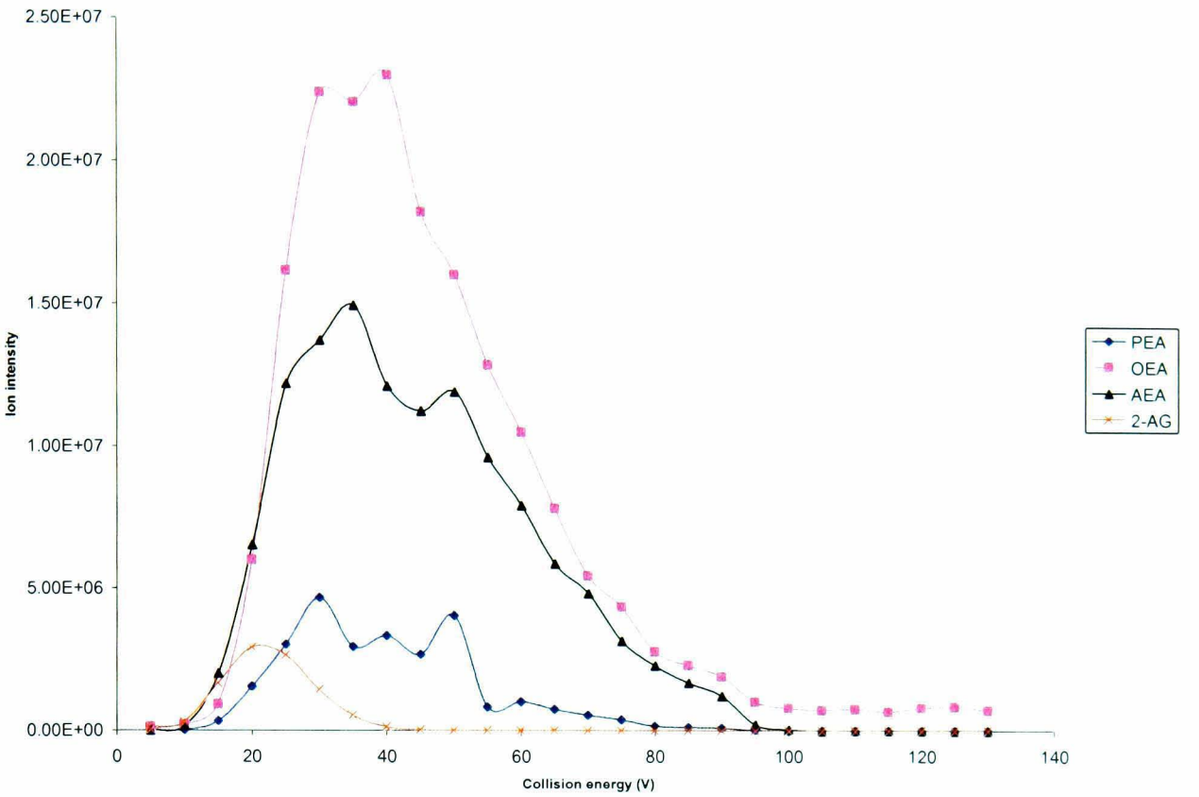

Figure 3.5. Optimum collision energies for the PI and NL survey scans. NAEs have a wide, optimum CE to choose from. 2-AG demonstrates that the MAGS have a smaller range from which a collision energy will provide the required product ions for identification.

3.3.2 Development of PI and NL scan modes

AEA C20:4, PEA C16:0 and OEA C18:0 reference standard solutions were used to develop survey scans for NAEs, and MAG 2-AG C20:4 for MAGs. All reference standards produced a strong $[M+H]^+$ pseudomolecular ion. MS/MS product ion spectra rather than EPI spectra were employed to determine suitable product ions for precursor ion or neutral loss scans due to differences between results of the two scan functions, see section 3.3.5. EPI was subsequently used for analyte identification latter on.

The pseudomolecular ion of AEA fragments under CID to produce an informative pattern of product ions; see Figure 3.6. The *m/z* 330 $[M+H]^+$ (- 18) ion suggests a loss of H_2O from the pseudomolecular ion. Product ion *m/z* 287 $[M+H-C_2H_7NO]^+$ is the result of a cleavage of the amide bond with the loss of the ethanolamide moiety as a neutral, probably due to a charge migration mechanism. The ion *m/z* 269 is the likely result of the same cleavage but with the additional loss of water to form $[M+H-C_2H_7NO-H_2O]^+$, the mechanism of which is unknown at this time. A large *m/z* 62 ion was observed and can be attributed to the ethanolamine moiety, with the subsequent loss of $[M+H-C_{20}H_{30}O]$ as a neutral. Identification of these ions is consistent with that reported by other groups (Huang *et al.*, 2001; Kasai *et al.*, 2003; Koga *et al.*, 1997; Liu *et al.*, 2006). Similar fragmentation of the amide C-N bond has previously been observed in *N*-acylhomoserine lactones (Morin et al., 2003) and aromatic amides (Tu and Harrison, 1998). Ions *m/z* 259 $[M+H-C_3H_7NO_2]^+$ and 245 $[M+H-C_4H_9NO_2]^+$ are the likely results of cleavages along the acyl chain, close to the amide group and indicative of the length and saturation of the acyl chain, along with *m/z* 287 and 269. A very recent publication has attempted to assign the multitude of product ions from *m/z* 91 up to 259 that result from CID of AEA C20:4 and of other unsaturated NAEs and MAGs (Thomas et al., 2009). Such ions are thought to occur due to charge remote fragmentation, a common mechanism for long chain alkyls to undergo, assuming collision energies are high enough (Cheng and Gross, 2000). Where product ions have been assigned structures, it is difficult to use these ions to ascertain structures of unknowns, due to the high and potentially confusing number of ions which occur under

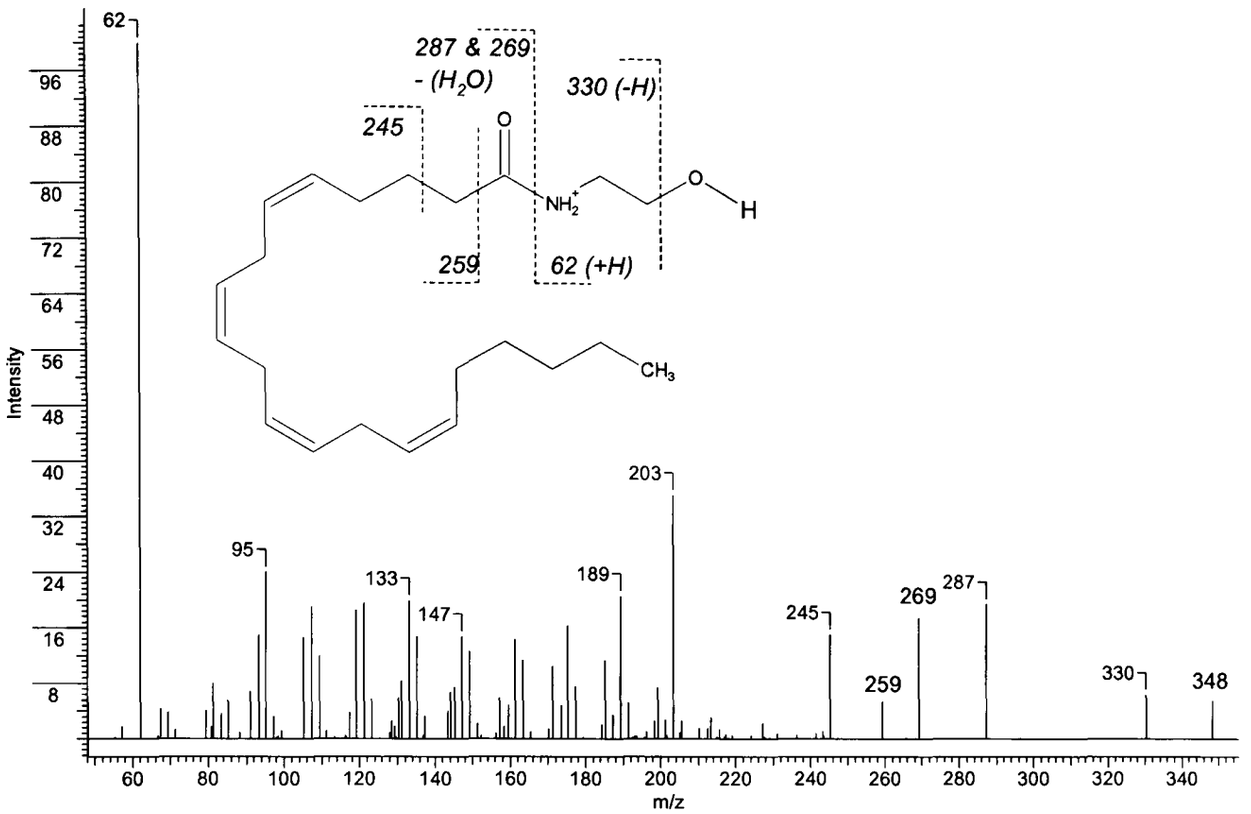

Figure 3.6. MS/MS spectra of NAE AEA C20:4 collected by direct infusion ESI$^+$ mode. A curtain gas of 15, capillary voltage of 4000V, source temperature of 175°C , gas values of 25 (no units), collision gas of 9 (no units) and collision energy of 20 V were used. The most intense pseudomolecular ion was the protonated [M+H]$^+$ ion at *m/z* 348. High mass fragments of *m/z* 287, 259 and 245 provide information as to the length and saturation of the acyl chain. The ion *m/z* 62 is indicative of the ethanolamine moiety.

these conditions. Furthermore, this work has assigned *m/z* 259 and 245 not as bond cleavages close to the acyl bond, as described in Figure 3.6, but rather between the 2nd and 3rd and between the 3rd and 4th carbons next to the terminal end of the acyl chain, respectively. Theoretically, the source of these fragments could come from either location, and to clarify this point deuterated standards could be employed. Previous work conducted on *N*-arachidonylglycine (similar to AEA C20:4, with the same acyl chain but differs by a R-CONHCH$_2$COOH rather than R-CONHCH$_2$CH$_2$OH end moeity) using the accurate mass capabilities of a QTOF instrument identifies the *m/z* 245 ion resulting from the cleavage as described in Figure 3.6 rather than close to the terminal carbon (Huang et al., 2001). Nevertheless, the question as to the exact source of these two ions does not affect their use as a diagnostic tool for the identification of AEA C20:4 or of other NAEs where standards are not available.

OEA C18:1 and PEA C16:0 provided significantly different spectra (Figure 3.7 and Figure 3.8, respectively). OEA C18:1 demonstrated a reduced intensity of the high mass ions resulting from the amide cleavage (and resulting loss of water) compared to the polyunsaturated AEA C20:4, and no ions indicative of the cleavage of the acyl chain were detected. The strongest, high mass ions were the protonated pseudomolecular ion $[M+H]^+$ and the loss of water $[M+H - 18]^+$, with the additional loss of ·OH radical (or NH_3) $[M+H - 17]^+$ at *m/z* 308.3 and 309.3, respectively. An intense ion at *m/z* 62, indicative of the ethanolamine moiety, was present. The spectrum was consistent with others previously reported (Koga *et al.*, 1997; Richardson *et al.*, 2007).

NAE PEA C16:0, with an unsaturated acyl chain, demonstrated less fragmentation, leading to higher mass ions, than monosaturated NAE OEA C18:1 and polyunsaturated AEA; see Figure 3.8. Neither ions resulting from the amide cleavage nor any from the acyl chain were detected. The lack of these diagnostic ions was independent of the collision energy. As with NAE OEA C18:1, the strongest high mass ions are the protonated pseudomolecular ion $[M+H]^+$ and the loss of water $[M+H-18]^+$ with the additional loss of ·OH radical (or NH_3) $[M+H-17]^+$ at *m/z* 282.3 and 283.3, respectively.

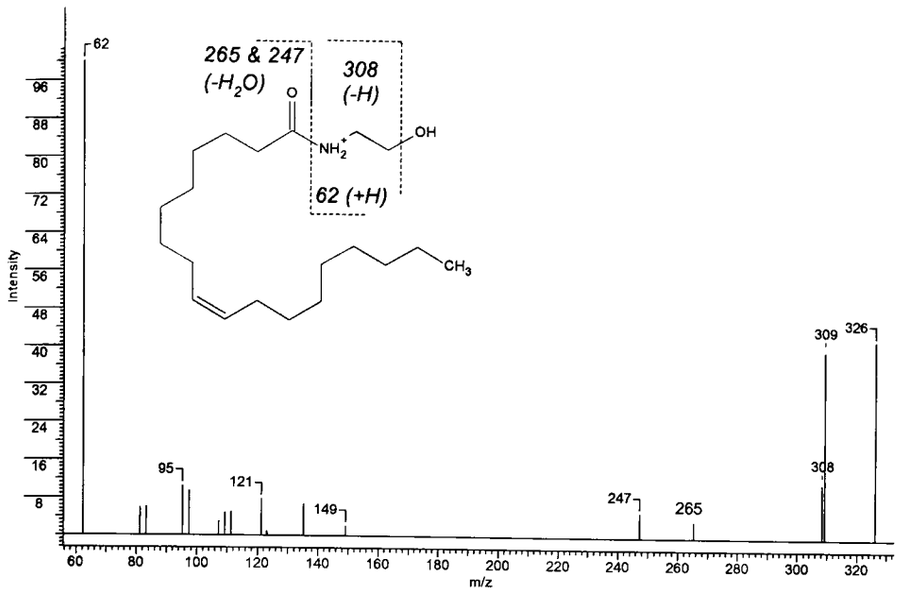

Figure 3.7. MS/MS spectra of NAE OEA C18:1 under ESI$^+$ CID conditions. A curtain gas of 15, capillary voltage of 4000V, source temperature of 175°C , gas values of 25 (arbitrary units), collision gas of 9 (arbitrary units) and collision energy of 20 V were used. There is a lack of high mass fragmentation occurring from the acyl chain, unlike the polyunsaturated AEA. Fragmentation from the cleavage of the amide bond and subsequent loss of water is present, but at lower relative levels compared to AEA. The ion *m/z* 62, indicative of the ethanolamine moiety, is present.

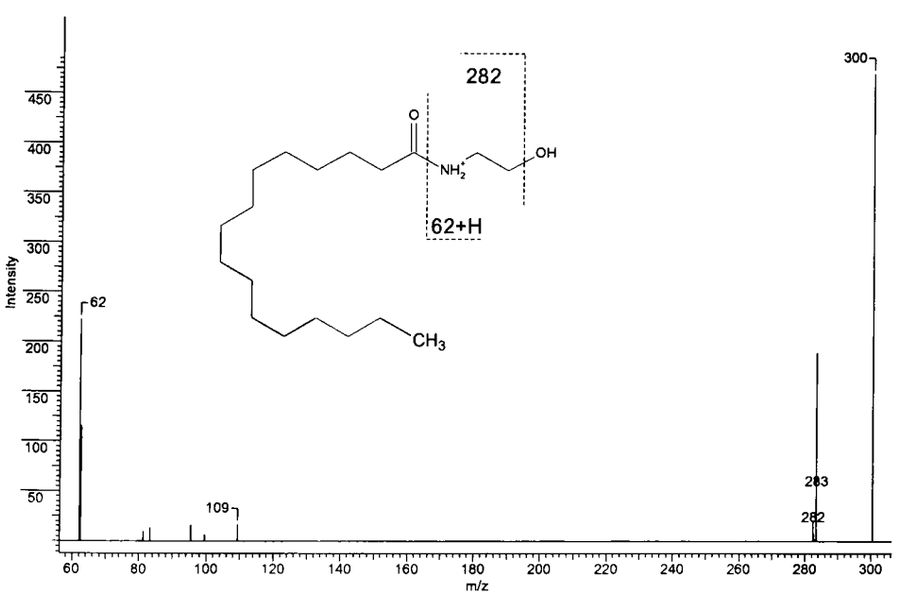

Figure 3.8. MS/MS spectra of NAE PEA C16:0 under ESI$^+$ CID conditions. A curtain gas of 15, capillary voltage of 4000V, source temperature of 175°C , gas values of 25 (arbitrary units), collision gas of 9 (arbitrary units) and collision energy of 20 V were used. There is a lack of high mass fragmentation occurring from the acyl chain unlike the polyunsaturated AEA. Additionally, fragmentation from the cleavage of the amide bond is not detected. The ion *m/z* 62, indicative of the ethanolamine moiety, is present.

An intense ion at *m/z* 62, indicative of the ethanolamine moiety, is present. The spectrum is consistent with another reported (Richardson et al., 2007). AEA C20:4, PEA C16:0 and OEA C18:1 fragmentation under CID conditions produces the ethanolamine *m/z* 62 product ions. As this ion is indicative of the ethanolamine group and structurally core to all NAEs, it was chosen as the identifier for a PI survey scan.

MAG 2-AG C20:4 MS/MS spectra can be found in Figure 3.9. There are strong similarities between the fragmentation pattern of MAG 2-AG C20:4 and AEA C20:4. The *m/z* 287 ion is the result of a cleavage of the ester linkage $[M+H - C_3H_8O_3]^+$, and 269 is likely the further fragmentation of that ion by the loss of H_2O $[M+H - C_3H_8O_3 - H_2O]^+$. Ions *m/z* 259 $[M+H-C_4H_8O_4]^+$ and *m/z* 245 $[M+H-C_5H_{10}O_4]^+$ are the probable results of cleavages along the acyl chain close to the ester linkage. Such a fragmentation pattern might be expected as both AEA C20:4 and 2-AG C20:4 have the same acyl chain. Where NAEs produce an ethanolamine ion under CID, MAGs do not form a glycerol product ion. However, the ion *m/z* 287 cleaves from the pseudomolecular ion to produce a neutral of 92 amu, the neutral glycerol moiety. This neutral allows the use of an NL survey scan in identifying MAGs. The fragmentation ions compare well against the previously reported literature (Richardson et al., 2007).

Noladin Ether (NE), a known CB1 agonist (Hanus et al., 2001), has been detected in rat brain (but not spleen, heart or liver) (Fezza et al., 2002). This analyte is structurally similar to MAG 2-AG C20:4, and differs only in the bridge between the glycerol and acyl chain -the former linkage having ether where the latter is an ester. Fragmentation under CID conditions (see Figure 3.10) yields a loss of *m/z* 273 at the same location as MAG 2-AG C20:4 yields *m/z* 287 - $[M+H-C_3H_8O_3]^+$; consequently both compounds demonstrate a neutral loss of 92 Daltons. Therefore a neutral loss scan of 92 Daltons will not be specific for MAGs but also NE and structural analogues (Richardson et al., 2007). However, where both endogenous compounds fragment to form $[M+H-C_3H_8O_3]^+$ under CID, only MAG 2-AG C20:4 fragments to form $[M+H-C_3H_8O_3-H_2O]^+$, the loss of water from that ion. Consequently this is a diagnostic ion which can be used to discriminate between the ester and ether linked analogue.

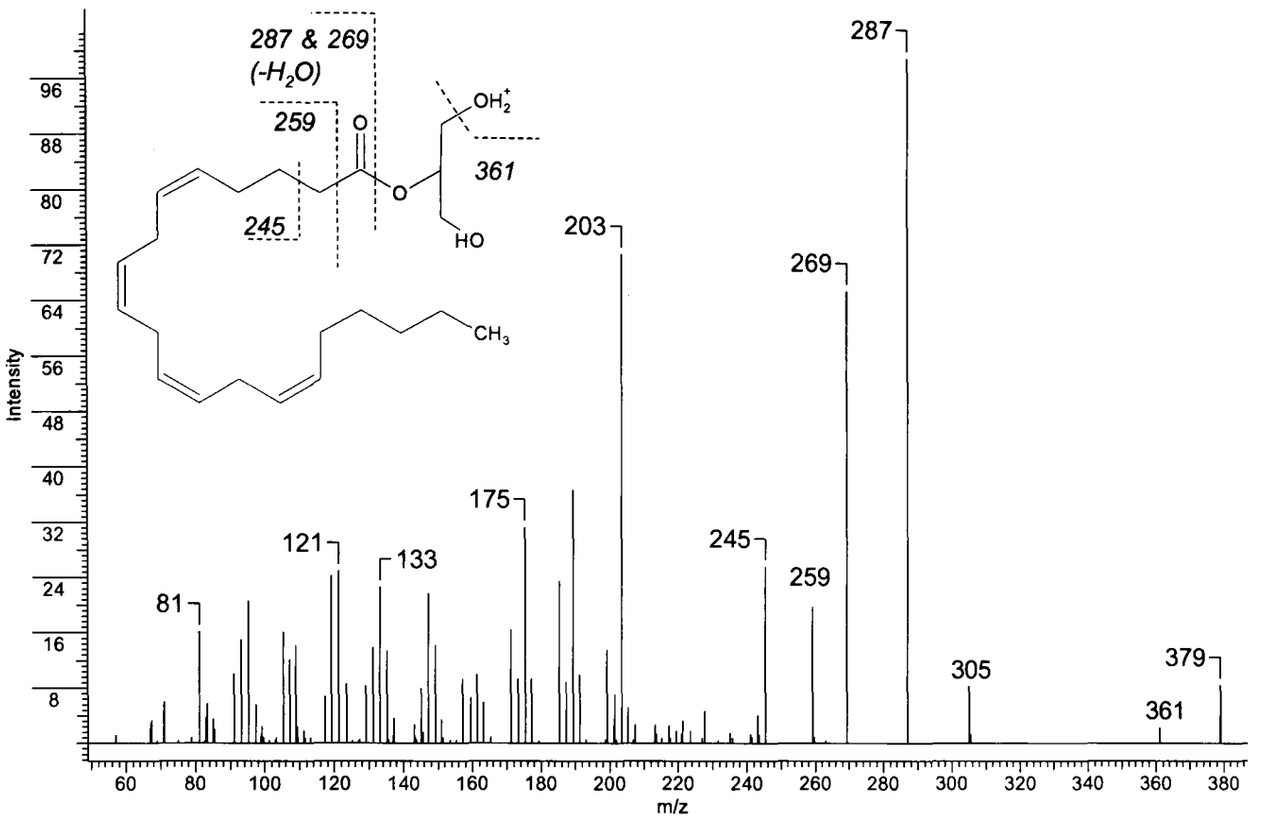

Figure 3.9. MS/MS spectra of MAG 2-AG C20:4 collected by direct infusion ESI$^+$. A curtain gas of 15, capillary voltage of 4000 V, source temperature of 175°C, gas values of 25 (arbitrary units), collision gas of 9 (arbitrary units) and collision energy of 25 V were used. The most intense pseudomolecular ion was the protonated [M+H$^+$] ion at *m/z* 379. High mass fragments of *m/z* 287, 259 and 245 provide information as to the length and saturation of the acyl chain (as with AEA, due to the C20:4 acyl chain). The site of protonation is a best estimate.

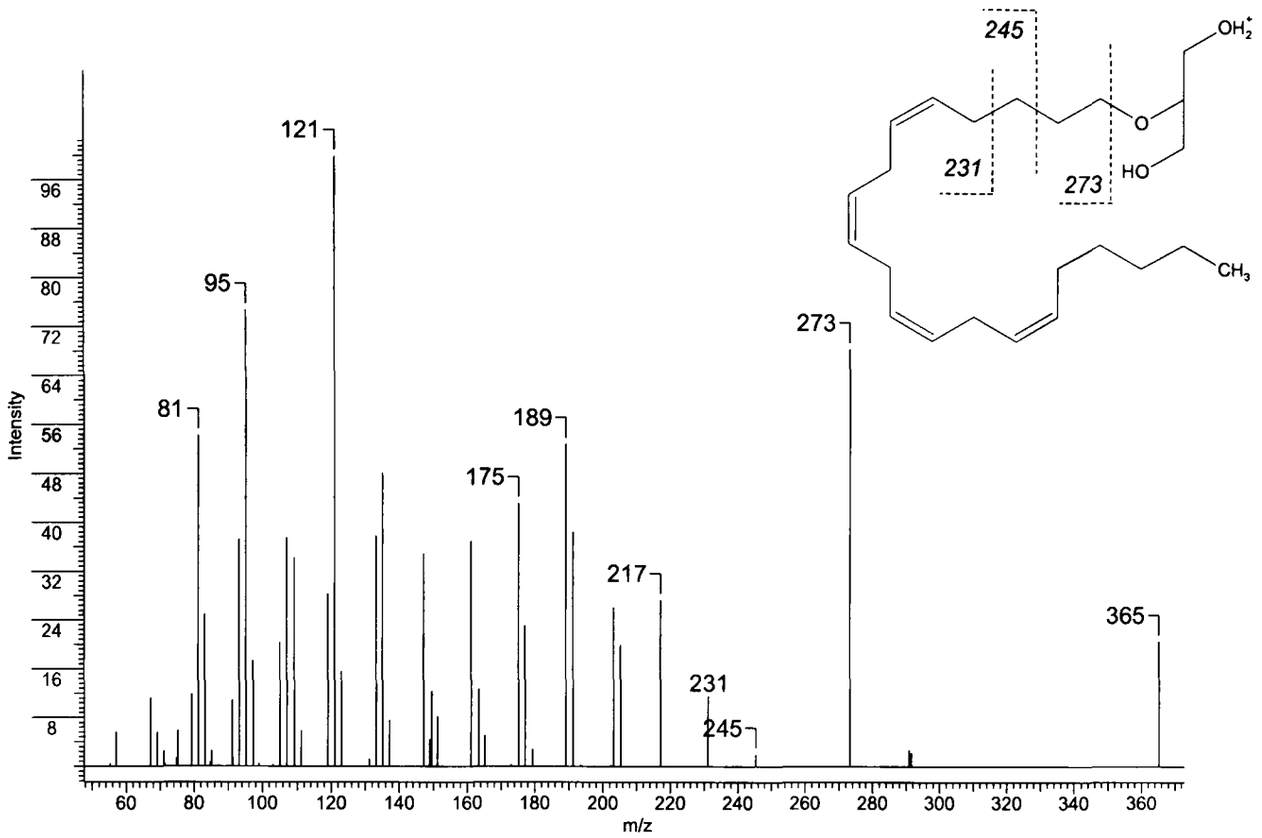

Figure 3.10. MS/MS spectra of Noladin Ether collected by direct infusion ESI$^+$. A curtain gas of 15, capillary voltage of 4000 V, source temperature of 175°C, gas values of 25 (arbitrary units), collision gas of 9 (arbitrary units) and collision energy of 25 V were used. The most intense pseudomolecular ion was the protonated [M+H$^+$] ion at *m/z* 365. High mass fragments of *m/z* 273, 245 and 232 provide information as to the length and saturation of the acyl chain. The site of protonation is a best estimate.

3.3.3 Testing precursor ion and neutral loss survey scans on reference standards

To demonstrate that the precursor ion and neutral loss survey scans were able to correctly identify NAEs and MAGs in a chromatographic run, the methods were tested against their respective reference standards. AEA C20:4, OEA C18:1 and PEA C16:0 were made up to a concentration of 500nM in ethanol. MAG 2-AG C20:4, which has poor ionization efficiency under ESI^+ conditions in comparison with NAEs (Richardson et al., 2007), was made up separately at 10 μM in ethanol. Injections of the two mixes were made and separation was carried out as specified in section 3.2.5.7. MS analysis was performed by the two survey scans coupled with EPI product ion spectra.

The extracted chromatograms of the precursor ion and neutral loss survey scans can be seen in Figure 3.11. All analytes were successfully detected, and the resulting EPI spectra generated matched those obtained from direct infusion experiments of the reference standards.

3.3.3.1 Structural variations of NAE and MAG metabolites and compatibility with survey methodology

Where metabolites have strong structural similarities to NAEs and MAGs, there remains the possibility that variations could cause an incompatibility with either the LC or mass spectrometry to the extent that detection is not observed. Additions to the ethanolamine or glycerol moieties, or changes to the acyl chain that in turn change fragmentation of the molecule, leading to the lack of these signature ions being formed, would render such analytes undetectable by the methods described here. Furthermore, changes to the acyl chain that cause an increase in polarity of the molecule could have a detrimental effects on the chromatography. To look into this possibility, prostaglandinglycerols standards were used to access the suitability of the methodology for at least one class of metabolite. Prostaglandinglycerols PGE_2-G, PGD_2 and $PGF_{2\alpha}$ were purchased and analyzed by the NL method. Using this method, all three compounds were detected. The

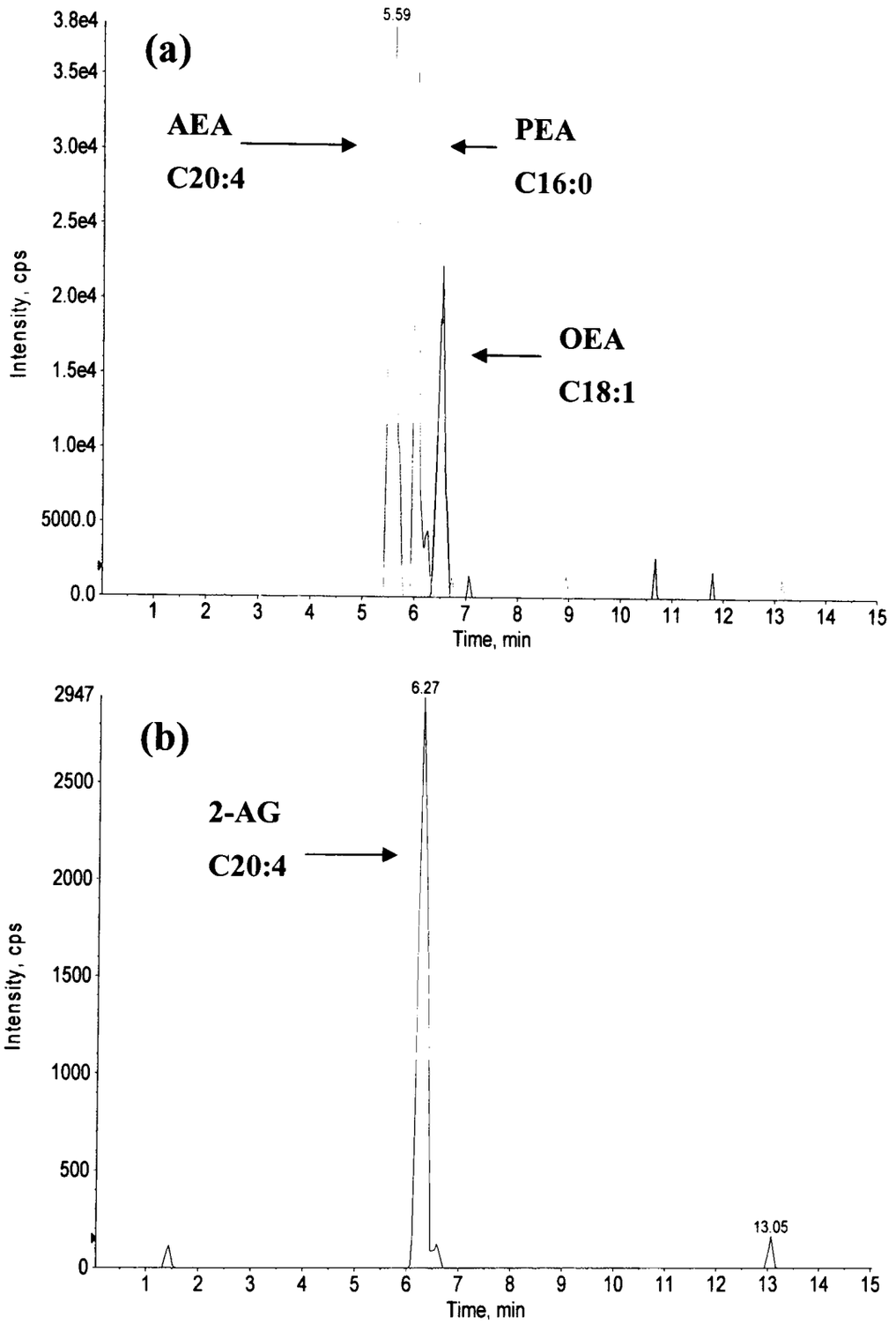

Figure 3.11. Extracted ion chromatograms of (a) NAE AEA C20:4, NAE OEA C18:1 and NAE PEA C16:0 and (b) MAG 2-AG C20:4 from precursor ion and neutral loss survey scan respectively. The resulting EPI spectra generated for each analyte matched those obtained from direct infusion experiments.

chromatography was not ideal, with elution of the analytes around 2 minutes demonstrating little retention on the column; nevertheless, they were detected and EPI spectra obtained to confirm identification. The results provide greater confidence that the methodology is suitable for metabolites of MAGs, and in all likelihood NAEs, where the ethanolamine or glycerol moieties remain intact. Where known metabolites are not detected, this is in all probability due to concentrations below the LLOD of the methodology rather than other limitations of the method.

3.3.4 Further use of NAE and MAG reference standards for identifying fragmentation pattern trends

3.3.4.1 NAEs

Where nucleotides fragment to form common ions i.e. loss of a base or the loss of two phosphates, NAEs and MAGs do not appear to have those common ions but rather common neutral losses. Further work was therefore required to better understand the trends in product ion formation from the families of NAEs and MAGs. Additional standards docosatetraenoyl ethanolamide (DEA, C22:4 ethanolamine), dihomo – γ – linolenoyl ethanolamide (C20:3 ethanolamine) and 2-linoleoyl glycerol (2-LG, C18:2 glycerol) were infused in ESI^+ and fragmented under the same CID conditions as the other NAEs and MAGs. Resulting EPI spectra were compared to AEA and 2-AG EPI spectra respectively to identify trends in the product ion spectra

DEA C22:4 acyl chain is longer than AEA C20:4 by C_2H_4 and this difference is borne out in the product ions; see Figure 3.12. The diagnostic ions resulting from cleavages between the amide bond *m/z* 315 $[M+H-C_2H_7NO]^+$ and *m/z* 297 $[M+H-C_2H_7NO-H_2O]^+$, as well as the acyl chain *m/z* 287 $[M+H-C_3H_7NO_2]^+$ and *m/z* 273 $[M+H-C_4H_9NO_2]^+$ are present. Where DEA differs from AEA by an increase of the acyl chain by C_2H_4 (28 amu), these ion fragments also differ by +28amu from those detected in AEA. As expected, the pseudomolecular ion (and loss of water $[M+H - 18]^+$ is also increased by +28amu. The presence of these ions provides information as to the length and saturation of the acyl chain

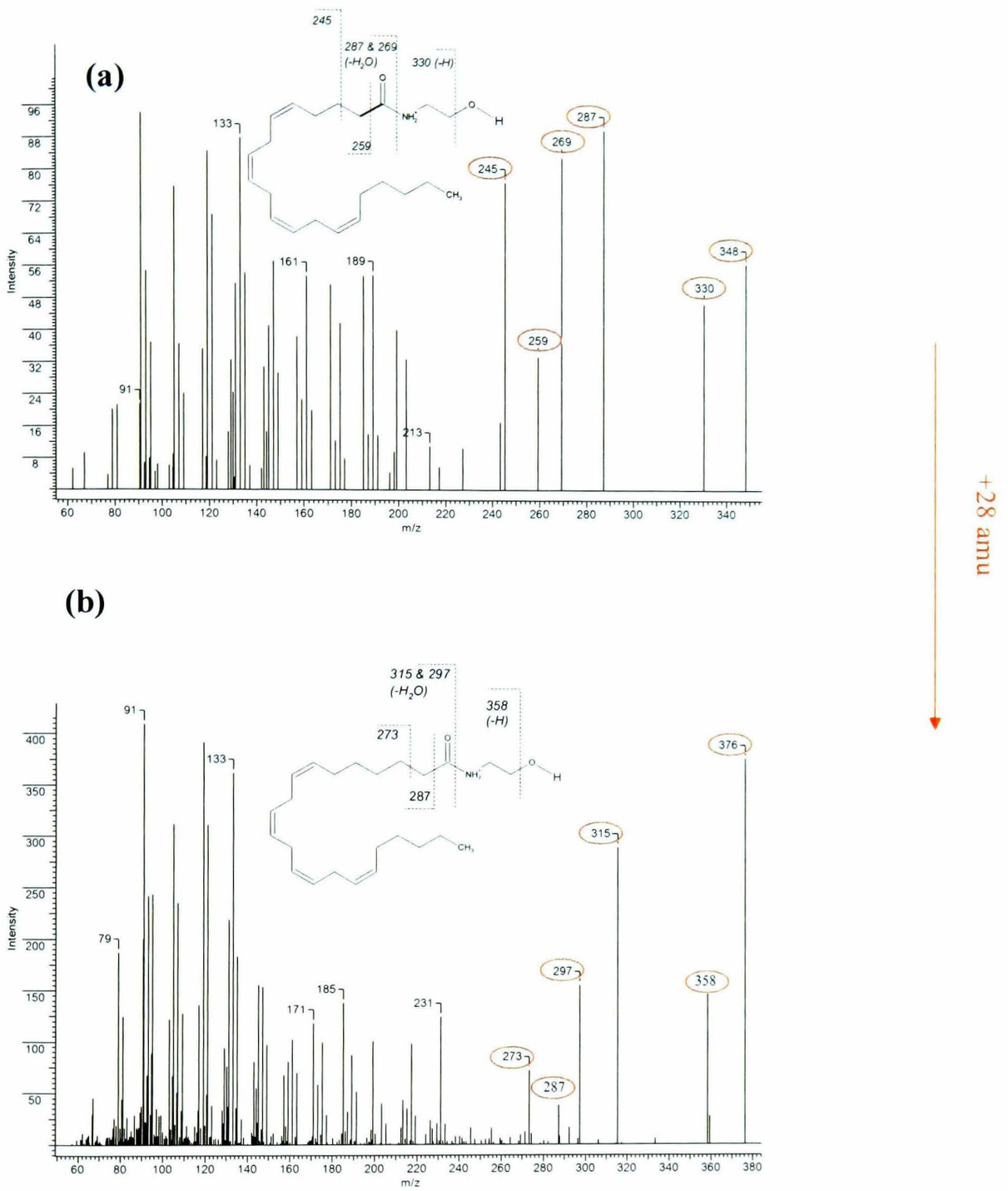

Figure 3.12. EPI spectra of (a) AEA C20:4 and (b) DEA C22:4 standards. A comparison of these two spectra aided the comprehension of fragmentation patterns and identification of structural similar compounds. DEA C22:4 has a longer acyl chain than NAE AEA C20:4 by C_2H_4 (28 amu), hence the molecular weight is +28 amu greater than NAE AEA C20:4. Ions indicative of the acyl chain length and saturation in (a) AEA C20:4 *m/z* 287, 269 and 245 have also increased by 28 amu in spectrum (b); consequently, these ions are diagnostic when calculating the length and saturation of the acyl chain.

Dihomo – γ –linolenoyl ethanolamide (C20:3) acyl chain differs to AEA C20:4 by one double bond i.e. 2H. Again, C20:3 product ions of NAE demonstrate this difference; see Figure 3.13. Dihomo – γ –linolenoyl ethanolamide has one less double bond, but the same acyl chain length, when compared to AEA; consequently the pseudomolecular ion and the loss of water is 2 amu greater. The ions resulting from the cleavage of the amide bond *m/z* 289 $[M+H-C_2H_7NO]^+$ and subsequent loss of water $[M+H-C_2H_7NO-H_2O]^+$ are also 2 amu greater than those observed with AEA. Where AEA demonstrates 2 cleavages along the acyl chain, dihomo – γ –linolenoyl ethanolamide has one, *m/z* 261 $[M+H-C_3H_7NO_2]^+$.

There appears to be a trend that ions resulting from the carbon – carbon cleavage of the acyl chain are less likely to occur as the acyl chain becomes more saturated. Acyl chain fragments $[M+H-C_3H_7NO_2]^+$ and $[M+H-C_4H_9NO_2]^+$ are detected in NAE AEA C20:4 and DEA C22:4. Only $[M+H-C_3H_7NO_2]^+$ is detected in dihomo – γ –linolenoyl ethanolamide (C20:3) and it is not observed in NAE OEA C18:1 or NAE PEA C16:0. MS/MS spectra of NAE Linoleoyl EA C18:2 from other sources (Kasai et al., 2003) and online lipid web sites (http://www.lipidmaps.org/) also demonstrate a lack of these two ions. Furthermore, the presence of the high mass ions, resulting from the cleavage of the amide bond (and loss of water), $[M+H-C_2H_7NO]^+$, $[M+H-C_2H_7NO-H_2O]^+$, appears to be less abundant with an increase in saturation of the acyl chain. Whereas they are clearly present in AEA C20:4, DEA C22:4 and NAE C18:2, their intensity is low in monounsaturated OEA C18:1 and not detectable in saturated PEA C16:0. These trends have not, to the best of the authors knowledge, been previously reported in the endocannabinoid literature.

3.3.4.2 MAGs

2-LG C18:2 has 2 less double bonds and C_2H_4 less on the acyl chain than 2-Ag C20:4 and the product ions reflect the difference. MAG 2-LG C18:2 was infused under the same conditions as MAG 2-AG C20:4 and formed a strong $[M+H]^+$ pseudomolecular ion; see Figure 3.14. The product ion spectrum is similar to that of 2-AG under CID

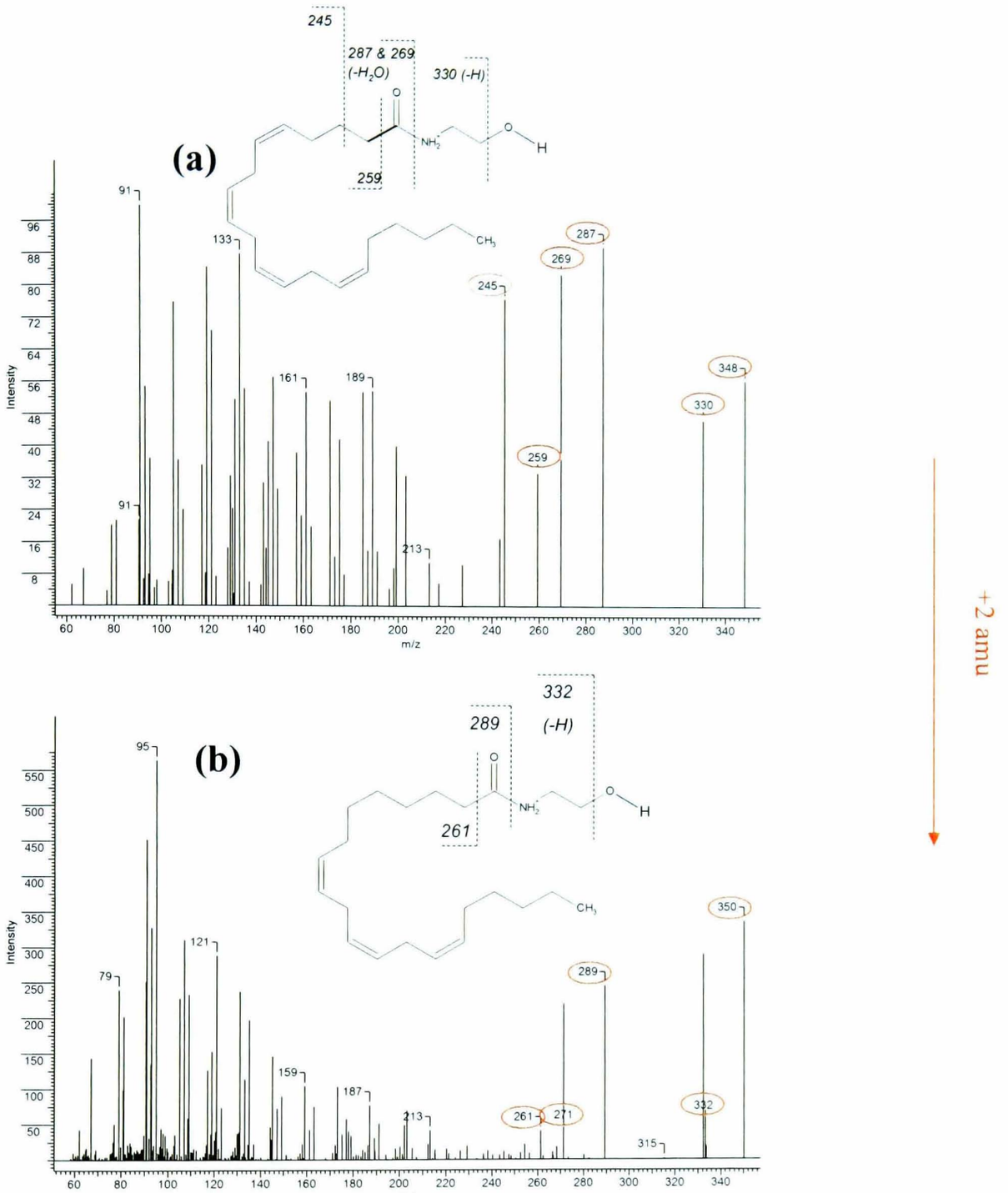

Figure 3.13. EPI spectra of standards (a) AEA C20:4 and (b) NAE dihomo – γ –linolenoyl ethanolamide C20:3. A comparison of these two spectra aided the comprehension of fragmentation patterns and identification of structural similar compounds. NAE dihomo – γ –linolenoyl ethanolamide C20:3 has one less double bond, but the same acyl chain length compared to AEA; consequently, the psudomolecualr ion and the loss of water is 2 amu greater. The ions resulting from the cleavage of the amide bond and subsequent loss of water are also 2 amu greater than those detected in AEA. Where AEA C20:4 demonstrates 2 cleavages along the acyl chain, NAE dihomo – γ –linolenoyl ethanolamide C20:3 has one.

conditions. The cleavage of the ester linkage occurs, as does the subsequent loss of water (*m/z* 263 and 245). The mass difference of MAG 2-AG C20:4 and MAG 2-LG C18:2 is 24 amu; consequently, these fragments are *m/z* 24 less than those detected in 2-AG C20:4 (*m/z* 287 and 269). Unlike 2-AG C20:4 fragmentation along the acyl chain, $[M+H - C_4H_8O_4]^+$ and $[M+H - C_5H_{10}O_4]^+$ does not appear to occur.

MAG 2-LG C18:2 has a notable lack of fragmentation along the acyl chain compared to polyunsaturated 2-AG C20:4. A similar trend is observed with monosaturated and saturated compounds OEA C18:1 and PEA C16:0 compared to polyunsaturated NAE AEA C20:4. This observation would indicate that there is a trend for the polyunsaturated chains to fragment to a greater degree under CID conditions. Such a trend in MAGs has not been previously noted in the literature. It has been previously reported, however, that the degree of acyl chain saturation has a substantial effect on the fragmentation pattern of fatty acid methyl esters under EI (Murphy, 1993), be it by mechanisms involving free radicals or by different product ions.

The trends in acyl chain length / saturation and the associated pseudomolecular ion $[M+H]^+$ and the loss of water observed in NAEs and MAGs have previously been observed in phospholipids and employed as a means of identification (Wang *et al.*, 2005). Furthermore the same approach (along with other product ions) have been used in the identification of acyl-homoserine lactones (Ortori *et al.*, 2007). Consequently, the use of the $[M+H]^+$ and $[M+H - H_2O]^+$, coupled with other product ions observed from NAE and MAG reference standards could be employed to identify other analytes for which reference standards were not available. A systematic list of compounds with varying acyl chain lengths and degrees of saturation was tabulated for NAEs and MAGs to aid in identification of unknowns (see Table 3.3 and Table 3.4). It is assumed that acyl chains will have an even number of carbons, due to the formation of fatty acids via acetyl CoA (Stryer, 1999). The pseudomolecular ion and subsequent loss of water are listed, providing initial mass and identification for each analyte. Ions indicative of the cleavage of amide or ether linkage (and subsequent loss of water) were included, as these provide additional information on the length and saturation of the acyl chain (Kasai et al., 2003),

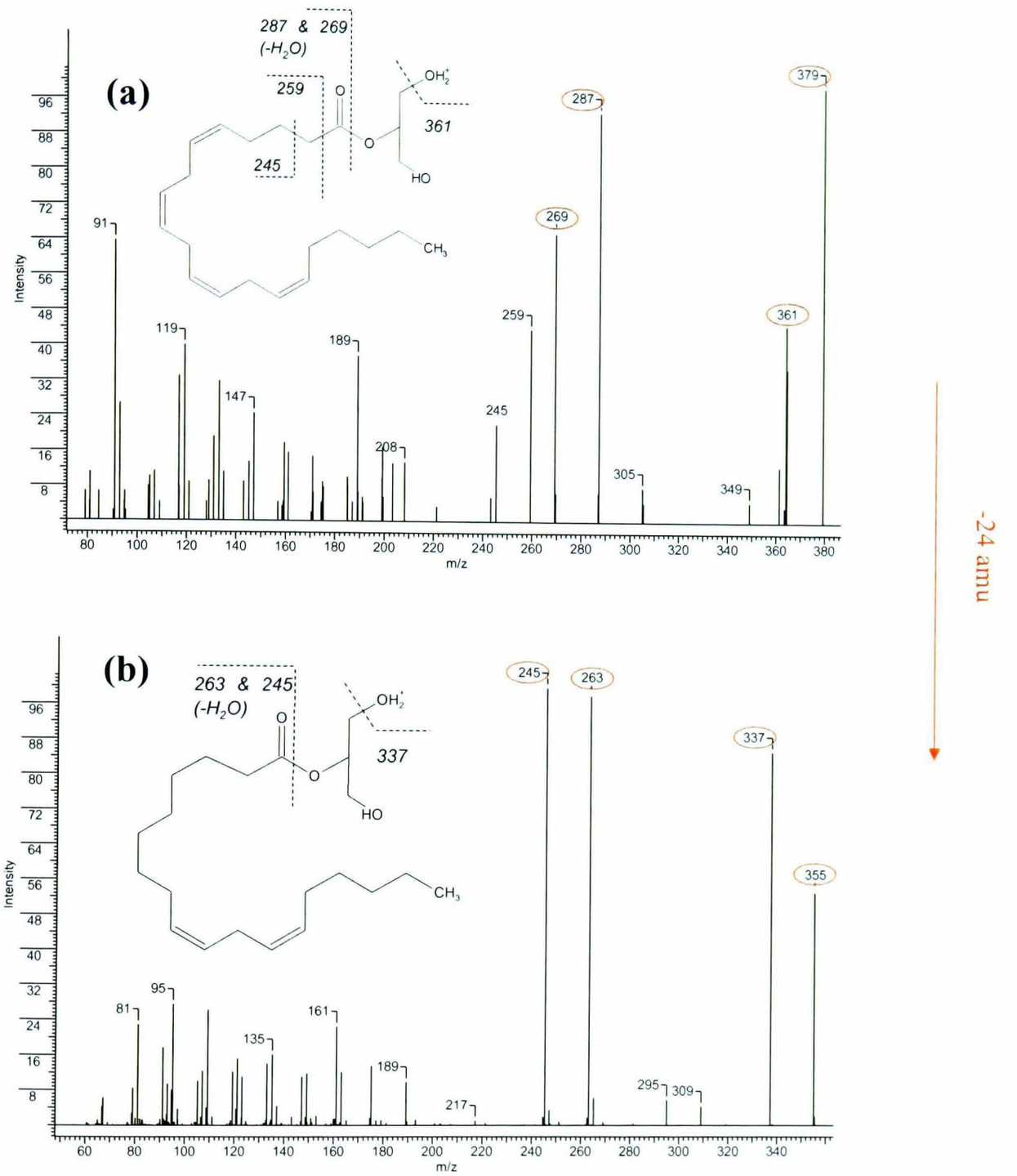

Figure 3.14. EPI spectra of MAG 2-AG C20:4 (a) and MAG 2-LG C18:2 (b) standards infused. A comparison of these two spectra aided the comprehension of fragmentation patterns and identification of structural similar compounds. MAG 2-LG C18:2 has a shorter, di-saturated acyl chain compared to MAG 2-AG C20:4 by C2 (24 amu); hence the molecular weight is -24 amu less than MAG 2-AG C20:4. Ions from the cleavage of the ester linkage, indicative of the acyl chain in MAG 2-AG C20:4 (a) 287 (and the subsequent loss of water 269), have also decreased by 24 amu in spectrum MAG 2-LG C18:2 (b); consequently, these ions are diagnostic when calculating the length and saturation of the acyl chain.

Table 3.3. A table of theoretical and experimental NAE molecular ions and prominent product ions under CID conditions. Those in bold are obtained under experimental conditions with standards. All other compounds are the theoretical protonated pseudomolecular ions and expected product ions that may occur. Although $[H+M]^+$ - 18 and $[H+M]^+$ - 17 are observed experimentally, only $[H+M]^+$ - 18 has been included in the list

Acyl Chain	$[M+H]^+$	Product Ions (*m/z*)				
C24:8	396.3	378.3	335.3	317.3	307.3	293.3
C24:7	398.3	380.3	337.3	319.3	309.3	295.3
C24:6	400.3	382.3	339.3	321.3	311.3	297.3
C24:5	402.3	384.3	341.3	323.3	313.3	299.3
C24:4	404.4	386.3	343.3	325.3	315.3	301.3
C24:3	406.4	388.3	345.3	327.3	317.3	303.3
C24:2	408.4	390.3	347.3	329.3		
C24:1	410.4	392.3	349.3	331.3		
C24:0	412.4	394.3				
C22:7	370.3	352.3	309.3	291.3	281.3	267.3
C22:6	372.3	354.3	311.3	293.3	283.3	269.3
C22:5	374.3	356.3	313.3	295.3	285.3	271.3
C22:4 (DEA)	**376.3**	**358.3**	**315.3**	**297.3**	**287.3**	**273.3**
C22:3	378.3	360.3	317.3	299.3	289.3	275.3
C22:2	380.4	362.3	319.3	301.3		
C22:1	382.4	364.3	321.3	303.3		
C22:0	384.4	366.3				
C20:6	344.3	326.3	283.3	265.3	255.3	241.3
C20:5	346.3	328.3	285.3	267.3	257.3	243.3
C20:4 (AEA)	**348.3**	**330.3**	**287.3**	**269.3**	**259.3**	**245.3**
C20:3	**350.3**	**332.3**	**289.3**	**271.3**	**261.3**	**247.3**
C20:2	352.3	334.3	291.3	273.3		
C20:1	354.3	336.3	293.3	275.3		
C20:0	356.4	338.3				
C18:6	316.2	246.3	203.3	185.3	175.3	161.3
C18:5	318.2	274.3	231.3	213.3	203.3	189.3
C18:4	320.3	302.3	259.3	241.3	231.3	217.3
C18:3	322.3	304.3	261.3	243.3	233.3	219.3
C18:2	**324.3**	**306.3**	**263.3**	**245.3**		
C18:1 (OEA)	**326.3**	**308.3**	**265.3**	**247.3**		
C18:0	**328.3**	**310.3**				
C16:5	290.2	272.3	229.3	211.3	201.3	187.3
C16:4	292.2	274.3	231.3	213.3	203.3	189.3
C16:3	294.2	276.3	233.3	215.3	205.3	191.3
C16:2	296.3	278.3	235.3	217.3		
C16:1	298.3	280.3	237.3	219.3		
C16:0 (PEA)	**300.3**	**282.3**				

Table 3.4. A table of theoretical and experimental MAG $[H+M]^+$ pseudomolecular ions and prominent product ions under CID conditions. Those in bold are obtained under experimental conditions with standards. All other compounds are the theoretical protonated pseudomolecular ions and expected product ions that may occour.

Acyl Chain	$[M+H]^+$	Product Ions (*m/z*)				
C24:8	427.3	409.3	335.3	317.3	307.3	293.3
C24:7	429.3	411.3	337.3	319.3	309.3	295.3
C24:6	431.3	413.3	339.3	321.3	311.3	297.3
C24:5	433.3	415.3	341.3	323.3	313.3	299.3
C24:4	435.3	417.3	343.3	325.3	315.3	301.3
C24:3	437.3	419.3	345.3	327.3		
C24:2	439.3	421.3	347.3	329.3		
C24:1	441.3	423.3	349.3	331.3		
C24:0	443.3	425.3	351.3	333.3		
C22:7	401.3	383.3	309.3	291.3	281.3	267.3
C22:6	403.3	385.3	311.3	293.3	283.3	269.3
C22:5	405.3	387.3	313.3	295.3	285.3	271.3
C22:4	407.3	389.3	315.3	297.3	287.3	273.3
C22:3	409.3	391.3	317.3	299.3		
C22:2	411.3	393.3	319.3	301.3		
C22:1	413.3	395.3	321.3	303.3		
C22:0	415.3	397.3	323.3	305.3		
C20:6	375.3	357.3	283.3	265.3	255.3	241.3
C20:5	377.3	359.3	285.3	267.3	257.3	243.3
C20:4 (2-AG)	**379.3**	**361.3**	**287.3**	**269.3**	**259.3**	**245.3**
C20:3	381.3	363.3	289.3	271.3	261.3	247.3
C20:2	383.3	365.3	291.3	273.3		
C20:1	385.3	367.3	293.3	275.3		
C20:0	387.3	369.3	295.3	277.3		
C18:6	347.3	329.3	255.3	237.3	227.3	213.3
C18:5	349.3	331.3	257.3	239.3	229.3	215.3
C18:4	351.3	333.3	259.3	241.3	231.3	217.3
C18:3	353.3	335.3	261.3	243.3	233.3	219.3
C18:2 (2-LG)	**355.3**	**337.3**	**263.3**	**245.3**		
C18:1	357.3	339.3	265.3	247.3		
C18:0	359.3	341.3	267.3	249.3		
C16:5	321.3	303.3	229.3	211.3	201.3	187.3
C16:4	323.3	305.3	231.3	213.3	203.3	189.3
C16:3	325.3	307.3	233.3	215.3	205.3	191.3
C16:2	327.3	309.3	235.3	217.3		
C16:1	329.3	311.3	237.3	219.3		
C16:0	331.3	313.3	239.3	221.3		

although they are not detected for saturated NAEs. Ions resulting from the fragmentation of the acyl chain were also included for polyunsaturated NAEs and MAGs, but not for monosaturated or saturated chains - as the EPI of standards demonstrate, these analytes do not fragment to form these ions.

Where a range of standards was available to base these proposed ions on for NAEs (C22:4 to C16:0), only two were available for the MAGs. Although the end moiety of MAGs is different from NAEs, other constituents of the molecules are the same; consequently, there are strong similarities between the EPI spectra of the 2 classes of compounds. This is demonstrated by the spectra of NAE AEA C20:4 compared to MAG 2-AG C20:4 and of NAE C18:2 compared to MAG C18:2. The predicted product ions of MAGs in Table 3.4 are subsequently based not only on the two MAG standards available but also on data obtained from NAE standards.

The list was subsequently employed in the identification of MAGs and MAGs in biological tissues.

3.3.5 Differences in MS/MS spectra and EPI Spectra

It was noted that there are differences in the spectra obtained from the QqQLIT when captured in MS/MS or EPI mode. Product ion survey scans are performed in MS/MS mode, and are undertaken by fixing the first quadrupole for the *m/z* of the pseudomolecular ion. Fragmentation occurs in the collision cell and product ions are observed by scanning the third quadrupole through the appropriate mass range. Alternatively, the EPI spectrum is obtained slightly differently, although the first steps are the same. The first quadrupole is fixed for *m/z* of the pseudomolecular ion. Fragmentation occurs in the collision cell and the resulting product ions pass into the third quadrupole. However, rather than being scanned out, ions are stored for a predetermined time as the quadrupole is acting as a linear ion trap, following which the ions are expelled and recorded.

Marked differences in the spectra were noticeable for NAEs at the lower mass range. The low mass ethanolamine ion *m/z* 62 present in AEA C20:4, OEA C18:1 and PEA C16:0 MS/MS spectra are absent in the EPI spectra (see Figure 3.15). Such a difference could be attributed to the low mass cut-off rule that ion traps suffer from (Raymond, 1997), where product ions have to be within one third of the mass of the pseudomolecular ion in order to be stable in the ion trap. Ions outside that range are unstable and are lost from the trap. The QqQLIT, however, has been reported to not be effected by this issue (Hager and YvesLeBlanc, 2003).

After discussions with an ABI technical representative, it is clear that the reasons for the lack of the *m/z* 62 product ion under EPI conditions is that low mass ions (<75amu) are not stable in the ion trap (irrespective of the *m/z* of the original pseudomolecular ion) and are not retained long enough for them to be identified. This does not appear to affect the stability of ions of this mass when the ion trap is run as a quadrupole. To the best of the author's knowledge, this has not been reported in the literature. PI surveys scans were run in MS/MS mode and not affected by this issue and it was taken into account when interpreting EPI spectra.

3.3.6 Limit of detection

The LLOD for PI 62 and NL 92 survey scans (coupled with EPI scanning) was calculated on standards NAE AEA C20:4, NAE OEA C18:1, NAE PEA C16:0 and MAG 2-AG C20:4. Three injections were carried out per concentration. Results can be seen in Table 3.5. The LLODs are could be described by two criteria. The more common description being the lowest concentration which demonstrates an extracted ion chromatogram with a S:N ration of 3:1 or greater. In practice, it was difficult to obtain a peak with such a S:N and hence those concentrations demonstrating a peak S:N closest to 3:1 were selected The second, perhaps more specific to the QqQLIT, is the lowest concentration which generated a recognizable EPI spectrum. The latter is dependent not only on instrument

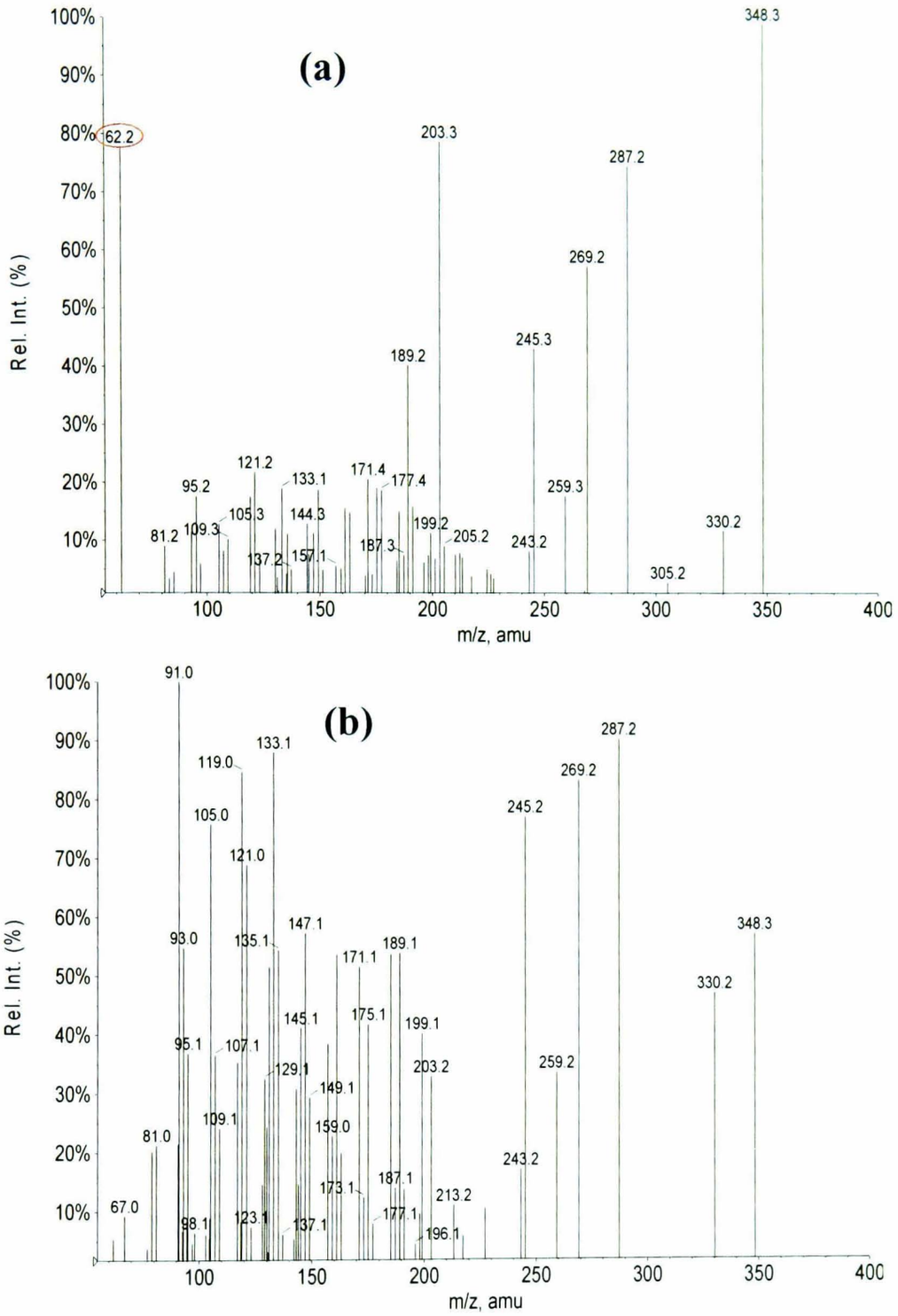

Figure 3.15. Comparison of MS/MS and EPI spectra of the same NAE AEA C20:4 reference standard solution generated under the same CID conditions. Spectrum (a) is obtained by MS/MS mode where product ions are sequentially scanned by the third quadrupole. Structurally significant *m/z* 62 ethanolamine ion is observed. Spectrum (b) is obtained by EPI mode where product ions are stored and expelled from the third quadrupole, acting as a linear ion trap. The diagnostic ion *m/z* 62 is not present.

sensitivity but also a threshold set in the software to limit false positives. In samples with a high matrix background signal, it would be likely that this LLOD might be increased. The LLOD for both criteria are described in Table 3.5 The LLODs obtained are higher than previous targeted SRM approaches (Richardson et al., 2007) by approximately an order of magnitude, as is expected due to the extended scan speed of the survey scan compared to a targeted SRM method. The LLOD of MAG 2-AG C20:4 is considerably higher than that of the NAEs. This has been previously noted (Richardson et al., 2007) and is thought to be due to ionization efficiency under the conditions used. Greater sensitivity for 2-AG C20:4 has been achieved by the addition of silver to replace the proton as the adduct (Kingsley and Marnett, 2007). The resulting fragmentation is sparse, however, with only the loss of water. With the deficiency of structurally diagnostic ions, this approach lacks the specificity for a precursor ion or neutral loss survey scan. Ironically, 2-AG C20:4 is abundant in rat brain at far greater levels than AEA C20:4, which it could be said, makes up for the lack of sensitivity (Richardson *et al.*, 2007; Williams *et al.*, 2007).

The silver adduct of AEA C20:4, unlike 2-AG C20:4, was demonstrated to have few of the sensitivity advantages of a protonated pseudomolecular ion.

Table 3.5. The LLOD of the survey scan employed to detect NAEs and MAGs. The LLOD was calculated on two criteria. The lowest concentration demonstrated an extracted ion chromatogram peak with a S:N ration of 3:1 or greater or the the lowest concentration to generate an EPI spectrum.

Compound	Limit of Detection (pMol on column)	*S/N*	Limit of Detection with EPI spectrum (pMol on column)
AEA C20:4	0.25	6	0.5
OEA C18:1	0.20	17	0.5
PEA C16:0	0.25	12	0.5
2-AG C20:4	2.5	20	37.5

3.3.7 Identification of NAEs and MAGs in rat brain

PI62 and NL92 survey scans were undertaken on rat brain (n=6) to identify all NAEs and MAGs above the limit of detection. Both methods detected a range of NAEs and MAGs in rat brain extract that were varying in acyl chain length and saturation. The identification of analytes was performed by reference to retention times and comparison of EPI spectra where standards were available. Where this was not possible, product ion spectra were compared with theoretical ions listed in Table 3.3 and Table 3.4. Additionally, accurate mass was obtained by use of TOF MS and compared against the theoretical monoisotopic masses. Detected NAEs and MAGs are demonstrated in Table 3.6 and Table 3.7. A TIC of the precursor ion and neutral loss scan can been observed in Figure 3.16.

3.3.7.1 NAEs Detected in Rat Brain

Table 3.6. NAEs detected in rat brain tissue using PI62 survey scan coupled with EPI. Compounds were additionally identified by TOF and the mass error in ppm is stated. ND indicates that the compound was not detected using TOF.

Acyl Chain	$[M+H]^+$	RT (min)	Expected Product ions (*mz*)	$[M+H^+]$ (*m/z*) measure by TOF	Error (ppm)
C24:1	410.4	10.6	392.3	410.4025	7.9
DEA C22:4	376.3	7.10	358.3, 315.3, 297.3, 287.3, 273.3	ND	ND
C22:1	382.4	9.73	364.3, 321.3, 303.3	382.3693	3.5
AEA C20:4	348.3	5.30	330.3, 287.3, 269.3, 259.3, 245.3	348.2901	1.1
C20:1	354.3	8.08	336.3, 311.3, 293.3, 275.4	354.3374	2.1
C20:0	356.4	9.51	338.3	356.3532	2.5
C18:2	324.3	5.5	306.3, 263.3, 245.3	324.2876	6.5
OEA C18:1	326.3	6.17	308.3, 265.3, 247.3	326.3053	0.2
C18:0	328.3	7.36	310.3	328.3225	4.6
PEA C16:0	300.3	5.80	282.3	300.2907	3.3

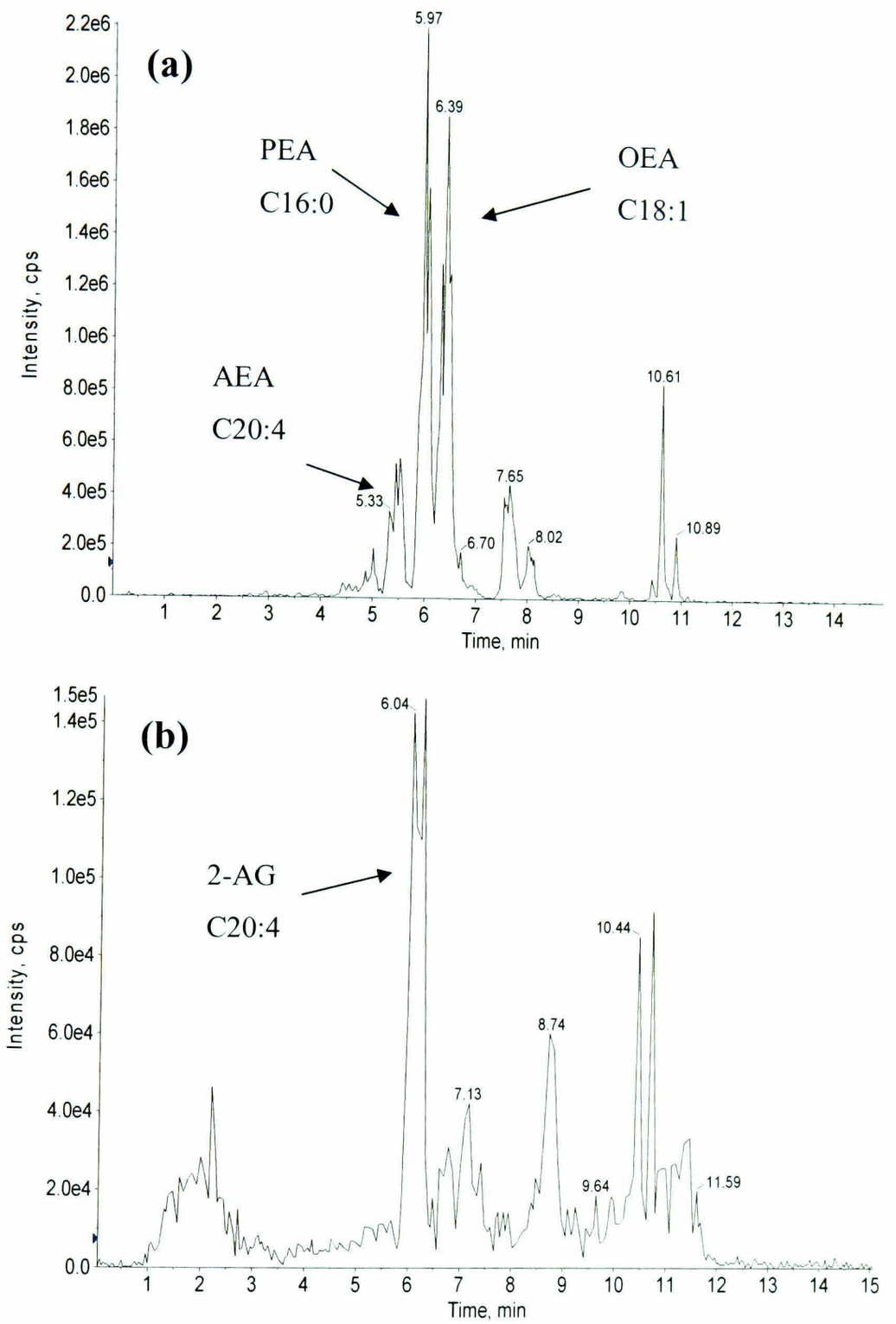

Figure 3.16. Total ion currents of (a) precursor ion survey scan identifying AEA C20:4, PEA C16:0, OEA C18:1 and (b) neutral loss survey scan identifying 2-AG C20:4 in rat brain extract. Confirmation of identification was undertaken by retention time and EPI spectra. Peak splitting may be due to a feature of the instrument switching between various scan modes.

DEA C22:4 was detected and demonstrated an EPI spectrum consistent with that obtained from a standard, with the loss of water and the ions formed from the cleavage of the amide bond and acyl chain, See Figure 3.17. The retention times were also consistent. However, it would be fair to say the intensity of the pseudomolecular ion is greater and the lower mass fragments less intense in the biological DEA C22:4 compared to DEA C22:4 standard. AEA C20:4 was detected and demonstrated an EPI spectrum consistent with that of AEA C20:4 standard, See Figure 3.17. The loss of water is observed as are ions occurring from the cleavage of the amide bond and acyl chain. The retention time was consistent with that observed with standards. NAE OEA C18:1 was detected in rat brain. The EPI spectra and retention time is consistent with that obtained from reference standards. The protonated pseudomolecular ion is observed along with the loss of water. Additionally, ions originating from the amide bond cleavage are observed although, as expected, relative intensities are very low. See Figure 3.18. NAE PEA C16:0 was detected in rat brain. The EPI spectra and retention time is consistent with that obtained from standards. The protonated pseudomolecular ion is observed along with the loss of water. See Figure 3.18

The identification of known NAEs demonstrated the capability of the methodology to profile NAEs in biological matrix. Furthermore, an additional six NAEs were tentatively identified by this method and are described below

Tentative identification of other NAEs in rat brain

For NAEs identified by the survey scan, but where no standards were available, the EPI spectrum was compared with theoretical product ions listed in tables Table 3.3. Additionally, the spectrum was compared with a compound of similar structures where a standard was available. Furthermore, the accurate mass was measured for all compounds detected, using LC-TOF-MS and the mass error calculated in ppm (although not all were detected, due to a lack of sensitivity of the LC-TOF-MS instrumentation).

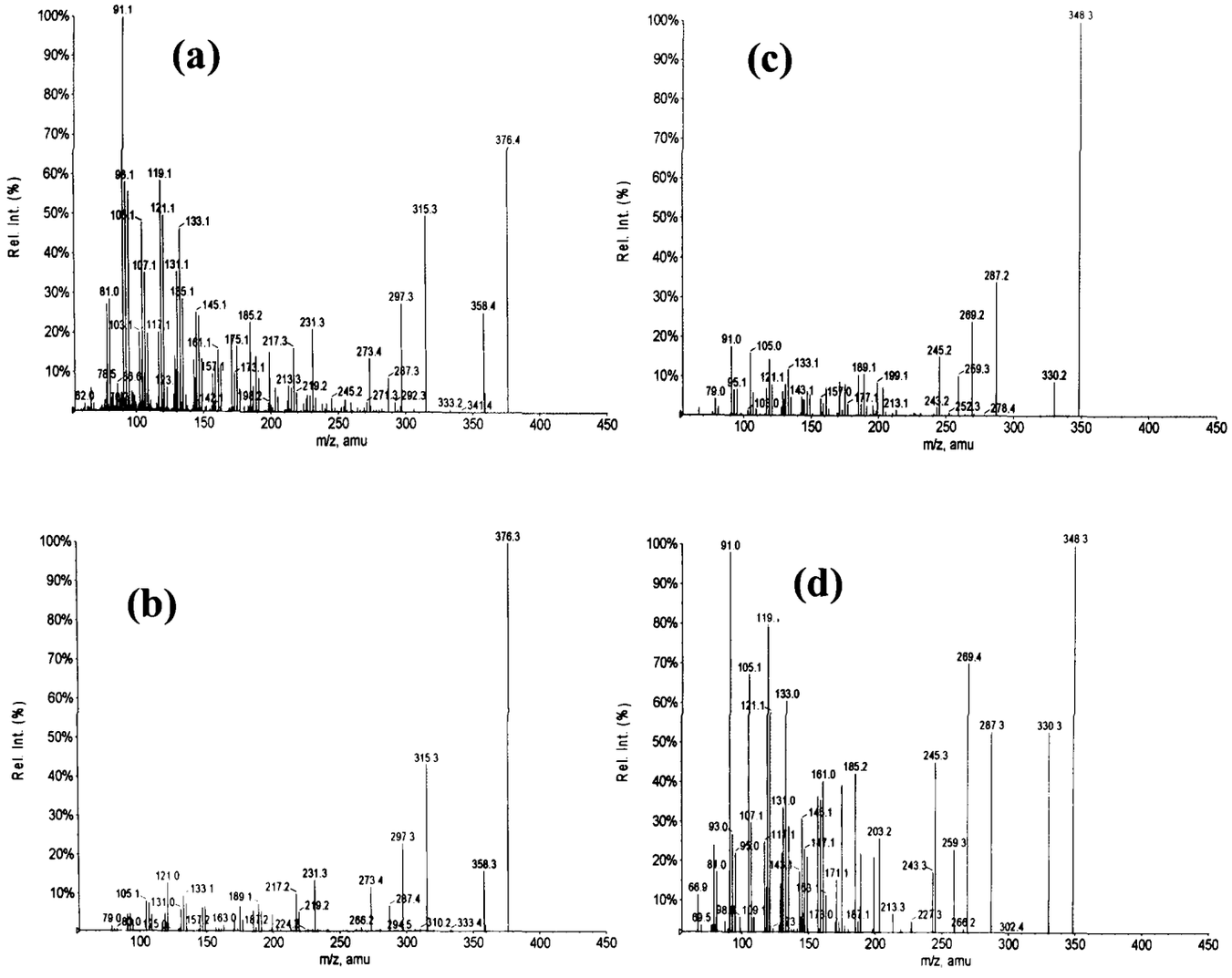

Figure 3.17. Comparison of DEA C22:4 and AEA C20:4 EPI spectra from reference standards and extracted rat brain tissue. EPI spectrum of (a) DEA C22:4 standard spectrum and (b) detected in rat brain show similar fragmentation ions. Additionally, (c) NAE AEA C20:4 reference standard EPI spectrum and (d) detected in rat brain show similar fragmentation ions.

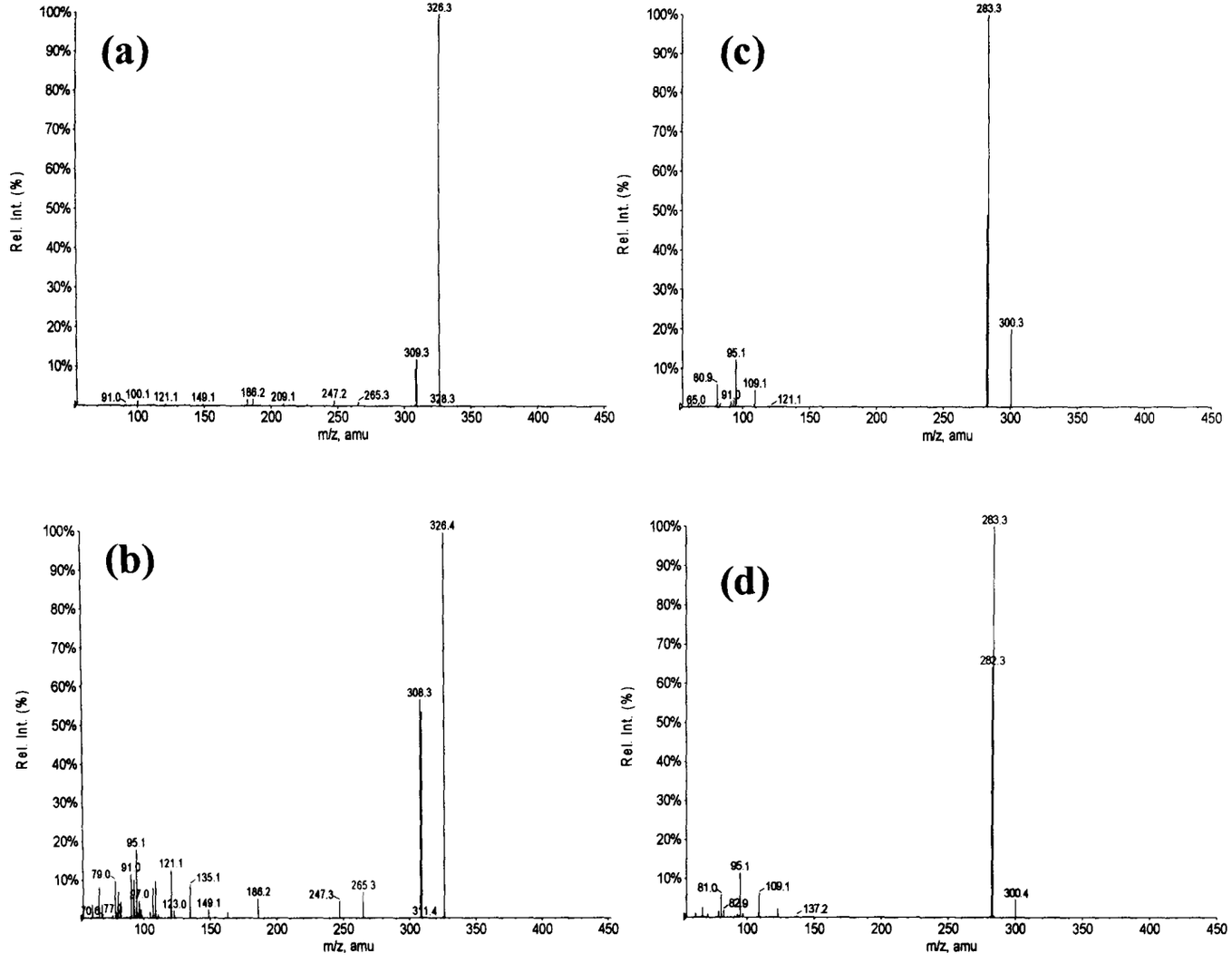

Figure 3.18. Comparison of standard and extracted EPI spectra of OEA C18:1 and PEA C16:0. EPI spectra of (a) OEA C18:1 standard spectrum and that detected in rat brain (b) show similar fragmentation ions. EPI spectrum of (c) PEA C16:0 refernce standard and that detected in rat brain (d) demonstrate a similar fragmentation pattern.

NAE C24:1 was tentatively identified by the precursor ion survey scan. Further identification of the analyte was undertaken by the comparison of the EPI spectra with theoretical ions in Table 3.3. Additionally, the EPI spectra were compared to NAE OEA C18:1, another monosaturated NAE for which standards were available; see Figure 3.19. NAE C24:1 has a longer acyl chain by C_6H_{12} (84 amu); consequently, the $[M+H]^+$ ion is 84 amu greater than NAE OEA C18:1. The subsequent loss of 17 ($^{\cdot}OH$) *m/z* 393.5 and 18 (H_2O) *m/z* 392.5 is also 84 amu greater than those fragments detected from C18:1. The presence of a high mass ion, indicative of amide bond cleavage $[M+H-C_2H_7NO]^+$ (*m/z* 349.3), is present, but at low intensity; however, the subsequent ion indication of the loss of water from this ion, $[M+H-C_2H_7NO-H_2O]^+$, was not observed. As low mass ions are also not observed this could be due to insufficient collision energy. As observed with NAE OEA C18:1 standard no fragments from the cleavage of the acyl chain are observed. The measurement of this compound by TOF gave a 7.9 ppm error from the theoritical monoisotopic mass. This is slightly higher than the expected mass error range for this instrument (± 5ppm); This could conclude that the strength of confidence in the identification of this analyte is not as perhaps as strong as other NAEs, althoug known MAG 2-AG C20:4 also demonstarted a slightly larger than expected mass error

Two additional monounsaturated NAEs were detected: NAE C20:1 and NAE C22:1. The prominent diagnostic ions match those listed in Table 3.3. In the same theme with NAE C24:1, the EPI spectra of these two compounds were compared with reference standard OEA C18:1; see Figure 3.20. NAE C20:1 and NAE C22:1 differ from OEA C18:1 by an extension of the acyl chain by C_2H_4 (28amu) and C_4H_8 (56amu), respectively. Consequently, the pseudomolecular ion and the subsequent loss of water of each analyte is 28 amu and 56 amu greater. The ions indicative of the amide bond cleavage $[M+H-C_2H_7NO]^+$ and the subsequent loss of water $[M+H-C_2H_7NO-H_2O]^+$ are also respectively 28 amu and 56 amu greater compared to those observed from NAE OEA C18:1. Analytes were observed by LC-TOF-MS with a ppm mass error of 0.2 and 3.3, providing additional confirmation of their identification.

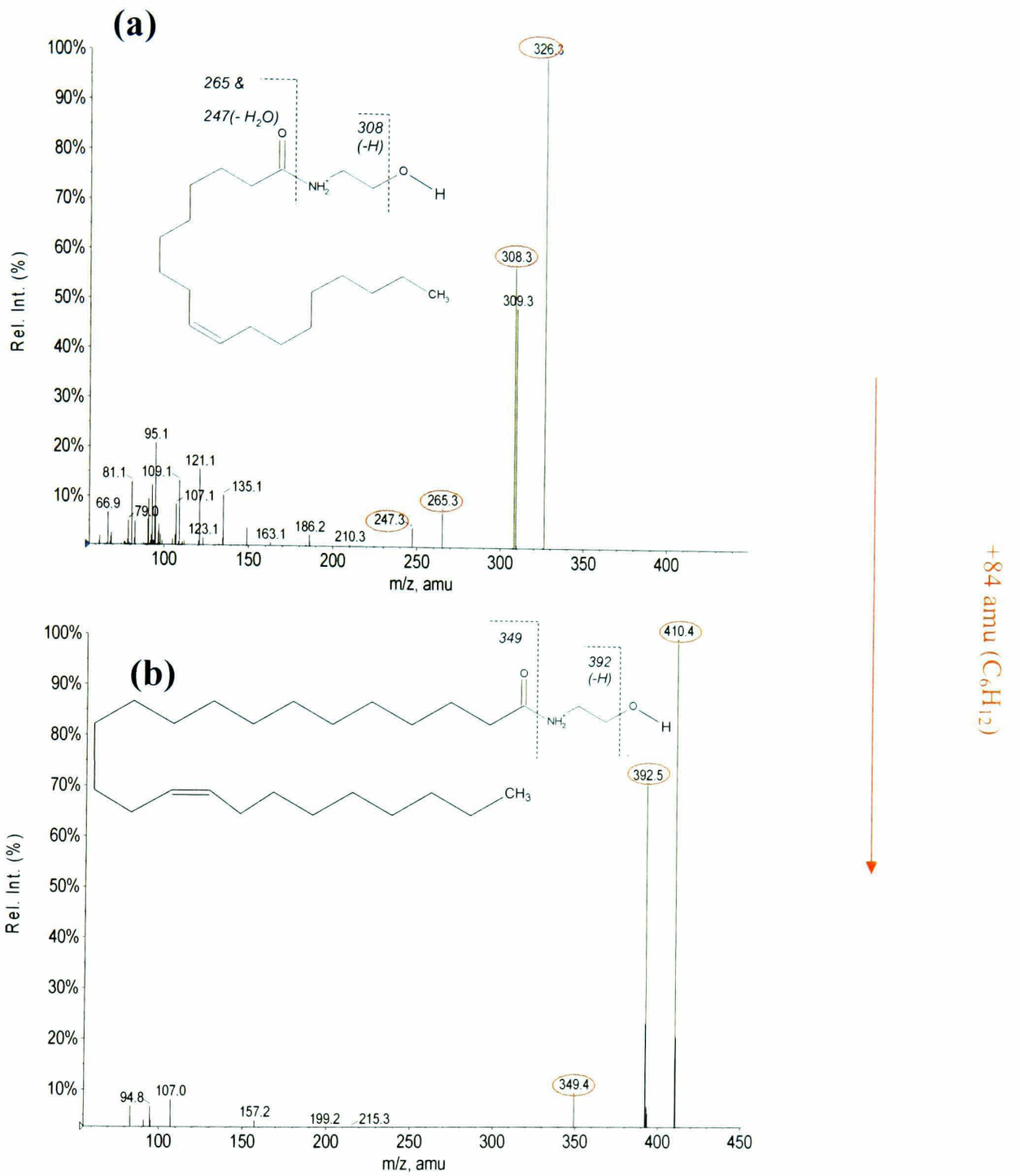

Figure 3.19. Identification of NAE C24:1. EPI spectra of (a) OEA C18:1 and (b) NAE C24:1 from rat brain. NAE C24:1 has a longer acyl chain by C_6H_{12} (84 amu); consequently the $[M+H]^+$ ion is 84 amu greater than OEA C18:1. The loss of 17 ($^{\cdot}OH$ or NH_3) and 18 (H_2O) is also 84 amu greater than OEA C18:1. The presence of a high mass ion, indicative of amide bond cleavage, is present, but the subsequent loss of water from that ion was not detected. The double bond position of C24:1, not determined by this method, was placed in position n-9 for the purpose of drawing the structure.

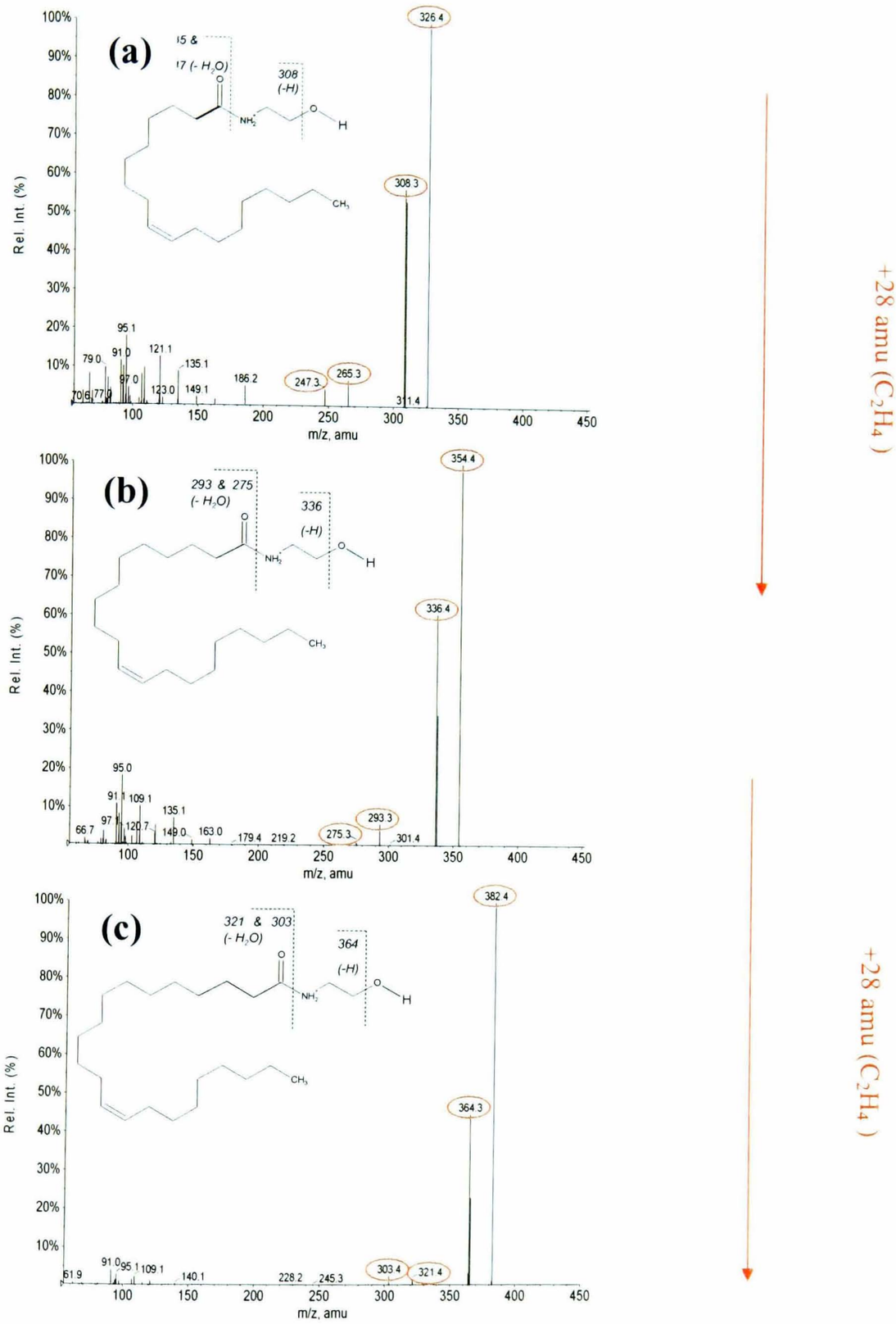

Figure 3.20. Comparison EPI spectra of (a) OEA C18:1 standard and (b)C20:1 and (c) C22:1 detected in rat brain using a PI62 survey scan. Compared to OEA C18:1, C20:1 and C22:1 differ by an increase to the acyl chain by C_2H_4 (28amu) and C_4H_8 (56amu), respectively; consequently the pseudomolecular ion, the loss of water and the two ions indicative of the amide cleavage also increase by 28 and 56 amu, respectively. The double bond position of C22:1 and C20:1, not determined by this method, was placed in position n-9 for the purpose of drawing the structure.

Saturated NAEs, NAE C18:0 and NAE C20:0, were detected and identification was aided by comparisons with Table 3.3. As with saturated acyl chains, diagnostic ions were limited to the pseudomolecular ion and the loss of H_2O and $^{\cdot}OH$ or NH_3. Additional identification was made by comparing them with the EPI spectrum of NAE PEA C16:0; see Figure 3.21. NAE C18:0 and NAE C20:0 differ from NAE C16:0 by C_2H_4 (28amu) and C_4H_6 (56 amu) respectively. Consequently, the $[M+H]^+$ of NAE C18:0 and NAE C20:0 are 28amu and 56 amu greater than NAE C16:0. Additionally, ions indicating the loss of water $[M+H - H_2O]^+$ (18 amu) and $[M+H - {}^{\cdot}OH]^+$ or NH_3 (17 amu) are also 28 amu and 56 amu greater, respectively. As with the NAE C16:0 EPI spectrum, NAE C18:0 and NAE C20:0 spectra demonstrate no fragmentation of the amide bond or acyl chain, resulting in few diagnostic ions. With fewer ions the confidence in such identifications could be deemed to be weaker than those with a greater abundance of confirmatory ions. Nethertheless, both analytes were observed by LC-TOF-MS with a ppm mass error of 4.6 and 2.5, providing additional confirmation to their identification.

Unsaturated NAE C18:2 was identified by comparison with Table 3.3. Additional identification was made by comparing spectra with reference standard NAE OEA C18:1; see Figure 3.22. NAE C18:2 differs from OEA C18:1 by one additional double bond; consequently, the $[M+H]^+$ of NAE C18:2 is 2 amu less than OEA C18:1. Additionally, ions indicating the loss of water $[M+H - H_2O]^+$ (18 amu) and $[M+H - {}^{\cdot}OH]^+$ or NH_3 (17amu) are also 2 amu less. Ions indicative of a cleavage across the amide bond $[M+H-C_2H_7NO]^+$ (*m/z* 263.3) and subsequent loss of water $[M+H-C_2H_7NO-H_2O]^+$ (*m/z* 245.3) are also 2 amu less compared to those observed from NAE OEA C18:1.

Retention time patterns

To provide further confidence in the identification of NAEs detected, the trends in retention times were observed and compared against standard materials. As reversed phase chromatography is employed as a tool for separation, it would be expected that shorter acyl chains would elute faster than longer acyl chains, due to fewer interactions with the stationary phase. Additionally, compounds with fewer double bonds will elute

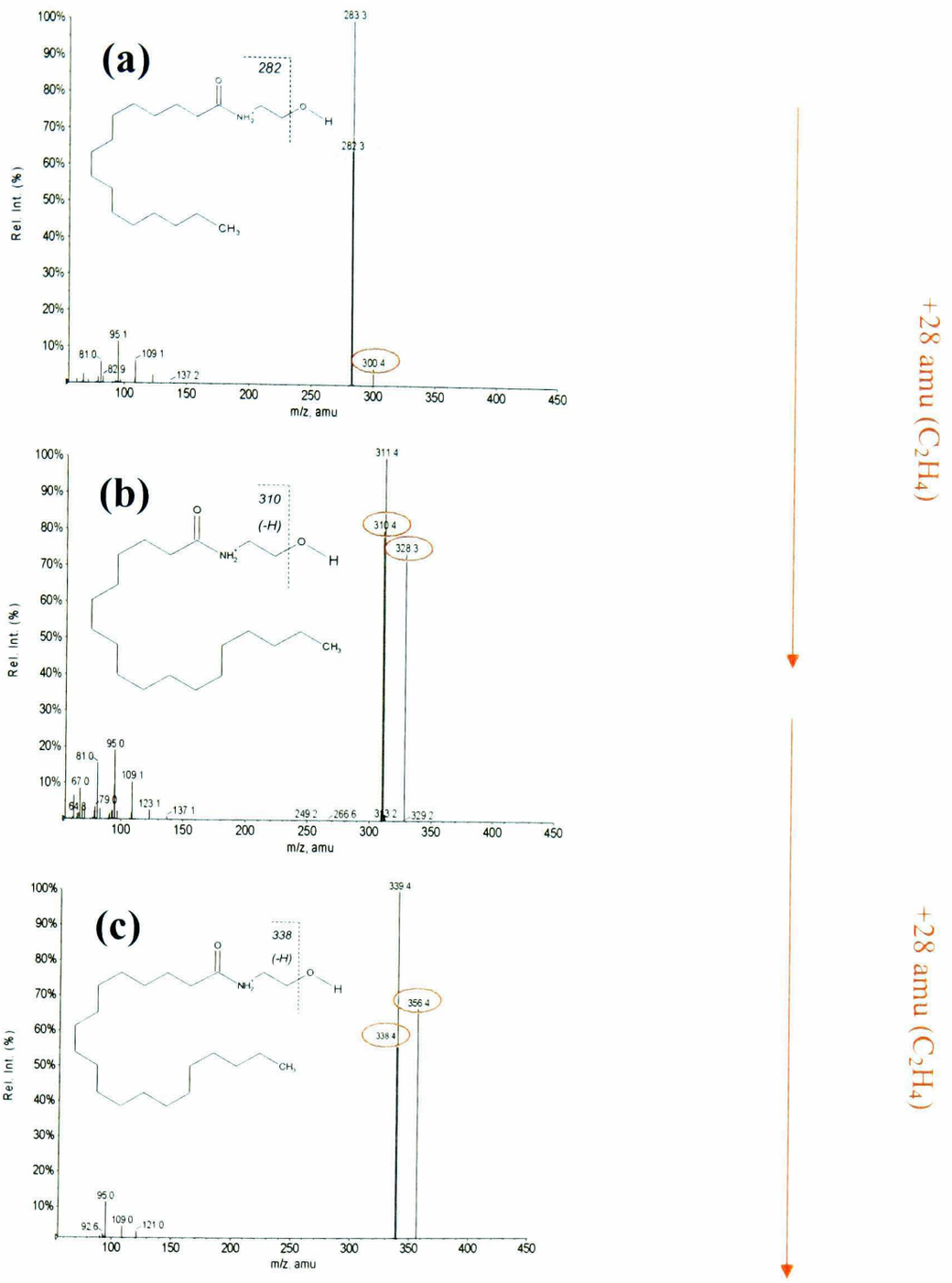

Figure 3.21. A comparison of EPI spectra of (a) PEA C16:0 reference standard, (b) NAE C18:0 and (c) NAE C20:0 identified in rat brain. NAE C18:0 and NAE C20:0 differ from NAE PEA C16:0 by C_2H_4 (28amu) and C_4H_6 (56 amu). Consequently, the $[M+H]^+$ of NAE C18:0 and NAE C20:0 are 28amu and 56 amu greater than C16:0. Additionally, ions indicating the loss of water $[M+H - H_2O]^+$ (18 amu) and $[M+H - {}^{\cdot}OH]^+$ or NH_3 (17amu) are also 28 amu and 56 amu greater, respectively (only $[M+H - H_2O]^+$ are ringed in this example). In spectra (b) and (c) only the loss of ${}^{\cdot}OH$ or NH_3 has been labeled by the software. As with PEA C16:0 EPI spectrum, NAE C18:0 and NAE C20:0 spectra demonstrate no cleavage of the amide bond or acyl chain.

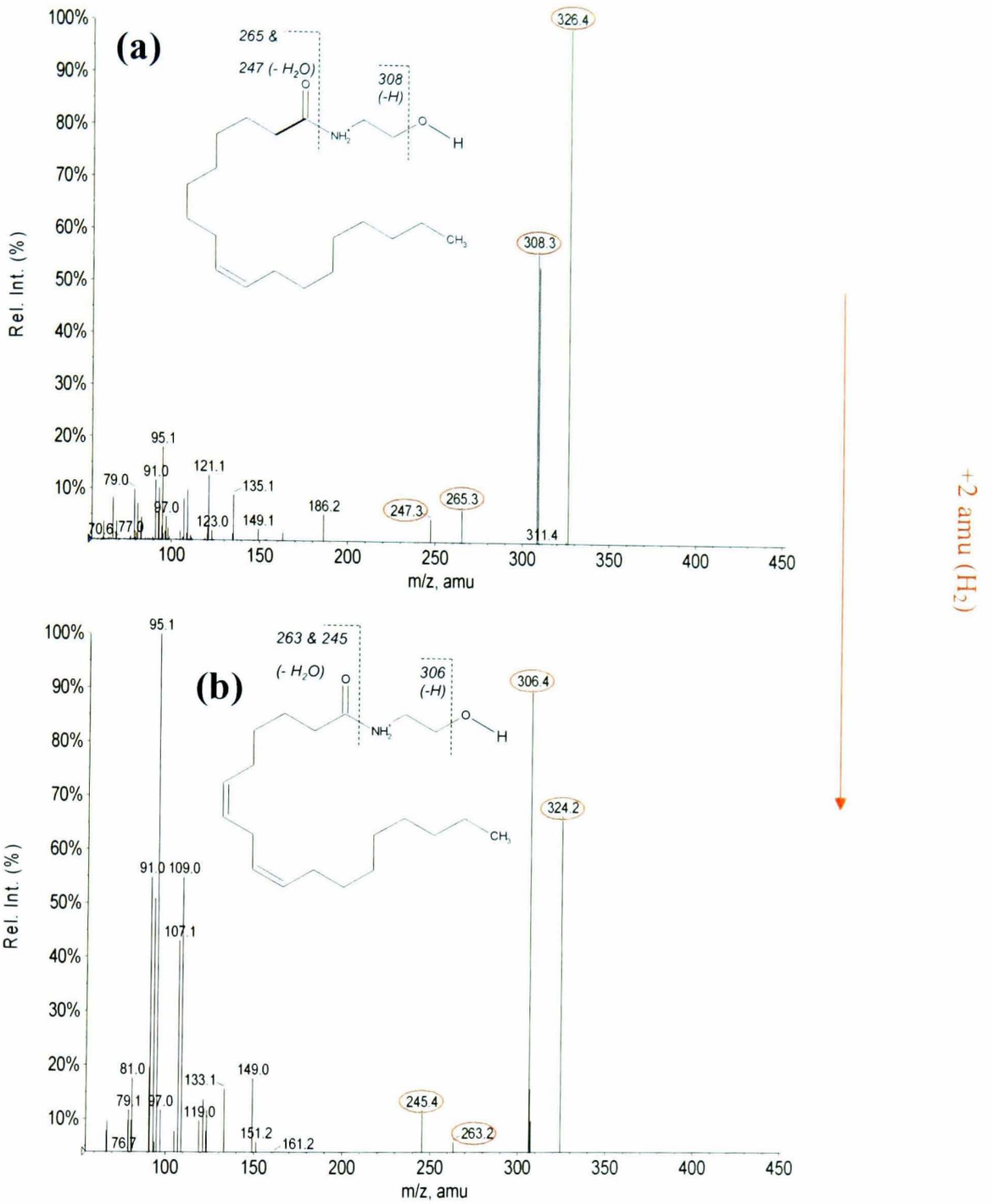

Figure 3.22. A comparison of EPI spectra of OEA C18:1 standard and NAE C18:2 identified in rat brain. NAE C18:2 has a less saturated acyl chain by one double bond, resulting in a lack of H_2 (2amu), and consequently the $[M+H]^+$ of NAE C18:2 is 2 amu less than OEA C18:1. Additionally, ions indicating the loss of water $[M+H - H_2O]^+$ (18 amu) and $[M+H - {}^{\cdot}OH]^+$ or NH_3 (17amu) are also 2 amu less. Only the Loss of H_2O has been labeled in this instance. Ions indicative of a cleavage across the amide bond $[M+H-C_2H_7NO]^+$ (*m/z* 263.3) and subsequent loss of water $[M+H-C_2H_7NO-H_2O]^+$ (*m/z* 245.3) are also 2 amu less compared to those observed from OEA C18:1. The location of the double bonds in NAE C18:2 are unknown but have been nominally placed at the n-9 position for the purpose of drawing the structures.

later than polyunsaturated compounds. This separation is due to the *cis* double bonds which cause the acyl chain to bend, resulting in a reduction of the tight packing between the acyl chain and the stationary phase required for hydrophobic interactions. Such patterns in retention times have previously been observed in phosphatidylcholine species on C18 stationary phase (Kuksis, 1987). It can be seen from Table 3.6 that analytes detected, when compared against reference standards, follow these trends. For example, NAE PEA C16:0, NAE C18:0 and NAE C20:0 elute in order: from shortest to longest acyl chain. The same can be seen for NAE OEA C18:1, NAE C20:1, NAE C22:1 and NAE C24:1, which also elute in order, with the shortest acyl chain first. Additionally, OEA C18:0, NAE C18:1 and NAE C18:2 elute in that order. With the increase in the number of double bonds, attraction to the stationary phase is reduced and resulting retention times are shorter.

Use of the nitrogen rule for analyte identification

One additional piece of evidence corroborating the identification of the purposed analytes is their adherence to the nitrogen rule. A compound that contains no, or an even number, of nitrogens will have an even molecular weight mass. Consequently, a compound that contains an odd number of nitrogens will have an odd molecular weight mass (McLafferty and Turecek, 1993). All NAEs contain one nitrogen atom; hence it would be expected that the molecular weight of each compound would be odd. This is the case for all NAEs detected.

3.3.8 Biological relevance of NAEs detected in rat brain

NAE AEA C20:4, the first of the endocannabinoids to be discovered, has been previously identified in rat brain alongside entourage compounds OEA C18:1 and PEA C16:0 (Richardson *et al.*, 2007; Williams *et al.*, 2007).

DEA C22:4, reported here, has previously been observed in porcine brain tissue (Hanus et al., 1993) and has been demonstrated to exhibit endocannabinoid effects to the same extent as NAE AEA C20:4 (Barg et al., 1995). Although clearly a relevant NAE in the

endocannabinoid story, this analyte has been studied very little in comparison to NAE AEA C20:4; this is predominantly due to a lack of standards (Fowler, 2007).

NAE C24:1 ethanolamine, reported here, has been previously identified in mouse brain (Leung et al., 2006). By the use of NAPE-PLD(-/-) and NAPE-PLD(+/+) mice, they demonstrated that NAE C24:1 ethanolamine was biosynthesized via NAPE-PLD. Similar results were observed for other unsaturated and monounsaturated NAEs (PEA C16:0, C18:0, OEA C18:1, and C20:0). Additional work (Nomura et al., 2008) demonstrated that by inhibiting FAAH and MAGL (known NAE and MAG metabolizing enzymes), C24:1 ethanolamine levels in mice brain increase along with other NAEs and MAGs. Further work (Saghatelian et al., 2004) also concludes that NAE C24:1 ethanolamine is a ligand for FAAH. Whether NAE C24:1 ethanolamine is a substrate for CB1 or CB2 has yet to be reported. However, considering that the acyl chain is monounsaturated and does not have the same degree of saturation as known CB1 & CB2 substrates (Ahn *et al.*, 2008; Sheskin *et al.*, 1997), it seems unlikely.

NAE C18:0 (Leung *et al.*, 2006; Maccarrone, 2006; Saghatelian *et al.*, 2004) and NAE C18:1 (Mulder and Cravatt, 2006) are previously reported NAEs. Although substrates for FAAH along with NAE C20:4 (Nomura *et al.*, 2008; Saghatelian *et al.*, 2004), they are not routinely measured along with entourage compounds NAE PEA C16:0 and NAE OEA C18:1.

NAEs C18:2 has been demonstrated *in vitro* to be inactive against the CB_1 receptor. NAE C20:0 has not been assessed; however, considering the lack of double bonds along the acyl chain, it would be unlikely that it would demonstrate any activity (Sheskin et al., 1997). Both compounds have been demonstrated to be substrates for fatty acid amide hydrolase (Nomura et al., 2008) and have the potential for being entourage compounds, competing with NAE AEA C20:4 for metabolism.

NAE C20:0 has previously been identified in mouse brain (Leung et al., 2006) and was demonstrated to be metabolized by FAAH along with other NAEs - AEA C20:4, OEA

C18:1 and PEA C16:0. The CB_1 and CB_2 activity of this NAE has not been accessed as with others; however, as with C22:1, the lack of double bonds along the acyl chain may preclude a direct effect on the cannabinoid receptors (Sheskin et al., 1997).

NAE C20:1 has been identified previously in rat frontal cortex using a targeted approach (Williams et al., 2007) as well as in mouse brain (Saghatelian et al., 2004). However, in the latter study NAE C20:1 was not detected in wild-type mice but only in FAAH knock-out mice, animals incapable of generating FAAH, an enzyme known to be involved in the catabolism of NAEs, including AEA C20:4, OEA C18:1 and PEA C16:0. Studies conducted *in vitro* to determine CB_1 and CB_2 activity have demonstrated little effect on the endocannabinoid receptors (Sheskin et al., 1997) however, as a ligand for FAAH, this is an important analyte to study when profiling NAEs

NAE C20:3, a known CB_1 agonist (Hanus et al., 1993) previously identified in porcine brain, was not detected in brain extractions analyzed here. Presumably this is due to endogenous levels below the LLOD of this methodology.

NAE C22:1 has been observed once before in mouse brain (and spine) (Saghatelian et al., 2004). As with NAE C20:1, NAE C22:1 was not detected in wild-type mice but only in FAAH knock-out mice, animals incapable of generating FAAH. Activity towards CB_1 and CB_2 receptors has not been assessed. Previous work (Sheskin et al., 1997) demonstrates that ligands for CB_1 and CB_2 require at least three double bonds along the acyl chain; it appears unlikely that this NAE will have a direct effect on the cannabinoid receptors. However, as a substrate for FAAH, this analyte is likely to exert an entourage effect towards AEA C20:4 and hence is an important analyte to profile when investigating the endocannabinoid system.

The analytes detected by this method have been previously identified in biological tissue (rat or mouse); however, such identifications have been an accumulation of a number of methodologies. Such methods have focused predominantly on targeted approaches, relying on reference standards or on more global approaches comparing two or more

tissue states and observing the associated changes. The precursor ion methodology described here has successfully identified a range of NAEs, which previous methods have been unable to achieve. A number of the NAEs are commonly studied; however, a number are not, and an analytical method capable of identifying the scope of analytes observed here is valuable in the field of endocannabinoids.

3.3.8.1 MAGs detected in rat brain

Table 3.7. MAGs detected in rat brain tissue using NL92 survey scan coupled with EPI. Each compound was additionally identified by TOF and the mass error in ppm is stated. ND indicates the compound was not detected using TOF.

Acyl Chain	$[M+H]^+$	RT	Prominent Product Ions	$[M+H]^+$ *(m/z) measured by TOF*	Error (ppm)
C22:4	407.3	7.10	389.3, 333.3, 315.3, 297.3, 287.3, 273.3	407.3161	1.3
2-AG C20:4	379.3	5.92	361.3, 305,3 287.3, 269.3, 259.3, 245.3	379.2879	9.5
C20:3	381.3	6.52	363.5, 307.3, 289.3, 271.3, 261.3, 247.3	ND	ND
C18:1	357.3	6.89	339.3, 283.3, 265.3, 247.3	357.2994	1.5
C18:0	359.3	7.6	341.3, 285.3, 267.3, 249.3	359.3151	1.4
C16:0	331.3	6.7	313.3, 257.3, 239.3, 221.3	331.2832	3.3

It was demonstrated in section 3.3.2 that both MAGs, containing an ester linkage, and noladin ether, containing an ether linkage, produce a neutral loss of 92amu under CID in positive. However, there is some variability as to reported levels of NE in brain tissues in rat. An early publication reports levels of 1 – 65 pmol/g (Fezza et al., 2002) where later publications demonstrated NE in rat brain, if detected, of 0.2pmol/g (Oka *et al.*, 2003; Richardson *et al.*, 2007). The latter values are below the LLOD of the NL scan employed here and would theoretically not be detected by this technique. In practice, this was found to be the case, and NE was not detected in brain tissue by this methodology.

MAGs detected and confirmed by reference standards

2-AG C20:4 was detected and demonstrated an EPI spectrum consistent with that of 2-AG C20:4 reference standard; see Figure 3.23. The loss of water from the pseudomolecular ion is present as are ions indicative of the amide bond cleavage (*m/z* 287.2 *and* 269.2) and fragmentation along the acyl chain (*m/z* 259.3 and 245.3). The monoisotopic mass calculated by LC-TOF-MS was slightly higher than expected, at 9.5 ppm, where the expected mass error should range between ± 5.0 ppm.

Tentative identification of other MAGs

MAG C22:4 was tentatively identified by the neutral loss survey scan. Initial identification was based on theoretical ions in Table 3.4. Additional confirmation was obtained from a comparison with MAG 2-AG C20:4. MAG C22:4 has a longer acyl chain by C_2H_4 (28 amu), and consequently the $[M+H]^+$ ion is 28 amu greater than MAG 2-AG C20:4. Ions indicative of the loss of water $[M+H - H_2O]^+$ (*m/z* 333) as well as ions from the cleavage of the ester linkage $[M+H-C_3H_8O_3]^+$ (*m/z* 315), $[M+H-C_3H_8O_3-H_2O]^+$ (*m/z* 297) and acyl chain $[M+H-C_4H_8O_4]^+$ (*m/z* 287) are also +28 amu greater than those detected from 2-AG; see Figure 3.24. In this instance only one of the two expected acyl chain fragments was observed. The psuedomolecular ion is the base peak, demonstrating that the collision energy used may be less than optimal for this compound, resulting in fewer product ions and hence the lack of the second acyl chain fragment. Measurement by LC-TOF-MS of this compound observed the monoisotopic mass to within 1.3 ppm of the theoretical value addings additional evidence to the correct assessment of this analyte.

MAG C20:3 was detected by the NL92 survey scan. To aid in the identification, a comparison of diagnostic product ions was made against theoretical ions listed in Table 3.4. Additionally, the EPI spectrum was compared against that of MAG 2-AG C20:4 standard; see Figure 3.25. MAG C20:3 is structurally similar to 2-AG C20:4, varying by one double bond on the acyl chain; the consequence being that the mass of the two compounds varies by 2 amu (H_2). As can be seen when comparing the two spectra, MAG C20:3 has a pseudomolecular ion 2 amu greater that MAG 2-AG C20:4.

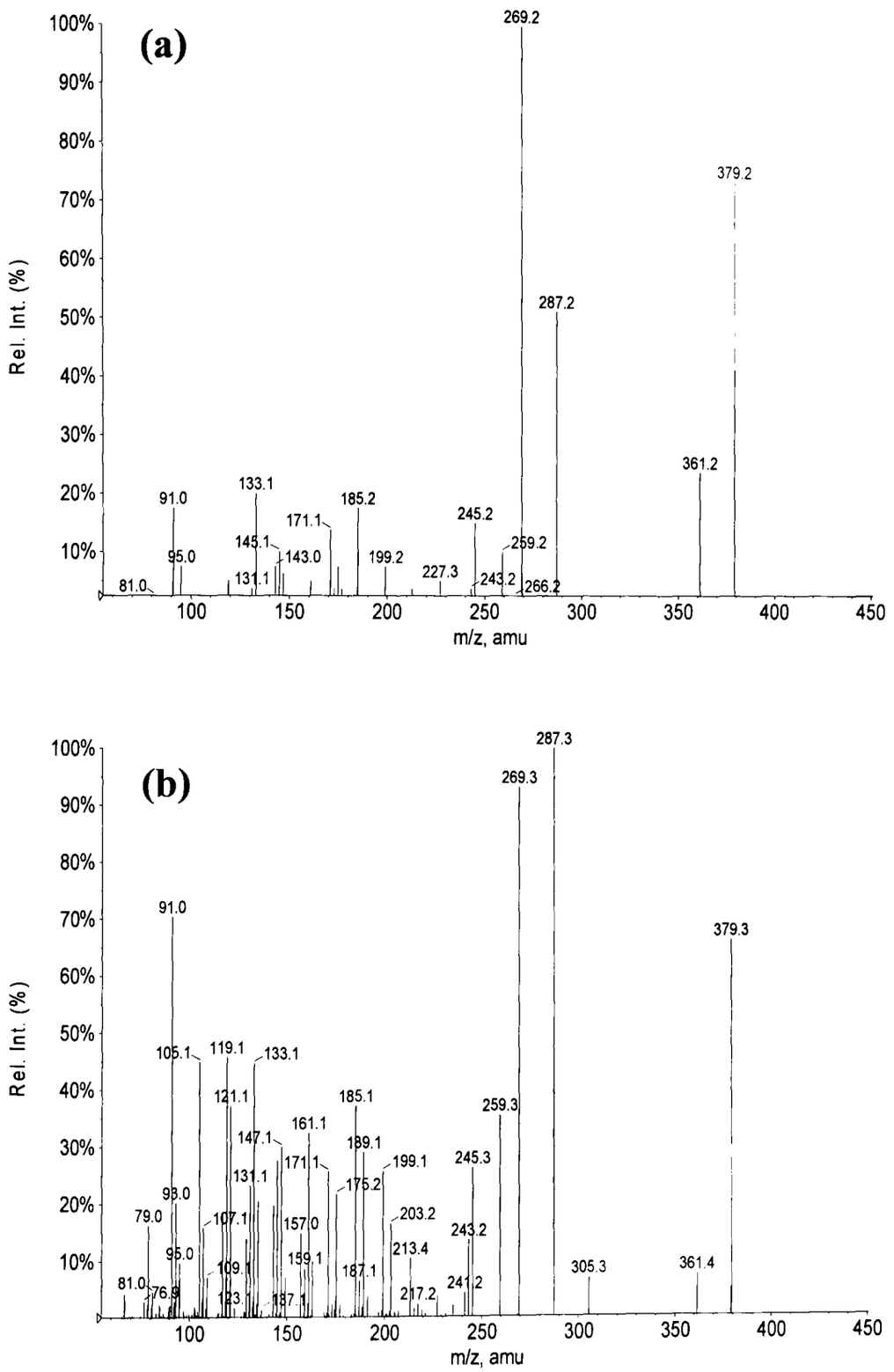

Figure 3.23. A comparison of 2-AG C20:4 EPI spectra obtained from (a) standards and (b) rat brain tissue. The fragmentation patters are very similar. The loss of water from the pseudomolecular ion is present as are ions indicative of the amide bong cleavage (*m/z* 287.2 and 269.2) and fragmentation along the acyl chain (*m/z* 259.3 and 245.3)

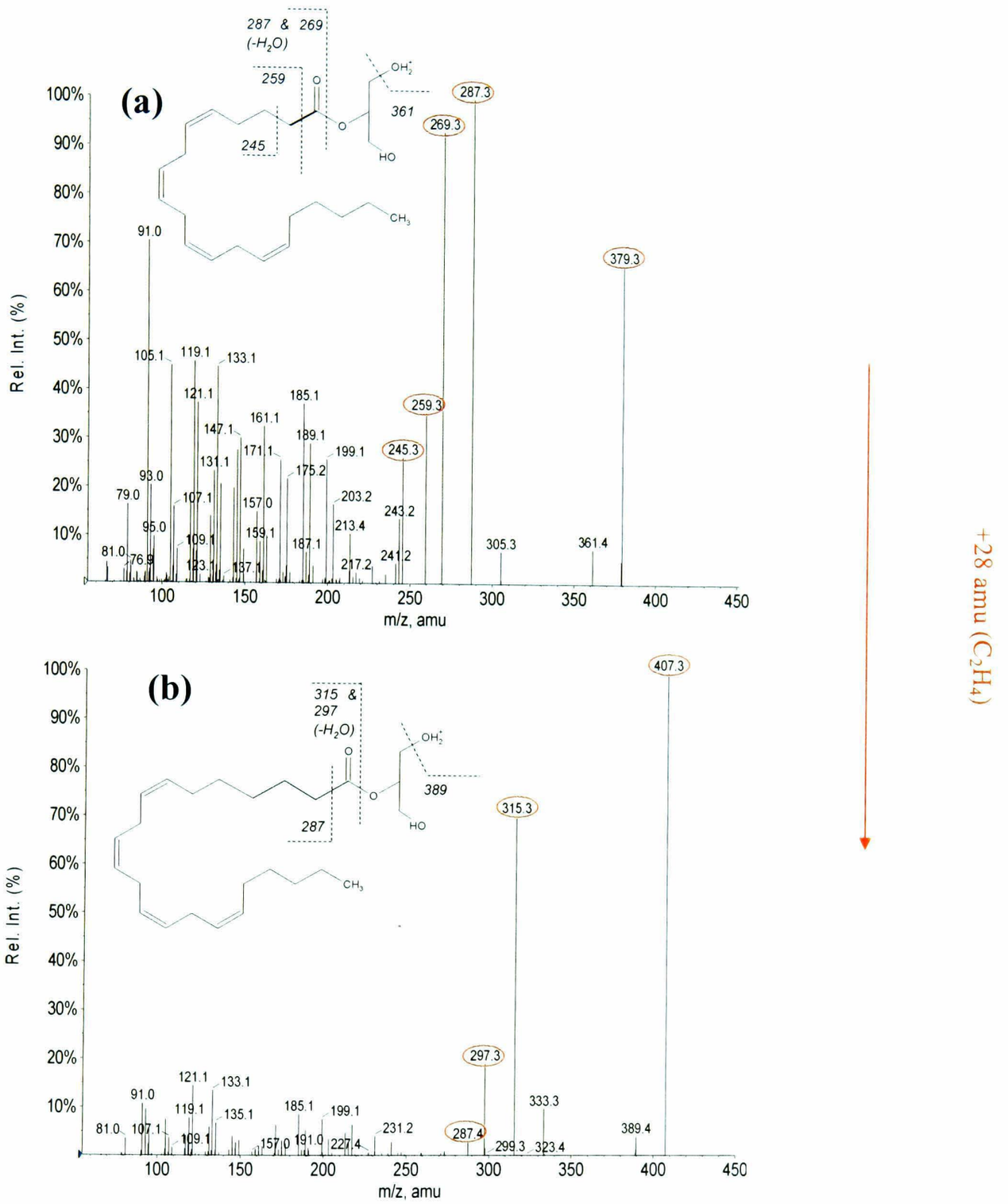

Figure 3.24. Tentative identification of MAG C22:4. EPI spectra of (a) reference standard 2-AG C20:4 and (b) MAG C22:4 from rat brain. MAG C22:4 has a longer acly chain by C_2H_4 (28 amu) and consequently the $[M+H]^+$ ion is 28 amu greater than MAG2-AG C20:4. Ions at 333, 315, 297 and 287, indicative of fragmentation around the ester bond and the acyl chain, are also +28amu greater than those detected in MAG2-AG C20:4 EPI spectra.

Furthermore, ions indicative of the loss of water $[M+H - H_2O]^+$ (*m/z* 363.3) as well as ions from the cleavage of the ester linkage $[M+H-C_3H_8O_3]^+$ (*m/z* 289.3), $[M+H-C_3H_8O_3-H_2O]^+$ (*m/z* 271.3) and acyl chain $[M+H-C_4H_8NO_4]^+$ (*m/z* 261.3) are also +2 amu. There was only one fragment originating from the cleavgae of the MAG C20:3 acyl chain, whereas MAG 2-AG C20:4 demonstrates two. This could be due to less saturation, as, looking at MAG standards, it was observed that MAG C18:2 demonstrated no acyl chain fragmention. No TOF measurement was obtained for this analyte, presuambly because the endogenous level was below the detection limit of the instrument.

MAG C18:1 and MAG C18:0 were also detected in rat brain by the NL92 survey scan. Diagnostic product ions match theoretical values predicted in Table 3.4. The protonated pseudomolecular ions are present, as are the subsequent loss of water $[M+H - H_2O]^+$ as well as the ions indicative of the ester cleavage. For further confirmation, both MAG C18:1 and MAG C18:0 EPI spectra were compared against 2-LG C18:2 standard because there was a clear structural incremental variation in these compounds, with a loss of saturation from MAG C18:0 through to 2-LG C18:2. Figure 3.26 shows the EPI spectra of C18:2 (2-LG) standard and MAG C18:1 and MAG C18:0 detected in rat brain. The three compounds vary by the addition of one double bond from C18:0 to C18:2, with the decrease of 2 amu (H_2), respectively. Consequently each $[M+H]^+$ decreases by 2 amu, respectively. Furthermore, the productions also demonstrate this pattern. The ion formed by the loss of water from the pseudomolecular ions also decreases by 2 amu, as do the ions indicative of a cleavage across the ester linkage $[M+H-C_3H_8O_3]^+$ and $[M+H-C_3H_8O_3-H_2O]^+$. Measurements by LC-TOF-MS of both MAG C18:0 and MAG C18:1 provide good additional evidence that the identification of these two compounds (mass errors of -2.8 and 3 ppm, respectively) is correct. It should be noted, however, that the product ion intensities resulting from the ester linkage (and loss of water) for MAG C18:0 are relatively low compared to MAG C18:1 and reference standard MAG 2-LG C18:2. This could be due to the lack double bonds along the acyl chain, although a mechanistic reason for this is unknown at this time. Certainly another saturated MAG tentatively identified, MAG C16:0, also demonstrates very low intensity ester linkage fragments. Additionally,

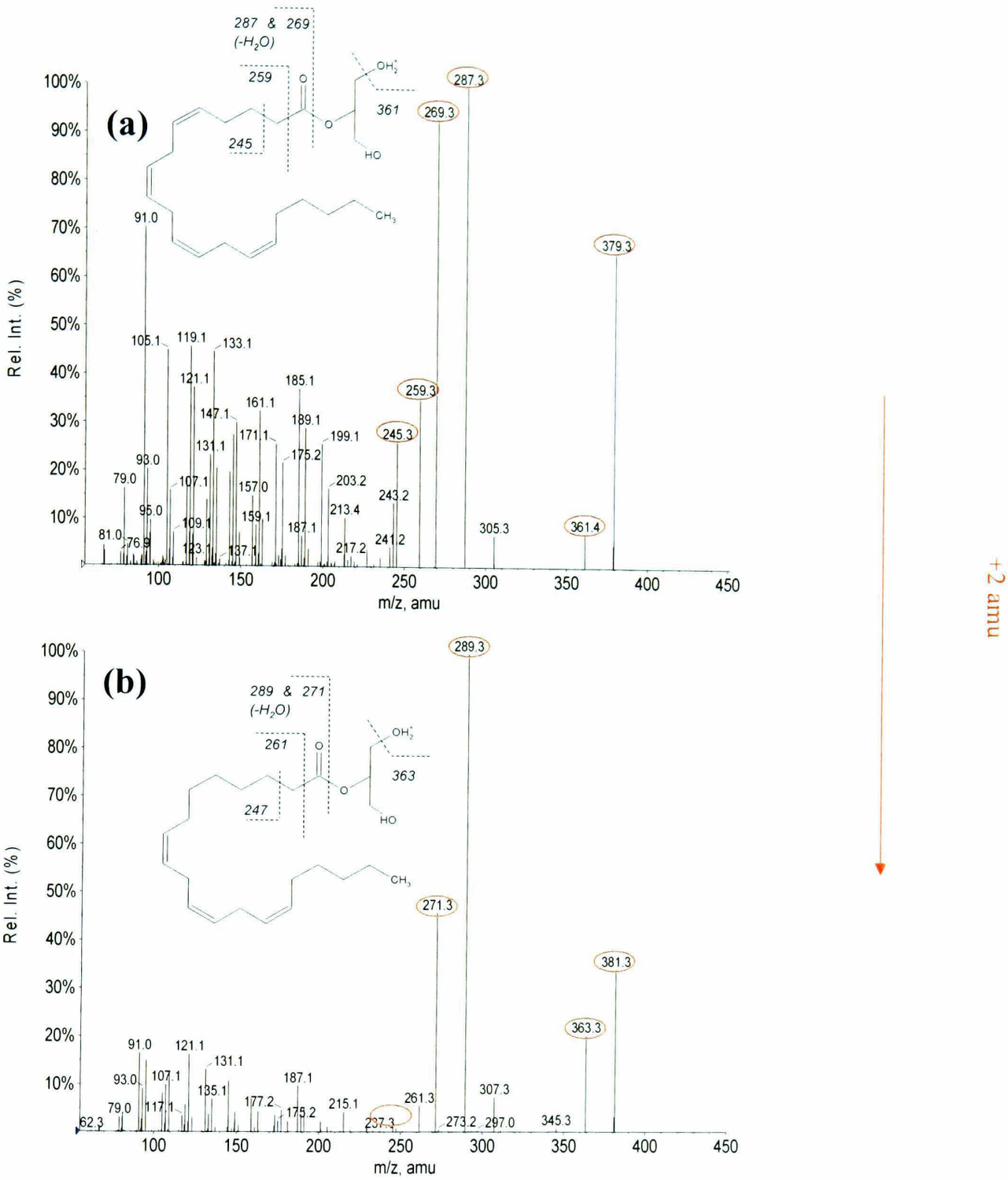

Figure 3.25. Tentative identification of MAG C20:3. EPI spectra of (a) reference standard 2-AG C20:4 standard and (b) MAG C20:3 from rat brain. C20:3 has one less double bond compared to MAG 2-AGC20:4 and consequently the $[M+H]^+$ is 2 amu greater. Additionally, the loss of water $[M+H - H_2O]^+$ (*m/z* 363.3) and the ions resulting from the ester linkage (*m/z* 289.3 and 271.3) and acyl chain cleavage (*m/z* 261.3 and 247.2 – not labled) are 2 amu greater compared to the fragments orginating from MAG 2-AGC20:4,

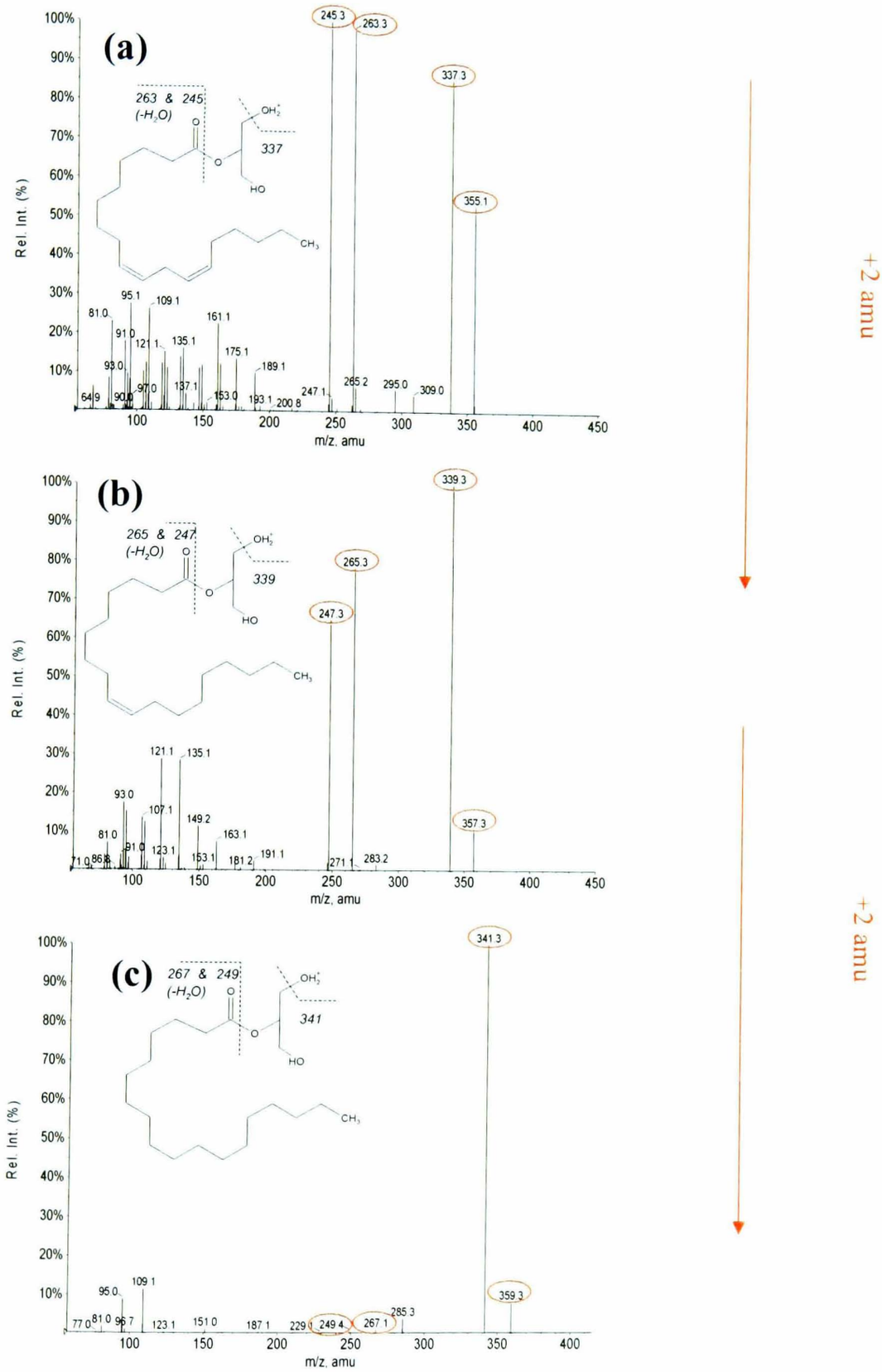

Figure 3.26. EPI spectra of (a) 2-LG C18:2 reference standard and tentative identified (b) MAG C18:1 and (c) MAG C18:0 detected in rat brain by NL92 survey scan. The three compounds vary by the lack of one double bond from MAG C18:2 to MAG C18:0 and consequently the $[M+H]^+$ increase by 2 amu. The ion formed by the loss of water from the pseudomolecular ions also increases by 2 amu, as do the ions indicative of a cleavage along the acyl chain.

saturated NAE reference standard PEA C16:0 demonstrates no fragmentation of the amide bond where polyunsaturated AEA C20:4 demonstrated a high degree of fragmentation. Nevertheless, with such a difference in intensity of ions for the purposed MAG C18:0, it could be said the identification of this analyte is not as strong as other MAGs listed here.

MAG C16:0 was identified by the NL92 survey scan. Diagnostic product ions match with those listed in Table 3.4 although $[M+H-C_3H_8O_3-H_2O]^+$ the cleavage of the ester linkage followed by the loss of water was not detectable. Additional confirmation was made by comparing EPI spectra of MAG C16:0 with standard 2-LG C18:2; see Figure 3.27. MAG C16:0 has a shorter acyl chain compared to MAG C18:2 by C_2H_4 and 4 additional hydrogens because of its saturated acyl chain, resulting in a mass difference of 24 amu. Hence the $[M+H]^+$ is *m/z* 24 less than 2-LG C18:2, and consequently the loss of water and the ion indicative of cleavage from the ether linkage is also *m/z* 24 less than those observed from 2-LG C18:2. Additional confirmation of identification was made by use of LC-TOF-MS, where the monoisotopic mass was measured to be within 1.5 ppm of the expected value.

As observed with MAG C18:0 EPI spectrum, the relative intensity of the ions resulting from the cleavage of the ester linkage is very low.

Further evidence of identification using the nitrogen rule

MAGs, as with NAEs, follow the nitrogen rule. MAGs do not contain a nitrogen atom and consequently it would be expected that the molecular masses would be even (McLafferty and Turecek, 1993). This is the case for all MAGs detected.

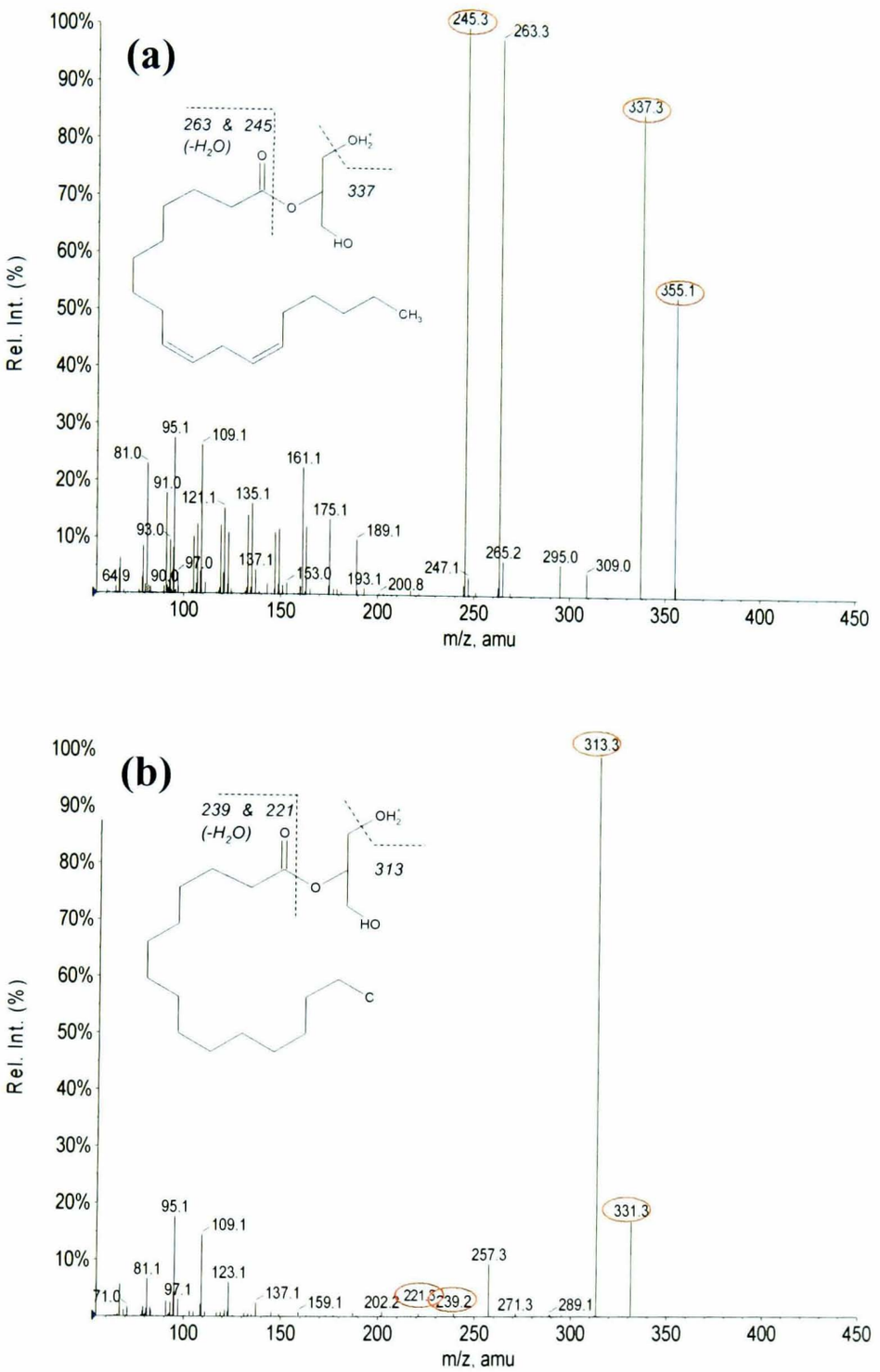

Figure 3.27. A comparison of the EPI spectra of (a) MAG 2-LG C18:2 reference standard and (b) MAG C16:0 detected in rat brain. MAG C16:0 has a shorter acyl chain compared to MAG 2-LG C18:2 by C_2H_4 and 4 additional hydrogens (because it is fully saturated), resulting in a mass difference of 24 amu. Hence the $[M+H]^+$ is *m/z* 24 less than MAG 2-LG C18:2, and consequently the loss of water (*m/z* 313.3) and the ion indicative of cleavage from the ether linkage (*m/z 239.2* and *211.3)* are also *m/z* 24 less than those observed from MAG 2-LG C18:2.

Identified MAGs in biological tissue

2-AG C20:4 is a well characterized endocannabinoid and has been identified by previous targeted methodologies (Richardson *et al.*, 2007; Williams *et al.*, 2007). 2-LG C18:2, observed previously (Richardson et al., 2007) in various brain regions, was not identified by this technique. Where it is has been observed previously, concentrations were in the region of two orders of magnitude less than MAG 2-AG C20:4, ranging from 0.1 to 4.3 nmol/g. Although it is difficult to perform a direct comparison and identify these as on-column concentrations, it suggests that MAG 2-LG C18:2 is below the LLOD for this technique in rat brain.

MAG C18:1 identified by this methodology has been demonstrated *in vitro* to have little affinity as CB1 or CB2 receptor agonists, unlike 2-AG C20:4 (Sugiura et al., 2000). However, MAG C18:1 (along with MAG C16:0) has been determined to be catabolised by MAGL, an enzymatic degradation route of 2-AG C20:4 (Nomura *et al.*, 2008). As such the resulting competition between these MAGs and 2-AG C20:4 for catabolism by MAGL portray them as possible entourage compounds along with 2-LG C18:2. As 2-LG C18:2 has been demonstrated *in vitro* to potentiate the effect of 2-AG C20:4 on motor behaviour (Ben-Shabat *et al.*, 1998) the role of MAG C18:1, although not fully explored in the area of endocannabinoids, is also likely to play a similar role.

MAG C18:0 has been previously reported in rat brain (Saghatelian et al., 2004). The role, if any, of unsaturated MAG C18:0 on the endocannabinoid systems is currently unknown. However, considering C18:2 has been demonstrated *in vivo* and *in vitro* (Ben-Shabat et al., 1998) to show entourage effects, and considering that monounsaturated MAG C18:1 is a substrate for MAGL (Nomura et al., 2008), it is possible that this compound also undergoes similar catabolomic pathways and warrants further investigation.

MAG C22:4, identified here, has been synthesized and demonstrated to have little affinity for CB_1 or CB_2 receptors compared to 2-AG C20:4 (Sugiura *et al.*, 1999; Sugiura *et al.*,

2000). It has not, to the best of the author's knowledge, been previously identified in biological tissue.

C20:3, also observed by this method in rat brain tissue, has previously been tested for CB_1 or CB_2 activity (Sugiura *et al.*, 1999; Sugiura *et al.*, 2000). Unlike C22:4, C20:3 demonstrated comparable activity to C20:4, but only in the n-9 double bond configuration. C20:3n-6 and C20:3n-3 demonstrated considerably less activity. The location of the double bonds in MAG C20:3 identified by this methodology cannot be identified at this current time, so a possible physiological role cannot be confirmed.

3.3.9 NAE and MAG Metabolites

It has been demonstrated that both AEA C20:4 and 2-AG C20:4 can be catabolised via various enzymatic pathways to form a number of new compounds. These structures maintain either an ethanolamine or glycerol moiety and hence could potentially be identified by the PI62 or NL92 survey scan methods.

3.3.9.1 Metabolism by cyclooxygenases-2

Whereas catabolism of arachidonic acid by cyclooxygenase-2 forming prostaglandins is well established, it has also been observed for endocannabinoids *in vitro* studies (Kozak *et al.*, 2004; Kozak *et al.*, 2002a; Yang *et al.*, 2005). Both AEA C20:4 and 2-AG C20:4 have been shown to be a substrate for cyclooxygenase-2 metabolism to form ethanolamide and glycerol esters forms of PGE_2, PGD_2 and $PFG_{2\acute{\alpha}}$. Using the PI and NL survey scan methodologies, these metabolites were not identified in rat brain tissue. Such findings are in agreement with the current literature. Although endocannabinoids are a potential substrate for cyclooxygenase-2, only where FAAH activity has been disrupted are cyclooxygenase-2 metabolites of anandamide been observed *in vivo* (Weber et al., 2004).

3.3.9.2 Metabolism by cytochrome P450 and lipoxygenase

Both AEA C20:4 and 2-AG C20:4 are known substrates for lipoxygenase. *In vitro* studies have shown 2-AG C20:4 to be metabolized by lipoxygenase to 12-hydroxyeicosatetraenoicacid glyceryl ester and 15-hydroxyeicosatetraenoic acid glyceryl ester. Both metabolites are structurally similar to MAG 2-AG C20:4, but with oxidation on the 12^{th} and15^{th} carbon from the ester linkage (Kozak *et al.*, 2002b; Moody *et al.*, 2001). The survey scans for both ethanolamines and glycerol groups did not identify any lipoxygenase metabolites of AEA C20:4, 2-AG C20:4 or any of their structural analogs. Where those lipoxygenase metabolites have been previously identified *in vitro*, such metabolites have not been identified *in vivo*. If such compounds are present it is assumed they are below the limit of detection of this technique.

Cytochrome P450 from human kidney and liver microsomes has been demonstrated *in vitro* to oxygenate anandamide to form single monooxygenated hydroxyeicosatetraenoic acids (HETEs) and epoxyeicosatrienoic acids (EETs), like species including 20-HETE - ethanolamide, 14, 15-EET - ethanolamide and 5,6-EET – ethanolamide. Where these results were obtained *in vitro* from human CP450, Wistar rat brains have also been demonstrated to contain a form of this enzyme (Warner and Gustafsson, 1994), leading to the possibility that such metabolites could be formed. Such metabolites have a similar product ion pattern compared to NAE AEA C20:4 (Bornheim *et al.*, 1995; Snider *et al.*, 2007) and hence would in theory be detected by this methodology if present in concentrations above the LLOD. As no oxygenated compounds such as these were detected in brain samples, it is assumed that they are not present, below the LLOD or that other synthesis / metabolomic pathways are involved.

3.4 Conclusion

The application of survey scans coupled with full product ion spectra has successfully identified a range of endocannabinoid and structural analogs in rat brain. Known NAEs DEA C22:4, AEA C20:4, OEA C18:1 and PEA C16:0, for which standards were available, were identified. Additionally NAE C24:1, NAE C18:0, NAE C20:1 and NAE C22:1, for which standards were not available, were also identified. MAGs 2-AG C20:4 was identified, as well as MAG C22:4, MAG C20:3, MAG C18:1, MAG C18:0 and MAG C16:0, for which standards were not available. To the best of the author's knowledge, MAG C22:4 has not been previously identified in biological tissues.

It has been demonstrated that the method outlined in this chapter has the sensitivity and specificity to identify compounds containing ethanolamine or glycerol moiety and to produce full product ion spectra for further confirmation. Compounds for which standards were not available have been identified based on product ion spectra compared to structurally related standards with the addition of accurate mass measurments. This additional evidence provides greater confidence in the identification of less saturated analytes which form fewer structurally significant ions. To take the identification of these compounds to completion, synthesis of standards would be the most appropriate way. By comparison of retention times and product ion spectra a more complete identification could be made.

This methodology has demonstrated an advantage over other targeted and global methodologies employed in the field of endocannabinoids by identifying a greater profile of NAEs or MAGs. Targeted approaches to date have not demonstrated the range of NAEs and MAGs observed with this technique because of the reliance on standards, a number of which are not commercially available and can be difficult to synthesize in the laboratory. Global methodologies, comparing differences between a control and an enzyme deficient tissue, successfully identified known and novel endocannabinoid-like structures (Saghatelian et al., 2004). However, the identification of analytes lacked the specificity of the approach described in this chapter, basing identification on the

pseudomolecular ion. Further work, however, was required to complement the technique to identify unknowns, using FT-ICR and MS/MS of standards compounds. A limitation of this approach is that only analytes affected by the absence of the knocked out / removed enzymes are identified; those analytes which may be biologically significant but not affected by the chosen variation in the samples are not observed.

A limitation of the proposed identification of NAEs and MAGs is the inability to identify double bond location on the acyl chain. It was attempted by the study of the AEA C20:4 and 2-AG C20:4 EPI spectra but due to the large number of ions resulting from fragmentation of the acyl chain, it was difficult to assign double bond location with confidence.

Fast atom bombardment (FAB) coupled with CID has been previously used for the structural elucidation of NAEs (Kasai et al., 2003). Pseudomolecular ions formed by lithium adducts $[M+Li]^+$ demonstrated greater fragmentation along the acyl chain compared to $[M+H]^+$ species and enable the determination of double bond location. It is unclear as to whether an ethanolamine ion or glycerol neutral loss would be generated under CID from pseudomolecular ions formed by lithium adducts, and hence be detected by the PI62 or NL92 survey scan. Such an approach could be complementary to the survey scans. With the identification of NAEs and MAGs known a targeted approach could be taken to isolate on the $[M+Li]^+$ and fragment to produce a product ion spectra that may identify double bond location.

Atmospheric pressure chemical ionization has been demonstrated to identify double bonds' location in polyunsaturated fatty acid methyl esters (Van Pelt et al., 1999). By the addition of acetonitrile adducts across the double bond, and subsequent product ions formed under CID, the location of unsaturated bonds was accomplished. Whether the characteristic ion and neutral of the ethanolamine and glycerol moieties would be observed with acyl chain adducts is unclear. Again, in a similar vein, this approach could be attempted as an additional, targeted step if double bond location became of critical importance.

Where the approach taken here is an effective method for identifying NAEs and MAGs, the method could equally be applied for the profiling of other endocannabinoids that vary in the end moiety. *N*-acyl taurines, with a distinctive end moiety that fragments under CID to generate the representative *m/z* 124 ion (Saghatelian et al., 2004), could be targeted using the surveying methodology. *N*-arachidonylalanine also form under CID an end moiety detectable by a precursor ion or neutral loss survey scan (Huang et al., 2001). Both compounds and structural analogues could be applicable to the use of this methodology.

Whereas this method has demonstrated the ability to identify and profile NAEs and MAGs in rat brain, the approach could be taken and applied to other tissue. The roles of all the NAEs and MAGs identified here are not fully defined within the sphere of endocannabinoids and the variation of such compounds in different tissues has not been fully investigated. The profile of NAEs and MAGs in other tissues would be valuable to the investigation and understanding of the endocannabinoid system, and these are considered in the next chapter.

CHAPTER 4

4 The identification and Distribution of NAEs and MAGs in Rat Tissue Determined by Precursor and Neutral Loss Survey Scans

4.1 Introduction

Following the successful identification of NAEs and MAGs in brain tissue, a further study was conducted using the QqQLIT precursor ion and neutral loss survey scans coupled with EPI spectra to profile and compare NAEs and MAGs in a variety of rat tissues. Where work to date has investigated the role of endocannabinoids in tissues outside the nervous system, the focus has predominantly been on the well-established endocannabinoids, for which standards are readily available. Little work has been undertaken to identify the range of NAEs and MAGs present. This methodology has the potential to provide a comprehensive profile of related NAEs and MAGs along with metabolites, if present in sufficiently high concentrations.

4.1.1 NAE and MAG profiles in rat tissue

To date there have been few reports of comparative NAE and MAG profiles in mammalian tissues. Most studies have focused on tissue-specific analysis, identifying a relatively small number of specific NAEs and MAGs in a given tissue. The result of this approach is invariably narrow, often ignoring known CB1 and CB2 agonists because of the unavailability of reference standards (Fowler, 2007). Some methods that have profiled a wider range of analytes have limitations. One approach employed TLC coupled with GC-MS to profile MAGs in rat brain, liver, spleen, lung, kidney and plasma (Kondo et al., 1998a). Although successfully identifying C20:4 and C18:0, C18:2 and C22:6 glycerol, the method lacked the selectivity to discriminate MAG species with 14, 16 or 18 carbons on the acyl chain.

An alternative, more selective approach was taken using SPE and GC-MS to identify a number of NAEs and MAGs in kidney, testis, heart, liver, spleen and liver of rat (Schmid et al., 2000). Although identification of a number of analytes was achieved, the range was not as extensive as other targeted methods performed on single tissues (Nomura *et al.*, 2008; Williams *et al.*, 2007) or as comprehensive as the list of compounds identified in chapter 3. A further drawback to the GC-MS approach was the additional chemical derivatization stage required, which added complexity to the sample preparation.

Where investigations into various tissue types have been conducted, the approaches have been narrowly focused. A GC-MS method was applied to rat liver, spleen, lungs, heart, aorta, cortex, medulla, and papilla, investigating for changes in MAG 2-AG C20:4 following bile duct – ligation to simulate cholestatic liver disease (Avraham et al., 2008). Where 2-AG may be of sole interest to the investigation, an understanding of other MAGs and NAEs may have proved useful. Conversely, LC-MS/MS has been applied in the detection of NAE AEA C20:4 in various brain regions (hippocampus, cerebellum, striatum and thalamus) along with the spleen and the skin of rats and humans (Felder et al., 1996), but other NAEs, known CB_1 agonists or entourage compounds, were not investigated. This is not to say such work is not of great use, but a fuller profile of NAEs and MAGs was not achieved due to methodology limitations.

Previous work conducted in the reproductive tissues of rat has demonstrated a wider analysis of NAEs and MAGs than commonly observed in other tissues. HPLC coupled with a fluorescence detector have successfully identified PEA 16:0, NAE C16:1, NAE C18:0, OEA C18:1(n−7) , NAE C18:1(n−9), NAE C18:2(n−6) and AEA 20:4 (n−6) in rat testi (Sugiura et al., 1996), although the profile of NAEs identified was not complete. Furthermore, MAGs were not targeted in this analysis. The ability to analyze a larger profile of analytes compared to other work in the literature was due the group's ability to synthesis reference standards in house. A similar approach taken, again employing GC-MS, profiled NAEs and MAG C18:1n-9, MAG C18:1n-7, MAG C18:2n-6 and MAG C20:4n-6 (Schmid et al., 2000). As with the previous methods, reference standards, excluding AEA C20:4, were synthesised in house. TLC and GC-MS were also used in

the analysis of NAEs in rat testi, again identifying the same NAEs mentioned previously plus one additional not commonly identified in brain, NAE C22:5 (Kondo et al., 1998a).

An LC-MS approach has successfully been applied in the identification of NAEs in a number of brain regions as well as rat kidney, testi, liver, heart and thymus (Koga et al., 1997). Although a reasonable range of tissues were analysed, providing an understanding of the NAE distribution within the rat, only AEA C20:4, OEA C20:4 and PEA C20:4 were analysed, forsaking a number of other biologically significant NAEs and MAGs. Furthermore, identification was performed on the $[M+H]^+$ ion alone. Where such an approach is inherent within the instrumentation used, the use of full product ion spectra employed in this chapter will provide greater selectivity.

4.1.2 Tissues

The following tissues were selected for profiling: brain, spinal cord, heart, lungs, liver and testi. Selection was based on incorporating major organs and additionally where some previous work in the literature was available for comparison.

4.1.3 Aims

The aims of this section of work were as follows:

- Apply the methodology developed in chapter 3 to profile various tissues in rat
- Identify a wider profile of NAEs and MAGs present than previously determined in rat tissue.
- Identify other endogenous metabolites which contain an ethanolamine or glycerol moiety.

4.2 Methods and Materials

4.2.1 Chemicals

Acetonitrile, anhydrous chloroform, ethanol, toluene, ethyl acetate, hexane, ammonium acetate and formic acid were obtained from Fisher Scientific (Loughborough, UK). Anandamide, 2-AG, virodhamine, 2-LG, OEA, PEA, prostaglandin E2 glycerol ester, prostaglandin D2 glycerol ester, prostaglandin $F2_{\alpha}$ glycerol ester, deuterated anandamide (AEA-d8) and deuterated 2-AG (2-AG-d8) were obtained from Cayman Chemicals / Alexis (Nottingham, UK). HPLC grade water, purified using an Elga system to 18Ω (Elga, High Wycombe, UK), was used for all experiments. All glassware used in the EC extraction method was silanized using trichlorotrimethyl silane, obtained from Sigma–Aldrich (Steinheim, Germany), followed by wash stages with toluene and then methanol prior to use. All solvents and chemicals were of HPLC grade or higher. Mobile phases were filtered using 0.47 μm nylon filters (Whatman, Maidstone, UK)

4.2.2 Tissue collection

Tissues and organs were collected from six Sprague-Dawley rats (Charles River, UK). The animals were stunned by a blow to the head followed rapidly by decapitation, typically within 3–4 seconds. The animals underwent immediate dissection, recovering brain, heart, lungs, liver, testi and spinal tissue, following which collected tissues were immediately frozen on dry ice. All tissues were subsequently stored at -80°C until required. Tissue collection was carried out by Professor David Kendall, Dr. Victoria Chapman and Dr. Stephen Alexander, School of Biomedical Sciences, University of Nottingham. Mean weights and standard deviation of tissues are listed in Table 4.1

4.2.3 Tissue extraction

Tissues were extracted by the method detailed in the paper by Richardson *et al* (Richardson et al., 2007). Tissues were homogenized by hand in a silanized glass

homogenizer in 8 ml of ethyl acetate /hexane (9:1 v/v). 10% of its volume of water was added and the contents transferred to a centrifuge tube. Centrifugation was performed at 7000g for 15 min and the temperature maintained at 4°C. The supernatant was removed and the process repeated a further two times to optimize recovery. Supernatants were then subsequently pooled and the solvent removed by centrifugal evaporation.

Extractions were reconstituted in 200 µl ethanol and vortexed for 3 min. 100 µl was removed from each of the tissue replicates and then pooled, dried down and reconstituted in 100 µl of ethanol. This extract was analyzed by the two survey scan methodologies previously described in section [3.2], chapter 3. The remaining 100 µl of samples were refrozen and stored at -80 for further analysis where required.

Table 4.1. Mean weight (n=6) and standard deviation of tissues extracted from the Sprague-Dawley rats.

Statistic	Tissue					
	Brain (left hemisphere)	Heart	Lung	Liver	Testis	Spine
Mean Weight (g)	0.909	1.107	0.745	0.770	1.171	0.152
Stdev	0.026	0.101	0.038	0.043	0.159	0.019

4.2.4 Liquid chromatography and mass spectrometry methods

The same LC conditions detailed in section 3.2.5 in chapter 3 were used here. The parameters for both MS systems have been described in chapter 3. As with brain extracts, NAEs and MAGs were detected in the various tissues using a precursor ion *m/z* 62 and a neutral loss *m/z* 92 survey scans (coupled with an EPI scan). Accurate mass measurement using a TOF-MS was conducted where applicable as previously stated in section 3.2.5, chapter 3.

4.3 Results and Discussion

4.3.1 NAE and MAG profiles in rat tissues

Using a precursor ion and neutral loss survey scan coupled with full product ion spectra a number of known and unknown NAEs and MAGs were identified. Well-established AEA C20:4, OEA C18:1, PEA C16:0 and 2-AG C20:4 and 2-LG C18:2 were identified in tissues. Additionally, NAEs and MAGs previously observed in chapter 3 and for which reference standards were not available were also identified in the tissue extracts. Analytes not previously identified in chapter 3 were also observed in certain tissues. The resulting profiles of NAEs and MAGs demonstrate distribution is tissue dependent; see Table 4.2 and Table 4.3.

NAEs

Table 4.2 illustrates the range of NAEs detected, with acyl chains spanning from C16 up to C24 and containing between zero and 5 double bonds. NAE AEA C20:4, NAE OEA C18:1 and NAE PEA C16:0 were detected in all tissues except lung and heart, where NAE AEA C20:4 was not present or below the LLOD.

It is clear that there is a variation of NAE distribution dependent on the tissue. Spinal tissue and brain (described in section 3.3.5, chapter 3) clearly contains the majority, but not all, of the NAEs detected.

MAGs

A range of MAGs detected in the various tissues are listed in see Table 4.3. The acyl chains detected span from C16 up to C22 and contain between zero and five double bonds. As observed with NAE profiles, spinal cord tissue (and brain, described in section 3.3.5, chapter 3) contains the majority, but not all, of MAGs detected across the spectrum of tissues.

Table 4.2. NAEs detected in various rat tissues by the precursor – ion survey scan (*m/z* 62). There is a clear variation in the profile of NAEs in each tissue. A * indicates the detection of a chromatographic peak with the expected $[M+H]^+$ and the expected RT but no EPI triggered.

Acyl Chain	$[M+H]^+$	RT	Brain	Spinal cord	Testi	Heart	Liver	Lung
C24:1	410.4	10.6	✓	✓				
C22:5	374.3	5.98			✓			
DEA C22:4	376.3	7.10	✓	✓				
C22:1	382.3	9.68	✓	✓				
AEA C20:4	348.3	5.30	✓	✓	✓		✓*	
C20:1	354.3	7.86	✓	✓				
C20:0	356.3	9.22	✓*	✓				
C18:2	324.3	5.3	✓	✓*	✓		✓	
OEA C18:1	326.3	6.17	✓	✓	✓	✓	✓	✓
C18:0	328.3	7.36	✓	✓	✓	✓		✓
PEA C16:0	300.3	5.80	✓	✓	✓	✓	✓	✓

Table 4.3. A list of compounds detected in various rat tissues by the neutral loss survey scan (m/z 92) containing a glycerol moiety. There is a clear variation in the profile of MAGs in each tissue.

Acyl Chain	$[M+H]^+$	RT	Brain	Spinal cord	Teste	Heart	Liver	Lung
C22:5	405.3	6.58			✓			
C22:4	407.3	7.10	✓	✓	✓			✓
2-AG C20:4	379.3	5.92	✓	✓	✓	✓	✓	✓
C20:3	381.3	6.52	✓	✓				✓
C20:1	385.3	8.56		✓				
2-LG C18:2	355.3	5.97			✓	✓	✓	✓
C18:1	357.3	6.89	✓	✓	✓	✓	✓	✓
C18:0	359.3	8.42	✓	✓				
C16:0	331.3	6.7	✓	✓	✓		✓	✓

It was noticed that a few analytes expected to be detected were not observed by the precursor ion or neutral loss survey scans employed. This lack of detection is probably due to endogenous levels being below the LLOD of the methods. When compared to the targeted SRM approach developed in chapter 5, the survey scans are approximately ~5 to 10 times less sensitive. Nevertheless, the survey methods developed in chapter 3 and employed in this chapter have identified a range of NAEs and MAGs in the low pmol/g levels (Richardson et al., 2007) not previously achieved by other analytical methodologies. The distribution of NAEs and MAGs in each rat tissue will now be considered in detail.

4.3.1.1 NAEs and MAGs detected in rat testi

NAEs detected in rat testi

A number of NEAs were identified in rat testi (see Table 4.2), including the well-established endocannabinoid NEA AEA C20:4 and the entourage compounds NEA OEA C18:1 and NEA PEA C16:0. The identification of these compounds was undertaken by comparison of the retention time and EPI spectra with reference standards, as already described in section 3.3.3 chapter 3.

Additionally, NEA C18:2 and NEA C18:0, for which standards were not available, were also observed. These were previously observed in brain tissue and described in chapter 3. EPI spectra of NAEs detected in testi tissue can be found in Figure 4.1.

One other NAE was identified that had not been previously detected in rat brain by this method: NAE C22:5. Identification was based upon the EPI spectra compared to those hypothesized in Chapter 3. The pseudomolecular ion and resulting loss of water were observed. Ions indicative of the amide bond cleavage and subsequent loss of water, $[M+H-C_2H_7NO]^+$ and $[M+H-C_2H_7NO-H_2O]^+$, are also observed at *m/z* 313.3 and 295.3. Two ions originating from the cleavage of the acyl chain, $[M+H-C_3H_7NO_2]^+$ and $[M+H-C_4H_9NO_2]^+$, are also observed at *m/z* 285.3 and 271.3.

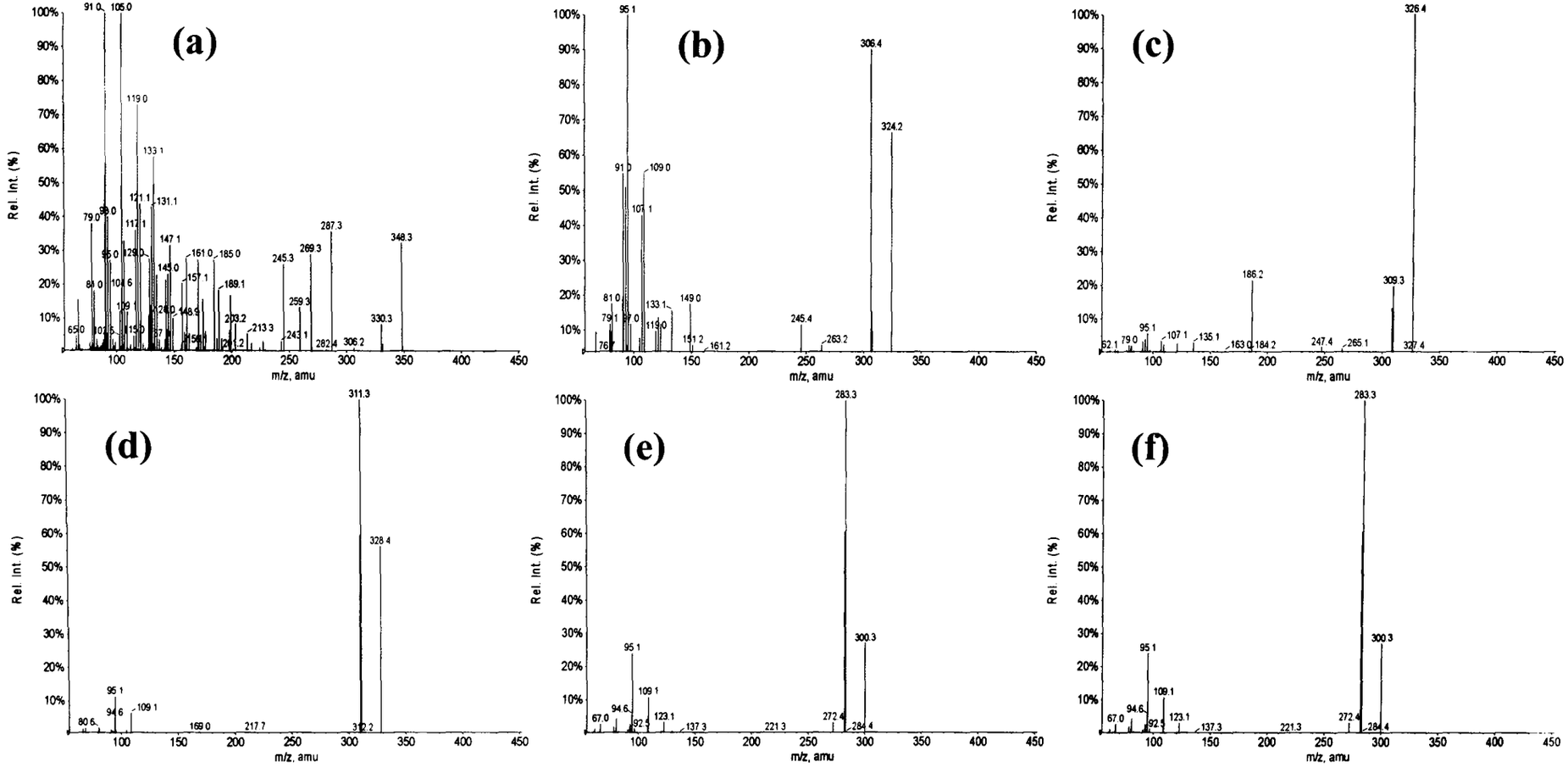

Figure 4.1. EPI spectra of NAEs detected in rat testi: (a) NAE C22:5, (b) NAE C20:4, (c) NAE C18:2, (d) NAE C18:1, (e) NAE C18:0 and (f) NAE C16:0.

Further confidence in identification was gained from the comparison of the EPI spectra with the reference standard spectra of NAE DEA C22:4; see Figure 4.2. NAE C22:5 has one additional double bond compared to NAE DEA C22:4; hence the pseudomolecular ion is 2 amu less, and the loss of water from $[M+H]^+$ is also 2 amu less, than that observed with NAE DEA C22:4. The two ions indicative of a cleavage across the amide bond, $[M+H-C_2H_7NO]^+$ and $[M+H-C_2H_7NO-H_2O]^+$ (*m/z* 313.3 and 295.3), and ions resulting from a cleavage of the acyl chain, $[M+H-C_3H_7NO_2]^+$ and $[M+H-C_4H_9NO_2]^+$ (*m/z* 285.3 and 271.3), are all 2 amu less than those observed from DEA C22:4.

One additional step was undertaken to provide further evidence as to the identification of this compound by accurate mass measurement using LC-TOF-MS. C22:5 was identified by retention time and the theoretical monoisotopic $[M+H]^+$, measured with an error of 1.5 ppm, providing additional confidence as to its identification.

MAGs detected in rat testi

A number of MAGs were identified in testi tissue. Commonly identified MAG 2-AG C20:4 and entourage compound 2-LG C18:2 were observed. Identification was confirmed by comparison of EPI spectra and retention times of standards. Additionally, MAG C22:4, MAG C18:1, and MAG C16:0 were also observed and identification was made as previously stated in chapter 3. EPI spectra of MAGs detected in testi tissue can be found in Figure 4.3.

Another observed MAG not previously identified in chapter 3 was MAG C22:5. Identification was based upon the EPI spectra compared to those hypothesized in Chapter 3. The pseudomolecular ion and resulting loss of water were observed. Ions indicative of the ester linkage cleavage and subsequent loss of water, $[M+H-C_3H_8O_3]^+$ and $[M+H-C_3H_8O_3-H_2O]^+$, are observed at *m/z* 313.3 and 295.3. Two ions originating from the cleavage of the acyl chain, $[M+H - C_4H_8O_4]^+$ and $[M+H - C_5H_{10}O_4]^+$, are also observed at *m/z* 285.3 and *m/z* 271.3.

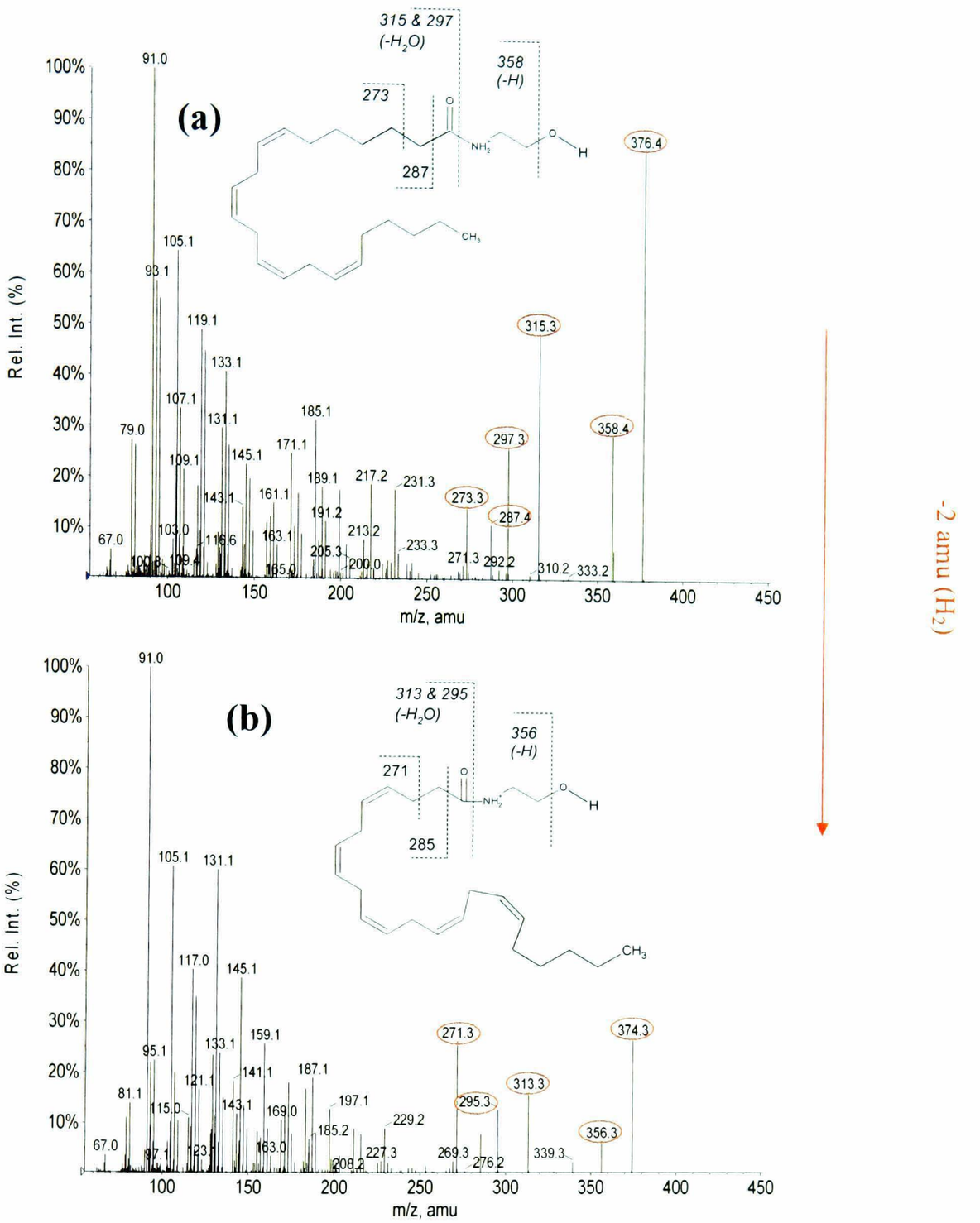

Figure 4.2. A comparison of EPI spectra from (a) DEA C22:4 reference standard and (b) NAE C22:5 extracted and detected in testi by precursor ion survey scan coupled with EPI. C22:5 has one extra double bond compared to C22:4 and is consequently H_2 (2 amu) less. This 2 amu difference is observed in the pseudomolecular ion and the subsequent loss of water. Additionally, the two ions indicative of a cleavage across the amide bond, $[M+H-C_2H_7NO]^+$ and $[M+H-C_2H_7NO-H_2O]^+$, and ions resulting from a cleavage of the acyl chain, $[M+H-C_3H_7NO_2]^+$ and $[M+H-C_4H_9NO_2]^+$, are all 2 amu less than those observed from DEA C22:4. The double bond locations of NAE C22:5 are not identified here, but nominally positioned at n-6 for the sake of the structure

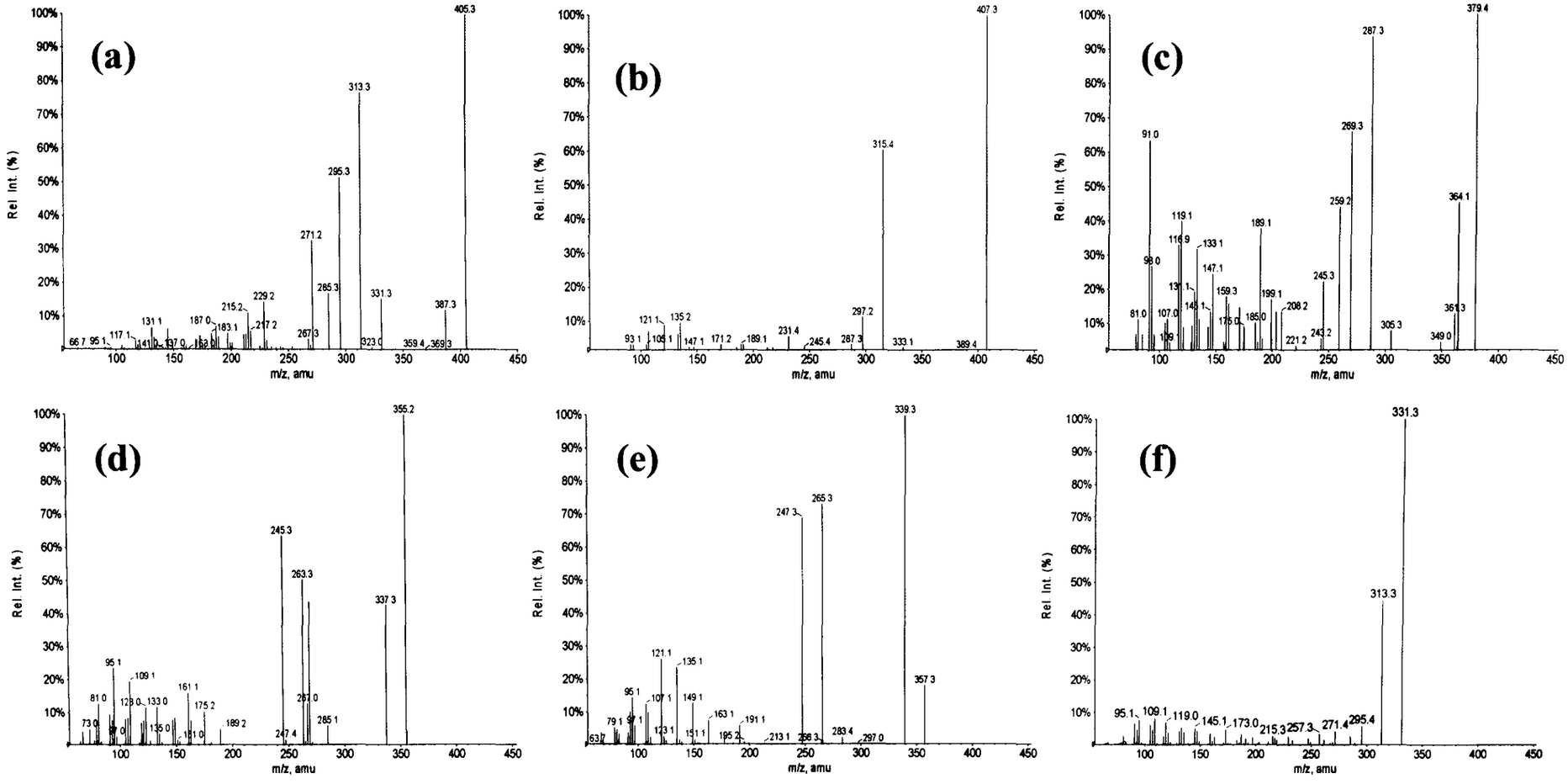

Figure 4.3. EPI spectra of MAGs detected in rat testi: (a) MAG C22:5, (b) MAG C22:4, (c) MAG C20:4, (d) MAG C18:2, (e) MAG C18:1 and (f) MAG C16:0

As an additional step to aid in the identification, comparison of the EPI spectrum with the standard spectrum of MAG 2-AG C20:4 was undertaken; see Figure 4.4. MAG C22:5 has one additional double bond and an extra C_2H_4 on the acyl chain compared to 2-AG C20:4. Consequently, $[M+H]^+$ of MAG MAG C22:5 (*m/z* 405) is 26 amu greater than that of 2-AG C20:4. The loss of water from the pseudomolecular ion is also 26 amu greater than that observed with 2-AG C20:4. The two ions indicative of a cleavage across the ester linkage, $[M+H-C_3H_8O_3]^+$ and $[M+H-C_3H_8O_3-H_2O]^+$ (*m/z* 313.2 and 295.3), and ions resulting from a cleavage of the acyl chain, $[M+H - C_4H_8O_4]^+$ and $[M+H - C_5H_{10}O_4]^+$ (*m/z* 285.2 and 271.4), are all 26 amu greater than those observed from MAG 2-AG C20:4.

To provide further evidence as to the identification of this compound, accurate mass measurements by LC-TOF-MS were employed. MAG C22:5 was identified by retention time pattern and the theoretical monoisotopic $[M+H]^+$ ion, with an error of 10.3 ppm. Such an error is slightly greater than expected of 5ppm, however, the known MAG 2-AG C20:4 was observed to have a mass error of 9.5 ppm.

Testi NAEs and MAGs in the literature

Previously targeted analyses of rat testi have identified more NAEs when compared to tissues such as brain, where work has predominantly been focused on AEA C20:4 and MAG 2-AG C20:4, the more routinely studied ECs. The range of analytes identified in the literature compare well with those detected by this method. Using TLC and HPLC, PEA C16:0, NAE C16:1, NAE C18:0, OEA C18:1, NAE C18:2 and AEA C20:4 have been reported (Sugiura et al., 1996). NAE C16:1 was not observed with the methodology described here. Where it has been previously observed it was the least abundant (0.9% of total NAE) of all NAEs encountered, and the lack of identification by this method is likely due to endogenous concentrations below the LLOD. NAE C22:5 identified here was not identified in the published reference, due to the nature of the targeted approach. An alternative method employing TLC and GC-MS identified C22:5 (n-6) NAE (Kondo et al., 1998b), along with PEA C16:0 , NAE C18:0, OEA C18:1n-7, n-9, NAE C18:2 and AEA C20:4.

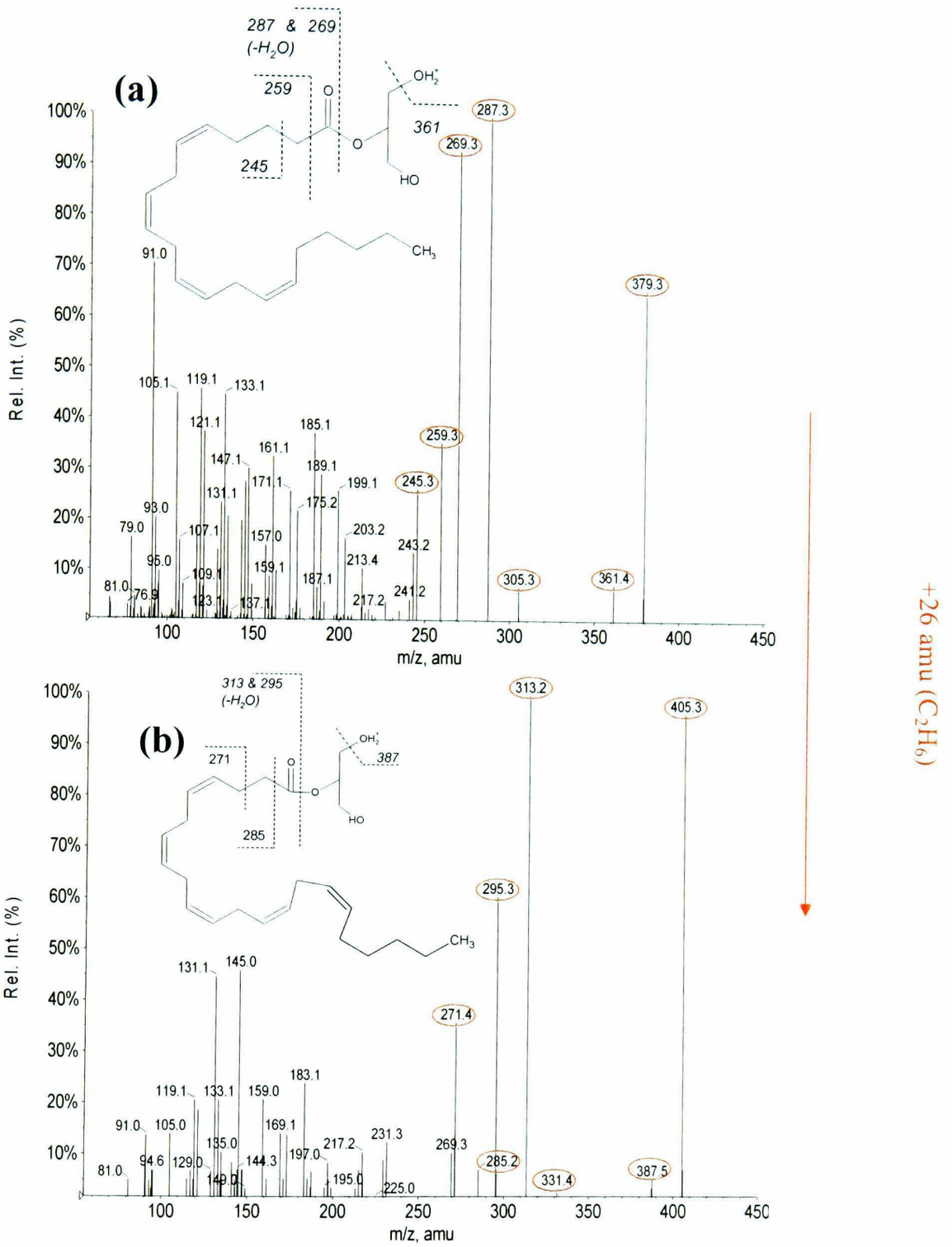

Figure 4.4. EPI spectra of 2-AG, C20:4 (a) and MAG C22:5 (b) detected in testi, but not in any other tissues analyzed by a NL survey scan. MAG C22:5 has one additional double bond and an extra C_2H_4 on the acyl chain compared to 2-AG C20:4. Consequently, the $[M+H]^+$ of MAG C22:5 is 26 amu greater than that of MAG 2-AG C20:4 (*m/z* 405.3). The loss of water is also 26 amu greater that that observed with 2-AG C20:4. The two ions indicative of a cleavage across the amide bond, $[M+H-C_3H_8O_3]^+$ and $[M+H-C_3H_8O_3-H_2O]^+$ (*m/z* 313.2 and 295.3), and ions resulting from a cleavage of the acyl chain $[M+H - C_4H_8O_4]^+$ and $[M+H - C_5H_{10}O_4]^+$ (*m/z* 285.2 and 271.4), are all 26 amu greater than those observed from MAG 2-AG C20:4. The double bond locations of MAG C22:5 are not identified here, but nominally positioned at n-6 for the sake of drawing the structure.

There are few studies of MAG profiles in testi to date; however, in confirmation of results presented here, MAG C18:1 (n-9, n-7), MAG C18:2 (n-6) and MAG C20:4 (n-6) were identified in a Zucker rat testi (Schmid et al., 2000) using SPE followed by a targeted GC-MS method (and an additional derivatization step). Despite extensive searching of the available literature, MAG C22:5, observed here, has not been found to be previously reported in rat testi.

4.3.1.2 NAEs and MAGs detected in rat liver

NAEs detected in rat liver

Known NAEs and endocannabinoid entourage compounds NAE OEA C18:1 and NAE PEA C16:0 were observed and identified by comparison with standard retention times and EPI spectra.

AEA C20:4 was identified by retention time and pseudomolecular ion only. In this instance both analytes were identified by the MS system; however, EPI was not triggered by the software because the intensities of both pseudomolecular ions were below the threshold determined to cause the instrument to switch to EPI mode. The setting of this threshold was applied to reduce the number of false positives resulting from background ions. As a result of the threshold, in conjunction with low endogenous intensities, no EPI were obtained. Despite the lack of EPI spectra there was sufficient evidence from the PI scan and the retention time to be reasonably confident of the identity of the peaks.

NAE C18:2, for which standards were not available, were also observed. Identification was made by comparison of theoretical product ions in section 3.3.4, chapter 3. EPI spectra of the NAEs detected in rat liver can be found in Figure 4.5.

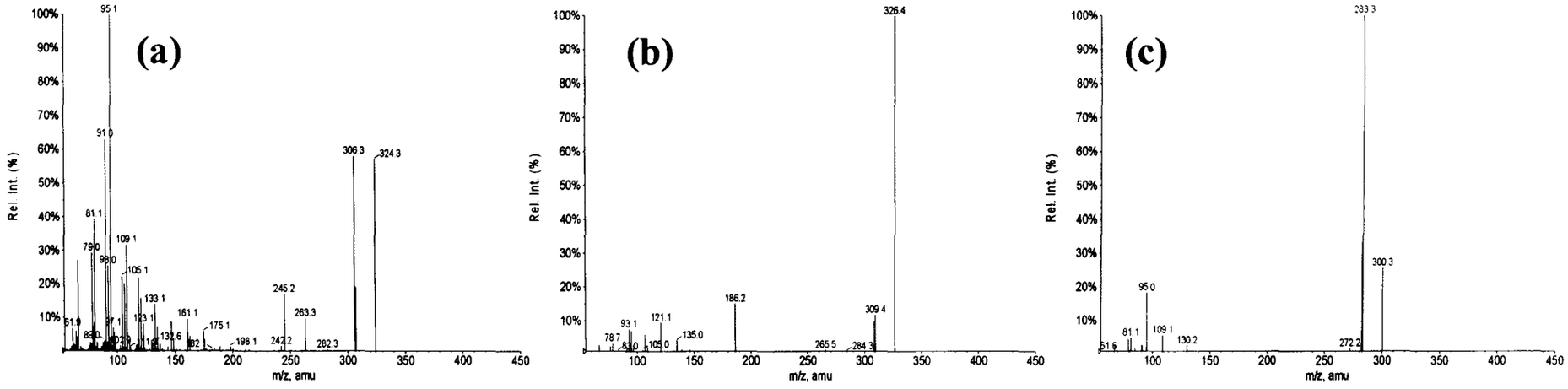

Figure 4.5. EPI spectra of NAEs detected in rat liver: (a) NAE C18:2, (b) NAE C18:1 and (c) NAE C16:0

MAGs detected in rat liver

Known MAGs 2-AG C20:4 and entourage compound MAG 2-LG C18:2 were observed in liver tissues and identification confirmed by comparison of EPI spectra and retention time with available standards.

MAG C18:1 and MAG C16:0, for which standards were not available, were also observed. Both compounds were previously described in section 3.3.4, chapter 3. EPI spectra can be found in Figure 4.6

Liver NAEs and MAGs in the literature

The profile of NAEs and MAGs identified here compares well with those previously obtained employing a GC-MS targeted method with a SPE clean up stage (Schmid et al., 2000). NAEs reported in that method were NAE C16:0, NAE C18:0, NAE C18:1n-9, NAE C18:1n-7 and NAE C18:2n-6. AEA C20:4 n-6 was not detected, however. NAE AEA C20:4 was identified here using the survey methodology, although endogenous levels were so low an EPI was not triggered and identification was consequently based on the pseudomolecular ion and the RT obtained from reference standards.

The same GC-MS method also identified MAG C18:1n-9, MAG C18:1n-7, MAG C18:2n-6 and MAG C20:4n-6. Again, such results compare well with the method detailed in this chapter, although MAG C16:0 was not identified by the targeted method but detected by the survey scan method described here.

4.3.1.3 NAEs and MAGs detected in rat heart

NAEs detected in rat heart

NAE OEA C18:1 and NAE PEA C16:0 were observed and identified by comparison of EPI spectra and retention time against standards. NAE AEA C20:4 was not observed, indicating that, if present, the endogenous levels fall below the LLOD of this method.

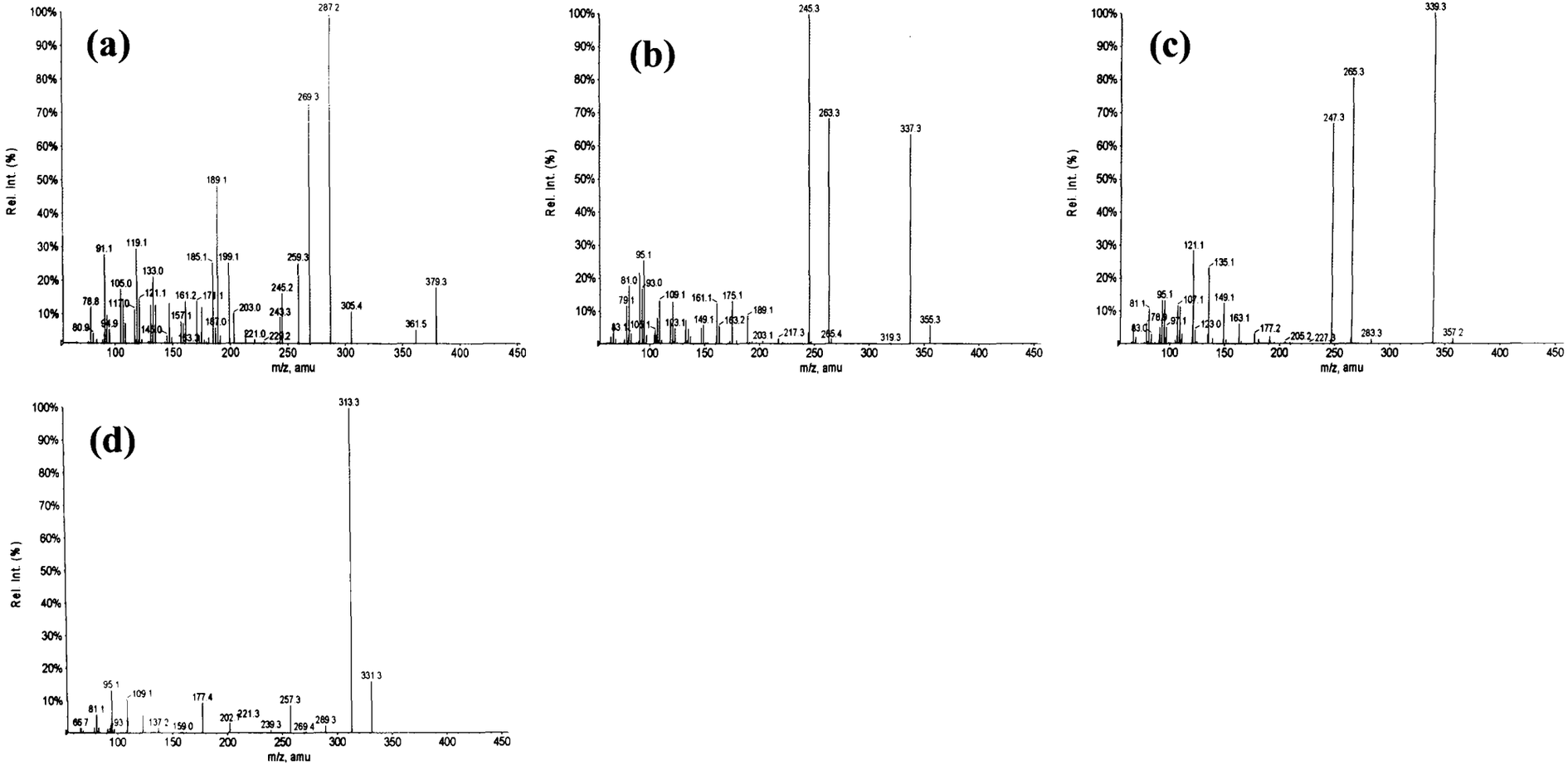

Figure 4.6 EPI spectra of MAGs detected in rat liver, (a) MAG C20:4, (b) MAG C18:2, (c) MAG C18:1 and (d) MAG C16:0

One other NAE was observed in heart tissue: C18:0. Identification was performed as described in section 3.3.5.1, chapter 3. EPI spectra of NAEs detected in rat heart tissue can be found in Figure 4.7

MAGs detected in rat heart

Heart tissue has a noticeable lack of MAGs compared to other tissues, with only three identified. MAG 2-AG C20-4 and MAG 2-LG C18:2 were observed, and identification confirmed by comparison of EPI spectra and retention time with available standards.

MAG C18:1, for which standards were not available, was also observed, and previously described in section 3.3.5.2, chapter 3.

Heart NAEs and MAGs in the literature

Previous analysis of heart tissue from a Zucker rat demonstrates similar NAE profiles to those observed here (Schmid et al., 2000). Employing a targeted method, using SPE and GC-MS with a derivatization step, NAE C16:0, NAE C18:0, NAE C18:1n-9, NAE C18:1n-7 and NAE C18:2n-6 were identified. NAE AEA C20:4n-6 was not identified, due to endogenous levels, nor was it observed by the survey method described in chapter 3. MAG C18:1n-9, MAG C18:1n-7, MAG C18:2n-6 and MAG C20:4n-6 were identified by the targeted GC-MS method. These results compare well with the MAGs detected by the survey scan method, which also identified MAG C18:1, MAG C18:2 and MAG C20:4.

4.3.1.4 NAEs and MAGs in rat lung

NAEs

Lung tissue appears to contain fewer detectable NAEs compared to other tissues examined. Neither AEA C20:4 nor DEA C22:4 were detected above the LLOD. OEA C18:1 and PEA C16:0 were observed and identified by comparison of EPI spectra and retention time with standards.

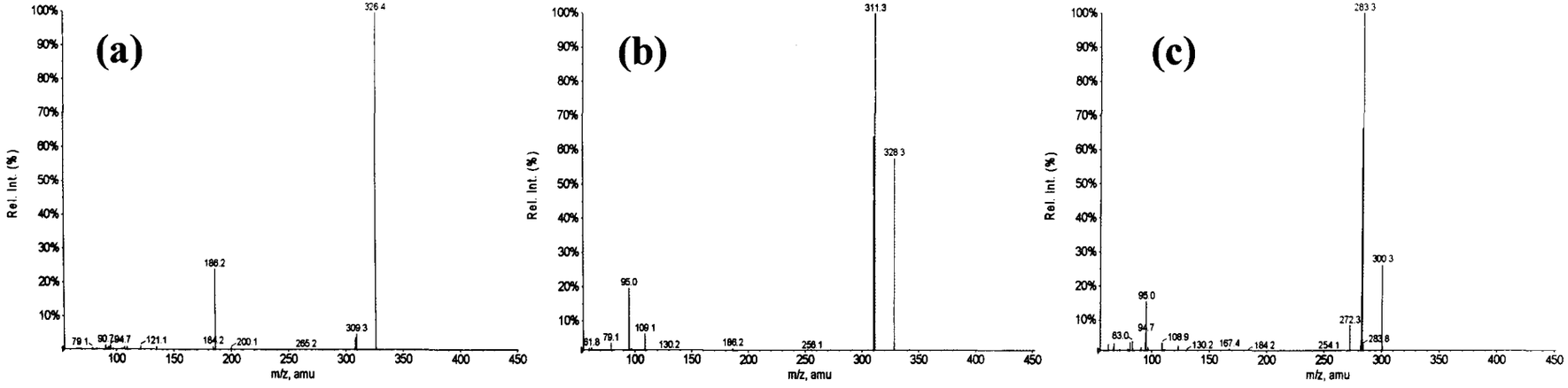

Figure 4.7. EPI spectra of NAEs detected in rat heart: (a) NAE C18:1, (b) NAE C18:0 and (c) NAE C16:0.

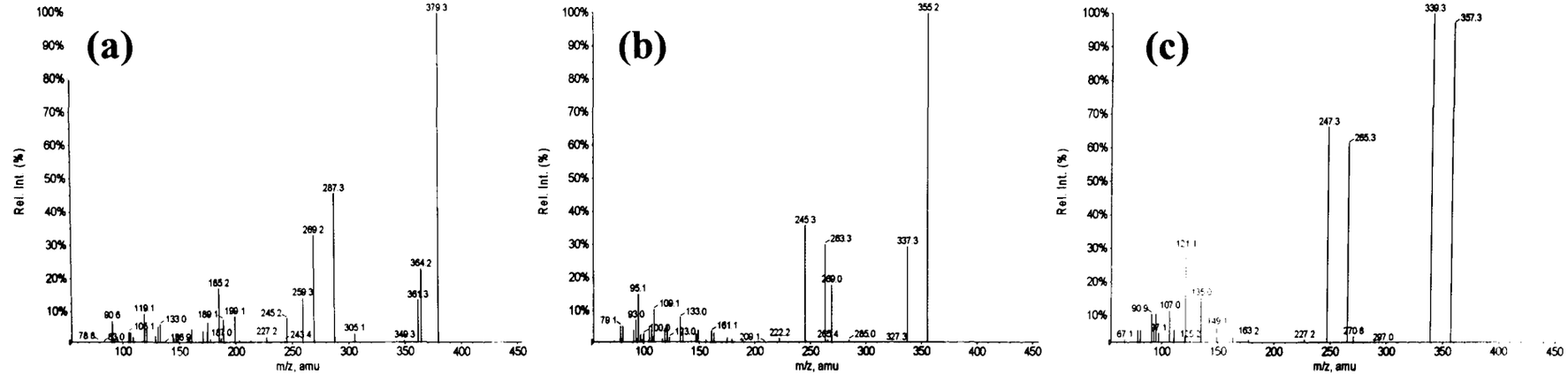

Figure 4.8. EPI spectra of MAGs detected in rat heart: (a) MAG C20:4, (b) MAG C18:2 and (c) MAG C18:1

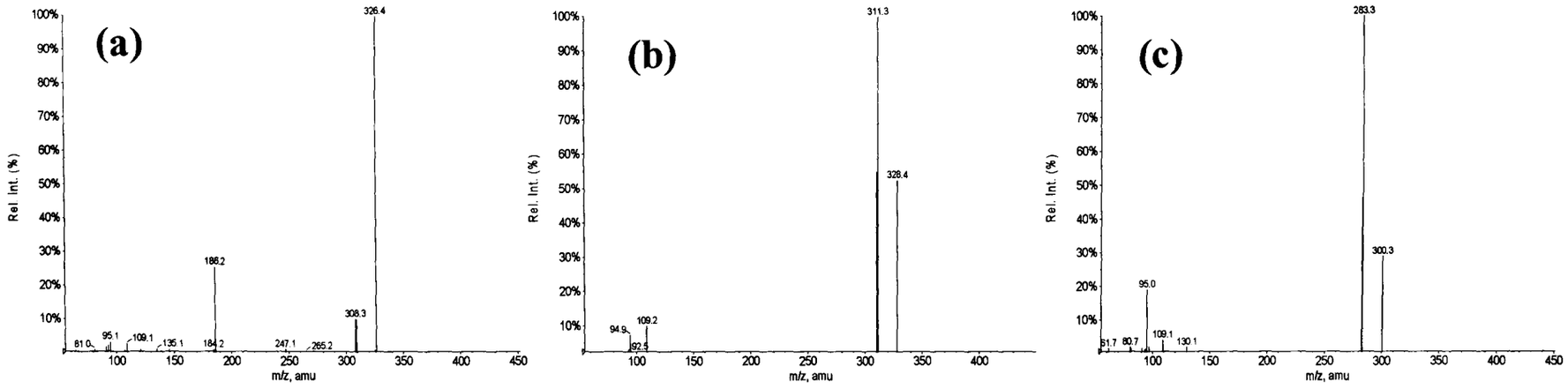

Figure 4.9. EPI spectra of NAEs detected in rat lung: (a) NAE C18:1, (b) NAE C18:0 and (c) NAE C16:0.

One other NAE was observed in lung tissue: C18:0. Identification was performed by comparison of product ions with theoretical ions listed in chapter 3. EPI spectra can be found in Figure 4.9.

MAGs

Lung extract demonstrates a varied number of MAGs. Commonly studied MAG 2-AG C20-4 and entourage compound MAG 2-LG C18:2 were observed. Confirmation was obtained by comparison of product ions and retention time of available standards.

MAG C22:4, MAG C20:3, MAG C18:1, and MAG 16:0 for which standards were not available, were observed. Previous identification has been described in section 3.3.5.2, chapter 3.

Lung NAEs and MAGs in the literature

AEA C20:4 was not identified in rat lung using the precursor ion survey method detailed in this chapter 3, furthermore endogenous levels fell below the limit of quantification in a previous, targeted GC-MS study (Yang et al., 1999). AEA C20:4 has, however, been identified in other rodent lung tissue, including mice (Weber et al., 2004) and guinea pig (Jia et al., 2002). As this endocannabinoid has been previously observed in lung tissue (albeit from other rodents), the lack of detection could be attributed to endogenous levels below the LLOD. Where there is little information in the literature regarding other NAEs in rat lung, entourage compounds OEA C18:1 and PEA C16:0 were identified, as well as NAE C18:0, by the methodology described here.

2-AG C20:4, identified by the neutral loss method presented here, has been previously identified in rat lung (Avraham et al., 2008). Another previous study (Kondo et al., 1998a) has profiled other MAGs, although a lack of selectivity prohibited the qualification and quantification of MAG C14:0, MAG C16:1, MAG C16:0 and MAG C18:1. MAG C18:0, MAG C18:2, MAG C20:4 and MAG C22:6 were quantified, however. These results do not compare well against those obtained by the method described in this chapter (MAG C22:4, MAG 2-AG C20:4, MAG C20:3,

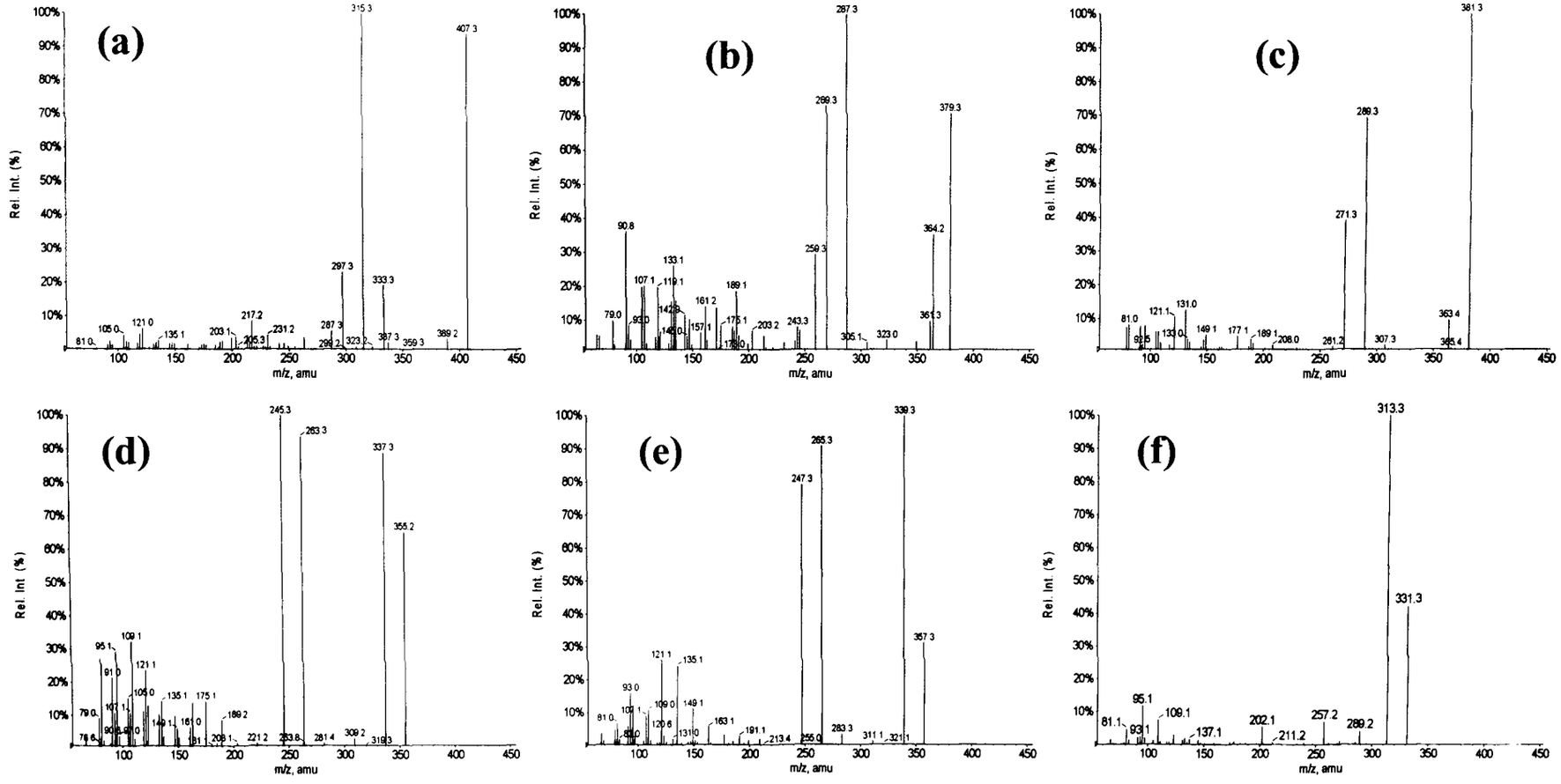

Figure 4.10. EPI spectra of MAGs detected in rat lung (a) MAG C22:4, (b) MAG C20:4, (c) MAG C20:3, (d) MAG C18:2, (e) MAG C18:1 and (f) MAG C16:0

MAG 2-LG C18:2 and C18:1). Analytes MAG C22:4 and MAG C20:3 were missed by the previous method. MAG C22:6 was not identified by the neutral loss method, presumably due to endogenous levels below the LLOD of the method, levels previously reported to be of an order of magnitude less than MAG 2-AG C20:4. The neutral loss survey method described in this chapter provides a greater, more complete picture of NAEs and MAGs in rat lung than previously reported.

MAG C20:3 was also demonstrated (Sugiura *et al.*, 1999; Sugiura *et al.*, 2000) to display similar activity as MAG 2-AG C20:4 against CB_1 and CB2 endocannabinoid receptors, but only in the n-9 double bond configuration.

4.3.1.5 NAEs and MAGs detected in rat spinal cord

NAEs

NAEs detected in spinal cord tissue cover the majority of analytes detected in other tissues. Known NAEs AEA C20:4 and DEA C22:4, along with entourage compounds OEA C18:1 and PEA C16:0, were observed and identified by comparison of EPI spectra and retention time with standards.

Other NAEs, for which standards were not available, were detected: NAE C24:1, NAE NAE C22:1, NAE C20:1, NAE C20:0, NAE C18:2, and NAE C18:0 Identification was performed as described in Chapter 3. EPI spectra can be found in Figure 4.11 and Figure 4.12.

MAGs

2-AG C20-4 and 2-LG C18:2 were identified by comparison of product ions and retention time compared to standards.

MAG C22:4, MAG C20:3, MAG C18:1 and MAG C16:0, for which standards were not available, were previously observed in chapter 3 and their identification described there. EPI spectra can be found in Figure 4.13.

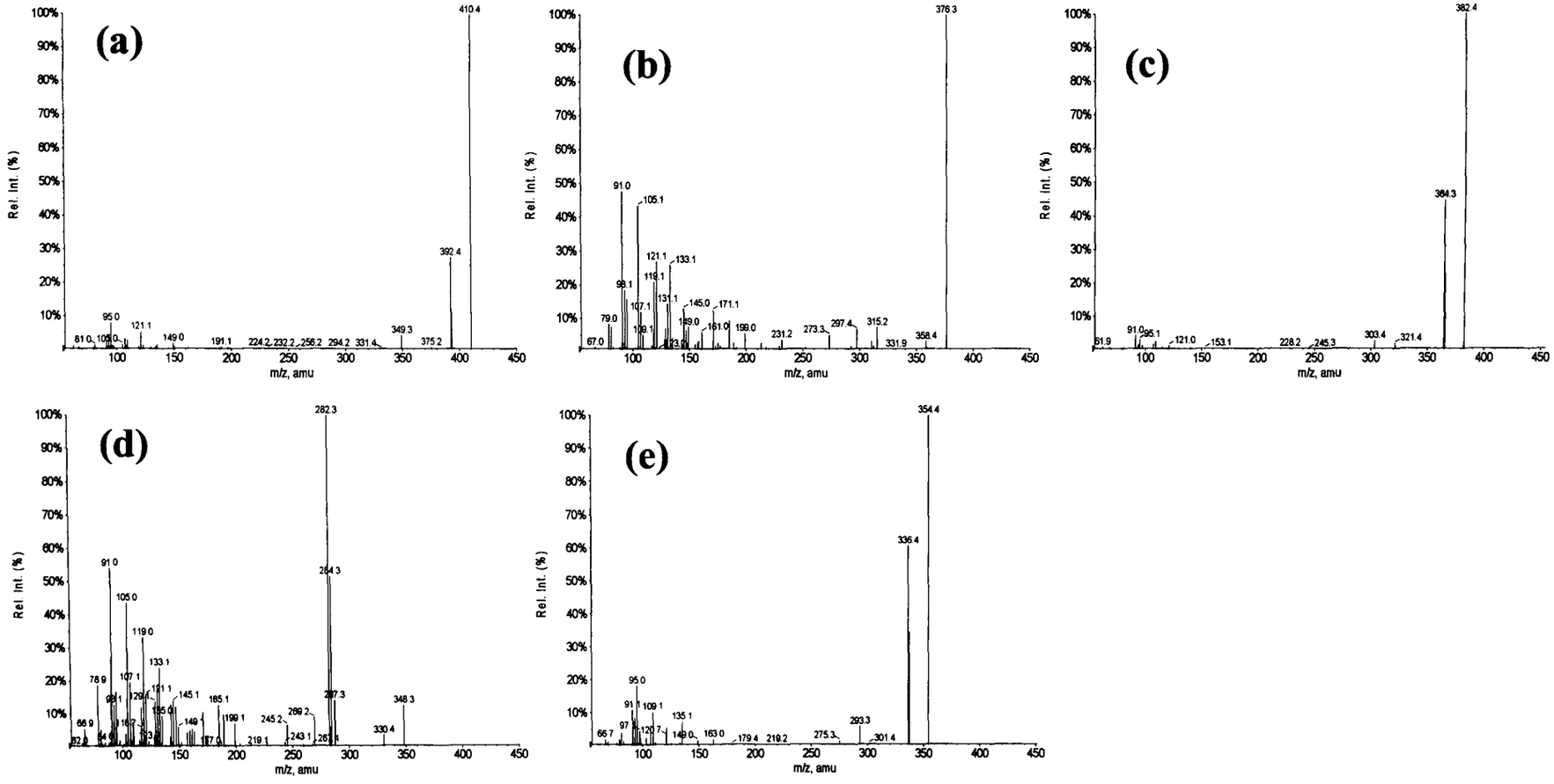

Figure 4.11. EPI spectra of NAEs detected in rat spinal cord: (a) NAE C24:1, (b) NAE C22:4, (c) NAE C22:1, (d) NAE C20:4, and (e) NAE C20:1.

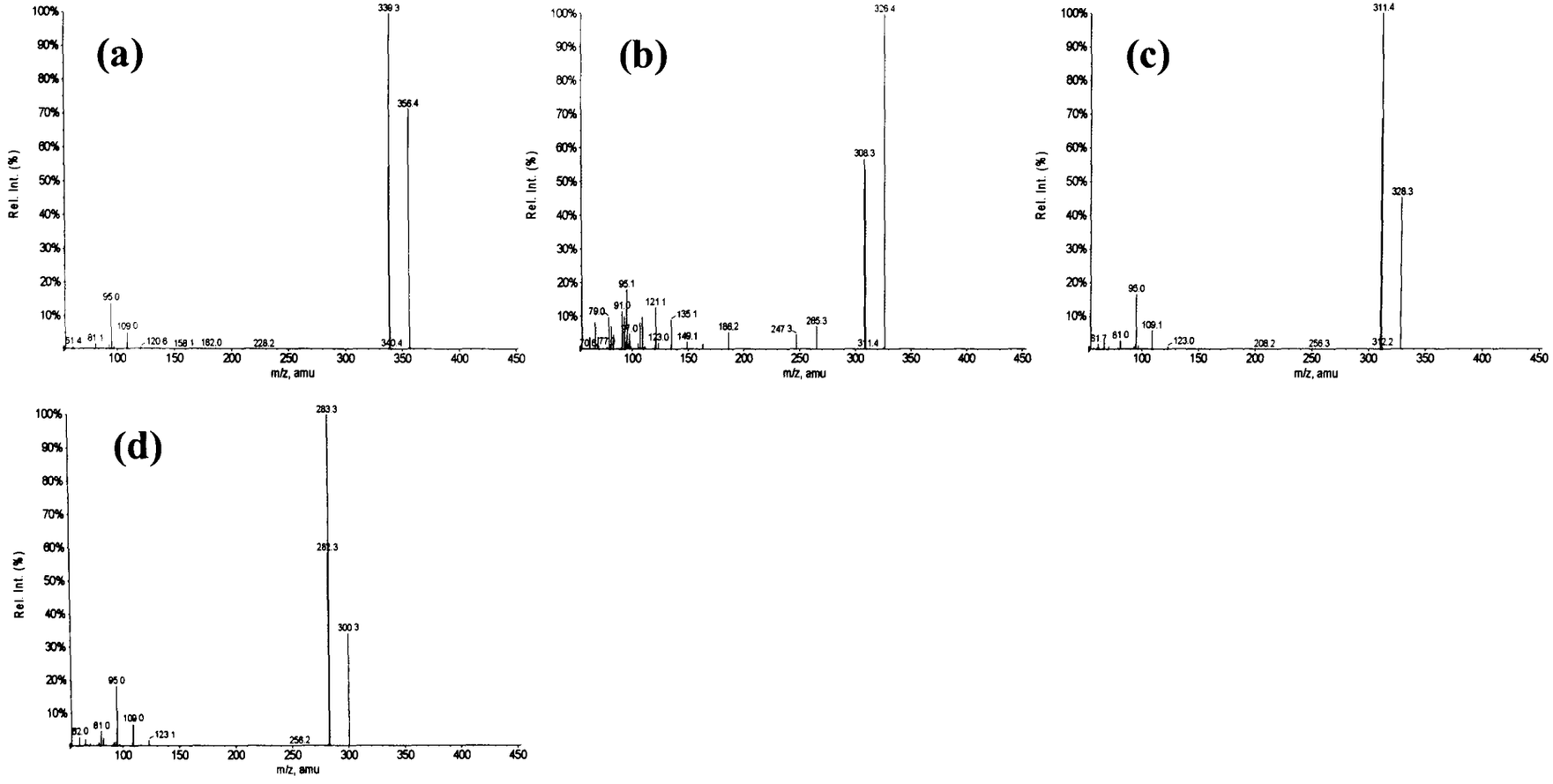

Figure 4.12 EPI spectra of NAEs detected in rat spinal cord: (a) NAE C20:0, (b) NAE C18:1, (c) NAE C18:0 and (d) NAE C16:0

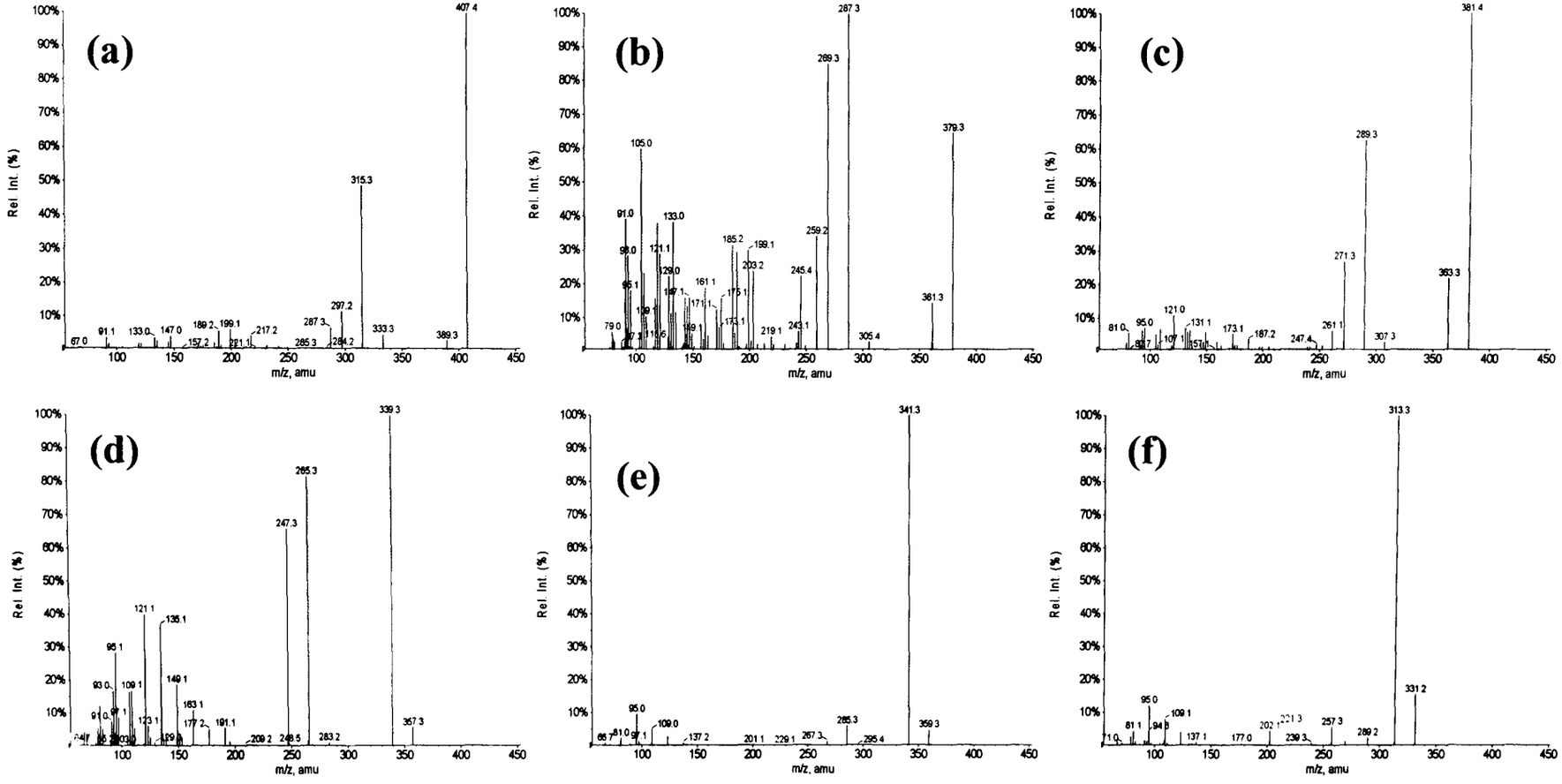

Figure 4.13. EPI spectra of MAGs detected in rat spinal cord: (a) MAG C22:4, (b) MAG C20:4, (c) MAG C20:3, (d) MAG C18:1, (e) MAG C18:0 and (f) MAG C16:0

An additional MAG was detected in rat spinal cord, MAG C20:1. To aid in the identification, a comparison of diagnostic product ions was made against theoretical ions listed in Table 4, Chapter 3. Additionally the EPI spectrum was compared against that of 2-AG C20:4 standard; see Figure 4.14. MAG C20:1 is structurally similar to 2-AG C20:4, varying by three double bonds on the acyl chain and consequently 6 amu. As can be seen when comparing the two spectra, MAG C20:1 has a pseudomolecular ion 6 amu greater that 2-AG C20:4. Additionally, ions indicative of the loss of water $[M+H-H_2O]^+$ (*m/z* 367.3) as well as ions from the cleavage of the ester linkage $[M+H-C_3H_8O_3]^+$ (*m/z* 293.3), $[M+H-C_3H_8O_3-H_2O]^+$ (*m/z* 275.3) are also +6 amu greater. The low mass ions from ~ *m/z* 91 to 200 commonly observed with MAG (and NAE) reference standards and are the result of fragmentation of the acyl chain, are at reletively low intensity. This lack of ions could be the result of the CE being slightly too low for this specific analtye.

Spinal Cord NAEs and MAGs in the literature

The commonly investigated NAEs have been measured numerous times in rat spinal cord. AEA C20:4 and PEA C16:0 have been reported in rat spinal tissue with investigations into spinal cord and peripheral injury on endocannabinoid levels (Garcia-Ovejero *et al.*, 2009; Petrosino *et al.*, 2007). AEA C20:4, OEA C18:1 and PEA C16:0 have been measured during the investigation of fatty acid amide hydrolase knockout mice and alternative metabolomic pathways (Mulder and Cravatt, 2006). Other NAEs have not been studied in such detail, although one investigation of spinal cord in fatty acid amide hydrolase knockout mice, using a global approach, identified NAE C16:0, NAE C18:0, NAE C18:1, NAE C20:0, NAE C20:1, NAE C22:0, NAE C22:1, NAE C24:1, NAE C24:0 and NAE C26:1 in wide type mice (Saghatelian et al., 2004) . These results compare well with those observed by the precursor ion survey scan method; see Table 4.2. Although NAE C24:0 and NAE C26:1 were not observed by the precursor ion survey scan method described in this chapter, such differences could be species dependent.

2-AG C20:4, a most abundant endocannabinoid, has been investigated in rat spinal tissue. Levels have been reported during investigation into spinal cord and peripheral injury on

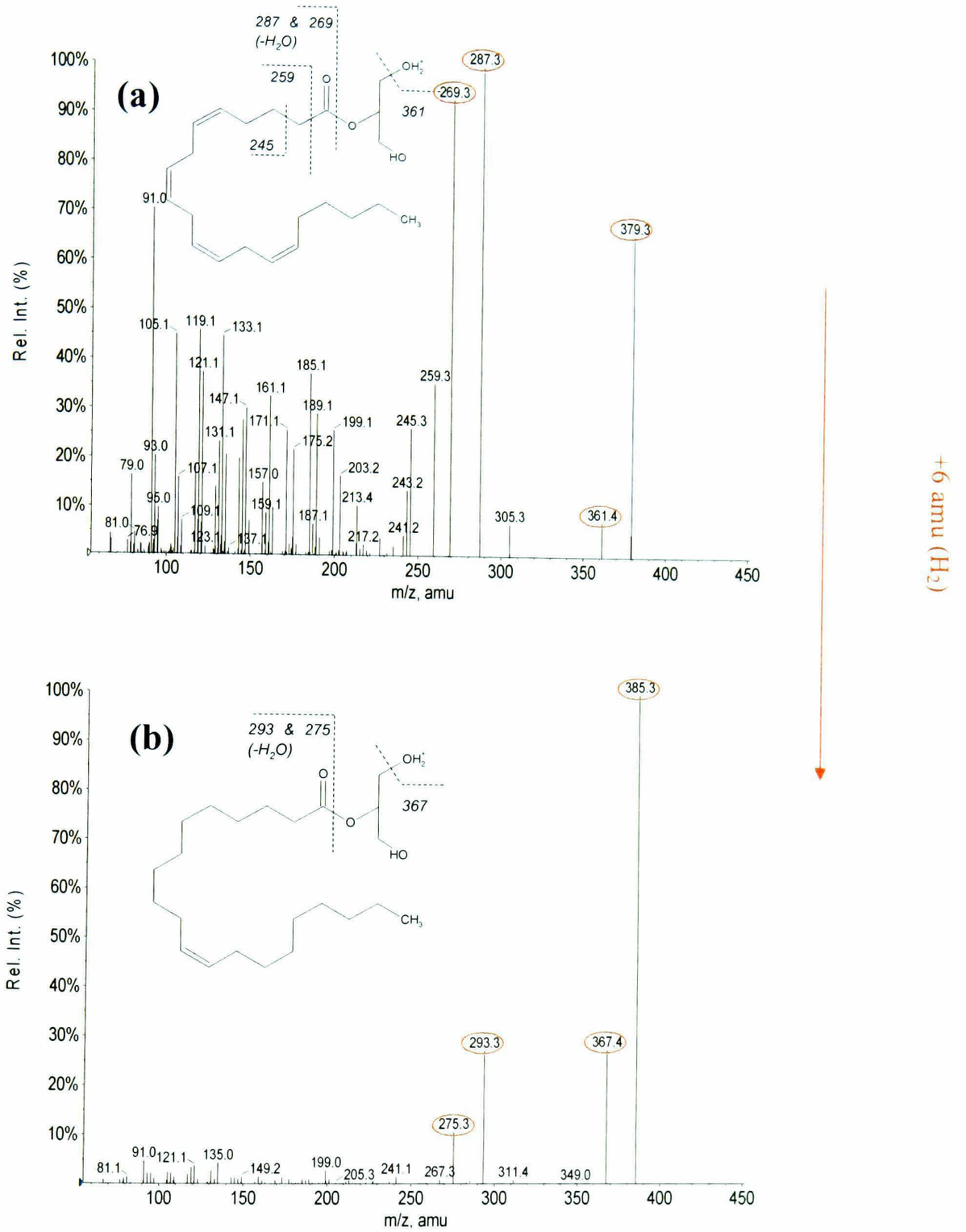

Figure 4.14. Identification of MAG C20:1. EPI spectra of (a) 2-AG C20:4 standard and (b) MAG C20:1 from rat spine. C20:1 has three less double bonds compared to MAG 2-AGC20:4, and consequently the $[M+H]^+$ is 6 amu greater. Additionaly the loss of water $[M+H]^+ - H_2O$ (*m/z* 367.3) and ions resulting from the ester linkage (*m/z* 293.3 and 275.3) are 6 amu greater, as compared to the fragments orginating from 2-AG C20:4. The double bond position, not determined by this method, was placed in position n-9 for the purpose of drawing the structure.

endocannabinoid levels (Garcia-Ovejero *et al.*, 2009; Petrosino *et al.*, 2007). MAG 2-AG C20:4 has also been assessed in its role as an analgesic under stress conditions (Suplita et al., 2006).

Other MAGs have not been studied in as much detail in rat spinal tissue. A global approach, mentioned previously, investigating fatty acid amide hydrolase knockout mice, observed MAG C16:0, MAG C18:0 and MAG C18:1 (Saghatelian et al., 2004). These MAGs were identified by the neutral loss method employed in this chapter, as were MAG C20:3 and MAG C22:4, which were not identified in the global method. Again, such differences could be species specific.

4.3.1.6 Discrepancies in NAE OEA C18:1 Spectra

It was noticed that EPI spectra of OEA C18:1 detected in testi, heart, lung, liver and spinal cord tissue had an additional product ion at *m/z* 186.2, which was not previously observed in OEA C18:1 extracted from brain tissue nor in OEA C18:1 reference standards. It was also noted, however, that the EPI spectra of reference standard OEA C18:1, analyzed on the same day as the tissue extracts, also demonstrated this product ion. While these spectra could be due to an additional co-eluting analyte and mis-identified as OEA C18:1, it is more likely the discrepancies originated from an isobaric source of contamination. Such a theory is substantiated by the presence of the additional product ion in the reference standard OEA C18:1 EPI spectrum run on the day of analysis.

Although not proven conclusively, the likely cause of the contamination is from the polypropylene glycols (PPG) reference standards used in the tuning of the instrument's resolution and sensitivity. The PPG standard solution used consists of a number of polymers varying in repeating units, of which one forms a doubly charged pseudomolecular ion at *m/z* 326, nominally isobaric with OEA C18:1. This PPG could be the cause of the unexpected *m/z* 186.2 product ion. It is unlikely that the PPG reference standard fragments to an *m/z* 62 product ion, as there is not a continuous triggering of EPI

scans throughout the chromatography run due to the continual presence of pseudomolecular ion fragmenting to form *m/z* 62 leaching from a post-column point. Nor did an additional *m/z* 326 pseudomolecular ion peak occur at a single time point other than when OEA C18:1 eluted. Consequently, the ion is only detected when the first quadrupole is selective for *m/z* 326 and when both NAE OEA C18:1 and the PPG standard enter the collision cell and product ions are scanned out under EPI conditions. The lack of an *m/z* 62 product ion from the PPG standard means the precursor ion scan is not adversely effected, nor would it cause a false positive if an SRM method were to be implemented, as a likely SRM transition for OEA C18:1 would be *m/z* 326 to 62. Nevertheless, all analysis following this experiment contained an additional cleaning step to remove any potential contamination and the issue did not subsequently arise.

4.3.2 Biological precursors and metabolites

4.3.2.1 NAE and MAG metabolites

Metabolites of prominent NAE and MAG (AEA C20:4 and 2-AG C20:4) identified in the literature are listed in Figure 4.15. It has been demonstrated that NAEs and MAG can be metabolized by cyclooxygenases-2 to form prostaglandins with either ethanolamine or glycerol end groups. Additionally, oxidation of the acyl chain has been demonstrated by enzymes cytochrome P450 and lipoxygenase. Tissue extracts, once analyzed by both the precursor ion and neutral loss survey scan methods, were examined for the presence of possible metabolites. This was performed by identifying and searching for the protonated pseudomolecular ions of metabolites previously identified in *in vitro* studies. Where an EPI spectrum was triggered from a sought $[M+H]^+$, the spectrum was studied for product ions which might be related to the purposed structure. However, as observed in brain tissues, no metabolites were identified.

Oxygenated metabolite derivative of arachidonic acid, determined to have been formed by cytochrome P450, have recently been detected in benign rat brain, kidneys and spleen (approximately 1g of tissue) (Chen et al., 2008) using a targeted LC-MS/MS method. The protonated pseudomolecular ions were not observed, but rather silver adducts with

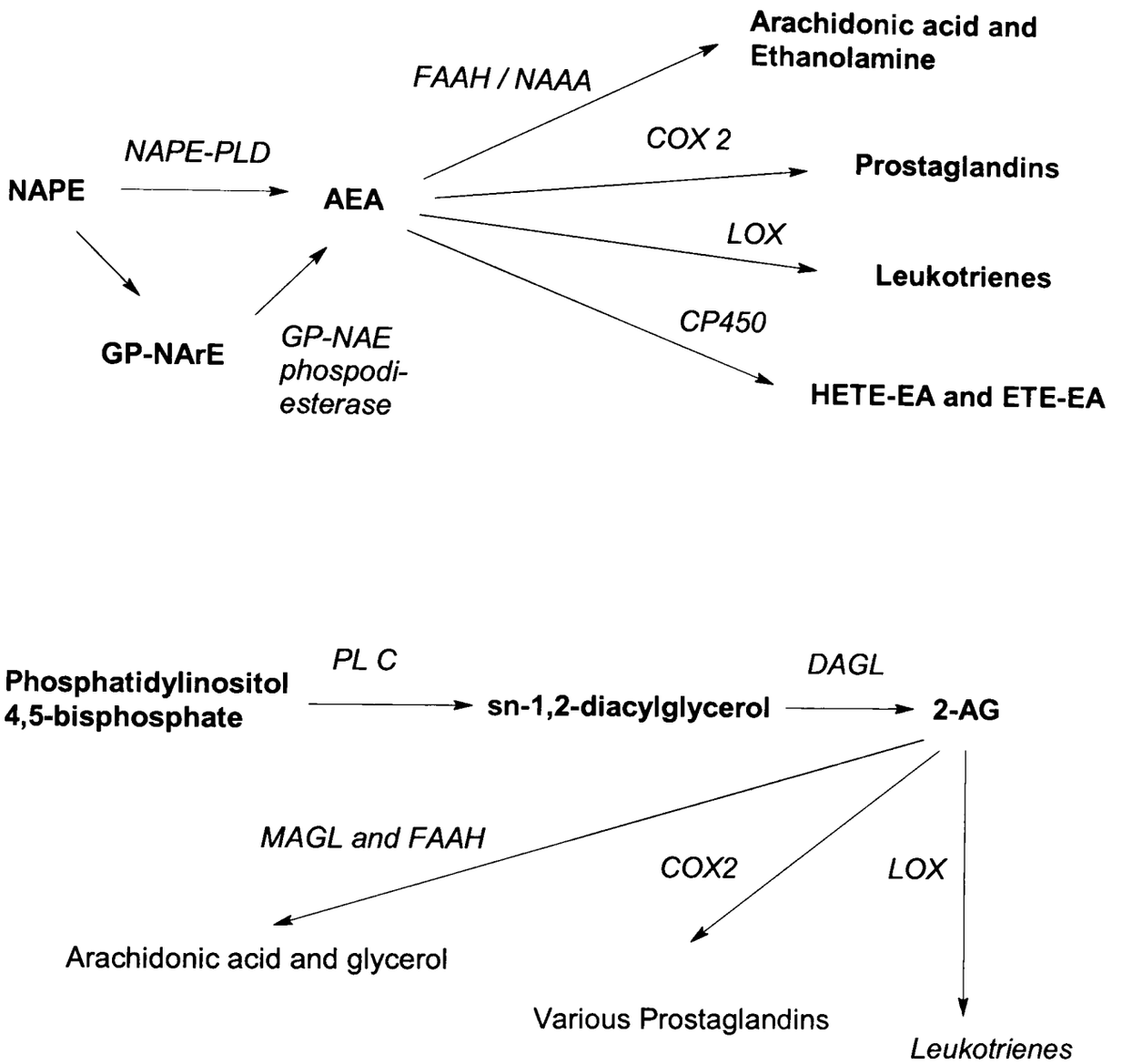

Figure 4.15. Biosynthetic and metabolomic pathways of AEA and 2-AG. Metabolomic pathways are similar to arachidonic acid, which metabolizes to form biologically active compounds. Abbreviations are *N*-acyl-phosphatidylethanolamines (NAPE), glycerophopspho-N-arachidonoylethanolamine (GP-NArE), fatty acid amide hydrolase (FAAH), cyclooxygenase (COX), lipoxygenases (LOX), cytochrome P450 (CP450), hydroxyeicosatetraenoic acid ethanolamine (HETE-EA), epoxyeicosatrienoic acid ethanolamine (ETE-EA), monoacylglycerol lipase (MAGL) and diacylglycerol lipase (DAGL). Based on information in publications (Ahn *et al.*, 2008; Moody *et al.*, 2001; Simon and Cravatt, 2008; Snider *et al.*, 2007; Yu *et al.*, 1997).

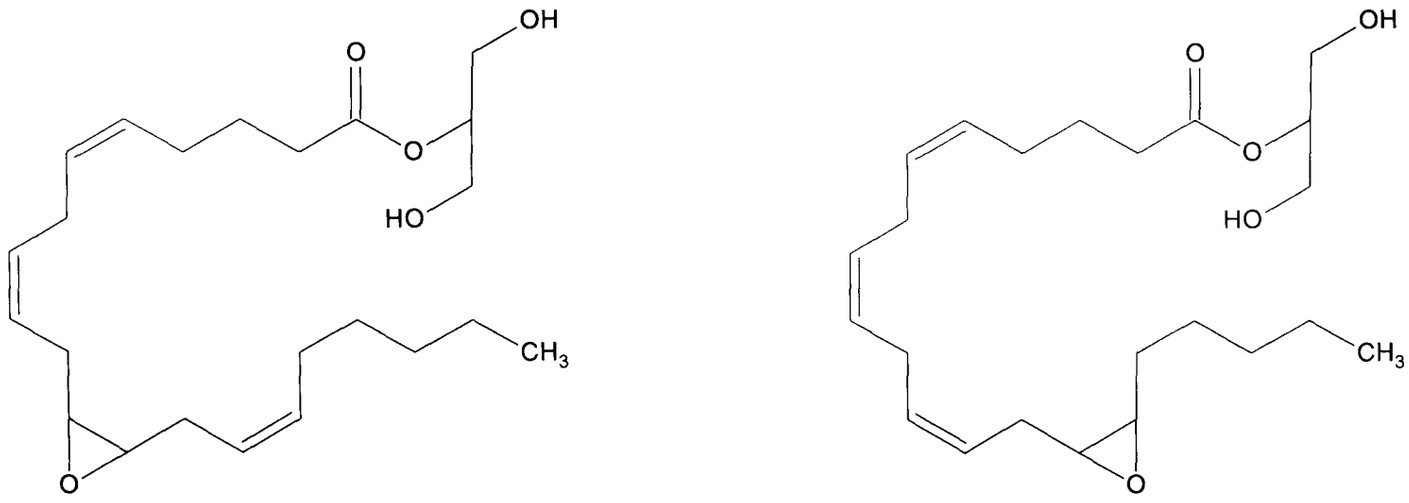

Figure 4.16. 2-(11,12 - epoxyeicosatrienoyl glycerol), two epoxides detected in rat spleen, kidney and brain (Chen et al., 2008). These epoxides were not detected by the neutral loss survey scan methodology employed here. The structure is similar to that of 2-AG, so fragmentation would be expected to lead to a neutral loss of 92, the glycerol group indicating that if present endogenous levels are below the LLOD of the neutral loss survey scan method.

the addition of $AgBF_4$. Two 2-epoxyeicosatrienoyl glycerols (2-EG) were identified, (2-11,12-EG) and (2-14,15 – EG), which vary in the site of oxygenation across the double bond. Although thought to be metabolite derivative of arachidonic acid, a glycerol moiety is present, making identification by the neutral loss survey scan described in chapter 3 a possibility. It was demonstrated that kidney and spleen had roughly comparable levels of each 2-EG, whereas brain contained predominantly the 11,12-EG form. Neither of these metabolites were identified using the survey scan approach described here in any of the tissues analyzed. Structurally both of these epoxides are similar to 2-AG (see Figure 4.16), and hence it is probable a neutral loss of 92 would be observed in CID conditions. The fact that neither analytes are observed with this method is most likely due to endogenous levels being below LLOD of this method.

4.3.2.2 Biological precursors

NAE precursors

Although biosynthetic pathways of NAEs have not been fully established (Ahn et al., 2008), a number of precursors have been previously identified in mouse (Liu *et al.*, 2006; Simon and Cravatt, 2008) and rat (Astarita et al., 2008) brain tissue; see Figure 4.17. These precursors, however, were not identified in rat tissues analyzed by the precursor ion and neutral loss methods described in chapter 3. Although each compound in Figure 4.17 is different, there are strong structural similarities: each analyte contains the AEA C20:4 structure attached to a phosphate group. This linkage onto the ethanolamide moiety may hinder *m/z* 62 product ion formation under CID and consequently preclude these analytes from detection by the precursor ion survey scan discussed here.

A previous study of phosphoanandamide does not provide direct evidence for the lack of an *m/z* 62 product ion under CID, but goes someway to suggest this is the case (Liu *et al.*, 2006). It was demonstrated that the analyte cleaves between the carbon and the terminal oxygen of the ethanolamine moiety, resulting in a PO_4H_2 neutral. This cleavage and the subsequent loss of the oxygen remove the possibility of an *m/z* 62 ethanolamine ion being formed by further fragmentation. Additionally, there appears to be no evidence of a

cleavage resulting in an ion containing an intact NAE AEA C20:4 group, which could undergo further fragmentation, resulting in a *m/z* 62 ion. Because of the structural similarities of the analytes in Figure 4.17 and the addition of a phosphate group attached to the ethanolamide moiety, it is unlikely they will generate an *m/z* 62 ion under CID, hence precluding detection by the precursor ion survey scan described in this chapter

Alternative reasons for the lack of detection could be endogenous levels, which could lie below the limit of detection of the survey scan methods described here. Lack of protonation of the analytes in positive ESI is not necessarily a reason for lack of observation. With the phosphate group, the analytes will de-protonate, as was observed with diacyl-NAPE (Astarita *et al.*, 2008); however, phosphoanandamide was identified as a $[M+H]^+$ ion. None of the NAE biological precursors described in Figure 4.17 have been identified using the survey scan methodology described in this chapter and a number of possible reasons for that have been discussed. Nevertheless, with strong structural similarities these compounds may be identifiable with an alternative survey scan, possibly targeting the phosphate group.

MAG precursors

A limitation of the instrument was observed that highlighted the care required when assigning the pseudomolecular ion from a neutral loss (or precursor ion) survey scan. The neutral loss survey scan of nerve tissue identified a pseudomolecular ion at *m/z* 647.6 that fragmented under CID to generate a neutral loss of 92amu. The instrument subsequently performed an enhanced resolution scan on the identified pseudomolecular ion. The resulting spectrum did not identify *m/z* 647.6 as the monoisotopic ion, as would be expected. Rather, it identified the M+2 isotope of an ion at *m/z* 645.6; see Figure 4.18. The instrument subsequently selected the most intense ion present, *m/z* 645.6, for EPI and ignored the ion *m/z* 647.6. There could be two explanations for the presence of the *m/z* 645.6 ion. The mass accuracy of the neutral loss survey scan could be +2amu in error.

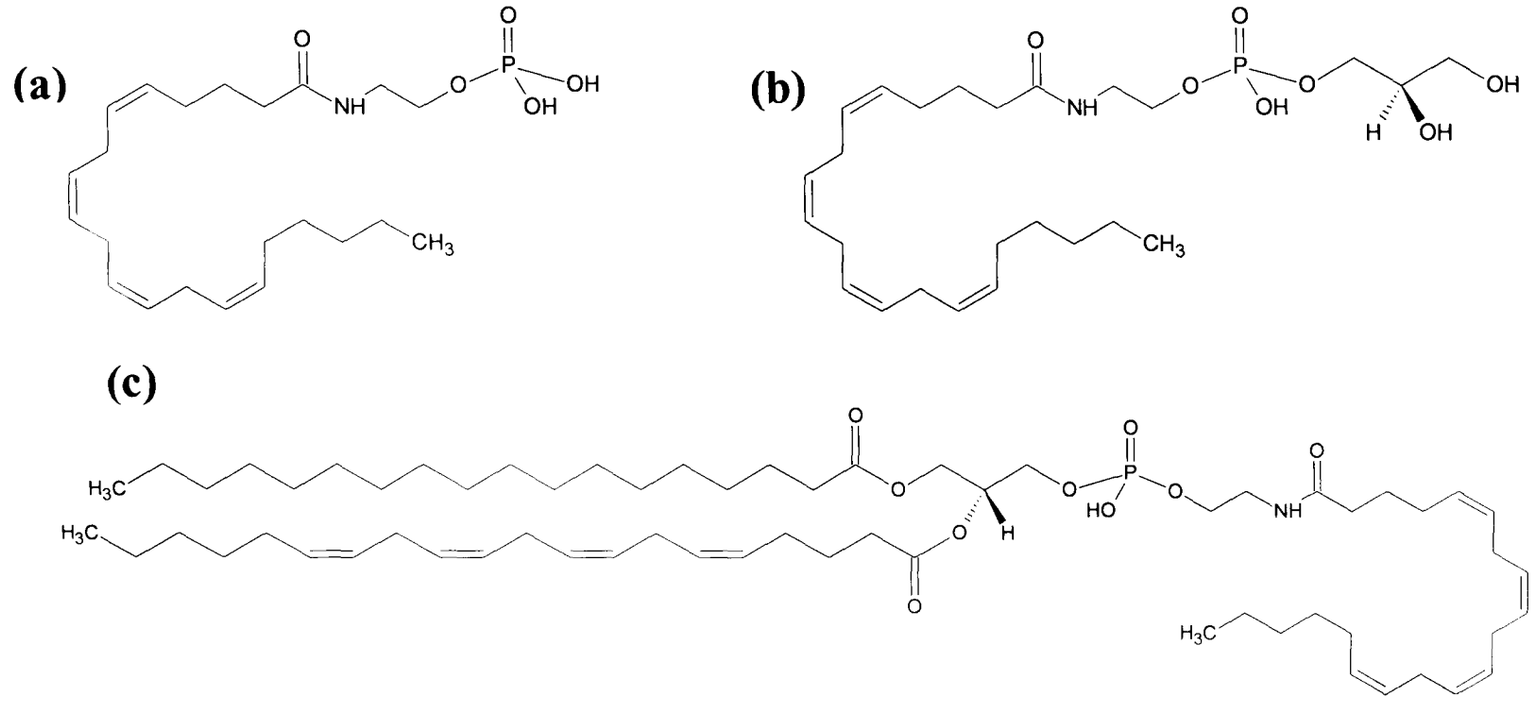

Figure 4.17. Three biological precursors of AEA that have been previously identified in the literature: (a) Phosphoanandamide (Liu *et al.*, 2006) identified in mouse brain tissue under positive ESI conditions, (b) (Simon and Cravatt, 2008) and (c) diacyl-NAPE with *sn*-1 C18:0 and *sn*-2 C20:4 from rat brain under negative ESI conditions. None of the above were identified by the precursor ion survey scan method in the tissues analyzed.

However, this was previously assessed and the mass accuracy was deemed to be at most +0.5amu, and hence is unlikely to be the cause. Alternatively, a second compound co-eluted with *m/z* 647.6 has an *m/z* within ±10 amu of the ion selected by the neutral survey (and hence is included in the enhanced resolution scan) and is also in greater abundance. Because the second ion is observed in the enhanced resolution scan and demonstrates a more intense signal, it is selected to undergo EPI and the ion observed to lose a neutral of 92amu. Such mis-identification demonstrates a limitation of the system. The system can wrongly select an ion for EPI because of a co-eluting, more intense ion. It is possible to run the instrument without the enhanced resolution scan, however, the resolution and clarity of the neutral loss (or precursor ion) scans make it difficult to ascertain with confidence the isotopic pattern, and hence the charge state, of the pseudomolecular ion.

This mis-identification was only observed once. If, however, such an event occurred regularly, it could be addressed by further sample cleanup, reducing the number of possible extraneous analytes in the matrix.

Ironically, the pseudomolecular ion and EPI spectra of the ion *m/z* 645.6, incorrectly selected for EPI, could be a 2-AG precursor and of interest in understanding the roles of MAGs (DAG, 1-octadecanoyl-2-(5Z,8Z,11Z,14Z-eicosatetraenoyl)-sn-glycerol) (Bisogno *et al.*, 1999). DAG (644.5 amu), if protonated, could form a pseudomolecular ion, with a monoisotopic mass of *m/z* 645.5. The detected pseudomolecular ion at *m/z* 645.6 is consistent with a singularly charged protonated DAG molecule, and subsequent EPI spectra of *m/z* 645.6 is consistent with the structure of DAG; see Figure 4.19. Nevertheless, *m/z* 645.5 was not triggered by the NL92 survey scan, although a neutral loss of 92 amu is present. Therefore this compound will not be assigned as DAG; however, the EPI spectra have strong similarities to 2-AG and warrant further investigation.

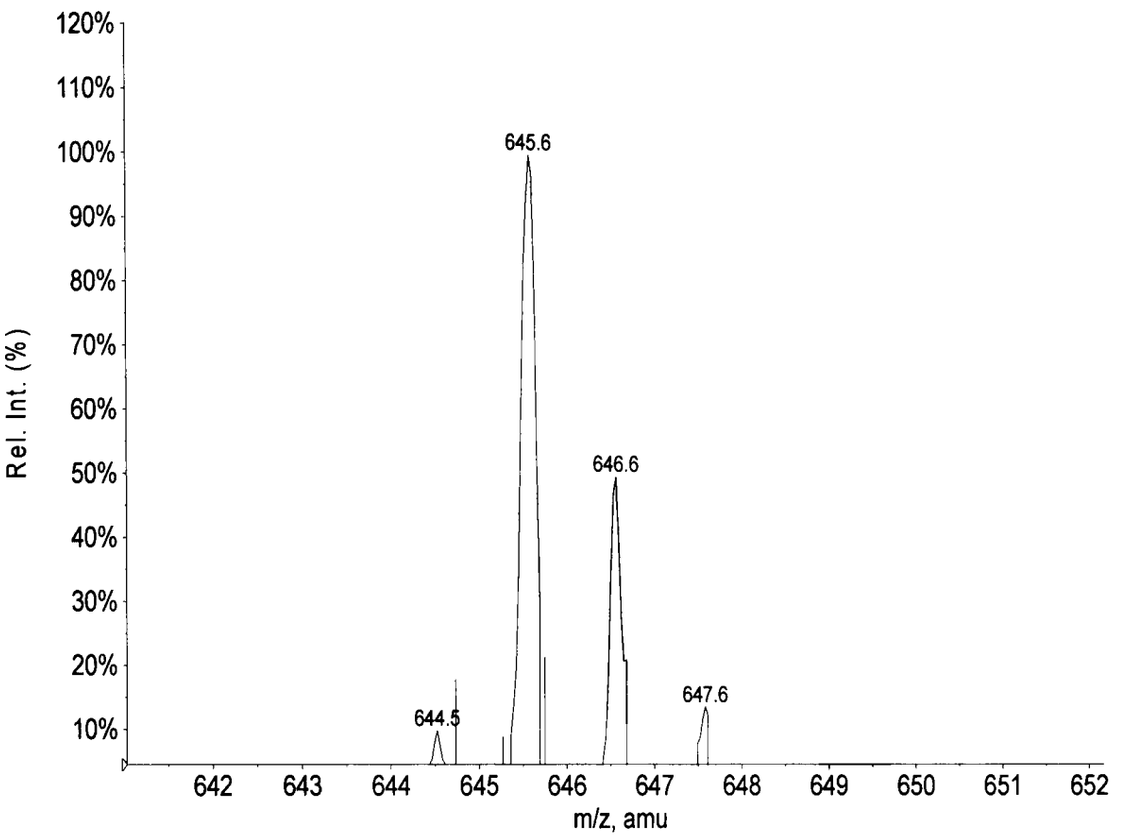

Figure 4.18. The enhanced resolution scan of a compound identified by NL92 survey scan detected in nerve tissue. The pseudomolecular ion *m/z* 647.6 identified by NL92 survey scan is not the monoisotopic ion, as expected, but rather M+2. This indicates that the mass accuracy of the NL survey scan is 2 amu in error; (previous work demonstrated a mass accuracy +0.5amu) or that a co-eluting analyte with a pseudomolecular ion *m/z* 645.6 is present.

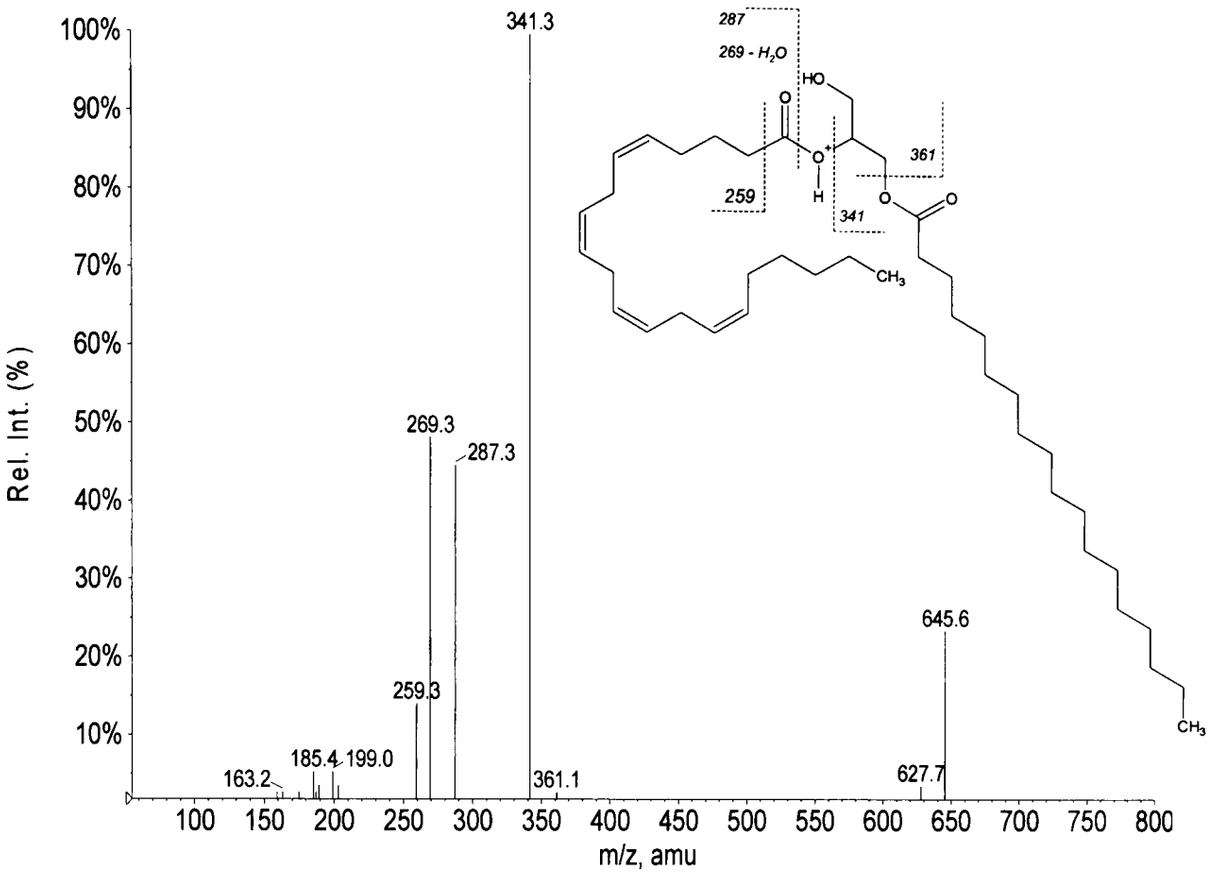

Figure 4.19. The EPI spectrum of compound *m/z* 645.5 detected from nerve tissue recovered immediately after death. The pseudomolecular ion and EPI spectrum are consistent with DAG, an MAG 2-AG C20:4 precursor.

4.3.3 Trends in the distribution of NAEs and MAGs in rat tissues

It is noticeable that there is a variation in the profile of NAEs and MAGs detected across the tissues and that each tissue does not contain the same analytes. Some caution has to be taken when comparing profiles of NAEs and MAGs in different tissues without quantification. Concentrations of analytes vary between tissues. Tissues with low endogenous levels of analytes may demonstrate unusual profiles; this is not due to gross differences, but because analytes may be present at concentrations below the LLOD of this methodology. Previous quantitative analysis (Schmid *et al.*, 2000) indicates that NAE and MAG levels in testi, heart and liver are within an order of magnitude of each other. Levels of AEA C20:4 and MAG 2-AG C20:4 in brain are roughly of an order of magnitude higher than those in the non-CNS tissues (Richardson *et al.*, 2007), but OEA C18:1 and PEA C16:0 are substantially higher. Nevertheless, broad observations can be made from the results obtained from this study.

A notable observation is the presence of C22:5 NAE and MAG in testi, but not in any other tissue examined in this chapter. C22:5 NAE has only been identified previously 3 times; however, C22:5 MAG, despite an intensive search of the literature, has not been previously found. The selective presence of these compounds could indicate a specific role involved in the reproductive system. The effect on cannabinoid receptors CB_1 and CB_2 by C22:5 NAE and MAG has yet to be determined. Due to the similar structure of DEA C22:4 (n-6), a known CB_1 agonist, it is possible that NAE C22:5 could play a part in the endocannabinoid system. Where the location of the double bonds along the acyl chain of this analyte (n-3 or n-6) has not been identified here, previous work has identified the bond position to be n-6 (Kondo *et al.*, 1998a). According to previous work (Sheskin *et al.*, 1997), the position of the double bonds (as well as the number, which is required to be at least three) affects the activity of NAEs, with the n-6 series being greater than n-3. The activity of MAG C22:5 is difficult to estimate. The activity of MAG C20:5n-3 at CB_1 and CB_2 receptors is similar to that of 2-AG C20:4n-6, but MAG C22:4n-6 is relativity low, indicating that the effect of acyl chain length is more critical

for MAGs compared to NAEs (Sugiura *et al.*, 1999; Sugiura *et al.*, 2000). The role of C22:5 NAE and MAG warrants further investigation.

A trend is apparent with the longer acyl chain monosaturates. While monounsaturated OEA C18:1 is common amongst all tissues examined, C20:1, C22:1 and C24:1 NAE appear to only occur (above detectable limits) in brain and spinal tissue. Where synthesis and catabolism of C20:1 and C22:1 remains unclear, C24:1 has been demonstrated to be synthesized via NAPE-PLD in mice (Leung *et al.*, 2006) and catabolised by FAAH (Saghatelian *et al.*, 2004), the same synthesis and degradation routes as other monounsaturated and unsaturated NAEs (C16:0 - PEA, C18:0, C18:1 – OEA, and C20:0). What is interesting is the absence (or below-detection levels) of C24:1 ethanolamine in tissues other than brain when NAEs demonstrated to be synthesized and metabolized by the same routes are present in detectable levels. Such an observation could be explained by a highly selective metabolomic route in these tissues, not present in brain or spinal cord, which has yet to be determined. Whether C24:1 ethanolamine is a substrate for CB1 or CB2 has yet to be reported. However, considering the acyl chain is monounsaturated and does not have the same degree of saturation as known CB1 & CB2 substrates (Ahn *et al.*, 2008; Sheskin *et al.*, 1997), it seems unlikely.

NAE C20:3, first observed along with C22:4 in brain tissue (Hanus *et al.*, 1993), has not been identified in brain and spinal cord tissue nor in any other tissues by this method. With the use of standards, it is known to be identified by the precursor ion scanning method presented in chapter 3. This observation would indicate that, if present, C20:3 NAE is below the LLOD of this method.

NAE C22:4, a known CB_1 agonist that is rarely studied in comparison to C20:4, was not detected across the range of tissues analyzed, instead predominantly residing in brain and spinal tissues. Again, this may be an issue of low endogenous levels or indicating that alternative synthesis and catabolomic pathways are present

The NAE profiles of testi, heart, liver and lung have similar, but not identical, profiles. There is a trend in the non-CNS tissues for shorter, less saturated acyl chain NAEs compared to neural tissues. The exception is the identification of C20:4 and C22:4, known CB_1 agonists. MAG profiles are different from those of NAEs. Heart, liver, testi, lung and liver appear to contain mid-chain MAGs from C18 to C22, whereas brain and spinal cord also cover the shorter range of MAG down to C16.

4.3.4 Occurrence of NAEs and MAGs and free fatty acids

It could be questioned as to whether the distribution of NAEs or MAGs in tissues may be directly related to the distribution of free fatty acids. Although NAEs and MAGs are not generally thought to be synthesized directly from free fatty acids, and although the formation of AEA C20:4 from ethanolamine and arachidonic acid has been demonstrated to be possible *in vitro* (Devane and Axelrod, 1994), the distribution of free fatty acids could impinge on the distribution of NAE or MAG precursors. According to reported but unpublished work (Sugiura *et al.*, 1996), there is not a common distribution of NAEs and free fatty acids in rat brain. The profile of free fatty acids in rat heart does not appear to be similar to NAEs or MAGs either. The presence of short chain saturated or monounsaturated free fatty acids is comparable to the presence of NAE and MAG analogs, however; where C20:4, C20:5, C22:4, C22:5 and C22:6 free fatty acids were observed in rat heart (Yaffee *et al.*, 1980), the NAE and MAG equivalents, excluding MAG C20:4, were not observed.

4.4 Conclusions

The use of precursor ion and neutral loss survey scans coupled with obtaining full product ion spectra has successfully profiled a range of NAEs and MAGs in various rat tissues. The majority of NAEs and MAGs detected in brain tissue are also observed in other tissues, although there were tissue specific variations. A profile of the NAEs and MAG in each tissue demonstrates differences between each tissue and prominent differences between non CNS tissues and brain / spinal cord. It was observed that the CNS tissues contain a range of NAEs from C16 through to C24 and various degrees of unsaturation (0-4) where peripheral tissues generally contain shorter (C16 – C18) NAEs with 0 to 2 double bonds, although AEA C20:4 was found in liver and testi. Furthermore C22:5 was also observed in teste. MAG profiles across the tissues appear to be more uniform compared to NAEs although heart tissue was only found to contain 2-AG C20:4, 2-LG C18:2 and MAG C18:1. NAE C22:5 and MAG C22:5 were identified in rat testi but not in any other tissue. If these analytes are present in tissues other than testi, their endogenous levels fall below the LLOD for this methodology. The presence of these two compounds in testi might suggest a specific role with the reproductive system.

A noticeable profile of NAE C24:1, NAE C22:1 and NAE C20:1 was observed in brain and spinal tissue, but not in any other tissue analyzed. The reason for their selective presence is unclear at this time.

The NAE and MAG profiles in each tissue are more comprehensive than those previously reported, the majority of which have reported a limited number of NAEs and MAGs. This again highlights the advantage of this alternative approach, where NAEs and MAGs have been identified in tissues not because of a preconceived understanding of what may be present but by structural similarities which they all possess.

The lack of NAE or MAG metabolites identified in the tissues analyzed was slightly disappointing but perhaps not surprising. The majority of endocannabinoid metabolites previously reported have been identified *in vitro*. Two oxygenated metabolites of arachidonic acid have been previously identified in rat brain, which in theory would be detectable using the neutral loss survey scan. These metabolites were not identified, presumably due to endogenous levels below the LLOD.

AEA C20:4 precursors were not detected in any tissue in this study. While this may be due to low endogenous levels, a more likely explanation is the inability of the molecules to fragment and yield a *m/z* 62 production, due to the attachment of the ethanolamine moiety with a phosphate group. This is an inherent limitation of such methodology. Precursors or metabolites of NAEs or MAGs that contain enough of a structural difference could affect the fragmentation and result in a lack of identification. For metabolites of NAEs and MAGs that demonstrate greater structural similarity, such as prostaglandin analogs, it has been demonstrated that the lack of detection is not for this reason.

The work in this chapter has highlighted a limitation of this method. In nerve tissue a compound ($[M+H^+]$ *m/z* 647.6) was identified by the neutral loss survey scan to possess a neutral loss of 92amu. The subsequent enhanced resolution scan chose an ion at *m/z* 645.6 to be selected to EPI, due to its greater intensity compared to *m/z* 647.6. Although the ion *m/z* 645.6 fragmented to display a product ion spectra that resembled diacylgycerol, a known 2-AG precursor, the wrong ion was selected for EPI by the software. This point demonstrates that the selection of ions for EPI is not only dependent on the identification during the survey scan, but also on the intensity of ions observed when an enhanced resolution scan is taken. The most intense ion observed by the software in enhanced resolution mode will be selected for EPI, not necessarily the ion observed by the survey scan to be of interest. This issue was only observed once with these samples; however, if this was to occur more frequently, further work would be required to either clean up the samples using different front end methods or to adjust the chromatography so that such compounds did not co-elute with analytes of interest.

While this method has demonstrated the profiles of NAEs and MAGs to differ depending on the tissue, the concentrations of the analytes would provide additional information. A limitation of this method is the lack of quantification, due to sensitivity combined with low endogenous analyte concentrations. The number of data points across an analytical peak can be increased by an increase of tissue material, but this is not a practical option when investigating small quantities of rodent tissues. An alternative approach would be to use the data obtained from these survey scans and to build up a targeted method capable of quantification. The combination of both methods would have the potential of identifying and measuring NAE and MAG levels previously not observed before, and this approach is investigated in the next chapter.

CHAPTER 5

5 Combining survey scans and targeted LC-MS-MS analysis to study post-mortem changes in NAE and MAG lipid classes in rat tissues

5.1 Introduction

5.1.1 Quantification of NAEs and MAGs

The purpose of the work outlined in this chapter was to develop a method to provide a quantitative profile of NAEs and MAGs detected in rat tissues previously identified qualitatively in chapters 3 and 4. Previous analytical methods for NAEs and MAGs have been limited, predominantly by the availability of reference standards to a relatively small list of key compounds (Fowler, 2007). As such, the profile of NAEs and MAGs reported in previous studies is not complete and potentially useful information may be missed due to lack of a comprehensive profiling method. Consequently, a quantitative methodology expanding the range of NAEs and MAGs measured was the focus of this chapter, based on the range of NAEs and MAGs identified in rat tissue in the previous chapter.

The precursor ion and neutral loss survey scan methods used in chapters 3 and 4 identified a wider range of NAEs and MAGs in rat tissue than previously reported by other methods. This was due to the alternative approach taken, using precursor ion and neutral loss survey scans to identify analytes based on structural similarities rather than relying on reference standards. However, the sensitivity of the precursor / neutral loss survey approach is limited when compared with targeted methods, due to the time taken for quadrupoles to scan through the desired mass range (Hoffman and Stroobant, 2005). Where a number of NAEs and MAGs are at relatively low concentrations, as is expected in rat tissues (low pmol / g) (Richardson *et al.*, 2007; Williams *et al.*, 2007), the use of the survey scan method is unlikely to provide sufficient sensitivity to analyse the full

complement of NAEs and MAGs previously detected due to endogenous levels and limited tissue sample.

The alternative was to design a targeted LC-MS/MS approach that would be expected to benefit from an increase in sensitivity, and which incorporated all of the NAEs and MAGs identified in the previous survey scans. Such an approach afforded advantages not open to other previously reported targeted methods.

The approach of developing an SRM methodology based on the understanding of analyte fragmentation from a limited number of reference standards has been previously demonstrated (Scholz *et al.*, 2005). Although concerned with the metabolism of xenobiotic compounds rather than endogenous metabolites, the approach taken was similar. By the use of a limited number of *N*-acetyl-*L*-cysteine standards, MS/MS spectra were obtained and a common neutral loss was observed from a sub-structure common to all analytes. SRM transitions were subsequently prepared for a wider range of known analytes, for which standards were not employed. The precursor ion was known and the product ion identified by the understanding of the neutral loss. This approach, using MS/MS spectra to identify a common moiety across a number of structurally similar compounds and to generate SRM transitions from such, is similar to the tactic taken in this chapter.

5.1.2 Post-mortem changes in tissue levels of NAEs and MAGs

A number of papers have detailed the effects of post-mortem changes in NAEs and MAGs levels post-mortem in mammalian brain tissue (Kempe *et al.*, 1996; Patel *et al.*, 2005; Schmid *et al.*, 1995; Sugiura *et al.*, 2001). These studies have not only illustrated that NAE and MAG levels change substantially post-mortem, but also that not all NAE and MAG concentration profiles post-mortem are the same. Such an observation has led to the conclusion that there may be multiple synthetic or degradation pathways involved in the metabolism of NAEs and MAGs that may have selective substrate specificity. To date, only a relatively small number of NAEs and MAGs have been measured at various

time points post-mortem. However, by applying the data obtained in chapters 3 and 4, a quantification of a far wider range was possible.

Due to the interest in AEA C20:4 and availability of reference standards, this NAE has been the focus of several post-mortem tissue studies. AEA C20:4 levels have been observed to increase in rat brain by two orders of magnitude when tissue was left at room temperature for five hours post-mortem; furthermore, levels continue to rise for up to 48 hours (Kempe *et al.*, 1996). Further work conducted on pigs, cows and sheep also display similar increases, although not to the same degree, with levels approximately doubling after five hours and continuing for up to 24 hours. Similar increases were also observed with OEA C18:1, PEA C16:0 and NAE C18:0 (Schmid *et al.*, 1995).

Further work conducted on FAAH knock-out mice (as FAAH is known to degrade NAEs) and URB597 (a FAAH inhibitor) treated animals demonstrated that relative increases of OEA C18:1 and PEA C16:0 varied from AEA C20:4 over a period of 24 hours post mortem, suggesting alternative metabolism mechanisms were involved .

Conversely for MAGs, 2-AG C20:4 levels in mouse brain were studied over 24 hours post-mortem and demonstrated an overall decrease (Patel *et al.*, 2005).

Where it has been demonstrated that NAE and MAG levels are affected post-mortem, the number of NAEs and MAGs measured have been relatively small and focused predominantly in brain tissue. Applying a quantitative method to profile the wider range of NAEs and MAGs detected in the tissues discussed in chapter 4 will highlight possible differences in metabolisms currently unreported. This chapter further extends the application of the methods described in chapters 3 and 4. By employing the data of NAEs and MAGs detected in the previous two chapters into a quantitative method an approach far broader in the scope than previous methods is achieved.

5.2 Aim

The aims of this section of work were as follows

- Produce a quantitative method for the analysis of all the NAEs and MAGs identified in rat tissues in Chapters 3 and 4 based on the EPI spectra obtained in those chapters and the limited reference standards available.
- Quantify and compare the levels of NAEs and MAGs in rat tissues when dissected immediately after death and five hours post-mortem.

5.3 Methods

5.3.1 Liquid chromatography and survey scanning mass spectrometer methods

The parameters for LC - MS survey scanning used have been described previously in section 3.3.1 chapter 3. Briefly, all extracts from tissues collected five hours post-mortem were analyzed using the precursor ion *m/z* 62 and a neutral loss *m/z* 92 survey scans (coupled with an EPI scan) to identify NAEs and MAGs present.

5.3.2 Establishing a multiple reaction monitoring method

The precursor ion and neutral loss profiling methods detailed in chapters 3 and 4 successfully identified a number of known and unknown NAEs and MAGs in rat tissues and organs. To provide quantitative information of the analytes detected, a more sensitive approach was deemed necessary, especially if further studies were to analyze smaller tissue weights. Triple quadrupole instruments performing quantification experiments commonly operate in multiple reaction monitoring mode, performing analyses which are sensitive and selective (Hoffman and Stroobant, 2005). Reference standards are commonly required to optimize instrumental parameters but also to select which product ions (and retention times, if liquid chromatography is employed) are appropriate for the identification of each analyte (Richardson *et al.*, 2007; Williams *et al.*, 2007). By combining results from the precursor ion and neutral loss approaches with a targeted SRM approach, it was possible to operate a multiple reaction monitoring method without the full range of reference standards. A full understanding of analyte product ions were available from the two survey scans, allowing multiple reaction monitoring transitions (the setting of the first and last quadrupole allowing a specific pseudomolecular ion, and resulting production ion, through to the detector (Hoffman and Stroobant, 2005)) to be applied without all the relevant reference standard materials. Declustering potentials and collision energies for analytes where reference standards were unavailable were estimated using NAE and MAG standard analogues.

5.3.2.1 SRM Transitions

For the NAEs DEA C22:4, AEA C20:4, OEA C18:1 and PEA C16:0, SRM transitions were chosen by the direct infusion of each reference standard and by selecting the $[M+H]^+$ pseudomolecular ion and the most intense product ion. For all NAEs this ion was *m/z* 62, the ethanolamine ion. In the case of 2-AG C20:4 and 2-LG C18:2, no glycerol product ion was formed under CID conditions; rather, a neutral and an ion corresponding to the acyl chain ion were formed. This ion, *m/z* 287.3 and 263.3 (2-AG C20:4 and 2-LG C18:2, respectively), was selected, again based on relative abundance. Previous targeted endocannabinoid work has employed the same transitions (Jhaveri *et al.*, 2006; Richardson *et al.*, 2007; Thomas *et al.*, 2009; Williams *et al.*, 2007).

Where standards were not available for NAEs and MAGs, SRM transitions were selected on the data obtained from EPI spectra in chapter 3. SRM transitions chosen for NAEs follow the same trend as those NAEs where standards were available. The $[M+H]^+$ pseudomolecular ion identified in the EPI scan and the *m/z* 62, the ethanolamine ion, were chosen; see Table 5.1. Transitions for MAGs again follow a similar pattern to those where standards were available; the $[M+H]^+$ pseudomolecular ion identified in the EPI survey scan and the product ion resulting from a cleavage of the ester linkage, see Table 5.2.

5.3.2.2 Declustering potentials and collision energies optimization

Declustering potentials for reference standard NAEs DEA C22:4, AEA C20:4, OEA C18:1, PEA C16:0 and 2-AG C20:4 were optimized by the direct infusion of standards and by systemically increasing the declustering potential (0 up to 400 V) while monitoring the pseudomolecular ion for the maximum intensity. For NAEs and MAGs, where a reference standard was not available, declustering potentials were based on experimental values obtained from structural analogues AEA C20:4 and 2-AG C20:4 respectively. Where the voltage chosen may not be optimum, it is a best estimate and this approach has been used before (Gillum *et al.*, 2008; Scholz *et al.*, 2005). For NAEs it can be seen in figure 4, chapter 3 that the optimum declustering potential for NAE

reference standards C20:4 to C16:0 is relatively broad and changes of ± 25 V for any of the reference standards infused would have little effect on sensitivity. Consequently, the voltage selected should be acceptable for NAEs and MAGs where reference standards were not available.

Optimum collision energies for reference standard DEA C22:4, AEA C20:4, OEA C18:1, PEA C16:0, 2-AG C20:4 and 2-LG C18:2 were obtained by direct infusion of standards and by systemically increasing the collision energy (0 up to 130 V) while monitoring the relevant product ion for the maximum intensity. For NAEs where standards were not available, the same value obtained for AEA C20:4 was used. For MAGs where standards were not available, the collision energy of 2-AG was selected.

The collision energies for analytes where reference standards are not available were based on a structural analogue. For NAEs it can be seen in figure 5, chapter 3 that the optimum collision energy for NAE reference standards C20:4 to C16:0 is relatively broad and changes of ± 20 V for any of the reference standards infused would have little effect on sensitivity. Consequently, the voltage selected should be acceptable for NAEs and MAGs where references standards were not available. A list of the chosen declustering potentials and collision energies can be found in Table 5.1 and Table 5.2.

5.3.3 Internal standards

AEA-d8 and 2-AG-d8 were used as internal standards for NAEs and NAGs respectively. It is fair to say that the use of a wider number of deuterated internal standards has been reported for the quantification of NAEs and MAGs (Williams *et al.*, 2007); however, in that instance, synthesis of these standards was performed inhouse. The use of just one deuterated reference standard for NAEs and one for MAGs has been employed previously where in-house synthesis was not an option (Gillum *et al.*, 2008; Jhaveri *et al.*, 2006; Richardson *et al.*, 2007; Thomas *et al.*, 2009)

Table 5.1. SRM transitions, collision energies and declustering potentials selected for NAEs previously identified by PI survey scan in chapters 3 and 4. Where standards were not available, the parent ion and product ion transition were obtained from the precursor ion survey scan and resulting EPI spectra. The chosen *m/z* 62.3 product ion represents the ethanolamine moiety of each compound. Collision energies and declustering potentials were either obtained from reference standards or, where not available, the structural analogue AEA C20:4.

Acyl Chain	Precursor ion (*m/z*)	Product Ion (*m/z*)	Collision Energy (V)	Declustering Potential (V)
C24:1	410.4	62.3	41	51
C22:5	374.3	62.3	41	51
DEA C22:4	376.3	62.3	35	60
C22:1	382.4	62.3	41	51
C22:0	384.4	62.3	41	51
AEA C20:4	348.3	62.3	41	51
C20:1	354.3	62.3	41	51
C20:0	356.4	62.3	41	51
C18:2	324.3	62.3	41	51
OEA C18:1	326.3	62.3	35	70
C18:0	328.3	62.3	41	51
C16:1	298.3	62.3	41	51
PEA C16:0	300.3	62.3	35	50

Table 5.2. SRM transitions, collision energies and declustering potentials selected for MAGs previously identified by the neutral loss survey scan in chapters 3 and 4. Where standards were not available the parent ion and product ion transition were obtained from the neutral loss survey scan and resulting EPI spectra. The chosen product ion represents the acyl chain resulting from a cleavage of the ester linkage. Collision energyies and declustering potentials were either obtained from reference standards, or where not possible, a structural analogue 2-AG C20:4.

Acyl Chain	Precursor ion (*m/z*)	Product Ion (*m/z*)	Collision Energy (V)	Declustering Potential (V)
C22:5	405.3	313.3	17	60
C22:4	407.3	315.3	17	60
2-AG C20:4	379.3	287.3	17	60
C20:3	381.3	289.3	17	60
C20:2	383.3	291.3	17	60
C20:1	385.3	293.3	17	60
2-LG C18:2	355.3	263.3	20	90
C18:1	357.3	265.3	17	60
C18:0	359.3	267.3	17	60
C16:1	329.3	237.3	17	60
C16:0	331.3	239.3	17	60

Optimum collision energies and declustering potentials of the two deuterated standards were selected by direct infusion and by increasing the required voltages where appropriate. SRM transitions were selected on the basis of the most intense signal.

5.3.4 Validation of the method

5.3.4.1 Accuracy and precision

The accuracy and precision of the SRM method were evaluated intraday by the use of available standards AEA C20:4, OEA C18:1, PEA C16:0, 2-AG C20:4 and 2-LG C18:2. Standards at 3 concentrations covering the range of expected endogenous levels (0.05, 0.5, 5 nmol/g for NAEs and 0.75, 0.5 and 10 mol/g for MAGs) were extracted as described in chapter 3, section 3.2.3 (n=5) along with a calibration, (see section 5.3.7.1) and the results were evaluated in accordance to published guidelines (US Department of Health and Human Services, 2001).

5.3.4.2 Determination of the LLOQ

Calculating the lower limits of quantification (LLOQ) for all analytes was not possible due to unavailability of reference standards. Therefore, a general approach was taken to access the LLOQ in rat tissue by using AEA C20:4 d8 and 2-AG C20:4 d8 to represent NAEs and MAGs respectively. When deuterated standards behave as close to the non-dueterated standards as possible, it negates issues surrounding endogenous analyte levels and the need to remove them from calculations. The use of deuterated AEA C20:4 and 2-AG C20:4 have previously been compared against non-deuterated AEA C20:4 and 2-AG C20:4 for the assessment of recoveries and demonstrated to provide comparable results (Kingsley and Marnett, 2007).

Brain, liver, lung, and testi (tissue wet weights of ~100mg, n=6) were spiked with deuterated standards (concentrations 0.01, 0.02, 0.04, 0.06, 0.08 and 0.1 μM for NAEs and 0.1, 0.3, 0.5, 0.7, and 0.9 nM for MAGs) and extracted as detailed in section 3.2.3, chapter 3. Once samples were extracted and solvent removed by evaporation,

reconstitution was performed with 100 µl of ethanol. Extracts were analyzed using the SRM method described in section 5.3.2. The LLOQ was selected as the lowest concentration which demonstrated acceptable reproducibility of RSD less than 20% and a chromatographic peak with an S:N of no less the 10:1 (US Department of Health and Human Services, 2001; Williams *et al.*, 2007).

5.3.4.3 Determination of recoveries

The recoveries of AEA C20:4 d8 2-AG C20:4 d8 were calculated in rat tissues by spiking in deuterated standards close to the limit of quantification. The use of deuterated standards for recoveries has previously been demonstrated to be comparative to non-deuterated standards (Kingsley and Marnett, 2007). Rat brain, liver, lung and testi (~50mg, n=6) were spiked with AEA C20:4 d8 and 2-AG C20:4 d8 at post-reconstituted concentrations of 0.06 µM and 0.5 µM, respectively prior to extraction. Samples were extracted as previously described in section 3.2.3, chapter 3 and reconstituted in ethanol. Subsequently, extracted and non-extracted AEA C20:4 d8 2-AG C20:4 d8 (present at the same theoretical concentration) were analyzed.

5.3.4.4 Determination of Ion Suppression

Ion suppression effects were assessed in rat brain tissues using deuterated standards of AEA C20:4 and 2-AG C20:4. Rat brain (~100mg wet weight, n=6) were extracted as previously detailed in chapter 3, section 3.2.3. Extracts were spiked at the point of reconstitution with AEA C20:4 d8 and 2-AG C20:4 d8, resulting in a concentration of 0.5 µM and 1.0µM, respectively. AEA C20:4 d8 and 2-AG C20:4 d8 (0.5 µM and 1.0µM, respectively) matrix free reference standards were analyzed alongside spiked reference standards. The level of ion suppression relative to the 100% value was determined for each analyte. The use of deuterated standards for the evaluation of ion suppression has been previously assessed (Richardson *et al.*, 2007)

5.3.5 Rat tissue collection five hours post mortem

Tissues and organs were collected from six Sprague-Dawley rats (Charles River, UK). The animals were stunned by a blow to the head followed rapidly by decapitation, typically within 3–4 seconds. The animals were left in a fume cupboard for five hours at room temperature, following which tissues brain, heart, lungs, liver, testi and spinal tissue were dissected. Following dissection, tissues were immediately frozen on dry ice. All tissues were subsequently stored at -80°C until required. For tissue samples collected immediately after death, sample recovery was the same as described in chapter 4. Tissue collection was carried out by Professor David Kendall, Dr. Victoria Chapman and Dr. Stephen Alexander in the School of Biomedical Sciences at the University of Nottingham.

5.3.6 Tissue extraction

Tissues were extracted by the method detailed in the paper by Richardson *et al* (Richardson *et al.*, 2007). Tissues were homogenized by hand in a silanized glass homogenizer in 8 ml of ethyl acetate: hexane (9:1 v/v). 10% of its volume of water was added and the contents transferred to a centrifuge tube. Centrifugation was performed at 7000g for 15 minutes and the temperature maintained at 4°C. The supernatant was removed and the process repeated a further two times to optimize recovery. Supernatants were then subsequently pooled and the solvent removed by centrifugal evaporation.

Extractions were reconstituted in 200 µl ethanol and vortexed for 3 minutes. 100 µl was removed from each of the tissue replicates and pooled, dried down and reconstituted in 100 µl of ethanol, pooling and concentrating each tissue's extract for analysis by the two survey scan methodologies. The remaining 100 µl of samples were refrozen and stored at -80°C for SRM analysis. The samples underwent two freeze-thaw process prior to SRM analysis; however, previous work has demonstrated that these physical changes to the extracts have little effect on NAE and MAG concentrations (Williams *et al.*, 2007).

5.3.7 Tissue Analysis

5.3.7.1 Calibration curves

For quantification, calibration curves were produced using AEA C20:4, OEA C18:1, PEA C16:0 and MAGs 2-AG C20:4 and 2-LG C18:2 reference standards. Each standard was taken through the same extraction procedure as tissue samples (described in section 3.2.3, chapter 3). Reference standard concentrations used were 0.005, 0.01, 0.02, 0.03, 0.04, 0.05, 0.1, 0.5, 0.75, 1.0, 2.5, 5, 7.5, 10 and 50μM for each analyte. Reference standards DEA C20:4 and NAE C18:0 are currently commercially available but were difficult to obtain at the time of this work, and so were not included in the calibration.

For quantitative analysis of NAEs without available standards, it would have been possible to use peak areas alone and then to compare relative variations between tissue states as applied previously (Saghatelian and Cravatt, 2005; Saghatelian *et al.*, 2004). Without standards for each individual analyte, absolute quantification was not possible; however it was possible to obtain a semi-quantitative estimate by the use of one of the closely structurally related NAE or MAG calibrations. Such values should be reasonably accurate, but errors might occur due to variation in the analyte ionization efficiency for each compound compared to the reference standard. For analytes where a calibration curve was obtained, direct comparison between the results obtained here and those in the literature would be possible.

It has been previously noted that acyl chain length has an effect on the ionization efficiency of lipid-like compounds under ESI (Koivusalo *et al.*, 2001; Ortori *et al.*, 2007). Consequently, taking this factor into account, NAEs and MAGs where reference standards were not available were assigned a calibration line dependant on the acyl chain length; see Table 5.4 and Table 5.5.

5.3.7.2 Survey Scan of tissue extracts

Precursor ion and neutral loss survey scans were conducted on pooled tissues extracts for animals that were left for five hours post-mortem prior to dissection. Survey scans on tissues collected immediately post-mortem have been reported in section 4.3.1, chapter 4.

5.3.7.3 SRM analysis tissue extracts

Analysis using the SRM method was conducted on rat tissue extracts from samples recovered immediately after death and five hours after death (n=6 in each case).

5.3.7.4 Statistical analysis of post-mortem data

Levels of NAEs and MAGs recovered immediately after death and five hours post-mortem were tested for statistical significance by a Mann Whitney two-tailed test. This approach is a non-parametric method, determining the significant differences between the medians of two data sets, and does not rely on the data to have a Gaussian distribution (Roger, 1989). Such an approach has previously been employed in the comparison of endocannabinoid data (Jhaveri *et al.*, 2006).

Table 5.3. Weights of tissues extracted from the Sprague-Dawley rats five hours post-mortem. n=6.

Statistic	Tissue					
	Brain (left hemisphere)	Heart	Lung	Liver	Testis	Spinal cord
Mean Weight / g	0.939	0.947	0.764	0.769	1.065	0.143
Stdev	0.084	0.066	0.052	0.031	0.053	0.019

Table 5.4. Acyl chain length of NEAs and the calibration standard employed in quantification.

Acyl Chain	Calibration line employed
C24:x – C20:x	AEA C20:4
C18:x	OEA C18:1
C16:x	PEA 16:0

Table 5.5. Acyl chain length of MAGs and the calibration standard employed in quantification.

Acyl Chain	**Calibration line employed**
C22:x – C20:x	2-AG C20:4
C18:x– C16:x	2-LG C18:2

5.4 Results and discussion

5.4.1 Validation of the targeted SRM method

5.4.1.1 Accuracy and Precision

Accuracy and precision of the method can be found in Table 5.6. The results demonstrate reasonable accuracy and reproducibility. The accuracy is normally expected to be within 15 % of the expected outcomes (US Department of Health and Human Services, 2001), the majority of values obtained were within these tolerances. The accuracy of 5.0 nmol/g 2-AG C20:4 and 0.75nmol/g for 2-LG C18:2 were slightly outside however (74.1 and 76.8 respectively). The method also demonstrated reasonable precision, with the majority of values being below 15%, however PEA 16:0, 2-AG C20:4 and 2-LG C18:2 demonstrated slightly higher than expected values of 21.1, 18.7 and 25.8 % at 5 and 10 nmol/g, respectively. Nevertheless, the majority of values are within expected tolerances and are comparable with previous work (Richardson *et al.*, 2007)

5.4.1.2 Lower limit of quantification for SRM method

The LLOQs for rat tissues can be seen in Table 5.7. The relative standard deviations for AEA C20:4 d8 in brain are higher than the expected < 20% (US Department of Health and Human Services, 2001). This was due to a sampling error, leading to the analysis of only 3 out 6 extracts. However, the peaks for all three injections gave a S:N ration of 10:1 or greater, an alternative definition for the LLOQ (Williams *et al.*, 2007) and were subsequently allowed. There are no differences in LLOQs between tissues for 2-AG C20:4 d8, and very similar results are obtained for AEA C20:4 d8 in the different tissues. Previous reported LLOQ levels of 10 pmol/g for AEA and 100 pmol/g for MAG (Richardson *et al.*, 2007) compare well with those observed here.

As reference standards are not available for all the analytes analyses by this methodology, it is not possible to accurately assess the limit of quantification for all analytes. Therefore, as a best estimate, the limit of quantification for AEA C20:4 was applied to all

NAEs and consequently the limit of quantification for 2-AG C20:4 was applied to all MAGs.

5.4.1.3 Recoveries

The recoveries of AEA d8 and 2-AG d8 from rat brain, lung, liver, and testi can be found in Table 5.7. The levels of recovery are reasonable and are comparable with previous results (Kingsley and Marnett, 2007). AEA C20:4 recovery in testi was, however, slightly lower than results obtained from other tissues. Previous work has demonstrated however slightly better percentage recoveries, with levels in the mid- to high nineties and this could be due to the use of different extraction solvents and incorporating solid phase extraction (Richardson *et al.*, 2007; Williams *et al.*, 2007).

The validation demonstrates that the method is suitable for the analysis of NAEs and MAGs in post-mortem tissues. Where a full validation of this method would be preferable, as outlined by various publications (Hartmann *et al.*, 1998; US Department of Health and Human Services, 2001), this is not possible due to unavailability of the majority of analytes of interest. Nevertheless, it was necessary to demonstrate the suitability of the method for the use which it was intended. By the use of deuterated standards AEA C20:4 d8 and 2-AG C20:4 d8, this has been successfully undertaken. The LLOQ, reproducibility, recoveries, intraday accuracy and ion suppression have been assessed and have been demonstrated acceptable in comparison to previous work in this area (Kingsley and Marnett, 2007; Richardson *et al.*, 2007; US Department of Health and Human Services, 2001; Williams *et al.*, 2007).

Table 5.6 Intraday accuracy of and precision of NAEs and MAGs. (n=5)

Analyte	Concentration (nmol / g)		Accuracy Mean % Variation from expected	Precision (%RSD)
AEA C20:4	0.05	low	102.5	13.9
	0.50	medium	93.6	14.8
	5.00	high	99.7	11.5
OEA C18:1	0.05	low	114.9	10.0
	0.50	medium	110.8	8.1
	5.00	high	111.1	21.1
PEA C16:0	0.05	low	110.3	17.2
	0.50	medium	112.6	8.2
	5.00	high	111.7	8.5
2-AG C20:4	0.75	low	86.4	8.3
	5.00	medium	74.1	6.9
	10.00	high	85.7	18.7
2-LG C18:2	0.75	low	76.8	10.2
	5.00	medium	96.9	14.9
	10.00	high	83	25.8

Table 5.7 The lower limit of quantification and % recovery of C20:4 AEA d8 and C20:4 MAG d8. Recoveries were calculated on deuterated reference standards close to the LLOQ but ion suppression was calculated on deuterated reference standards at 0.5 μM and 1.0μM, respectively.

Tissue	LLOQ of AEA C20:4 d8 (n=6)		LLOQ of 2-AG C20:4 d8 (n=6)		% Recovery of AEA C20:4 d8	% Recovery of MAG C20:4 d8
	LLOQ (pmol/g)	%RSD	LLOQ (pmol/g)	%RSD	(n=6)	(n=6)
Brain	2 (n=3)	42.2	50 (n=3)	13.3	83.1 (n=3)	89.9 (n=3)
Liver	4	18.2	50	16.9	87	82
Lung	4	21	50	12	85.1	81.9
Testi	2	7.8	50	10.3	69.6	88.7

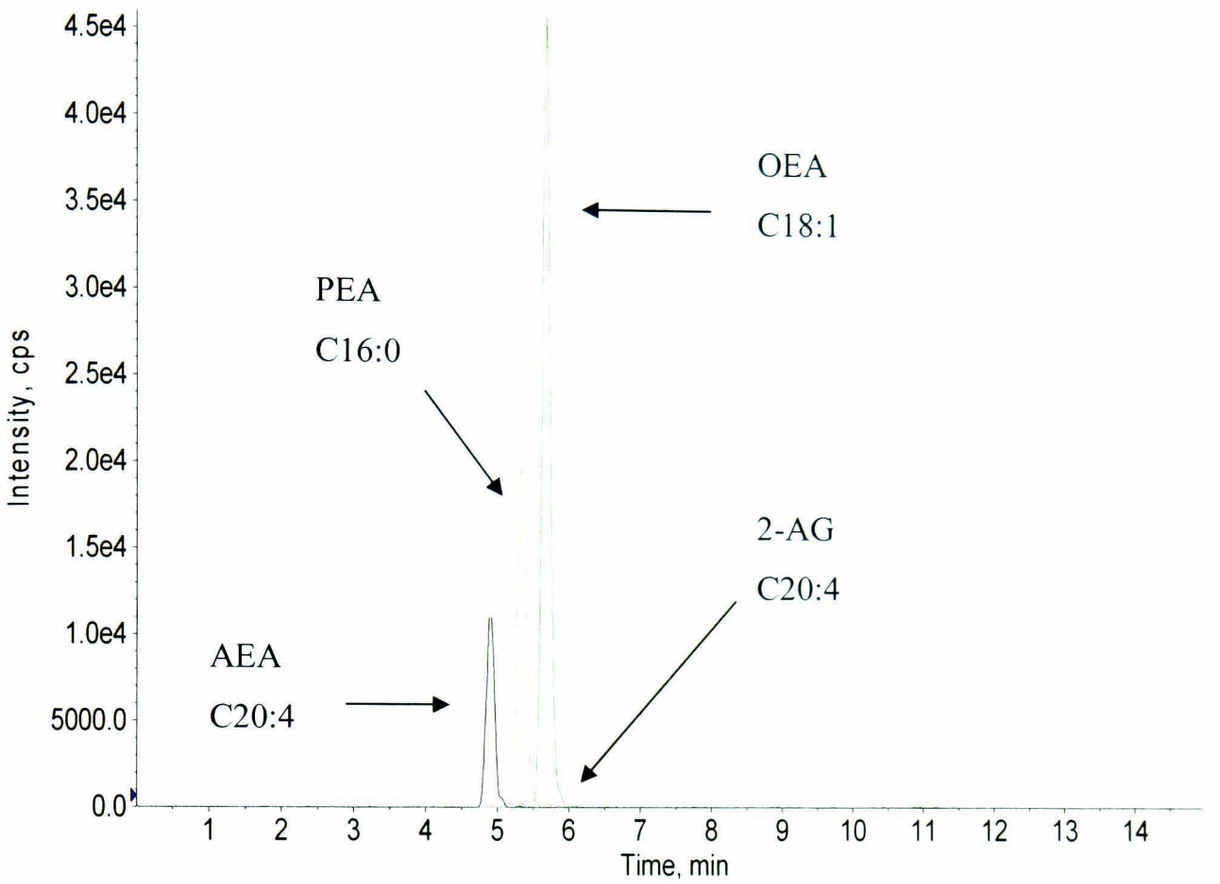

Figure 5.1. Extracted ion chromatograms of AEA C20:4, OEA C18:1, PEA C16:0 and 2-AG C20:4 reference standards analyzed with an SRM method, demonstrating the method works on NAE and MAG reference standards.

5.4.1.4 Ion Suppression

The ion suppression effects of brain tissue are demonstrated in Table 5.7. The effects were relatively small and comparable with previous evaluations of 83% and 96% (Richardson *et al.*, 2007)

5.4.2 Calibration and linearity

Table 5.8 demonstrates the slope of the lines and linear regression for the NAEs and MAGs calibrated.

The initial range of calibrants used, from 0.01 μM to 50 μM, was relatively large but represented changes in post mortem tissues for some analtyes. In the instance of AEA C20:4, endogenous levels were relatively low and such a range was excessive; consequently, to improve accuracy of the quantification, a smaller calibration range was used in practice. For OEA C18:1 and PEA C16:0, the endogenous levels, particularly five hours post-mortem, were high enough to justify using the range stated. The slopes of the line were forced through zero. A number of analytes around the limit of detection were better represented by this approach.

Table 5.8. Calibrations of NAE and MAG reference standards.

Calibrant	Equation of the line	R^2	Calibration range used (μM)
AEA C20:4	y=0.8792x	0.9997	0.01 – 1.0
OEA C18:1	y=1.4704x	0.9979	0.01 – 50.0
PEA C16:0	y= 1.503x	0.9986	0.01 – 50.0
2-AG C20:4	y=0.2632x	0.9994	0.5 – 50.0
2-LG C18:2	y=0.2750x	0.9981	0.5 – 50.0

NAEs and MAGs, for which reference standards were not available, were quantified using the calibrations of structural analogue reference standards. Such an approach does not necessarily provide data that would be as accurate as if individual calibrations were employed, but it does provide an estimate of concentrations for which comparisons can be made. The choice of calibration for each analyte was based on acyl chain length in an attempt to account, to some degree, for the differences in ionization efficiencies previously observed in structurally similar acyl chain-containing compounds (Koivusalo *et al.*, 2001; Ortori *et al.*, 2007). See Table 5.9 and Table 5.10.

Where C24:1, C22:5, C22:4, C22:1, C20:1 and C20:0 use the AEA C20:4 calibration, the endogenous levels of these analytes varied by a thirtyfold difference. So to improve accuracy, the calibration range was tailored to fit with levels detected and hence the slope of the line varies slightly. The same can be seen for C18:2 and C18:0. These two NAEs use the same calibration obtained from reference standard OEA C18:1, but there was a fivefold difference in concentrations; therefore the range of the calibration was adjusted accordingly, and the slope of the calibration line employed reflects that variation. The calibration line employed for each NAE (and MAG) was the same, independent of tissue.

MAGs were also detected at differing levels and, as seen with NAEs, the calibration range employed in quantification was dependant on endogenous levels detected. Table 5.10 illustrates the equation of the line and calibration range employed for MAGs where reference standards were unavailable.

The quantification of NAEs where a full complement of reference standards are not available has been previously demonstrated. Using AEA d4 and OEA d4, a two-point calibration line was constructed to quantify all NAEs detected in various biological tissues (Clement *et al.*, 2003; Leung *et al.*, 2006; Nomura *et al.*, 2008).

NAE and MAG concentrations from tissues dissected immediately after death can be seen in Table 5.11 and Table 5.12. Standard deviations and relative standard deviations are also listed.

Table 5.9. NAEs and the reference calibration assigned to provide quantification. Where endogenous levels varied between analytes, the range of the calibration was adjusted accordingly.

NAE	Reference calibrant used	Equation of the line	Calibration range (μM)
C24:1	AEA C20:4	y=1.0009x	0.01 – 50.0
C22:5	AEA C20:4	y=1.0009x	0.01 – 50.0
C22:4	AEA C20:4	y=1.0009x	0.01 – 50.0
C22:1	AEA C20:4	y=1.0009x	0.01 – 50.0
C20:1	AEA C20:4	y=1.0009x	0.01 – 50.0
C20:0	AEA C20:4	y=0.8792x	0.01 – 1.0
C18:2	OEA C18:1	y=1.4173x	0.01 – 2.5
C18:0	OEA C18:1	y=1.4704x	0.01 – 50.0

Table 5.10. MAGs and the reference calibration assigned to provide quantification. Where endogenous levels varied between analytes, the range of the calibration was adjusted accordingly.

MAG	Reference calibrant used	Equation of the line	Calibration range (μM)
C22:5	2-AG C20:4	y=0.2632x	0.5 - 50
C22:4	2-AG C20:4	y=0.2521x	0.5 - 10
C20:3	2-AG C20:4	y=0.2521x	0.5 - 10
C20:1	2-AG C20:4	y=0.2521x	0.5 - 10
C18:1	2-LG C18:2	y=0.2750x	0.5 - 50
C18:0	2-LG C18:2	y=0.2750x	0.5 - 50
C16:0	2-LG C18:2	y=0.2750x	0.5 - 50

The approach taken here, where SRM transitions have not originated from a complete set of reference standards but from full product ion spectra and an understanding of the fragmentation of a group of analytes has previously been employed (Scholz *et al.*, 2005), be it metabolism of xenobiotic compounds rather than endogenous metabolites, the approach taken was similar. In this instance, SRM transitions were coupled with a full product ion scan and consequently demonstrate a slight decrease in sensitivity due to increase scan time. Where they argue that the slight loss in sensitivity is warranted by the increased selectivity of the full product ion spectra obtained, the approach taken here employs a precursor ion / neutral loss survey scan coupled with EPI spectra for initial identification. Therefore the more sensitive SRM alone method was employed.

5.4.3 Quantification of NAEs and MAGs in rat tissues collected immediately after death

5.4.3.1 General observations

Levels of NAEs and MAGs in rat tissues can be found in Table 5.11 and Table 5.12 respectively, as well as total NAEs and MAGs in each tissue in Figure 5.2. Variation of NAE and MAG tissue distribution, previously observed in chapter 4, is more prominent with addition of concentrations. Non CNS tissues generally contain the shorter, more saturated NAEs; where longer chain NAEs are present, they occur at lower concentrations, although testi contain NAE C22:5. Brain and spinal tissue contains a greater range of NAEs. It is notable that MAGs do not follow the same pattern as NAEs. There is generally a greater distribution of both long and short chain MAGs in non-CNS tissues than observed with NAEs. The fact that NAE and MAG profiles are dissimilar is perhaps not surprising, as the synthesis routes of the two classes of compounds are believed to be separate (Ahn *et al.*, 2008).

Reproducibility of NAEs and MAGs measurements, using the relative standard deviation (RSD), are generally within 20%, although some are higher than this value, particularly those present at lower concentrations. Nevertheless, the quantitative data provide a

Table 5.11. Quantification of NAEs in rat tissues. Mean, standard and relative standard deviation (%RSD) are stated (n=6). Analytes below the limit of detection are listed by a -.

Tissue	Statistic	NAE Concentration (pmol/g)											Total (pMol/g)
		C24:1	C22:5	C22:4	C22:1	C20:4	C20:1	C20:0	C18:2	C18:1	C18:0	C16:0	
Brain	Mean	67.1	-	4.2	19	2.6	20.6	37.2	12.2	85.1	58.9	86.8	393.7
	Stdev	30.4	-	1.4	6.1	0.6	8.4	15.4	1.7	17.8	13.8	22.7	
	%RSD	45.4	-	33.5	32	22.5	40.8	41.5	13.9	20.9	23.5	26.1	
Liver	Mean	-	-	-	-	-	-	-	14.6	9.6	-	69.6	93.8
	Stdev	-	-	-	-	-	-	-	6.4	7.1	-	19.8	
	%RSD	-	-	-	-	-	-	-	43.7	73.7	-	28.4	
Heart	Mean	-	-	-	-	-	-	-	4.1	10	11.8	15.6	41.5
	Stdev	-	-	-	-	-	-	-	1.5	2.8	3	5.3	
	%RSD	-	-	-	-	-	-	-	35.6	27.8	25.3	33.7	
Lung	Mean	-	-	1.5	-	-	2.8	-	14.7	41.5	37.7	36.9	135.1
	Stdev	-	-	0.3	-	-	0.5	-	4.3	10.2	10.6	9.7	
	%RSD	-	-	20.1	-	-	17.8	-	29.1	24.4	28.1	26.4	
Testi	Mean	-	89.7	12.5	-	11	2.2	-	29.3	50.4	85.2	254.7	535
	Stdev	-	19.7	2.7	-	1.8	0.3	-	6.5	8.7	21.1	76.9	
	%RSD	-	22	22	-	16.1	15.2	-	22.3	17.2	24.7	30.2	
Spinal Cord	Mean	936.1	-	37.9	275.3	7.3	532.8	600.7	27.6	895.8	917.1	923.3	5153.9
	Stdev	237.6	-	5.7	68.8	1.8	140.2	182.1	3.9	115.4	187.2	83.2	
	%RSD	25.4	-	15.1	25	24.6	26.3	30.3	14.2	12.9	20.4	9	

Table 5.12. Quantification of MAGs in rat tissues (n=6). Mean, standard and relative standard deviation (%RSD) are stated (n=6). Analytes below the limit of detection are listed by a -.

Tissue	Statistic	MAG Concentration (nmol/g)									Total (nmol/g)
		C22:5	C22:4	C20:4	C20:3	C20:1	C18:2	C18:1	C18:0	C16:0	
Brain	Mean	0.2	0.6	11.1	0.5	-	0.2	6.8	0.3	2.1	21.8
	Stdev	0.1	0.2	2.8	0.2	-	0.1	3.2	0.1	0.6	
	%RSD	35.6	31.9	24.9	33.3	-	36.1	46.6	46.3	28	
Liver	Mean	-	0.3	3.3	-	0.2	7.2	15.4	1.4	5.4	33.2
	Stdev	-	0.1	0.8	-	0	2.3	5.1	0.3	2.2	
	%RSD	-	36.5	23.5	-	14.6	31.9	33.1	21.2	41.7	
Heart	Mean	-	-	0.5	-	-	0.2	0.4	0.2	0.3	1.6
	Stdev	-	-	0.1	-	-	0.1	0.1	0.1	0.1	
	%RSD	-	-	24.2	-	-	33.9	38	35.4	27.4	
Lung	Mean	-	0.9	5.6	1	-	2.4	4.5	0.5	1.5	16.4
	Stdev	-	0.2	1.4	0.3	-	0.3	0.9	0.1	0.1	
	%RSD	-	26.9	25.9	26.2	-	12.8	18.9	12.8	4.7	
Testi	Mean	2.4	0.5	3.3	0.5	-	1.4	3	0.6	3.6	15.3
	Stdev	0.7	0.2	1	0.2	-	0.4	0.8	0.2	1.1	
	%RSD	30.1	33	30.9	33.7	-	30.3	25.4	32.6	31	
Spinal Cord	Mean	-	1.4	31.4	2.9	4.4	1.1	31.5	2.5	4.1	79.3
	Stdev	-	0.2	4.5	0.7	0.6	0.2	4.9	0.8	0.5	
	%RSD	-	15.8	14.2	26	13.6	16.5	15.5	33.5	13.4	

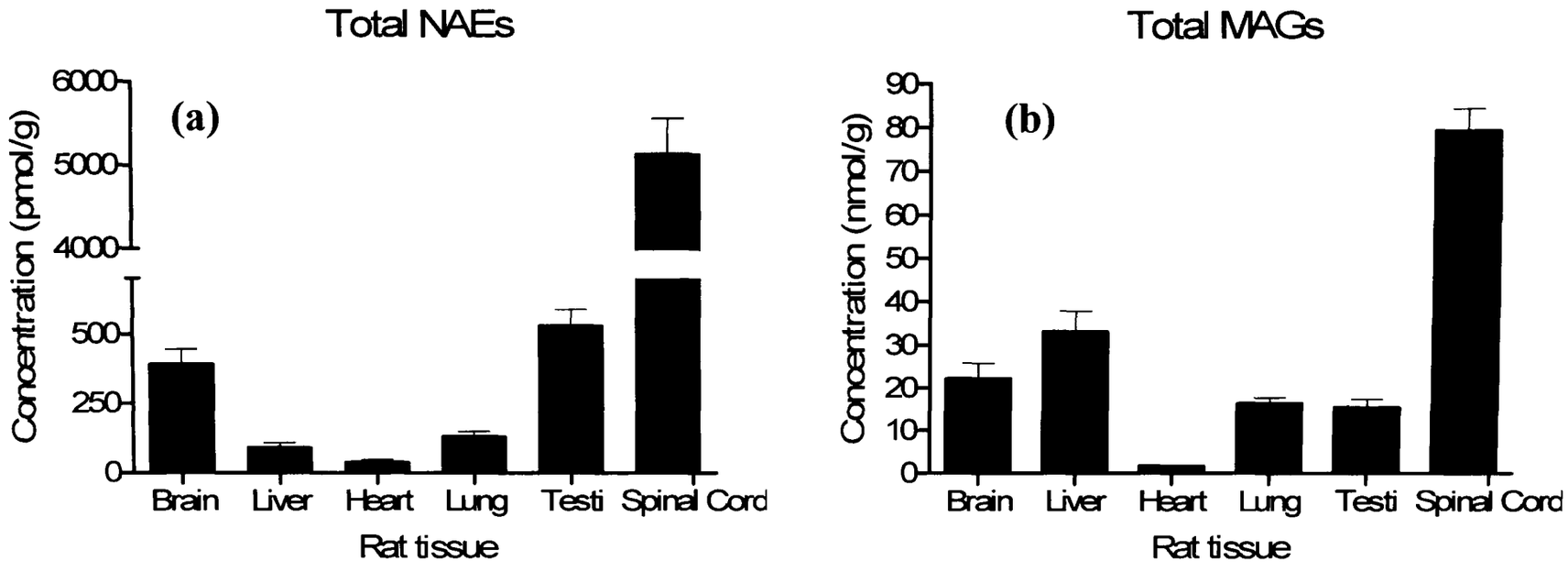

Figure 5.2 Plots illustrating the total amounts of (a) NAEs and (b) MAGs in the rat tissues analyzed. Error bars are standard error of the mean

profile of NAE and MAG distribution in rat tissue previously not reported in the scientific literature.

Although repetitious, NAE and MAG levels quantified in tissues have been further tabulated and compared with levels in the literature.

5.4.3.2 NAE and MAG levels in rat brain tissue

Brain (and spinal cord) tissue contains the widest range of NAEs in the tissue analyzed. Levels of AEA C20:4 detected here (2.6 ± 0.6 pmol/g) compare well against those reported from rat frontal cortices at 4.9 pmol/g (Williams *et al.*, 2007) and are close but slightly lower than those observed in a variety of rat brain regions, which ranged from 10.2 to 32.6 pmol/g (Richardson *et al.*, 2007). OEA C18:1 measured here at 85.1 pmol/g were slightly higher than those previously reported from the frontal cortex, 36.1 pmol/g. Levels of NAEs previously observed in the literature vary considerably, but the levels reported here are within the extremes of 60 to 1600 pmol/g (Koga *et al.*, 1997; Richardson *et al.*, 2007). PEA C16:0 levels reported here (86.8 ± 22.7 pmol/g) fall some way below the level recorded in various brain tissues (716 – 5000 pmol/g) (Richardson *et al.*, 2007) by an order of magnitude, and are similarly distant from those observed previously from the frontal cortex (521 pmol/g) (Williams *et al.*, 2007). Such variation in the literature suggests that differences in reported endogenous levels can be expected although there is not, as of yet, a reasonable explanation.

C24:1 levels in rat brain have not been detailed before, as far as it is possible to ascertain, but they have in mice. Levels described here at 67.1 pmol/g, are similar to those in mouse, 29 ~ 50 pmol/g (Leung *et al.*, 2006; Nomura *et al.*, 2008). NAE C20:0, NAE C18:2, and NAE C18:0 have not been quantified in rat brain as far as can be ascertained. Again however, these compounds have been quantified in mice. C20:0 levels reported here (37.2 ± 15.4 pmol/g) are in close agreement with one previous study, 40 pmol/g (Leung *et al.*, 2006), and almost double when compared to 24 ± 1.9 pmol/g (Nomura *et al.*, 2008). NAE C18:0 levels observed here (58.9 ± 13.8 pmol/g) are less than those

published previously: ~155pmol/g and 333 ± 42 pmol/g (Leung *et al.*, 2006; Nomura *et al.*, 2008). It is difficult to draw strong conclusions from these results as comparisons are being made across species; however, all reported values are well within an order of magnitude of those reported in mice and provide reasonable confidence in the results obtained. As far as it can be ascertained, quantitative values for NAE C22:1 and NAE C20:1 in rat brain have not been previously published. NAE C22:4 has been quantified in cultures of mouse neurons, microglial cells and rat astrocytes (Walter *et al.*, 2002; Walter *et al.*, 2003), however it is difficult to draw a comparison between levels found in tissue and cell cultures. A comparison of NAE levels in brain can be found in Table 5.13.

2-AG C20:4 has been previously quantified in rat brain tissues (Kondo *et al.*, 1998a; Richardson *et al.*, 2007; Williams *et al.*, 2007) (10.9 – 30.3, 8.1, and 4.75 nmol/g) and correlate closely with the levels reported in this chapter: 11.1 ± 2.8 nmol/g . Levels detected in mouse brain are also reasonably comparable at 3.7 ± 1.0 nmol/g (Nomura *et al.*, 2008). 2-LG C18:2 levels of 0.2 ± 0.1 nmol/g correlates closely with a previous LC-MS method (Richardson *et al.*, 2007), which ranges from 0.11 – 4.3 nmol/g but differs by an order of magnitude with those previously described at 0.05 ± 0.04 nmol/g (Kondo *et al.*, 1998a). This discrepancy could be due to differences in extraction methodology.

MAG C22:5, MAG C22:4, MAG C20:3, MAG C18:1, MAG C18:0 and MAG C16:0 were quantified in rat brain tissue. MAG C18:1 (6.8 ± 3.2nmol/g) and MAG C16:0 (2.1 ± 0.6nmol/g) compare favourably with those previously quantified in rat frontal cortices at 2.0 and 3.1 nmol/g (Williams *et al.*, 2007). MAG C18:0, 0.3 ± 0.1 nmol/g, also compares favourably against other levels previously detected in rat brain at 0.18 ± 0.23 (Kondo *et al.*, 1998a). Furthermore, it should be mentioned that MAG C18:1 and MAG C16:0 also compare well with those previously quantified in mouse brain, 2.2 ± 0.6 and 1 ± 0.1 nmol/g (Nomura *et al.*, 2008). This suggested that some reasonable confidence can be placed on the 'semi-quantitative' results for MAGs in the brain, and levels quantified in mouse brain are roughly comparable with those in rat. Quantitative results of MAG C22:5, MAG C22:4, and MAG C20:3 in rat tissue have not, despite extensive searching, been found in the literature. A comparison of MAG levels can be found in Table 5.14

Two recent publications in the field of endocannabinoids have quantified a reasonable number of NAEs and MAGs (Leung *et al.*, 2006; Nomura *et al.*, 2008). Identification of analytes was based on the on the pseudomolecular ion (without the use of authentic standards for the majority of the analytes observed). Quantification of the detected analytes was performed by a two point calibration using AEA C20:4 d4 and OEA C18:1 d4 reference standards spiked into the extracts. The peak area for each analyte, based on the pseudomolecular ion, was quantified using the two point calibration line and not by individual reference standards (Leung *et al.*, 2006; Nomura *et al.*, 2008). It could be said that the specificity of the approach taken is not as robust as the MS/MS method employed here. The approach taken to quantify each analyte is not dissimilar to the method described in this chapter and negates the issue of reference standard availability, although in this chapter the use of reference standards with various acyl chain lengths have been employed to counter, to some degree, the issue of differing ionization efficiencies observed with such analytes.

Although the neutral loss survey scan employed in chapter 4 was unable to detect MAG C22:5 in brain, it was quantified in brain tissue by the SRM method described in this chapter, although levels were at the lower limit of quantification. This finding demonstrates that MAG C22:5 is not solely found in testicular tissue, but that levels in testi are an order of magnitude higher than in brain.

5.4.3.3 NAE and MAG levels in rat liver

Table 5.15 and Table 5.16 compare NAE and MAG levels in rat liver measured in this chapter with those in the literature. NAE levels are reasonably comparable to those previously reported, as are MAG levels, demonstrating these reported levels can be viewed with some confidence. An exception is C18:0, which was quantified here to be at levels an order of magnitude greater that previously measured. There is no clear explanation for this discrepancy at this time.

5.4.3.4 NAE and MAG levels in rat heart

Table 5.17 and Table 5.18 compare NAE and MAG levels measure here in rat heart tissue with those in the literature. Levels of both NAEs and MAGs are less than those previously reported. Although no obvious explanation is forthcoming, the extraction procedures were slightly different and could contribute to the differences observed. AEA C20:4, not detected by this method nor by a previous GC-MS approach in rat heart (Schmid *et al.*, 2000), was however previously quantified between the levels of 21 and 126 pmol/g by the use of an LC-MS method (Koga *et al.*, 1997). The SRM method described in this chapter can quantify AEA C20:4 down to such levels, suggesting LLOQ is not a cause for such a discrepancy. As the mentioned method used LC-MS rather than the more selective LC-MS/MS employed here, misidentification may be the cause of the discrepancy.

It is worth noting that DEA C22:4 and NAE C20:3, not observed in rat heart by the method described in this chapter was also not observed in a previous study which also analyzed this tissue type (Koga *et al.*, 1997)

5.4.3.5 NAE and MAG levels in rat Lung

A comparison of MAG levels measured here in rat lung with those in the literature can be found in Table 5.19. NAE DEA C22:4, NAE C20:1, NAE C18:2, OEA C18:1 and PEA C16:0 were quantified in rat lung, however it difficult to find other reported levels in the literature to compare against. Although one previous study attempted to quantify AEA C20:4, endogenous levels were below the limit of quantification for the methodology. OEA C18:1 and PEA C16:0 were not included in the analysis (Yang *et al.*, 1999). Similarly, work conducted on mouse lung, among other tissues, only focused on AEA C20:4 and prostamides, ignoring other NAEs (Weber *et al.*, 2004). The same can be said for the work on guinea pig, which again focused solely on AEA C20:4.

Table 5.13. A comparison of NAEs detected in rat brain with those observed in the literature.

NAE	Detected levels (pmol/g)	Previously detected levels (pmol/g)	Source	Comment
C24:1	67.1 ± 30.4	30.0(mouse brain)	(Leung *et al.*, 2006)	Although there is some variation with values presented in the literature, most NAEs compare favorably. PEA C16:0 levels, however, are low, although they sit inside a relatively wide window of values published
		29.0(mouse brain)	(Nomura *et al.*, 2008)	
C22:4	4.2 ± 1.4	-		
C22:1	19.0 ± 6.1	-		
C20:4	2.6 ± 0.6	10.2 – 32.6	(Richardson *et al.*, 2007)	
		4.9	(Williams *et al.*, 2007)	
		11.8 – 77	(Koga *et al.*, 1997)	
		2.5 (mouse brain)	(Leung *et al.*, 2006)	
		4.1	(Nomura *et al.*, 2008)	
C20:1	20.6 ± 8.4	-	-	
C20:0	37.2 ± 15.4	30.0 (mouse brain)	(Leung *et al.*, 2006)	
		24.0	(Nomura *et al.*, 2008)	
C18:2	12.2 ± 1.7	6.1		
C18:1	85.1 ± 17.8	60 – 1600	(Richardson *et al.*, 2007)	
		36.0	(Williams *et al.*, 2007)	
		7.3 – 929	(Koga *et al.*, 1997)	
		60.0 (mouse brain)	(Leung *et al.*, 2006)	
C18:0	58.9 ± 13.8	150.0 (mouse brain)	(Leung *et al.*, 2006)	
		333 (mouse brain)	(Nomura *et al.*, 2008)	
C16:0	86.8 ± 22.7	716 – 5000	(Richardson *et al.*, 2007)	
		522.0	(Williams *et al.*, 2007)	
		36.9 – 485	(Koga *et al.*, 1997)	
		110.0 (mouse brain)	(Leung *et al.*, 2006)	
		167	(Nomura *et al.*, 2008)	

Table 5.14 A comparison of MAGs detected in rat brain with those observed in the literature.

MAG	Detected levels (nmol/g)	Previously detected levels (nmol/g)	Source	Comment
C22:5	0.2 ± 0.1	-		Good comparable results with the literature
C22:4	0.6 ± 0.2	-		
C20:4	11.1 ± 2.8	10.9 – 30.0	(Richardson *et al.*, 2007)	
		3.7 (mouse brain)	(Nomura *et al.*, 2008)	
C20:3	0.5 ± 0.2	-		
C18:2	0.2 ± 0.1	0.11 – 4.3	(Richardson *et al.*, 2007)	
		0.05	(Williams *et al.*, 2007)	
C18:1	6.8 ± 3.2	2.0	(Williams *et al.*, 2007)	
		2.2 (mouse brain)	(Nomura *et al.*, 2008)	
C18:0	0.3 ± 0.1	-		
C16:0	2.1 ± 0.6	3.1	(Williams *et al.*, 2007)	
		1	Nomura *et al.*, 2008)	

Table 5.15 A comparison of NAEs detected in rat liver with those observed in the literature.

NAE	Detected levels (pmol/g)	Previously detected levels (pmol/g)	Source	Comment
C18:2	14.6 ± 6.4	-		Reasonable correlation between values recorded here and those in the literature
C18:1	9.6 ± 7.1	29.3 – 66.4	(Koga *et al.*, 1997)	
C16:0	69.6 ± 19.8	68.8 – 98.7	(Koga *et al.*, 1997)	
		0.89	(Kondo *et al.*, 1998a)	

Table 5.16 A comparison of MAGs detected in rat liver with those observed in the literature.

MAG	Detected levels (nmol/g)	Previously detected levels (nmol/g)	Source	Comment
C22:4	0.3 ± 0.1			Reasonable correlation between value
C20:4	3.3 ± 0.8	1.8	(Kondo *et al.*, 1998a)	recorded here and those in the literatur
		2.2 ± 1.07	(Avraham *et al.*, 2008)	although C18:0 is higher than previousl
C20:1	0.2	-		observed
C18:2	7.2 ± 2.3	1.27	(Kondo *et al.*, 1998a)	
C18:1	15.4 ± 5.1	-		
C18:0	1.4 ± 0.3	0.14	(Kondo *et al.*, 1998a)	
C16:0	5.4 ± 2.2	-		

Table 5.17. A comparison of NAEs detected in rat Heart with those observed in the literature.

NAE	Detected levels (pmol/g)	Previously detected levels (pmol/g)	Source	Comment
C18:2	4.1 ± 1.5	-		Levels slightly lower than those in the literature
C18:1	10.0 ± 2.8	52 - 232	(Koga *et al.*, 1997)	
C18:0	11.8 ± 3.0	-		
C16:0	15.6 ± 5.3	56 - 233	(Koga *et al.*, 1997)	

Table 5.18. A comparison of MAGs detected in rat heart with those observed in the literature.

MAG	Detected levels (nmol/g)	Previously detected levels (nmol/g)	Source	Comment
C20:4	0.5 ± 0.1	3.25	(Avraham *et al.*, 2008)	Levels slightly lower than those in the literature
C18:2	0.2 ± 0.1	-		
C18:1	0.4 ± 0.1	-		
C18:0	0.2 ± 0.1	-		
C16:0	0.3 ± 0.1	-		

NAE DEA C22:4, NAE C20:1 and NAE C18:2 were not observed in the precursor ion scan of rat lung; however, they were identified by the SRM method detailed in this chapter. As calculated levels were low and close to the lower limit of quantification, it is perhaps to be expected that more NAEs would be detected by the SRM method due to an increase in sensitivity over scanning methodologies. Identification was achieved by the SRM transitions listed in Table 5.1 and by retention times previously observed from precursor ion scans used on other tissues. It has not been possible to find levels in the literature to compare against and is thought (Scholz *et al.*, 2005) to be the first reported levels of these NAEs in rat lung.

The values for MAG 2-AG C20:4 reported here sit within the range of previously reported values. MAG C18:0 is also comparable with previous result, but MAG C18:2 is slightly higher than those published.

As far as it can be ascertained, MAG C22:4, MAG C20:3, MAG C18:1 and MAG C16:0 have not been previously quantified in rat lung.

5.4.3.6 NAE and MAG levels in rat testi

Table 5.20 compares NAE levels measured here in rat testi with those in the literature. AEA C20:4, OEA C18:1 and PEA C16:0 were all quantified by the SRM method described in this chapter. AEA C20:4 levels are double previously detected levels (Sugiura *et al.*, 1996). OEA C18:1 and PEA C16:0 levels are slightly greater, with those identified here being five- and three-fold greater than those in the literature.

NAE C22:5, NAE C22:4, NAE C20:1 and NAE C18:0 were additionally measured. NAE C22:5 levels vary considerably with those previously reported in the literature (Kondo *et al.*, 1998a; Richardson *et al.*, 2007; Williams *et al.*, 2007), being over an order of magnitude greater. NAE C18:0 was also calculated to be at higher levels here than those in the literature, at levels five-fold greater. MAG C22:5, NAE C22:4 and NAE C20:1, as far as it can be ascertained, have not been previously measure in rat testi

Table 5.19 A comparison of MAGs detected in rat lung with those observed in the literature.

MAG	Detected levels (nmol/g)	Previously detected levels (nmol/g)	Source	Comment
C22:4	0.9 ± 0.2	-		Levels fall within those observed in the literature except for C18:2 which are almost a magnitude higher.
C20:4	5.6 ± 1.4	0.59 ± 0.3	(Kondo *et al.*, 1998a)	
		13.7 ± 3.2	(Avraham *et al.*, 2008)	
C20:3	1.0 ± 0.3	-		
C18:2	2.4 ± 0.3	0.46 ± 0.37	(Kondo *et al.*, 1998a)	
C18:1	4.5 ± 0.9	-		
C18:0	0.5 ± 0.1	0.14 ± 0.31	(Kondo *et al.*, 1998a)	
C16:0	1.5 ± 0.1	-		

Table 5.20. A comparison of NAEs detected in rat Testi with those observed in the literature

NAE	Detected levels (pmol/g)	Previously detected levels (pmol/g)	Source	Comment
C22:5	89.7 ± 19.7	6.0	(Kondo *et al.*, 1998a)	Levels are generally higher than those presented in the literature
C22:4	12.5 ± 2.7	-		
C20:4	11.0 ± 1.8	5.0 6.0 ± 1.4	(Kondo *et al.*, 1998a; Sugiura *et al.*, 1996)	
C20:1	2.2 ± 0.3	-		
C18:2	29.3 ± 6.5	9.0 5.6 ± 1.8	(Kondo *et al.*, 1998a; Sugiura *et al.*, 1996)	
C18:1	50.4 ± 8.7	9.5		
C18:0	85.2 ± 21.1	21.4 ± 1.7	(Sugiura *et al.*, 1996)	
C16:0	254.7 ± 76.9	73.9 ± 7.5	(Sugiura *et al.*, 1996)	

It is worth noting that a reasonable variety of NAEs were observed in one previously reported method, in rat testi, compared to the majority of published work in this area (Sugiura *et al.*, 1996). The scope of analytes covered in this instance was possible in this instance by the in house synthesis of reference standards.

5.4.3.7 NAE and MAG levels in rat spinal cord

Table 5.21 and Table 5.22 compare NAE and MAG levels in rat spinal cord measured in this chapter with those in the literature. There is considerable variation in the literature concerning NAE and MAG (2-AG C20:4) levels. However, AEA C20:4 levels measured here are comparable with two previously reported values. OEA C18:1 is slightly less than previously reported levels and PEA C16:1 levels are within the ranges previously published. The lower level of these two were the result of rats which had undergone a sham operation 3 days prior to tissue collection, which might affect the normal levels. MAG C20:4 levels in the literature vary considerably; however, levels reported here fall within the range of previously reported values.

NAE C24:1, NAE C22:5, NAE C22:1, NAE C20:1, NAE C20:0, NAE C18:2 and NAE C18:0 were also semi-quantified in rat spinal cord tissue but, as far as can be ascertained, no quantification has been published to compare against.

In the data presented in this chapter there appears to be a general trend for NAEs in brain to be lower than those found in spinal cord. Although AEA C20:4 levels are similar between the two tissues, most other NAEs are almost an order of magnitude higher in spinal cord compared to brain. The levels in spinal cord observed here are generally in keeping with those previously reported (Garcia-Ovejero *et al.*, 2009; Huang *et al.*, 1999; Jhaveri *et al.*, 2006; Petrosino *et al.*, 2007; Suplita *et al.*, 2006). NAEs levels in mouse spinal cord (although a different species) were also found to be higher than those in brain, with NAE C16:0, NAE C18:1, NAE C18:0 and NAE C24:1 levels found to be six, five, eleven and eight-fold higher in spinal cord compared to brain (Saghatelian *et al.*, 2004). Elevated levels, although not to such extremes, were noted in a separate experiment in

Table 5.21. A comparison of NAEs detected in rat spinal cord with those observed in the literature.

NAE	Detected levels (pmol/g)	Previously detected levels (pmol/g)	Source	Comment
C24:1	936.1 ± 237.6	-		Levels reported fall within those previously published, although OEA C18:1 was observed to be slightly low
C22:4	37.9 ± 5.7	-		
C22:1	275.3 ± 68.8	-		
C20:4	7.3 ± 1.8	10	(Jhaveri *et al.*, 2006)	
		30	(Petrosino *et al.*, 2007)	
		11	(Suplita *et al.*, 2006)	
C20:1	532.8 ± 140.2	-		
C20:0	600.7 ± 182.1	-		
C18:2	27.7 ± 3.9	-		
C18:1	895.8 ± 115.4	1250	(Jhaveri *et al.*, 2006)	
C18:0	917.1 ± 187.2	-		
C16:0	923.3 ± 83.2	5000	(Jhaveri *et al.*, 2006)	
		260	(Petrosino *et al.*, 2007)	

Table 5.22. A comparison of MAGs detected in rat spinal cord with those observed in the literature

MAG	Detected levels (nmol/g)	Previously detected levels (nmol/g)	Source	Comment
C22:4	1.4 ± 0.2			Levels of 2-AG C20:4 are within the range of values previously published
C20:4	31.4 ± 4.5	76	(Jhaveri *et al.*, 2006)	
		14	(Suplita *et al.*, 2006)	
		1.25	(Petrosino *et al.*, 2007)	
		0.43	(Huang *et al.*, 1999)	
C20:3	2.9 ± 0.7	-		
C20:1	4.4 ± 0.6	-		
C18:2	1.1 ± 0.2	-		
C18:1	31.5 ± 4.9	-		
C18:0	2.5 ± 0.8	-		
C16:0	4.1 ± 0.5	-		

mouse, where levels were between three and four - fold higher in spinal cord compared to brain (Mulder and Cravatt, 2006)

5.4.4 Comparison of NAE and MAG levels recovered immediately after death and five hours after death

NAE and MAG levels quantified immediately after death and five hours post-mortem are plotted in a comparative format in Figure 5.3 and Figure 5.4. Statistical analysis was performed on the median of each group and not the mean, therefore it may be more accurate to display the data as individual concentration data points and the median, however, it is easier to follow the data as portrayed. Such an approach has been previously used in the analysis and presentation of endocannabinoid data (Jhaveri *et al.*, 2006). Where NEA or MAG level changes were deemed significantly different, they are highlighted in the figures and Table 5.23 and Table 5.24. In some instances, analytes were not measurable in tissue immediately after death but were present five hours post-mortem. In such instances, it is clear that a change in levels had occurred, but it was not possible to perform a statistical analysis. In such cases, a substitution method was employed by using a concentration half-way between zero and the LLOQ. Although such an approach has the limitation of potentially overestimating the level of the analyte (Baccarelli *et al.*, 2005), it is a simple method enabling statistical analysis to be undertaken.

5.4.4.1 Post-mortem NAE and MAG changes in brain

It can be observed in Table 5.23, Figure 5.3 and Figure 5.5 that all NAEs detected in brain tissue increased significantly ($P < 0.01$ for all but C22:4 and C24:1 which were $P < 0.05$) when tissue was left for five hours compared to dissection immediately after death. AEA C20:4 has been previously observed to increase over a five hour period post-mortem in rat brain (Kempe *et al.*, 1996) as well as AEA C20:4, OEA C18:1 and PEA C16:0 in mouse brain (Patel *et al.*, 2005) and, along with NAE C18:0, in pig, sheep and cow brain (Schmid *et al.*, 1995). Although it is clear all NAEs increase, it has been

previously demonstrated in mouse brain that the mechanisms involved are not the same for all NAEs (Patel *et al.*, 2005). Furthermore, it is interesting to observe that NAE C22:5, not detected in rat brain immediately after death, is observed five hours post-mortem.

NAE C24:1 and C20:0 were both observed in brain and spinal cord, however only levels in brain were significantly elevated five hours post-mortem ($P < 0.05$ and $P < 0.01$ respectively). This would suggest that there is a selective metabolic pathway for at least these two NAEs that is not common to both tissues. 2-AG C20:4 levels were observed to decrease five hours post-mortem in rat brain, however not to the extent to be deemed statistically significant (see Table 5.24), and do not drop to the extent observed in mouse brain (Patel *et al.*, 2005), which were approximately half of the original value. Where 2-AG C20:4, 2-LG C18:2, MAG C16:1 and C18:1, reported in Figure 5.4, have been previously investigated in rat brain post-mortem, the results published are not directly comparable because of the five minute time course used (Sugiura *et al.*, 2001). Other MAGs detected in this chapter, MAG C22:4, MAG C20:3, MAG C18:2, MAG C20:1 and MAG C18:1, were observed to increase slightly, but not to statistically significant levels. The increase of MAG C18:0 levels five hours post-mortem was considered to be statistically significant ($P < 0.05$), see Table 5.24. Such an increase is contrary to the majority of other MAGs, indicating that a specific pathway is involved in the brain (and also in all other tissues investigated in this chapter except heart). It has been previously noted that more than one selective MAG synthesis / degradation pathway is present in brain tissue which might explain the differences observed here, although in that instance the tissue was derived from mice (Sugiura *et al.*, 2001). As far as can be ascertained, the post- mortem changes of MAG C18:0 have not been previously reported.

5.4.4.2 Post-mortem NAE and MAG changes in rat spinal cord

Levels of AEA C20:4, OEA C18:1 and NAE C16:0 significantly increased ($P < 0.01$) after five hours post-mortem: see Figure 5.3, Figure 5.5 and Table 5.23 All other NAEs in spinal cord, except for C24:1 and C20:0, also significantly increase five hours post-

mortem. As NAE C24:1 and NAE C20:0 levels did not increase; it suggests a selective mechanism specific for these two NAEs. Furthermore it would appear such mechanisms are not shared by both spinal cord and brain. Such an observation has not, as far as can be ascertained, been previously reported.

The MAGs observed in spinal cord post-mortem follow a similar trend to those in brain tissue; see Figure 5.4. Where there are changes in MAG levels, they are not deemed statistically significant except for MAG C18:0, which again, as observed in brain tissue and other non CNS tissues except heart, increased by significant levels ($P < 0.01$) five hours post-mortem, see Table 5.24. There appears to be no literature regarding spinal cord MAGs post-mortem to compare against.

5.4.4.3 Post-mortem NAE and MAG changes in rat testi

Levels of AEA C20:4, OEA C18:1 and NAE C16:0, as well as of other NAEs detected, increased significantly after five hours post-mortem ($P < 0.01$), see Figure 5.3 and Table 5.23. NAE C24:1, NAE C22:1 and NAE C20:0 were not observed at either time point. It is worth noting that where brain and spinal tissue obtained certain NAEs five hours post-mortem which were not present immediately after death, notably C22:5, the reverse is not necessarily the same for testi. NAE C24:1 and NAE C22:1, not observed in testi immediately after death, are also not observed five hours post-mortem, indicating that mechanisms involved in post-mortem NAE increases are selective and not alike across all tissues. The exact mechanism is unknown at this time. There are no previous reports that can be found to compare the results obtained here.

Levels of 2-AG C20:4 did not significantly alter after five hours post-mortem as observed in brain and spinal cord. As observed with central nervous tissue, the levels of all other MAGs detected, excluding MAG C18:0, did not significantly change either, where as MAG C18:0 levels significantly increased ($P < 0.01$) after five hours post-mortem, see Table 5.24.

5.4.4.4 Post-mortem NAE and MAG changes in rat heart

AEA C20:4 was below the limit of quantification in heart tissues collected immediately after death and five hours post-mortem. OEA C18:1 and PEA C16:0 were observed, but demonstrated no significant increases after five hours post-mortem. This is in contrast to OEA C18:1 and PEA C16:0 observed in all other tissues in this chapter and to those observed in mouse brain (Patel *et al.*, 2005). Furthermore, no NAEs from C20:n up to C24:n, nor those with greater saturation than two double bonds, were observed in tissue recovered immediately after death, nor were levels observed to increase five hours post-mortem. It could be theorized that if such NAEs were present, they did not increase; otherwise it might be expected that they would reach recordable levels after five hours. However, this cannot be substantiated; as it is possible that even if levels did increase, they may still be below the limit of quantification after five hours. The lack of longer, less saturated NAEs, coupled with no observable increases in NAEs five hours post-mortem, might indicate that the synthesis or catabolic routes for NAEs in rat heart studied in this chapter are substantially different to those in other rat tissues.

2-AG C20:4 levels in rat heart dropped by approximately half after five hours post-mortem. Such a significant decrease ($P < 0.01$) is greater than those observed in brain or spine but in line with those observed in other non-CNS tissues, lung and liver. Levels of other MAGs do not however exhibit a significant drop in concentration.

5.4.4.5 Post-mortem NAE and MAG changes in rat liver

AEA C20:4, OEA C18:1 and PEA C16:0 levels all significantly increased after five hours post-mortem ($P < 0.05$), see Figure 5.3 and Table 5.23 . This observation is comparable with NAEs levels five hours post-mortem in mouse brain (Patel *et al.*, 2005) and AEA C20:4 in rat brain (Kempe *et al.*, 1996). Excluding NAE C22:1 and NAE C20:0, all other NAEs increased significantly. As observed in central nervous tissues, NAE C22:5 levels were observed to increase from below detectable levels to recordable values five hours post-mortem. A similar trend was observed for NAE C24:1, NAE C22:4 and AEA C20:4.

Excluding MAG C18:0, there is a general reduction in MAG levels five hours post-mortem. 2-AG C20:4, MAG C20:3, MAG C20:1 and MAG C18:1 decreases in levels post-mortem were deemed significant ($P < 0.05$). As observed in all tissues examined in this chapter except heart, MAG C18:0 levels increase significantly ($P < 0.01$), see Figure 5.4 and Table 5.24.

5.4.4.6 Post-mortem NAE and MAG changes in rat lung

It can be seen from Figure 5.3 and Table 5.23 that levels of AEA C20:4, OEA C18:1 and PEA C16:0, as well as NAE C22:4, NAE C20:1, NAE C18:2 and NAE C18:0, all significantly increase ($P < 0.01$ except for C20:1 which was $P < 0.05$) after five hours post-mortem. This observation is comparable with those measured in CNS tissues and with those previously measured in mouse brain (Patel *et al.*, 2005). Additionally, such increases compare well with other non-CNS tissues investigated here, except for heart. Worthy of note is the lack of NAE C22:5 after five hours post-mortem, which is detected in all tissues except lung and heart after five hours post-mortem. As with most tissues, there is little information in the literature to compare against

2-AG C20:4 levels were observed to significantly decrease five hours post-mortem ($P < 0.01$) as observed in liver and heart tissues, but not CNS tissues. Other MAG levels also significantly decreased: MAG C22:4, MAG C20:3, MAG C18:2 and MAG C18:1 ($P < 0.01$ except C18:1 which was $P < 0.05$). As observed in all tissues investigated in this chapter, MAG C18:0 levels increase significantly five hours post-mortem ($P < 0.01$).

It can be seen from the results that not all NAEs and MAGs react to the same degree five hours postmortem; this is especially true in the instance of MAG C18:0. Furthermore, the same changes are not observed across all tissue types. This could lead to the conclusion that the synthesis and / or catabolic pathways of these analytes may be selective for some of the analytes observed and are not necessary equivalent across all tissues. The theory that the formation of NAEs via at least two routes post-mortem has

been previously proposed (Patel *et al.*, 2005). Work conducted on FAAH knockout mice demonstrated that not all NAE levels changes postmortem in the same way over time, suggesting alternative metabolism mechanisms were involved. AEA C20:4, OEA C18:1, and PEA C16:0 in wild type mice were all observed to increase in tissues left at room

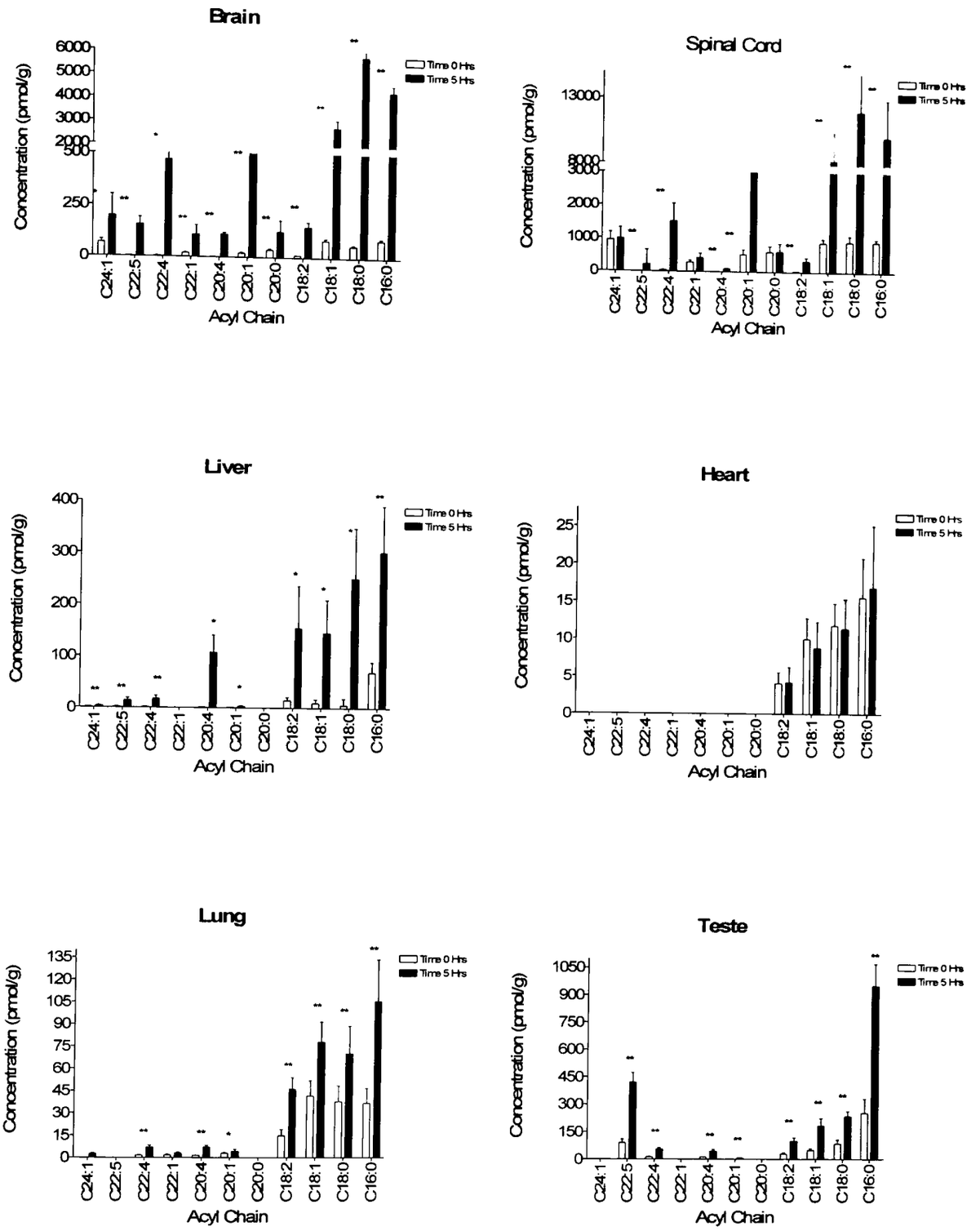

Figure 5.3. Graphical comparison of NAEs from rat tissues collected immediately after death and five hours post-mortem. Statistical tests were carried out using non-parametric Mann-Whitney (* $P < 0.05$, ** $P < 0.01$). To enable a statistical analysis to be performed against levels only detected five hours post-mortem, a nominal value halfway between zero and the limit of detection was selected.

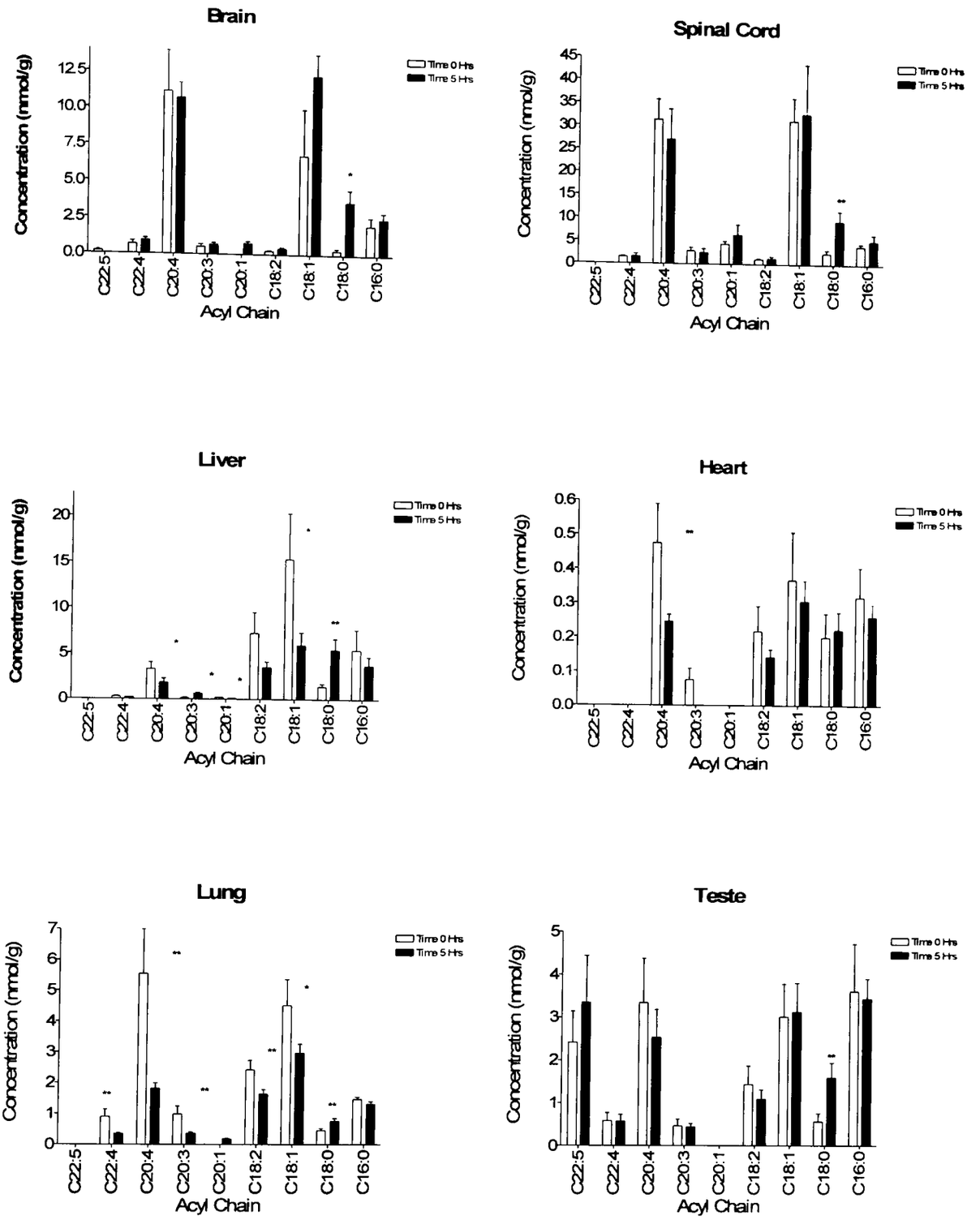

Figure 5.4. Graphical comparison of MAGs from rat tissues collected immediately after death and five hours post-mortem. Statistical tests were carried out using non-parametric Mann-Whitney (* $P < 0.05$, ** $P < 0.01$). To enable a statistical analysis to be performed against levels only detected five hours post-mortem, a nominal value halfway between zero and the limit of detection was selected.

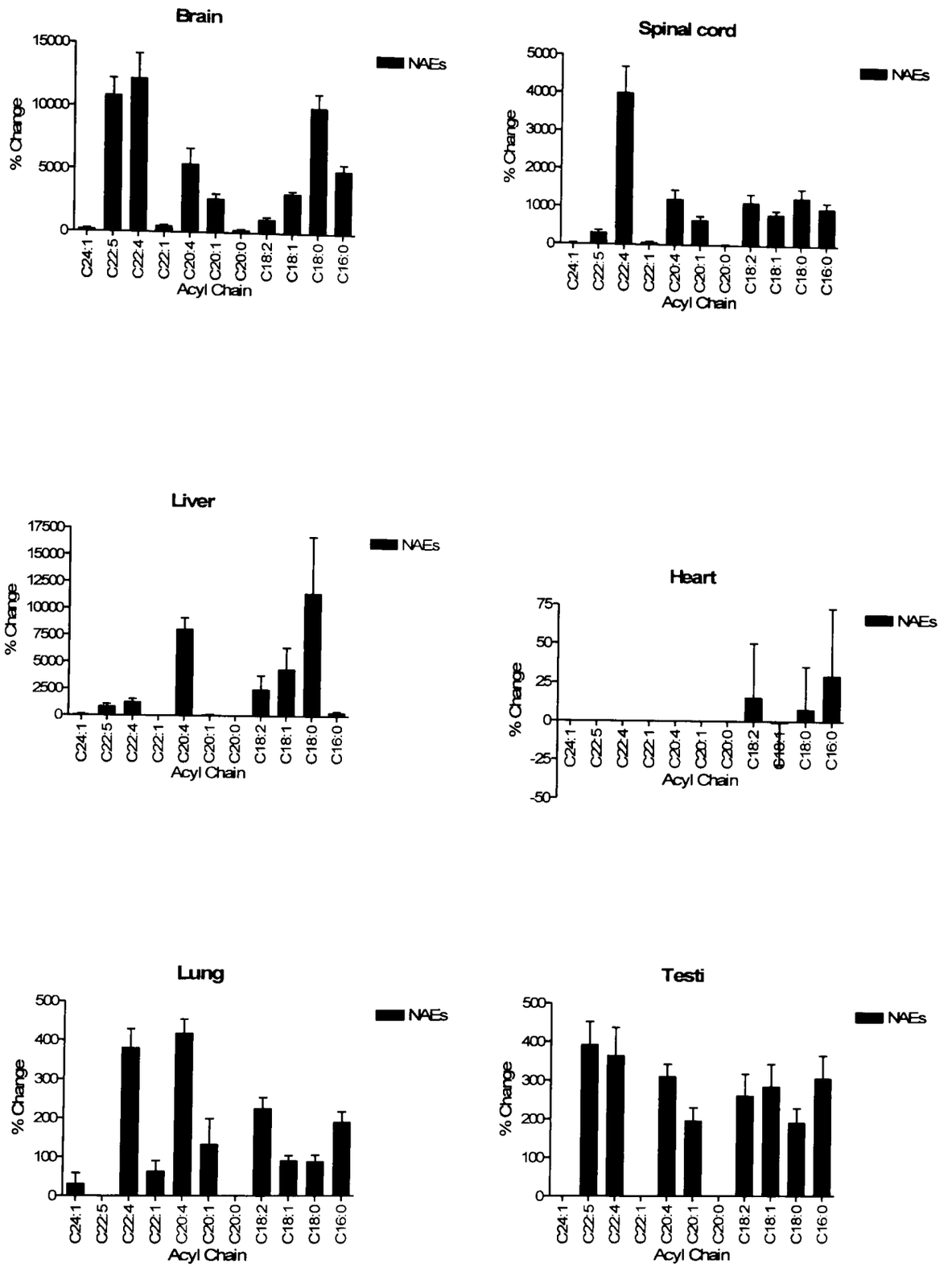

Figure 5.5. % variation between NAEs in tissues recovered immediately after death and five hours post-mortem. There is a general trend for NAE to increase five hours post-mortem.

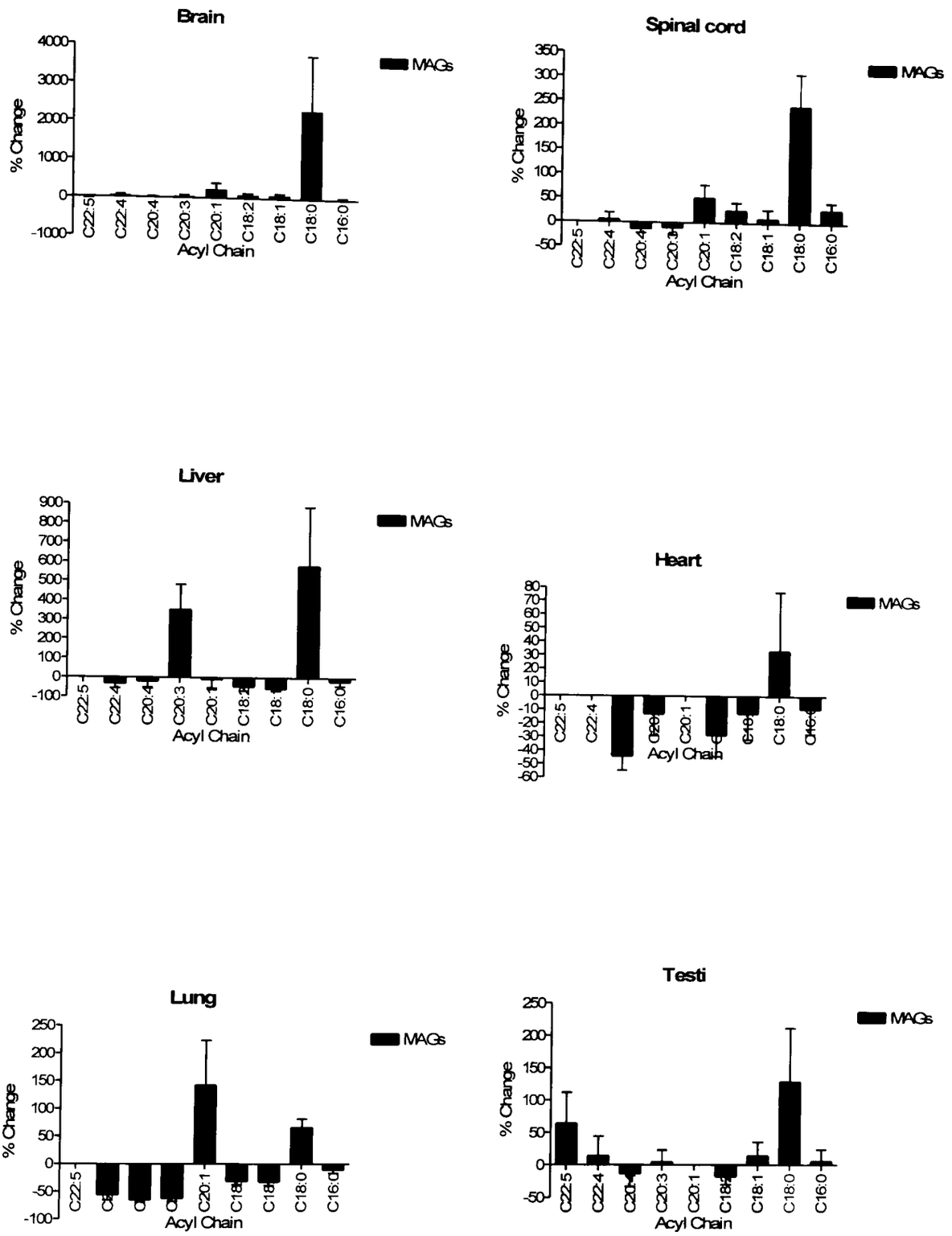

Figure 5.6. % variation between MAGs in tissues recovered immediately after death and five hours post-mortem. MAG C18:0 levels increase significantly in all tissue (except heart) compared to most other MAGs which decrease five hours post-mortem.

Table 5.23. A comparison of NAEs from tissues collected directly after death and those left for five hours post-mortem at room temperature. Statistical tested were carried out using non parametric Mann-Whitney (* $P < 0.05$, ** $P < 0.01$). NS indicates not significant and ND indicates not detected in either samples. Those characters in bold are where the analyte in tissue recovered immediately after death were below the limit of quantification. To enable a statistical analysis to be performed against levels detected five hours post-mortem, a nominal value halfway between zero and the limit of detection was selected.

Acyl Chain	Brain	Spinal cord	Testi	Heart	Liver	Lung
C24:1	*	NS	ND	ND	**	**NS**
C22:5	**	**	**	ND	**	ND
C22:4	*	**	**	ND	**	**
C22:1	**	*	ND	ND	ND	**NS**
C20:4	**	**	**	ND	*	**
C20:1	**	**	**	ND	*	*
C20:0	**	NS	ND	ND	ND	ND
C18:2	**	**	**	NS	**	**
C18:1	**	**	**	NS	*	**
C18:0	**	**	**	NS	*	**
C16:0	**	**	**	NS	**	**

Table 5.24. A comparison of MAGs from tissues collected directly after death and those left for five hours post-mortem at room temperature. Statistical tests were carried out using non-parametric Mann-Whitney (* $P < 0.05$, ** $P < 0.01$). NS indicates not significant and ND indicates not detected in either sample. Those characters in bold are where the analyte in one tissue group were below the limit of quantification. To enable a statistical analysis to be performed, a nominal value halfway between zero and the limit of detection was selected.

Acyl Chain	Brain	Spinal cord	Teste	Heart	Liver	Lung
C22:5	NS	ND	NS	ND	ND	ND
C22:4	NS	NS	NS	ND	NS	**
C20:4	NS	NS	NS	**	*	**
C20:3	NS	NS	NS	NS	*	**
C20:1	NS	NS	ND	ND	*	NS
C18:2	NS	NS	NS	NS	NS	**
C18:1	NS	NS	NS	NS	*	*
C18:0	*	**	**	NS	**	**
C16:0	NS	NS	NS	NS	NS	NS

temperature post mortem for up to 24 hours. However, where levels of OEA C18:1 and PEA C16:0 were considerably higher after 24 hours in FAAH knockout mice compared to wide type mice; AEA C20:4 levels however did not increase. Although AEA C20:4 levels immediately post mortem were higher than those detected in wild type, the levels did not rise to the extent observed in wild type mice 5 to 25 hours post mortem. This observation indicated that the increases of NAEs in wild type mice, and possibly other mammalian tissues, were not just the result of one mechanism.

MAGs 2-AG C20:4, 2-LG C18:2, MAG C16:1, and MAG C18:1 post mortem levels have also been assessed in rat brain (Sugiura *et al.*, 2001). Over a five minute time course post mortem, 2-AG C20:4 levels rapidly increased after one minute, followed by a rapid decrease, followed by a slower increase up to double original levels after 5 min. Conversely 2-LG C18:2 levels remain static throughout the 5 min time course. MAG C16:1 and C18:1 levels, measured together as they could not be discriminated, were demonstrated to increase approximately 3 fold after 5 min. As 2-AG C20:4, MAG C16:1 and C18:1 levels demonstrated different concentration profiles post mortem it demonstrates, as observed with NAEs, there are more than one synthesis or metabolomic routes taking place specific for some MAGs post-mortem.

5.4.4.7 Possible causes of NAE level changes in tissue 5 hours postmortem

There is a general trend for NAEs to increase (although to different degrees depending on the tissue) postmortem in all the tissue studied excluding the heart. It is difficult to ascertain from this study alone whether such increases (and the relative increases across the tissues) are due to continued / increased synthesis, differences in catabolism, chemical degradation (there was no pH control in the postmortem tissues) or a combination of factors

Postmortem NAE increases have been previously observed for AEA C20:4, OEA C18:1, and C16:0 PEA in mouse brain and have been speculated to be the result of continued synthesis via NAPE (overwhelming catabolism via FAAH) in particularly for OEA

C18:1 and C16:0 PEA. Furthermore alternative synthesis route post mortem have been speculated for AEA which are not thought to be prevalent in living rat (Patel *et al.*, 2005).

COX-2 may be responsible for differences in AEA C20:4 catabolism in rat liver and brain. It can be seen in Figure 5.5 that AEA C20:4 percentage increases post mortem in rat liver is slightly greater than that of brain (~7500 % increase compared to ~5000). It has previously been reported in mouse that COX-2 levels were undetectable in liver compared to brain (Naoi *et al.*, 2006) and gene expression for COX-2 levels in the liver of Wistar-Kyoto rats was less that those found in brain (Ivanov *et al.*, 2002). This difference in an enzyme known to catabolise AEA C20:4 may be responsible for the differences in percentage increases post mortem. It should be remembered however that prostamides, the result of AEA C20:4 catabolism by COX-2 were not detected by the precursor ion scan employed in chapter 4, therefore if this catabolism route is active, the resulting prostamides are at concentration too low for detection by the precursor ion method.

Another observation is the reduced percentage increase postmortem of NAEs in lung compared to brain tissue (DEA C22:4, AEA C20:4, AEA C20:4 ~ 30, 12.5, and 20 fold respectively) , see Figure 5.5. It has been demonstrated that NAAA, known to catabolise AEA C20:4, NAE C18:2, NAE C18:1, NAE C18:0, PEA C16:0, and NAE C14:0 (Ueda *et al.*, 2001) is present in rat lung tissue at levels ~14 times than found in brain (Tsuboi *et al.*, 2007). Such levels in the lung could be responsible for a greater rate of catabolism and result in a smaller increase of NAEs postmortem in lung tissue compared to brain, although it is fair to say that levels of NAAA in brain compared to lung are lower in some instances when compared to NAE percentage increases comparing the two tissues. The product of NAE catabolism by NAAA is ethanolamine and the respective arachdonic acid therefore if this metabolic route was prominent in postmortem lung tissue, the products would not be detectable by the precursor ion method described in chapters 3 and 4.

PEA C16:0 percentage increases post mortem in rat liver are considerably less than brain (~400% increase compared to 5000%). Such a decrease is not observed across the board

of NAEs and AEA 20:4 post mortem percentage increases in liver are slightly greater than in brain. Where the cause of this could be due to increased catabolism, it would be selective for PEA C16:0 but not AEA C20:4. As such it would appear that some of the synthesis / catabolism mechanisms at work in postmortem NAEs may be selective.

It is worth noting that bacteria could be an alternative cause to the postmortem changes of NAEs and MAGs observed in this chapter. Lung tissue would perhaps be most prone to this due to the direct access to organisms in the air. Further work could explore this possibility by identifying levels / increases of bacterial in tissues left for 5 hours post mortem compared to tissues salvaged immediately after death.

5.5 Conclusions

A quantitative method has been established for measuring a greater range of NAEs and MAGs than previously demonstrated. Previous approaches have predominantly been targeted and dependant on the availability of reference standards. Where more global efforts have been made, detectable analytes have generally been dependant on changes in levels between two or more samples. The approach taken here has widened the scope of analyte quantified by combining the information gathered on NAEs and MAGs by the precursor ion and neutral loss scans described in chapters 3 and 4 with a targeted SRM methodology. Hence this approach has combined the advantages of scanning for families of structural analogues with the specificity and sensitivity found with SRM approaches. The resulting method has quantified a wider range of NAEs and MAGs than previous targeted approaches.

Quantification of NAEs AEA C20:4, OEA C18:1 and PEA C16:1 and of MAGs 2-AG C20:4 and 2-LG C20:4 was successfully achieved in rat brain, spinal cord, heart, lung, liver and testi. Quantitative data, based on calibration curves derived from structural analogues, were also recorded for NAEs C24:1, C22:5, C22:4, C22:1, C20:1, C20:0, C18:2 and C18:0 and MAGs C22:5, C22:4, C20:3, C20:1, C18:1, C18:0, C16:0 providing a far greater distribution profile of these lipid compounds than previously reported. The profiles demonstrate that the distributions between tissues vary and that brain and spinal tissues contain the widest, but not a complete, distribution of NAEs and MAGs.

It should be noted that not all the fatty acid precursors of the NAEs and MAGs detected in this chapter can be synthesized by rat (Mathews *et al.*, 1998) and hence levels of analytes with a double bond position beyond C-9 will be to some degree diet dependant. Consequently the profile of NAEs and MAGs detected will vary depending on the feed of the animals.

Although a full validation of this method was not possible due to the unavailability of a substantial number of the analytes of interest, the method has been validated to a stage that demonstrates its suitability for the analysis of NAEs and MAGs.

By the use of this method a fuller profile of NAEs and MAGs has been recorded in rat tissues than has previously been observed. Where a number of such analytes do not directly affect the cannabinoid receptors, they can have an entourage effect on the CB_1 and CB_2 ligands and hence are important to measure when investigating the biological effects of this class of compounds. Furthermore, a wider range of NAEs and MAGs has been quantified five hours post-mortem than previously identified. It was found that not all NAE and MAG level changes postmortem are equivalent, indicating the possibility of selective synthesis / degradation pathways. Furthermore, differences in changes between tissues also indicate such pathways are not uniform across tissue types.

The targeted method developed in this chapter has been further applied to study the effects of acute / chronic administration of FAAH inhibitor (URN 597) on NAE and MAG profiles in rat tissue (data not included in this thesis)

CHAPTER 6

6 General Conclusions

The unique features of the QqQLit hybrid mass spectrometer have been assessed in the field of metabolite profiling by the analysis of three different families of endogenous metabolites; nucleotides, N-acyl ethanolamines, and mono-acylglycerols from bacterial and mammalian cells.

A method to profile phosphate containing endogenous metabolites, in particular nucleotide metabolites, was based around the identification of the phosphate moiety, which fragmented under CID to form a *m/z* 79 ion. A precursor ion scan was employed to identify the *m/z* 79 ion and full product ion spectra was used to confirm knowns or tentatively identify analytes where reference material was not immediately available. By applying the method to bacterial samples *Escherichia coli* MG1655 and *Pseudomonas aeruginosa,* a comprehensive profile of nucleotide was captured. Furthermore, a number of nucleotides for which reference standards were not available at the time were also identified. This approach has extended the number of nucleotides previously identified in targeted methods which generally have been focused on a relatively small subset. Due to the large number of possible nucleotides (≈ 30), endogenous levels and similar chemistry (Maybaum *et al.*, 1980), detection has been a challenge, especially without more selective methods such as MS. Where some methods have attempted to profile a broad range of nucleotides (Buckstein *et al.*, 2008; Cordell *et al.*, 2008; Tuytten *et al.*, 2002), such approaches have preselected the analytes and as such, the profile of nucleotides was not as complete as the profile obtained by the methods described here. By expanding the possible number of nucleotides identified, this methodology provides a more comprehensive profile of nucleotides than previous methods and would be beneficial in the study of nucleotide's biological function. Furthermore, this approach is not just specific for the analysis of nucleotides, but other phosphate containing analytes. Where it could be applied to the study of phospholipids, nucleotide sugars and sugar phosphates, the scope could be widened to the study of other larger phosphate bonded compounds

such as phosphorylated proteins and their respective peptide digest (Williamson *et al.*, 2006).

The use of this methodology was successful for the profiling of *N*-acyl ethanolamines (NAE) and monoacylglycerols (MAG). Ethanolamine and glycerol moieties enabled a precursor ion and neutral loss survey scans to be employed respectively. Application of this approach on rat-brain tissue identified not only analytes for which reference standards were available but also a number of analytes for which reference standards were not available. Furthermore, the application of the method on other rat tissues produced a wide profile of NAEs and MAGs not previously observed. Interestingly, the profile of rat testi was notably different to other tissues investigated due to the presence of MAG and NAE C22:5; analytes not detected in other tissues by this method. Furthermore, as far as it can be ascertained, MAG C22:5 has not been previously reported in rat tissues.

It is fair to say that a TIC of NAEs and MAG obtained from a precursor ion and neutral loss survey scan (see Figure 3.16) is noisy and appears to contain split peaks when in fact these are the result of single compounds. Although when processing the data analytes are not initially identified from a TIC, the resulting chromatogram is confusing. It is likely that this is a feature of the instrument due to switching between the various scan functions. To ascertain this it would be possible to repeat this experiment but run the instrument only in a survey scan mode (without the EPI scan) and look at the resulting TIC. Smoother peaks, with a loss in peak splitting would be expected.

The profile of NAEs and MAGs observed was considerable broader than previous methods. Targeted methods have previously identified a relatively small number of analytes due to the low availability of reference standards. Where more global profiling methods have successfully identified a wider number of NAEs and MAGs than targeted methods (Nomura *et al.*, 2008; Saghatelian and Cravatt, 2005), identification was commonly based on changes due to a biological intervention thus analytes not specifically affected by that intervention were not necessarily reported. Furthermore, in

these instances specification was not as rigid as the methods described in this thesis due to identification being solely based on the pseudomolecular ion. Where there are number of key NAEs and MAGs which interact directly with the endocannabinoid receptors, other NAEs and MAGs play a role as entourage compounds and it is important to profile all analytes within these families when studying their biological effects (Williams *et al.*, 2007). This methodology has demonstrated the capability to undertake this task.

Where the quantification capabilities of the phosphate survey method were accessed, this was not undertaken to the same degree with the two methods employed for identifying NAEs and MAGs. Further work could include evaluating the quantification capabilities of these two methods. Never the less a targeted approach employing the data obtained from the survey scans was successful, quantifying a more comprehensive number of NAEs and MAGs than previously published methods. It would be fair to say that a drawback to this approach is the additional time it required to quantify the analytes on a separate run.

The analytical approach taken in this thesis has been successful in the profiling of families of endogenous metabolites and sits in-between a targeted and global approach, offering the advantages of both. It is not as focused as a targeted method and as such is not limited to only identifying analytes preselected prior to analysis. Conversely, the method is not as open ended as global approaches, with an inherent bias towards a given class of analytes. The result of which is a method optimized to observe a range analyte and in theory more sensitive than an unbiased global approach. On balance it is a valuable methodology for metabolite profiling. Nevertheless, it might not be suitable for occasions where a given analysis requires greater sensitivity or when no preconception of analytes of interest are known, for which other approaches may be more appropriate.

A limitation of the method is the difficulty in identifying and confirming unknowns. Whilst GC-MS is relatively well supported with spectra libraries, LC-MS/MS is not, as yet, and of little use. The use of accurate mass can aid in the identification of unknowns but cannot be performed on the QqQLit and requires additional instrumentation.

At the start of this work (October 2005), the QqQLit was the only instrument capable of this approach. However, developments in mass spectrometry design since then have produced commercially available mass spectrometers potentially capable of the methodology employed in this thesis. For example, Waters have developed a new instrument, the Waters Xevo™ TQ MS[5], which is built on the design of a tandem quadrupole. With additional technology in the collision cell this instrument can produce full product spectra within time scales compatible with chromatography. This instrument could most likely perform precursor ion / neutral loss survey scans coupled with full product ion spectra as performed by the QqQLit. Furthermore, because the Waters Xevo™ TQ MS is designed to work with ultra high performance liquid chromatography, a separation technique based on HPLC but results in shaper chromatography peaks (2-3 sec), it is probable that the quadrupoles scan speeds are faster on this instrument than the QqQLit and hence could be advantageous in both sensitivity and possibly quantification.

Another instrument, manufactured by Thermo Scientific, could also be applied to this field of analysis; the LTQ Orbitrap™ velos[6]. This instrument is comprised of a linear ion trap and an Orbitrap™, enabling MS/MS fragmentation in the linear ion trap and accurate mass in the Orbitrap™. The scan speed of the ion trap is such that it is capable of performing a survey scan coupled with full product ion scan of ten of the most intense ions (consequently identifying structurally significant ions or calculating neutral losses), although this is not true precursor ion / neutral loss when compared to a tandem quadrupole instrument. Furthermore, being an iontrap, this part of the instrument would suffer from the one third rule. However, the Orbitrap™, capable of < 2 ppm mass accuracy and up to 100,000 FWHM resolution (at *m/z* 400) could be employed in the providing confirmation of identification or greatly aiding in the identification of unknowns. Potentially both of these two scan functions could be applied in one chromatography run.

---

[5] http://www.waters.com/waters/library.htm?locale=en_US&cid=10064408&lid=10046828 - accessed 18th June

[6] http://www.thermo.com/eThermo/CMA/PDFs/Product/productPDF_51627.pdf - accessed 18th June 2009

Hybridized techniques such as LC-MS/MS-NMR would also be advantageous to the analysis of metabolite profiling. Such combinations will no doubt become more accessible in the future and will be extremely useful in this field, providing sensitive analysis coupled with two independent techniques for the structural elucidation of unknowns.

Although these new instruments could potentially perform similar scans to the QqQLit, it is worth noting that there appears to be a divergence of roles for mass spectrometers which has positive implications for bioanalysis. Tandem quadrupole instruments were the workhorse for small molecule quantification and accurate mass instruments were employed predominantly in analyte identification and global analysis. However the latter instruments are slowly improving in dynamic range and sensitivity to the extent that they can perform quantification. A demonstration of this was recently published comparing an Orbitrap™ and an ABI 4000 tandem quadrupole (Zhang *et al.*, 2009a). Quantifying reference standards in rat plasma, the Orbitrap™ identified analytes by accurate mass measurements of their respective $[M+H]^+$ where the tandem quadrupole performed SRM. Comparable sensitivity was demonstrated. The tandem quadrupole required standards to optimize the electronics, whereas this was not necessary for the Orbitrap™. Furthermore, the scanning of the Orbitrap™ enables unknowns to be captured and identified post analysis. Similarly, there is an example of LC-TOF being used in the quantitative analysis of 101 pesticides (Ferrer and Thurman, 2007). As the capabilities of these instruments improve in sensitivity, selectivity and dynamic range, the traditional roles commonly held by mass spectrometers may blur further in the future. Such improvements in analytical instrumentation can only be a positive step for the challenging field of analytical biochemistry and metabolite profiling

References

Ahn K, McKinney MK, Cravatt BF (2008). Enzymatic pathways that regulate endocannabinoid signaling in the nervous system. *Chem Rev* **108:** 1687-707.

Annan RS, Huddleston MJ, Verma R, Deshaies RJ, Carr SA (2001). A multidimensional electrospray MS-based approach to phosphopeptide mapping. *Anal Chem* **73:** 393-404.

Antoni FA (2000). Molecular diversity of cyclic AMP signalling. *Front Neuroendocrinol* **21:** 103-32.

Astarita G, Ahmed F, Piomelli D (2008). Identification of biosynthetic precursors for the endocannabinoid anandamide in the rat brain. *J Lipid Res* **49:** 48-57.

Avraham Y, Magen I, Zolotarev O, Vorobiav L, Nachmias A, Pappo O *et al* (2008). 2-Arachidonoylglycerol, an endogenous cannabinoid receptor agonist, in various rat tissues during the evolution of experimental cholestatic liver disease. *Prostaglandins Leukot Essent Fatty Acids* **79:** 35-40.

Baccarelli A, Pfeiffer R, Consonni D, Pesatori AC, Bonzini M, Patterson Jr DG *et al* (2005). Handling of dioxin measurement data in the presence of non-detectable values: Overview of available methods and their application in the Seveso chloracne study. *Chemosphere* **60:** 898-906.

Barg J, Fride E, Hanus L, Levy R, Matus-Leibovitch N, Heldman E *et al* (1995). Cannabinomimetic behavioral effects of and adenylate cyclase inhibition by two new endogenous anandamides. *Eur J Pharmacol* **287:** 145-52.

Ben-Shabat S, Fride E, Sheskin T, Tamiri T, Rhee MH, Vogel Z *et al* (1998). An entourage effect: inactive endogenous fatty acid glycerol esters enhance 2-arachidonoyl-glycerol cannabinoid activity. *Eur J Pharmacol* **353:** 23-31.

Bisogno T, Melck D, De Petrocellis L, Di Marzo V (1999). Phosphatidic acid as the biosynthetic precursor of the endocannabinoid 2-arachidonoylglycerol in intact mouse neuroblastoma cells stimulated with ionomycin. *J Neurochem* **72:** 2113-9.

Bisogno T, Sepe N, Melck D, Maurelli S, De Petrocellis L, Di Marzo V (1997). Biosynthesis, release and degradation of the novel endogenous cannabimimetic metabolite 2-arachidonoylglycerol in mouse neuroblastoma cells. *Biochem J* **322 (Pt 2):** 671-7.

Bornheim L, Kim K, CHEN B, Correia A (1995). Microsomal Cytochrome P450-Mediated Liver and Brain Anandamide Metabolism. *Biochemical Pharmacology* **50:** 677 - 686.

Brindle JT, Antti H, Holmes E, Tranter G, Nicholson JK, Bethell HW *et al* (2002). Rapid and noninvasive diagnosis of the presence and severity of coronary heart disease using 1H-NMR-based metabonomics. *Nat Med* **8:** 1439-44.

Buchholz A, Takors R, Wandrey C (2001). Quantification of intracellular metabolites in escherichia coli K12 using liquid chromatographic-electrospray ionization tandem mass spectrometric techniques. *Anal Biochem* **295:** 129-137.

Buckstein MH, He J, Rubin H (2008). Characterization of nucleotide pools as a function of physiological state in Escherichia coli. *J Bacteriol* **190:** 718-26.

Bueno MJ, Aguera A, Gomez MJ, Hernando MD, Garcia-Reyes JF, Fernandez-Alba AR (2007). Application of liquid chromatography/quadrupole-linear Ion trap mass spectrometry and time-of-flight mass spectrometry to the determination of pharmaceuticals and related contaminants in wastewater. *Anal Chem* **79:** 9372-84.

Burns KL, Gelbaum LT, Sullards MC, Bostwick DE, May SW (2005). Iso-coenzyme A. *J Biol Chem* **280:** 16550-8.

Cai Z, Song F, Yang MS (2002). Capillary liquid chromatographic-high-resolution mass spectrometric analysis of ribonucleotides. *J Chromatogr A* **976:** 135-43.

Carrier EJ, Kearn CS, Barkmeier AJ, Breese NM, Yang W, Nithipatikom K *et al* (2004). Cultured rat microglial cells synthesize the endocannabinoid 2-arachidonylglycerol, which increases proliferation via a CB2 receptor-dependent mechanism. *Mol Pharmacol* **65:** 999-1007.

Ceglarek U, Kortz L, Leichtle A, Fiedler GM, Kratzsch J, Thiery J (2009a). Rapid quantification of steroid patterns in human serum by on-line solid phase extraction combined with liquid chromatography-triple quadrupole linear ion trap mass spectrometry. *Clin Chim Acta* **401:** 114-8.

Ceglarek U, Leichtle A, Brugel M, Kortz L, Brauer R, Bresler K *et al* (2009b). Challenges and developments in tandem mass spectrometry based clinical metabolomics. *Mol Cell Endocrinol* **301:** 266-71.

Chan W, Cai Z (2008). Aristolochic acid induced changes in the metabolic profile of rat urine. *J Pharm Biomed Anal* **46:** 757-62.

Chen JK, Chen J, Imig JD, Wei S, Hachey DL, Guthi JS *et al* (2008). Identification of novel endogenous cytochrome p450 arachidonate metabolites with high affinity for cannabinoid receptors. *J Biol Chem* **283:** 24514-24.

Chen P, Liu Z, Liu S, Xie Z, Aimiuwu J, Pang J *et al* (2009). A LC-MS/MS method for the analysis of intracellular nucleoside triphosphate levels. *Pharm Res* **26:** 1504-15.

Cheng C, Gross ML (2000). Applications and mechanisms of charge-remote fragmentation. *Mass Spectrom Rev* **19:** 398-420.

Cho WC (2007). Proteomics technologies and challenges. *Geno Prot Bioinfo* **5:** 77-85.

Clement AB, Hawkins EG, Lichtman AH, Cravatt BF (2003). Increased seizure susceptibility and proconvulsant activity of anandamide in mice lacking fatty acid amide hydrolase. *J Neurosci* **23:** 3916-23.

Coles R, Kharasch ED (2007). Stereoselective analysis of bupropion and hydroxybupropion in human plasma and urine by LC/MS/MS. *J Chromatogr B Analyt Technol Biomed Life Sci* **857:** 67-75.

Cordell RL, Hill SJ, Ortori CA, Barrett DA (2008). Quantitative profiling of nucleotides and related phosphate-containing metabolites in cultured mammalian cells by liquid chromatography tandem electrospray mass spectrometry. *J Chromatogr B Analyt Technol Biomed Life Sci* **871:** 115-24.

Coulier L, Bas R, Jespersen S, Verheij E, van der Werf MJ, Hankemeier T (2006). Simultaneous quantitative analysis of metabolites using ion-pair liquid chromatography-electrospray ionization mass spectrometry. *Anal Chem* **78:** 6573-82.

Cunnick WR, Cromie JB, Cortell R, Wright B, Beach E, Seltzer F *et al* (1972). Value of biochemical profiling in a periodic health examination program: analysis of 1,000 cases. *Bull N Y Acad Med* **48:** 5-22.

de Lago E, Petrosino S, Valenti M, Morera E, Ortega-Gutierrez S, Fernandez-Ruiz J *et al* (2005). Effect of repeated systemic administration of selective inhibitors of endocannabinoid inactivation on rat brain endocannabinoid levels. *Biochem Pharmacol* **70:** 446-52.

Devane WA, Axelrod J (1994). Enzymatic synthesis of anandamide, an endogenous ligand for the cannabinoid receptor, by brain membranes. *Proc Natl Acad Sci U S A* **91:** 6698-701.

Devane WA, Hanus L, Breuer A, Pertwee RG, Stevenson LA, Griffin G *et al* (1992). Isolation and structure of a brain constituent that binds to the cannabinoid receptor. *Science* **258:** 1946-9.

Di Marzo V (1998). 'Endocannabinoids' and other fatty acid derivatives with cannabimimetic properties: biochemistry and possible physiopathological relevance. *Biochim Biophys Acta* **1392:** 153-75.

Dierick JF, Dieu M, Remacle J, Raes M, Roepstorff P, Toussaint O (2002). Proteomics in experimental gerontology. *Exp Gerontol* **37:** 721-34.

Douglas D, Frank A, Mao D (2005). Linear Ion Traps In Mass Spec. *Mass Spectrom Rev* **24:** 1-29.

Dunn WB, Broadhurst D, Brown M, Baker PN, Redman CW, Kenny LC *et al* (2008). Metabolic profiling of serum using Ultra Performance Liquid Chromatography and the LTQ-Orbitrap mass spectrometry system. *J Chromatogr B Analyt Technol Biomed Life Sci* **871:** 288-98.

Dutta PK, O'Donovan GA (1987). Separation and quantitation of bacterial ribonucleoside triphosphates extracted with trifluroacetic acid, by an ion exchange high performance liquid chromatography. *Journal of Chromatography* **385:** 119-124.

Edelson-Averbukh M, Pipkorn R, Lehmann WD (2006). Phosphate group-driven fragmentation of multiply charged phosphopeptide anions. Improved recognition of peptides phosphorylated at serine, threonine, or tyrosine by negative ion electrospray tandem mass spectrometry. *Anal Chem* **78:** 1249-56.

Evans J, Wang TC, Heyes MP, Markey SP (2002). LC/MS analysis of NAD biosynthesis using stable isotope pyridine precursors. *Anal Biochem* **306:** 197-203.

Felder CC, Nielsen A, Briley EM, Palkovits M, Priller J, Axelrod J *et al* (1996). Isolation and measurement of the endogenous cannabinoid receptor agonist, anandamide, in brain and peripheral tissues of human and rat. *FEBS Lett* **393:** 231-5.

Feng X, Liu X, Luo Q, Liu BF (2008). Mass spectrometry in systems biology: an overview. *Mass Spectrom Rev* **27:** 635-60.

Ferrer I, Thurman EM (2007). Multi-residue method for the analysis of 101 pesticides and their degradates in food and water samples by liquid chromatography/time-of-flight mass spectrometry. *J Chromatogr A* **1175:** 24-37.

Fezza F, Bisogno T, Minassi A, Appendino G, Mechoulam R, Di Marzo V (2002). Noladin ether, a putative novel endocannabinoid: inactivation mechanisms and a sensitive method for its quantification in rat tissues. *FEBS Lett* **513:** 294-8.

Fiehn O (2001). Combining genomics, metabolome analysis, and biochemical modelling to understand metabolic networks. *Comp Funct Genomics* **2:** 155-68.

Fiehn O (2008). Extending the breadth of metabolite profiling by gas chromatography coupled to mass spectrometry. *Trends Analyt Chem* **27:** 261-269.

Fiehn O, Kopka J, Dormann P, Altmann T, Trethewey RN, Willmitzer L (2000). Metabolite profiling for plant functional genomics. *Nat Biotechnol* **18:** 1157-61.

Fontana A, Di Marzo V, Cadas H, Piomelli D (1995). Analysis of anandamide, an endogenous cannabinoid substance, and of other natural N-acylethanolamines. *Prostaglandins Leukot Essent Fatty Acids* **53:** 301-8.

Fowler CJ (2007). The contribution of cyclooxygenase-2 to endocannabinoid metabolism and action. *Br J Pharmacol* **152:** 594-601.

Fu J, Astarita G, Gaetani S, Kim J, Cravatt BF, Mackie K *et al* (2007). Food intake regulates oleoylethanolamide formation and degradation in the proximal small intestine. *J Biol Chem* **282:** 1518-28.

Gao L, Chiou W, Tang H, Cheng X, Camp HS, Burns DJ (2007). Simultaneous quantification of malonyl-CoA and several other short-chain acyl-CoAs in animal tissues by ion-pairing reversed-phase HPLC/MS. *J Chromatogr B Analyt Technol Biomed Life Sci* **853:** 303-13.

Garcia-Ovejero D, Arevalo-Martin A, Petrosino S, Docagne F, Hagen C, Bisogno T *et al* (2009). The endocannabinoid system is modulated in response to spinal cord injury in rats. *Neurobiol Dis* **33:** 57-71.

Gaskell SJ (1997). Electrospray : Principles and Practice. *J Mass Spectrom* **32:** 677 - 688.

Gillum MP, Zhang D, Zhang XM, Erion DM, Jamison RA, Choi C *et al* (2008). N-acylphosphatidylethanolamine, a gut- derived circulating factor induced by fat ingestion, inhibits food intake. *Cell* **135:** 813-24.

Griffiths WJ, Jonsson AP, Liu S, Rai DK, Wang Y (2001). Electrospray and tandem mass spectrometry in biochemistry. *Biochem J* **355:** 545-61.

Grob MK, rsquo, Brien K, Chu JJ, Chen DDY (2003). Optimization of cellular nucleotide extraction and sample preparation for nucleotide pool analyses using capillary electrophoresis. *J Chrom B* **788:** 103-111.

Hager J, YvesLeBlanc J (2003). High-performance liquid chromatography–tandem mass spectrometry with a new quadrupole/linear ion trap instrument. *J. Chromatogr A* **1020:** 3-9.

Hansen HH, Ikonomidou C, Bittigau P, Hansen SH, Hansen HS (2001). Accumulation of the anandamide precursor and other N-acylethanolamine phospholipids in infant rat models of in vivo necrotic and apoptotic neuronal death. *J Neurochem* **76:** 39-46.

Hanus L, AbuLafi S, Fride E, Breuer A, Vogel Z, Shalev DE *et al* (2001). 2-arachidonyl glyceryl ether, an endogenous agonist of the cannabinoid CB1 receptor. *Proc Natl Acad Sci USA* **98:** 3662-5.

Hanus L, Gopher A, Almog S, Mechoulam R (1993). Two new unsaturated fatty acid ethanolamides in brain that bind to the cannabinoid receptor. *J Med Chem* **36:** 3032-4.

Hartmann C, Smeyers-Verbeke J, Massart DL, McDowall RD (1998). Validation of bioanalytical chromatographic methods. *J Pharm Biomed Anal* **17:** 193-218.

Hennere G, Becher F, Pruvost A, Goujard C, Grassi J, Benech H (2003). Liquid chromatography-tandem mass spectrometry assays for intracellular deoxyribonucleotide triphosphate competitors of nucleoside antiretrovirals. *J Chromatogr B Analyt Technol Biomed Life Sci* **789:** 273-81.

Herrin GL, McCurdy HH, Wall WH (2005). Investigation of an LC-MS-MS (QTrap) method for the rapid screening and identification of drugs in postmortem toxicology whole blood samples. *J Anal Toxicol* **29:** 599-606.

Hoffman E, Stroobant V (2005). *Mass spectrometry - principles and applications*. Wiley.

Hoffmann Ed (1996). Tandem Mass Spectrometry: a Primer. *J Mass Spectrom* **31:** 129-137.

Hopfgartner G, Husser C, Zell M (2003). Rapid screening and characterization of drug metabolites using a new quadrupole–linear ion trap mass spectrometer. *Journal of Mass Spectrometry* **38::** 138-150.

Hopfgartner G, Varesio E, Tschappat V, Grivet C, Bourgogne E, Leuthold LA (2004). Triple quadrupole linear ion trap mass spectrometer for the analysis of small molecules and macromolecules. *J Mass Spectrom* **39:** 845-55.

Horning EC, Horning MG (1971). Metabolic profiles: gas-phase methods for analysis of metabolites. *Clin Chem* **17:** 802-9.

Howlett AC (2002). The cannabinoid receptors. *Prostaglandins Other Lipid Mediat* **68-69:** 619-31.

Huang SM, Bisogno T, Petros TJ, Chang SY, Zavitsanos PA, Zipkin RE *et al* (2001). Identification of a new class of molecules, the arachidonyl amino acids, and characterization of one member that inhibits pain. *J Biol Chem* **276:** 42639-44.

Huang SM, Strangman NM, Walker JM (1999). Liquid chromatographic-mass spectrometric measurement of the endogenous cannabinoid 2-arachidonylglycerol in the spinal cord and peripheral nervous system. *Zhongguo Yao Li Xue Bao* **20:** 1098-102.

Ingebretsen OC, Bakken AM, Segadal L, Farstad M (1982). Determination of adenine nucleotides and inosine in human myocard by ion-pair reversed-phase high-performance liquid chromatography. *J Chromatogr* **242:** 119-26.

IUPAC-IUBMB (1992). *Biochemical nomenclature and related documents*, 2nd edn.

Ivanov AI, Pero RS, Scheck AC, Romanovsky AA (2002). Prostaglandin E(2)-synthesizing enzymes in fever: differential transcriptional regulation. *Am J Physiol Regul Integr Comp Physiol* **283:** R1104-17.

Jhaveri MD, Richardson D, Kendall DA, Barrett DA, Chapman V (2006). Analgesic effects of fatty acid amide hydrolase inhibition in a rat model of neuropathic pain. *J Neurosci* **26:** 13318-27.

Jia Y, McLeod RL, Wang X, Parra LE, Egan RW, Hey JA (2002). Anandamide induces cough in conscious guinea-pigs through VR1 receptors. *Br J Pharmacol* **137:** 831-6.

Jones PM, Bennett MJ (2002). The changing face of newborn screening: diagnosis of inborn errors of metabolism by tandem mass spectrometry. *Clin Chim Acta* **324:** 121-8.

Kang J, Lee S, Kang S, Kwon HN, Park JH, Kwon SW *et al* (2008). NMR-based metabolomics approach for the differentiation of ginseng (Panax ginseng) roots from different origins. *Arch Pharm Res* **31:** 330-6.

Kasai H, TSUBUKI M, Kazunori T, HONDA T, UEDA H (2003). Analyses of anandamide and endocannabinoid-like compounds using collision-induced dissociation in fast atom bombardment ionization–mass spectrometry and gas chromatography/chemical ionization–mass spectrometry. *Anal Sci* **19:** 1593 -1598.

Kaushik VK, Kavana M, Volz JM, Weldon SC, Hanrahan S, Xu J *et al* (2009). Characterization of recombinant human acetyl-CoA carboxylase-2 steady-state kinetics. *Biochim Biophys Acta* **1794:** 961-7.

Keller BO, Sui J, Young AB, Whittal RM (2008). Interferences and contaminants encountered in modern mass spectrometry. *Anal Chim Acta* **627:** 71-81.

Kempe K, Hsu FF, Bohrer A, Turk J (1996). Isotope dilution mass spectrometric measurements indicate that arachidonylethanolamide, the proposed endogenous ligand of the cannabinoid receptor, accumulates in rat brain tissue post mortem but is contained at low levels in or is absent from fresh tissue. *J Biol Chem* **271:** 17287-95.

Kharbouche H, Sporkert F, Troxler S, Augsburger M, Mangin P, Staub C (2009). Development and validation of a gas chromatography-negative chemical ionization tandem mass spectrometry method for the determination of ethyl glucuronide in hair and its application to forensic toxicology. *J Chromatogr B Analyt Technol Biomed Life Sci* **877:** 2337-43.

Kingsley PJ, Marnett LJ (2007). LC-MS-MS analysis of neutral eicosanoids. *Methods Enzymol* **433:** 91-112.

Koga D, Santa T, Fukushima T, Homma H, Imai K (1997). Liquid chromatographic-atmospheric pressure chemical ionization mass spectrometric determination of anandamide and its analogs in rat brain and peripheral tissues. *J Chromatogr B Biomed Sci Appl* **690:** 7-13.

Koivusalo M, Haimi P, Heikinheimo L, Kostiainen R, Somerharju P (2001). Quantitative determination of phospholipid compositions by ESI-MS: effects of acyl chain length, unsaturation, and lipid concentration on instrument response. *J Lipid Res* **42:** 663-72.

Kondo S, Kondo H, Nakane S, Kodaka T, Tokumura A, Waku K *et al* (1998a). 2-Arachidonoylglycerol, an endogenous cannabinoid receptor agonist: identification as one of the major species of monoacylglycerols in various rat tissues, and evidence for its generation through Ca- dependent and - independent mechanisms. *Febs letters* **429:** 152 - 156.

Kondo S, Sugiura T, Kodaka T, Kudo N, Waku K, Tokumura A (1998b). Accumulation of various N-acylethanolamines including N-arachidonoylethanolamine (anandamide) in cadmium chloride-administered rat testis. *Arch Biochem Biophys* **354:** 303-10.

Kozak K, Prusakiewicz J, Marnett LJ (2004). Oxidative metabolism of endocannabinoids by COX - 2. *Curr Pharm Des* **10:** 659 - 667.

Kozak KR, Crews BC, Morrow JD, Wang LH, Ma YH, Weinander R *et al* (2002a). Metabolism of the endocannabinoids, 2-arachidonylglycerol and anandamide, into prostaglandin, thromboxane, and prostacyclin glycerol esters and ethanolamides. *J Biol Chem* **277:** 44877-44885.

Kozak KR, Gupta RA, Moody JS, Ji C, Boeglin WE, DuBois RN *et al* (2002b). 15-Lipoxygenase metabolism of 2-arachidonylglycerol. Generation of a peroxisome proliferator-activated receptor alpha agonist. *J Biol Chem* **277:** 23278-86.

Kuksis A (1987). *Chromatography of lipids in biomedical research and clinical diagnosis*, vol. 37. J Chrom Libr.

Laurentin H, Ratzinger A, Karlovsky P (2008). Relationship between metabolic and genomic diversity in sesame (Sesamum indicum L.). *BMC Genomics* **9:** 250.

Leung D, Saghatelian A, Simon G, Cravatt B (2006). Inactivation of N-acyl phosphatidylethanolamine phospholipase D reveals multiple mechanisms for the biosynthesis of endocannabinoids. *Biochemistry* **45:** 4720 - 4726.

Li A, Alton D, Bryant M, W S (2005). Simultaneously quantifying parent drugs and screening for metabolites in plasma pharmacokinetic samples using selected reaction monitoring information-dependent acquisition on a QTrap instrument. *Rapid Commun Mass Spectrom* **2005:** 1943–1950.

Lim HK, Chen J, Sensenhauser C, Cook K, Subrahmanyam V (2007). Metabolite identification by data-dependent accurate mass spectrometric analysis at resolving power of 60,000 in external calibration mode using an LTQ/Orbitrap. *Rapid Commun Mass Spectrom* **21:** 1821-32.

Lin H, Xu D, Chen H (1997). Simultaneous determination of purine bases, ribonucleosides and ribonucleotides by capillary electrophoresis-electrochemistry with a copper electrode. *J Chromatogr A* **760**.

Liu J, Wang L, Harvey-White J, Osei-Hyiaman D, Razdan R, Gong Q *et al* (2006). A biosynthetic pathway for anandamide. *Proc Natl Acad Sci U S A* **103:** 13345-50.

Liu Z, Chan KK, Wang JJ (2005). Tandem mass spectrometric analysis of cyclophosphamide, ifosfamide and their metabolites. *Rapid Commun Mass Spectrom* **19:** 2581-90.

Loregian A, Scremln C, Schiavon M, Marcello A, Palu G (1994). Quantitative analysis of ribonucleotide triphosphates in cell extracts by high-Performance liquid chromatography and micellar electrokinetic capillary chromatography; a comparative study. *Anal Chem* **66:** 2981-2984.

Lundin A, Thore A (1975). Comparison of methods for extraction of bacterial adenine nucleotides determined by firefly assay. *Appl Microbiol* **30:** 713-21.

Luo B, Groenke K, Takors R, Wandrey C, Oldiges M (2007). Simultaneous determination of multiple intracellular metabolites in glycolysis, pentose phosphate pathway and tricarboxylic acid cycle by liquid chromatography-mass spectrometry. *J Chromatogr A* **1147:** 153-64.

Maccarrone M (2006). Fatty acid amide hydrolase: A potential target for next generation therapeutics. *Curr Pharm Des* **12:** 759 - 772.

Maccarrone M, Attina M, Bari M, Cartoni A, Ledent C, Finazzi-Agro A (2001). Anandamide degradation and N-acylethanolamines level in wild-type and CB1 cannabinoid receptor knockout mice of different ages. *J Neurochem* **78:** 339-48.

Maccarrone M, Barboni B, Paradisi A, Bernabo N, Gasperi V, Pistilli MG *et al* (2005). Characterization of the endocannabinoid system in boar spermatozoa and implications for sperm capacitation and acrosome reaction. *J Cell Sci* **118:** 4393-404.

Maccarrone M, Valensise H, Bari M, Lazzarin N, Romanini C, Finazzi-Agro A (2000). Relation between decreased anandamide hydrolase concentrations in human lymphocytes and miscarriage. *Lancet* **355:** 1326-9.

Magnes C, Sinner F, Regittnig W, T P (2005). LC/MS/MS Method for Quantitative Determination of Long-Chain Fatty Acyl-CoAs. *Anal. Chem.* **77:** 2889-2894.

Martens-Lobenhoffer J, Becker A, Freude H, Bode-Boger SM (2009). Identification and quantification of the atypical metabolite ornithine-lactam in human plasma by liquid chromatography-tandem mass spectrometry (LC-MS/MS). *J Chromatogr B Analyt Technol Biomed Life Sci* **877:** 2284-9.

Mathews C, Van Holde k, Ahern k (1998). *Biochemistry*, Second edn. Prentice Hall.

Maybaum J, Klein FK, Sadee W (1980). Determination of pyrimidine ribotide and deoxyribotide pools in cultured cells and mouse liver by high-performance liquid chromatography. *J Chromatogr* **188:** 149-58.

McDonald JG, Thompson BM, McCrum EC, Russell DW (2007). Extraction and analysis of sterols in biological matrices by high performance liquid chromatography electrospray ionization mass spectrometry. *Methods Enzymol* **432:** 145-70.

McLafferty F, Turecek F (1993). *Interpretation of mass spectra*, Fourth edn. University Science Books.

Mechoulam R, Ben-Shabat S, Hanus L, Ligumsky M, Kaminski NE, Schatz AR *et al* (1995). Identification of an endogenous 2-monoglyceride, present in canine gut, that binds to cannabinoid receptors. *Biochem Pharmacol* **50:** 83-90.

Mechoulam R, Berry EM, Avraham Y, Di Marzo V, Fride E (2006). Endocannabinoids, feeding and suckling--from our perspective. *Int J Obes (Lond)* **30 Suppl 1:** S24-8.

Mechoulam R, Fride E, Marzo VD (1998). Endocannabinoids. *Eur J Pharmacol* **359:** 1 - 18.

Moody JS, Kozak KR, Ji C, Marnett LJ (2001). Selective oxygenation of the endocannabinoid 2-arachidonylglycerol by leukocyte-type 12-lipoxygenase. *Biochemistry* **40:** 861-6.

Morin D, Grasland B, Vallee-Rehel K, Dufau C, Haras D (2003). On-line high-performance liquid chromatography-mass spectrometric detection and quantification of N-acylhomoserine lactones, quorum sensing signal molecules, in the presence of biological matrices. *J Chromatogr A* **1002:** 79-92.

Movahed P, Jonsson BA, Birnir B, Wingstrand JA, Jorgensen TD, Ermund A *et al* (2005). Endogenous unsaturated C18 N-acylethanolamines are vanilloid receptor (TRPV1) agonists. *J Biol Chem* **280:** 38496-504.

Mueller C A , Weinmann W , Dresen S , Schreiber A, M G (2005). Development of a multi-target screening analysis for 301 drugs using a QTrap liquid chromatography/tandem mass spectrometry system and automated library searching. *Rapid Commun Mass Spectrom* **19:** 1332-1338.

Mulder AM, Cravatt BF (2006). Endocannabinoid metabolism in the mbsence of fatty acid amide hydrolase (FAAH): Discovery of phoshorycholine derivatives of N-acyl ethanolamines. *Biochemistry* **45:** 11267 - 11277.

Murphy RC (1993). *Mass Spectrometry of Lipids (Handbook of Lipid Research)*, First edn. Springer.

Naoi K, Kogure S, Saito M, Hamazaki T, Watanabe S (2006). Differential effects of selective cyclooxygenase (COX)-1 and COX-2 inhibitors on anorexic response and prostaglandin generation in various tissues induced by zymosan. *Biol Pharm Bull* **29:** 1319-24.

Nazar R, Lawford H, Wong J (1970). An improved procedure for extraction and analysis of cellular nucleotides. *Anal Biochem* **35:** 305 - 313.

Ng M, Blaschke TF, Arias AA, Zare RN (1992). Analysis of free intracellular nucleotides using high-performance capillary electrophoresis. *Anal Chem* **64:** 1682 - 1684.

Nguyen A, Luong J, Masson C (1990). Determination of nucleotides in fish tissues using capillary electrophoresis. *Anal Chem* **62:** 2490 - 2493.

Nikaido H, Vaara M (1985). Molecular basis of bacterial outer membrane permeability. *Microbiol Rev* **49:** 1-32.

Nomura DK, Blankman JL, Simon GM, Fujioka K, Issa RS, Ward AM *et al* (2008). Activation of the endocannabinoid system by organophosphorus nerve agents. *Nat Chem Biol* **4:** 373-8.

Obata T, Sakurai Y, Kase Y, Tanifuji Y, Horiguchi T (2003). Simultaneous determination of endocannabinoids (arachidonylethanolamide and 2-arachidonylglycerol) and isoprostane (8-epiprostaglandin F2alpha) by gas chromatography-mass spectrometry-selected ion monitoring for medical samples. *J Chromatogr B Analyt Technol Biomed Life Sci* **792:** 131-40.

Oka S, Tsuchie A, Tokumura A, Muramatsu M, Suhara Y, Takayama H *et al* (2003). Ether-linked analogue of 2-arachidonoylglycerol (noladin ether) was not detected in the brains of various mammalian species. *J Neurochem* **85:** 1374-81.

Oneill K, Shao XW, Zhao ZX, Malik A, Lee ML (1994). Capillary electrophoresis of nucleotides on ucon-coated fused silica columns. *Anal Biochem* **222:** 185-189.

Ortori CA, Atkinson S, Chhabra SR, Camara M, Williams P, Barrett DA (2007). Comprehensive profiling of N-acylhomoserine lactones produced by Yersinia pseudotuberculosis using liquid chromatography coupled to hybrid quadrupole-linear ion trap mass spectrometry. *Anal Bioanal Chem* **387:** 497-511.

Patel S, Carrier EJ, Ho WS, Rademacher DJ, Cunningham S, Reddy DS *et al* (2005). The postmortal accumulation of brain N-arachidonylethanolamine (anandamide) is dependent upon fatty acid amide hydrolase activity. *J Lipid Res* **46:** 342-9.

Pears MR, Cooper JD, Mitchison HM, Mortishire-Smith RJ, Pearce DA, Griffin JL (2005). High resolution 1H NMR-based metabolomics indicates a neurotransmitter cycling deficit in cerebral tissue from a mouse model of Batten disease. *J Biol Chem* **280:** 42508-14.

Perrett D, Herbert KE, Morris G, Simmonds HA (1989). Optimised conditions for the routine HPLC separation of nucleotides in cell extracts. *Adv Exp Med Biol* **253B:** 463-8.

Pertwee RG (2006). The pharmacology of cannabinoid receptors and their ligands: an overview. *Int J Obes (Lond)* **30 Suppl 1:** S13-8.

Petrosino S, Palazzo E, de Novellis V, Bisogno T, Rossi F, Maione S *et al* (2007). Changes in spinal and supraspinal endocannabinoid levels in neuropathic rats. *J neuropharm* **52:** 415-22.

Plumb RS, Johnson KA, Rainville P, Smith BW, Wilson ID, Castro-Perez JM *et al* (2006). UPLC/MS(E); a new approach for generating molecular fragment information for biomarker structure elucidation. *Rapid Commun Mass Spectrom* **20:** 1989-94.

Polson C, Sarkar P, Incledon B, Raguvaran V, Grant R (2003). Optimization of protein precipitation based upon effectiveness of protein removal and ionization effect in liquid chromatography-tandem mass spectrometry. *J Chromatogr B Analyt Technol Biomed Life Sci* **785:** 263-75.

Porter AC, Sauer JM, Knierman MD, Becker GW, Berna MJ, Bao J *et al* (2002). Characterization of a novel endocannabinoid, virodhamine, with antagonist activity at the CB1 receptor. *J Pharmacol Exp Ther* **301:** 1020-4.

Raamsdonk LM, Teusink B, Broadhurst D, Zhang N, Hayes A, Walsh MC *et al* (2001). A functional genomics strategy that uses metabolome data to reveal the phenotype of silent mutations. *Nat Biotechnol* **19:** 45-50.

Ramautar R, Mayboroda OA, Derks RJ, van Nieuwkoop C, van Dissel JT, Somsen GW *et al* (2008). Capillary electrophoresis-time of flight-mass spectrometry using noncovalently bilayer-coated capillaries for the analysis of amino acids in human urine. *Electrophoresis* **29:** 2714-22.

Raymond EM (1997). An introduction to quadrupole ion trap mass spectrometry. *J Mass Spectrom* **32:** 351-369.

Rea K, Roche M, Finn DP (2007). Supraspinal modulation of pain by cannabinoids: the role of GABA and glutamate. *Br J Pharmacol* **152:** 633-48.

Richards H, Das S, Smith CJ, Pereira L, Geisbrecht A, Devitt NJ *et al* (2002). Cyclic nucleotide content of tobacco BY-2 cells. *Phytochemistry* **61:** 531-7.

Richardson D, Ortori CA, Chapman V, Kendall DA, Barrett DA (2007). Quantitative profiling of endocannabinoids and related compounds in rat brain using liquid chromatography-tandem electrospray ionization mass spectrometry. *Anal Biochem* **360:** 216-26.

Rochfort SJ, Trenerry VC, Imsic M, Panozzo J, Jones R (2008). Class targeted metabolomics: ESI ion trap screening methods for glucosinolates based on MSn fragmentation. *Phytochemistry* **69:** 1671-9.

Roger B (1989). *Statistics - A guide to the use of statistical methods in the physical sciences*. John Wiley & Sons.

Saghatelian A, Cravatt BF (2005). Discovery metabolite profiling--forging functional connections between the proteome and metabolome. *Life Sci* **77:** 1759-66.

Saghatelian A, Trauger S, Want E, Hawkins E, Siuzdak G, Cravatt B (2004). Assignment of endogenous substrates to enzymes by global metabolite profiling. *Biochemistry* **43:** 14332-14339.

Sandlie I, Kleppe K (1982). Effect of caffeine on nucleotide pools in Escherichia coli. *Chem Biol Interact* **40:** 141-8.

Schmid PC, Krebsbach RJ, Perry SR, Dettmer TM, Maasson JL, Schmid HH (1995). Occurrence and postmortem generation of anandamide and other long-chain N-acylethanolamines in mammalian brain. *FEBS Lett* **375:** 117-20.

Schmid PC, Schwartz KD, Smith CN, Krebsbach RJ, Berdyshev EV, Schmid HH (2000). A sensitive endocannabinoid assay. The simultaneous analysis of N-acylethanolamines and 2-monoacylglycerols. *Chem Phys Lipids* **104:** 185-91.

Scholz K, Dekant W, Volkel W, Pahler A (2005). Rapid detection and identification of N-acetyl-L-cysteine thioethers using constant neutral loss and theoretical multiple reaction monitoring combined with enhanced product-ion scans on a linear ion trap mass spectrometer. *J Am Soc Mass Spectrom* **16:** 1976-84.

Schwab W (2003). Metabolome diversity: too few genes, too many metabolites? *Phytochemistry* **62:** 837-49.

Shaner RL, Allegood JC, Park H, Wang E, Kelly S, Haynes CA *et al* (2008). Quantitative analysis of sphingolipids for lipidomics using triple quadrupole and quadrupole linear ion trap mass spectrometers. *J Lipid Res.*

Sharkey KA (2006). Endocannabinoids: biology, mechanism of action and functions. *Int J Obes (Lond)* **30 Suppl 1:** S4-6.

Sheskin T, Hanus L, Slager J, Vogel Z, Mechoulam R (1997). Structural requirements for binding of anandamide-type compounds to the brain cannabinoid receptor. *J Med Chem* **40:** 659-67.

Simon GM, Cravatt BF (2008). Anandamide biosynthesis catalyzed by the phosphodiesterase GDE1 and detection of glycerophospho-N-acyl ethanolamine precursors in mouse brain. *J Biol Chem.*

Skoog D, Holler J, T N (1998). *Principles of Instrumental Analysis.*

Sleno L, Volmer DA (2004). Ion activation methods for tandem mass spectrometry. *J Mass Spectrom* **39:** 1091-112.

Snider NT, Kornilov AM, Kent UM, Hollenberg PF (2007). Anandamide metabolism by human liver and kidney microsomal cytochrome p450 enzymes to form hydroxyeicosatetraenoic and epoxyeicosatrienoic acid ethanolamides. *J Pharmacol Exp Ther* **321:** 590-7.

Snyder L, Kirkland J, Glajch J (1997). *Practical HPLC Method Developmant.*

Stitt M, Fernie AR (2003). From measurements of metabolites to metabolomics: an 'on the fly' perspective illustrated by recent studies of carbon-nitrogen interactions. *Curr Opin Biotechnol* **14:** 136-44.

Stryer L (1999). *Biochemistry*, 4 edn.

Sugiura T, Kodaka T, Nakane S, Miyashita T, Kondo S, Suhara Y *et al* (1999). Evidence that the cannabinoid CB1 receptor is a 2-arachidonoylglycerol receptor. Structure-activity relationship of 2-arachidonoylglycerol, ether-linked analogues, and related compounds. *J Biol Chem* **274:** 2794-801.

Sugiura T, Kondo S, Kishimoto S, Miyashita T, Nakane S, Kodaka T *et al* (2000). Evidence that 2-arachidonoylglycerol but not N-palmitoylethanolamine or anandamide is the physiological ligand for the cannabinoid CB2 receptor. Comparison of the agonistic activities of various cannabinoid receptor ligands in HL-60 cells. *J Biol Chem* **275:** 605-12.

Sugiura T, Kondo S, Sukagawa A, Nakane S, Shinoda A, Itoh K *et al* (1995). 2-Arachidonoylglycerol: a possible endogenous cannabinoid receptor ligand in brain. *Biochem Biophys Res Commun* **215:** 89-97.

Sugiura T, Kondo S, Sukagawa A, Tonegawa T, Nakane S, Yamashita A *et al* (1996). Enzymatic synthesis of anandamide, an endogenous cannabinoid receptor ligand, through N-acylphosphatidylethanolamine pathway in testis: involvement of Ca(2+)-dependent transacylase and phosphodiesterase activities. *Biochem Biophys Res Commun* **218:** 113-7.

Sugiura T, Yoshinaga N, Waku K (2001). Rapid generation of 2-arachidonoylglycerol, an endogenous cannabinoid receptor ligand, in rat brain after decapitation. *Neurosci Lett* **297:** 175-8.

Suplita RL, 2nd, Gutierrez T, Fegley D, Piomelli D, Hohmann AG (2006). Endocannabinoids at the spinal level regulate, but do not mediate, nonopioid stress-induced analgesia. *J neuropharm* **50:** 372-9.

Thomas S, Hopfgartner G, Giroud C, Staub C (2009). Quantitative and qualitative profiling of endocannabinoids in human plasma using a triple quadrupole linear ion trap mass spectrometer with liquid chromatography. *Rapid Commun Mass Spectrom* **23:** 629 - 638.

Tikhonov Yu V, Pimenov AM, Uzhevko SA, Toguzov RT (1990). Ion-pair high-performance liquid chromatography of purine compounds in the small intestinal mucosa of children with coeliac disease. *J Chromatogr* **520:** 419-23.

Tong H, Bell D, Tabei K, Siegel MM (1999). Automated data massaging, interpretation, and e-mailing modules for high throughput open access mass spectrometry. *J Am Soc Mass Spectrom* **10:** 1174-1187.

Triolo A, Altamura M, Dimoulas T, Guidi A, Lecci A, Tramontana M (2005). In vivo metabolite detection and identification in drug discovery via LC-MS/MS with data-dependent scanning and postacquisition data mining. *J Mass Spectrom* **40:** 1572-82.

Tsuboi K, Takezaki N, Ueda N (2007). The N-acylethanolamine-hydrolyzing acid amidase (NAAA). *Chem Biodivers* **4:** 1914-25.

Tu Y, Harrison AG (1998). Fragmentation of protonated amides through intermediate ion-neutral complexes: neighboring group participation. *J. Am. Soc. Mass. Spectrom.* **9:** 454-462.

Tuytten R, Lemiere F, Dongen WV, Esmans EL, Slegers H (2002). Short capillary ion-pair high-performance liquid chromatography coupled to electrospray (tandem) mass spectrometry for the simultaneous analysis of nucleoside mono-, di- and triphosphates. *Rapid Commun Mass Spectrom* **16:** 1205-15.

Ueda N, Yamanaka K, Yamamoto S (2001). Purification and characterization of an acid amidase selective for N-palmitoylethanolamine, a putative endogenous anti-inflammatory substance. *J Biol Chem* **276:** 35552-7.

US Department of Health and Human Services (2001). Guidance for industry : bioanalytical method validation.

Van Pelt CK, Carpenter BK, Brenna JT (1999). Studies of structure and mechanism in acetonitrile chemical ionization tandem mass spectrometry of polyunsaturated fatty acid methyl esters. *J Am Soc Mass Spectrom* **10:** 1253-62.

Villas-Boas SG, Rasmussen S, Lane GA (2005). Metabolomics or metabolite profiles? *Trends Biotechnol* **23:** 385-6.

Vogeser M, Hauer D, Christina Azad S, Huber E, Storr M, Schelling G (2006). Release of anandamide from blood cells. *Clin Chem Lab Med* **44:** 488-91.

Vogeser M, Schelling G (2007). Pitfalls in measuring the endocannabinoid 2-arachidonoyl glycerol in biological samples. *Clin Chem Lab Med* **45:** 1023-5.

Wagner JA, Hu K, Bauersachs J, Karcher J, Wiesler M, Goparaju SK *et al* (2001). Endogenous cannabinoids mediate hypotension after experimental myocardial infarction. *J Am Coll Cardiol* **38:** 2048-54.

Walker JM, Huang SM (2002). Endocannabinoids in pain modulation. *Prostaglandins Leukot Essent Fatty Acids* **66:** 235-42.

Walker JM, Krey JF, Chu CJ, Huang SM (2002). Endocannabinoids and related fatty acid derivatives in pain modulation. *Chem Phys Lipids* **121:** 159-72.

Walter L, Franklin A, Witting A, Moller T, Stella N (2002). Astrocytes in culture produce anandamide and other acylethanolamides. *J Biol Chem* **277:** 20869-76.

Walter L, Franklin A, Witting A, Wade C, Xie Y, Kunos G *et al* (2003). Nonpsychotropic cannabinoid receptors regulate microglial cell migration. *J Neurosci* **23:** 1398-405.

Wang C, Yang J, Gao P, Lu X, Xu G (2005). Identification of phospholipid structures in human blood by direct-injection quadrupole-linear ion-trap mass spectrometry. *Rapid Commun. Mass Spectrom.* **19:** 2443–2453.

Warner M, Gustafsson JA (1994). Effect of ethanol on cytochrome P450 in the rat brain. *Proc Natl Acad Sci U S A* **91:** 1019-23.

Weber A, Ni J, Ling KH, Acheampong A, Tang-Liu DD, Burk R *et al* (2004). Formation of prostamides from anandamide in FAAH knockout mice analyzed by HPLC with tandem mass spectrometry. *J Lipid Res* **45:** 757-63.

Weckwerth W, Loureiro ME, Wenzel K, Fiehn O (2004). Differential metabolic networks unravel the effects of silent plant phenotypes. *Proc Natl Acad Sci U S A* **101:** 7809-14.

Weiss B (2007). The deoxycytidine pathway for thymidylate synthesis in Escherichia coli. *J Bacteriol* **189:** 7922-6.

Wells JM, McLuckey SA (2005). Collision-induced dissociation (CID) of peptides and proteins. *Methods Enzymol* **402:** 148-85.

Werner A (1993). Reversed-phase and ion-pair separations of nucleotides, nucleosides and nucleobases: analysis of biological samples in health and disease. *J Chromatogr* **618:** 3-14.

Williams J, Wood J, Pandarinathan L, Karanian DA, Bahr BA, Vouros P *et al* (2007). Quantitative method for the profiling of the endocannabinoid metabolome by LC-atmospheric pressure chemical ionization-MS. *Anal Chem* **79:** 5582-93.

Williamson BL, Marchese J, Morrice NA (2006). Automated identification and quantification of protein phosphorylation sites by LC/MS on a hybrid triple quadrupole linear ion trap mass spectrometer. *Mol Cell Proteomics* **5:** 337-46.

Witkamp RF (2005). Genomics and systems biology--how relevant are the developments to veterinary pharmacology, toxicology and therapeutics? *J Vet Pharmacol Ther* **28:** 235-45.

Witters E, Roef L, Newton R, Van Dongen W, Esmans E, Van Onckelen H (1996). Quantitation of cyclic nucleotides in biological samples by negative electrospray tandem mass spectrometry coupled to ion suppression liquid chromatography. *Rapid Commun Mass Spectrom* **10:** 225-231.

Witters E, Van Dongen W, Esmans EL, Van Onckelen HA (1997). Ion-pair liquid chromatography-electrospray mass spectrometry for the analysis of cyclic nucleotides. *J Chromatogr B Biomed Sci Appl* **694:** 55-63.

Yaffee S, Gold A, Sampugna J (1980). Effects of prolonged starvation on plasma free fatty acid levels and fatty acid composition of myocardial total lipids in the rat. *J Nutr* **110:** 2490-6.

Yamashita M, Fenn J (1984). Electrospray ion source. Another variation on the free-jet theme. *J Phys Chem* **88:** 4451 - 4459.

Yang HY, Karoum F, Felder C, Badger H, Wang TC, Markey SP (1999). GC/MS analysis of anandamide and quantification of N-arachidonoylphosphatidylethanolamides in various brain regions, spinal cord, testis, and spleen of the rat. *J Neurochem* **72:** 1959-68.

Yang W, Ni J, Woodward DF, Tang-Liu DD, Ling KH (2005). Enzymatic formation of prostamide F2alpha from anandamide involves a newly identified intermediate metabolite, prostamide H2. *J Lipid Res* **46:** 2745-51.

Yu M, Ives D, Ramesha CS (1997). Synthesis of prostaglandin E2 ethanolamide from anandamide by cyclooxygenase-2. *J Biol Chem* **272:** 21181-6.

Zhang NR, Yu S, Tiller P, Yeh S, Mahan E, Emary WB (2009a). Quantitation of small molecules using high-resolution accurate mass spectrometers - a different approach for analysis of biological samples. *Rapid Commun Mass Spectrom* **23:** 1085-94.

Zhang WD, Yang XL, Cao J, Li P, Yang ZL (2009b). Identification of key metabolites of tectorigenin in rat urine by HPLC-MS(n). *Biomed Chromatogr* **23:** 219-21.

Zhao S, Jia L, Gao P, Li Q, Lu X, Li J *et al* (2008). Study on the effect of eicosapentaenoic acid on phospholipids composition in membrane microdomains of tight junctions of epithelial cells by liquid chromatography/electrospray mass spectrometry. *J Pharm Biomed Anal* **47:** 343-50.

Zhu Y, Wong PS, Zhou Q, Sotoyama H, Kissinger PT (2001). Identification and determination of nucleosides in rat brain microdialysates by liquid chromatography/electrospray tandem mass spectrometry. *J Pharm Biomed Anal* **26:** 967-73.